Intersubband Dynamics in Semiconductor Quantum Wells
– Linear and Nonlinear Response of Quantum Confined Electrons –

vorgelegt von
Diplom-Physikerin

Inès Waldmüller
aus Warendorf

Fakultät II - Mathematik und Naturwissenschaften
der Technischen Universität Berlin
zur Erlangung des akademischen Grades

Doktor der Naturwissenschaften
- Dr.rer.nat. -

genehmigte Dissertation

Promotionsausschuss:
Vorsitzender: Prof. Dr. E. Sedlmayr
Berichter: Prof. Dr. A. Knorr
Berichter: Prof. Dr. E. Schöll
Tag der wissenschaftlichen Aussprache: 16. Dezember 2004

Berlin 2005
D83

Contents

List of Figures

Nomenclature

α	absorption, page 57
$\mathbf{A}$	Vector potential, page 13
$\mathbf{B}$	magnetic field
$\mathbf{E}$	electric field
$\mathbf{j}$	current density
$\mathbf{k}_k$	2D wave number in the free propagation direction
$\mathbf{P}$	microscopic dipole density operator, page 26
$\mathbf{r}_\alpha$	particle position, page 12
$\mathbf{u}_M$	ion elongations, page 17
χ	electric susceptibility, page 57
ϵ_i	energy of electron in subband i (of quantum well w_i) with wave number $\mathbf{k}_i$ and spin σ_i, page 28
$\epsilon_{w_i,\mathbf{k}_i}$	energy dispersion, page 28
ϵ_{w_i,n_i}	bound state energy or subband energy, page 28
Γ^{cc}	intrasubband carrier-carrier scattering rate
Γ^{cp}	intrasubband carrier-phonon rate, page 92
$\Gamma_{\text{d}}^{i,\text{in}}$	diagonal in-scattering, page 54
$\Gamma_{\text{d}}^{i,\text{out}}$	diagonal out-scattering, page 54
$\hat{\psi}$	electron field operator, page 17
$\hat{n}_i$	$= d_i^\dagger d_i$ number operator, page 45
$\overline{\mathbf{P}}$	macroscopic polarization (dipole density), page 26
Ω_{ren}	renormalised Rabi frequency, page 73
Ω	Rabi frequency, page 50
Ω_{exc}	internal field due to the excitonic contribution, page 73
ϕ	scalar potential, page 13
ρ	charge density
σ	density operator
σ_k	electron spin
$\sigma_{\text{irr}}(t)$	irrelevant part of the density operator
$\sigma_{\text{rel}}(t)$	relevant part of the density operator
$\mathcal{T}_+$	time ordering operator, page 42

$\mathcal{T}_-$ time anti ordering operator, page 42

$\mathcal{L}(t)$ Liouville operator

$\underline{\mathbf{q}}$ 3D wavevector, page 52

Ξ_{d} diagonal correlation contribution for intersubband coherences, page 53

Ξ_{nd} non-diagonal correlation contributions for intersubband coherences, page 53

Ξ_{nl} nonlinear correlation contributions for intersubband coherences, page 53

$a_j^\dagger$ fermionic annihilation operator, page 17

a_j fermionic creation operator, page 17

$b_j^\dagger$ bosonic annihilation operator, page 17

b_j bosonic creation operator, page 17

$d_i^\dagger$ $=\sum_j U_{ij}^* a_j^\dagger$ transformed fermionic annihilation operator, page 45

d_i $=\sum_j U_{ij} a_j$ transformed fermionic creation operator, page 45

$D_{n1,n2}$ Dipole matrix element, page 51

$f^i_{\mathbf{k},\sigma}$ $= \sigma^{ii}_{\substack{\mathbf{k},\mathbf{k}\\ \sigma,\sigma}}$ occupation numbers, page 51

$g^{ab}_{\underline{\mathbf{q}}}$ Fröhlich matrix element, page 52

H total Hamiltonian

H_0 free particle Hamiltonian, page 28

$H_{0,\mathrm{e}}$ free-carrier Hamiltonian, page 18

$H_{0,\mathrm{p}}$ free-phonon Hamiltonian, page 18

H_{cc} carrier-carrier Hamiltonian, page 28

H_{cf} carrier-field Hamiltonian, page 28

H_{cp} carrier-phonon Hamiltonian, page 28

L standard Lagrangian

L_P particle Lagrangian

L_R Lagrangian for the electromagnetic field

L_{int} interaction Lagrangian

m_0 electron mass

m_α particle mass, page 12

n_k subband number

$n_{\underline{\mathbf{q}}}$ Bose function, page 92

$p^{12}_{\mathbf{k},\sigma}$ $= \sigma^{12}_{\substack{\mathbf{k},\mathbf{k}\\ \sigma,\sigma}}$ intersubband coherences, page 51

q_α particle charge, page 12

$V_q^{n_a n_b n_c n_d}$ Coulom matrix element, page 51

V_g potential of periodic lattice

V_{conf} confinement potential

w_k well number

W_{1234} $= V_{1234} - V_{2134}$, a concise notation for the difference of Coulomb matrix elements

CHAPTER I
Introduction

Since the beginning of ultrafast nonlinear optics, it is known, that coherently excited two-level systems exhibit Rabi oscillations [AE87]: a driving field $E(t)$ couples the two energy levels with optical dipole moment d_{12} and induces oscillations of the population in the levels with Rabi frequency $\Omega(t) = E(t)d_{12}/\hbar$. As Rabi oscillations are important for a broad range of technical applications such as quantum information processing, there has been considerably interest in the investigation of possible Rabi oscillations also in low-dimensional semiconductors. Thereby the focus was lying mostly on interband Rabi oscillations in quantum dots [BLS$^+$02, FWDK03, Vas04, SMM$^+$04] and quantum wells [BKL$^+$90]. Recently, also intersubband Rabi flopping between subbands in the conduction band of quantum wells is getting increasing attention [BC04, LRW$^+$04, MVO03].

At first sight, high excitation phenomena in intersubband systems appear to have a lot in common with the excitation of well-known atomic two-level systems, as the subbands have almost equal curvature and therewith a transition energy independent from the in-plane wave vector $\mathbf{k}$. However, this simplified picture is valid only on the basis of single-particle excitations, i.e. neglecting many-particle interactions such as carrier-carrier and carrier-phonon interaction. It is well known, that carrier-carrier and carrier-phonon interaction drastically reduce the similarities to two-level systems by introducing I. Hartree-Fock effects, which are dependent on a variety of sample parameters and yield time-dependent renormalizations of subband-dispersion and Rabi-frequency, and II. dephasing due to carrier-carrier and carrier-phonon scattering. Furthermore, the nonparabolicity of the conduction band can have a rather significant impact on the curvature of the subbands, strongest for small quantum wells, yielding different subband dispersions and thus a variety of possible transition frequencies. All the above can influence the ability to produce Rabi oscillations and therewith the coherent nonlinear control of populations in quantum wells considerably. Furthermore radiative coupling between individual quantum wells in a highly doped multiple quantum well system can also have a rather strong impact on Rabi oscillations of subband populations, much stronger than the impact of the mechanisms discussed above.

In the scope of this work, the linear and nonlinear response of intersubband systems shall thus be investigated - with respect to a possible coherent control of intersubband transitions and density oscillations. Thereby the impact of the various many-particle effects is investigated first in the linear regime and then in the nonlinear regime. The knowledge about the impact of the many-particle effects in the linear regime shall provide the basis to successfully control the nonlinear response of intersubband systems - in spite of taking into account the (in principle) counteracting many-particle effects.

A. Structure of this Work

In the following, first, the theoretical background for the investigation of intersubband transitions is provided. Starting point is the adaption of the Hamilton operator to the microscopic description of the sample of interest (Chapter II A). In this context, the necessary background informations for the description of semiconductor quantum wells are revised. Then, the crossover to the macroscopic quantities is made and the macroscopic polarization - the connection between microscopic and macroscopic equations - is determined (Chapter II B). The microscopic equations of motion for intersubband coherences (which yield the macroscopic polarization) and occupation numbers (which are the access to the investigation of density dynamics in the nonlinear regime) are derived

in Chapter III. For convenience, the equations are first derived in the density matrix approach in the Heisenberg picture which is a convenient approach for the desired many-body treatment. Additionally, the interesting points, namely the derivations of mean-field and correlation contributions - are also revised in the projector-operator theory in the Schrödinger picture. Here, the early distinction between relevant and irrelevant part of the density matrix (directly related to the distinction between mean-field and correlation contributions) simplifies the access to frequently used approximations such as the mean-field factorization and therewith hopefully enhances the understanding. Before the microscopic equations are then coupled to the macroscopic equations, which introduces radiative coupling and thus allows the description of multiple quantum well systems, first the derived microscopic contributions are investigated for the case of a very basic quantum well (Chapter IV). This is done in great detail for the example of a single quantum well, where local field effects can be neglected. Thereby, special attention lies on the nonlinear regime. Here the impact of the various many-particle effects on the observed density oscillations is studied. With regard to a possible coherent control of these oscillations, the attention is focused especially on the finding of methods or better of cases, where pure Rabi oscillations can be observed - despite destructive many-particle effects . In Chapter V, finally, the macroscopic equations are derived. Thereby, the theory is derived with a special attempt to cover a wide area of possible applications. Combining the presented components, the theory can either be used to only determine the fields in simplified multiple quantum wells samples, that is without respect to additional aspects such as different dielectric constants of well and barrier materials or reflections at an interface, or to determine the fields in more complex structures taking into account the latter. As examples, applications to both the linear and the nonlinear regime, are presented in Chapter VI. Last, we compare in Chapter VII numerical results of this work to recent experimental results.

CHAPTER II
Theoretical Background

A. Hamiltonian

In the following sections we derive the actual Hamiltonian for the considered quantum well system. First, we revise the general Hamiltonian for the description of charged particles interacting with an electromagnetic field. Next, we adapt the Hamiltonian to the description of intersubband transitions in semiconductor quantum wells using the formalism of second quantization. Last the actual matrix elements of the various contributions are determined.

1. Basics

In this section, the basics of the derivation of the general Hamiltonian are revised: From the Maxwell-Lorentz equations the standard Lagrangian is derived which then yields the Hamiltonian in $\mathbf{p} \cdot \mathbf{A}$ form.

a) Maxwell-Lorentz equations

The fundamental equations describing the dynamics of a system made up of charged particles (charge q_α, mass m_α, position $\mathbf{r}_\alpha(t)$) interacting with an electromagnetic field are the *Maxwell-Lorentz equations*. They consist of

I. the microscopic *Maxwell equations* relating electric field $\mathbf{E}(\mathbf{r},t)$ and magnetic field $\mathbf{B}(\mathbf{r},t)$

$$\nabla \cdot \mathbf{B}(\mathbf{r},t) = \quad 0 \tag{II.A.1a}$$

$$\nabla \times \mathbf{E}(\mathbf{r},t) = \quad -\frac{\partial}{\partial t}\mathbf{B}(\mathbf{r},t) \tag{II.A.1b}$$

$$\nabla \cdot \mathbf{E}(\mathbf{r},t) = \quad \frac{1}{\epsilon_0}\rho \tag{II.A.1c}$$

$$\nabla \times \mathbf{B}(\mathbf{r},t) = \quad \frac{1}{c^2}\frac{\partial}{\partial t}\mathbf{E}(\mathbf{r},t) + \frac{1}{\epsilon_0 c^2}\mathbf{j} \tag{II.A.1d}$$

to charge density $\rho(\mathbf{r},t)$ and current density $\mathbf{j}(\mathbf{r},t)$

$$\rho(\mathbf{r},t) = \quad \sum_\alpha q_\alpha \delta(\mathbf{r} - \mathbf{r}_\alpha(t)) \tag{II.A.2a}$$

$$\mathbf{j}(\mathbf{r},t) = \quad \sum_\alpha q_\alpha \dot{\mathbf{r}}_\alpha \delta(\mathbf{r} - \mathbf{r}_\alpha(t)) \tag{II.A.2b}$$

and

II. the *Newton-Lorentz equations* describing the dynamics of the charged particles under the influence of the electric and magnetic forces exerted by the fields

$$m_\alpha \frac{d^2}{dt^2}\mathbf{r}_\alpha(t) = q_\alpha[\mathbf{E}(\mathbf{r}_\alpha(t),t) + \dot{\mathbf{r}_\alpha}(t) \times \mathbf{B}(\mathbf{r}_\alpha(t),t)]\,. \tag{II.A.3}$$

The *Helmholtz theorem* [Muk95] states that any vector field can be written as the sum of a longitudinal and a transverse part

$$\mathbf{a}(\mathbf{r},t) = \mathbf{a}_L(\mathbf{r},t) + \mathbf{a}_T(\mathbf{r},t) \tag{II.A.4a}$$

$$\mathbf{a}_L(\mathbf{r},t) = -\frac{1}{4\pi}\nabla \int d^3r' \frac{\nabla\cdot\mathbf{a}(\mathbf{r}',t)}{|\mathbf{r}-\mathbf{r}'|}\,, \tag{II.A.4b}$$

$$\mathbf{a}_T(\mathbf{r},t) = \frac{1}{4\pi}\nabla \times \int d^3r' \frac{\nabla\times\mathbf{a}(\mathbf{r}',t)}{|\mathbf{r}-\mathbf{r}'|}\,. \tag{II.A.4c}$$

A longitudinal vector field is characterized by

$$\nabla\times\mathbf{a}_L(\mathbf{r},t) = 0 \qquad \text{or in reciprocal space} \qquad \mathrm{i}\,\mathbf{k}\times\tilde{\mathbf{a}}_L(\mathbf{k},t) = 0\,, \tag{II.A.5}$$

a transverse field by

$$\nabla\cdot\mathbf{a}_T(\mathbf{r},t) = 0 \qquad \Leftrightarrow \qquad \mathrm{i}\,\mathbf{k}\cdot\tilde{\mathbf{a}}_T(\mathbf{k},t) = 0\,. \tag{II.A.6}$$

Thus, in reciprocal space, the name longitudinal or transverse has a clear geometrical significance: for all wave vectors $\mathbf{k}$ a longitudinal vector field is parallel to $\mathbf{k}$ and a transverse field perpendicular to $\mathbf{k}$ [CTDRG89]. Considering Eq. (II.A.1) and Eq. (II.A.4)-Eq. (II.A.6) imposes the ansatz

$$\mathbf{B}(\mathbf{r},t) = \nabla\times\mathbf{A}(\mathbf{r},t)\,, \qquad \mathbf{E}(\mathbf{r},t) = -\tfrac{\partial}{\partial t}\mathbf{A}(\mathbf{r},t) - \nabla\phi(\mathbf{r},t)\,, \tag{II.A.7}$$

where the *vector potential* $\mathbf{A}(\mathbf{r},t)$ and the *scalar potential* $\phi(\mathbf{r},t)$ have been introduced. To determine the four unknown quantities A_x, A_y, A_z, ϕ uniquely, we have to impose another condition (gauge condition), as can be seen as follows: First we insert Eq. (II.A.7) into Eq. (II.A.1c) and Eq. (II.A.1d)

$$\nabla^2\phi + \frac{\partial}{\partial t}(\nabla\cdot\mathbf{A}) = -\frac{1}{\epsilon_0}\rho \tag{II.A.8}$$

$$\nabla\times(\nabla\times\mathbf{A}) + \frac{1}{c^2}\frac{\partial^2}{\partial t^2}\mathbf{A} + \frac{1}{c^2}\nabla(\frac{\partial}{\partial t}\phi) = \frac{1}{\epsilon_0 c^2}\mathbf{j}\,. \tag{II.A.9}$$

and then operate with $\frac{1}{c^2}\frac{\partial}{\partial t}$ on Eq. (II.A.8) and with ∇ on Eq. (II.A.9). Next, we subtract the resulting equations and obtain

$$\nabla\cdot(\nabla\times(\nabla\times\mathbf{A})) = \frac{1}{\epsilon_0 c^2}(\frac{\partial}{\partial t}\rho + \nabla\times\mathbf{j})\,. \tag{II.A.10}$$

The lhs of Eq. (II.A.10) is zero because it is the gradient of a curl and the rhs vanishes since it is the equation of continuity. Thus the four equations provided by are Eq. (II.A.8) and Eq. (II.A.9) are not linearly independent and we have to impose another condition to determine A_x, A_y, A_z, ϕ uniquely. We here use the so-called *Coulomb gauge* (or *transverse* or *radiation gauge*) [Jac98]

$$\nabla\cdot\mathbf{A} = 0\,, \tag{II.A.11}$$

where the vector field $\mathbf{A}$ is purely transverse. Then longitudinal and transverse part of the electric field are obtained as

$$\mathbf{E}_T(\mathbf{r},t) = -\frac{\partial}{\partial t}\mathbf{A}(\mathbf{r},t)\,, \qquad \mathbf{E}_L(\mathbf{r},t) = -\nabla\phi(\mathbf{r},t)\,. \tag{II.A.12}$$

The longitudinal component corresponds to the rearrangement of the charges, the transverse component is related to the induced currents. In this gauge, Eq. (II.A.8) simplifies to the Poisson equation which can be solved with [Nol97]

$$\phi(\mathbf{r},t) = \frac{1}{4\pi\epsilon_0}\int d^3r' \frac{\rho(\mathbf{r}',t)}{|\mathbf{r}-\mathbf{r}'|}\,. \tag{II.A.13}$$

This shows that in Coulomb gauge the potential is instantaneous and has no retardation. Applying the identity $\nabla \times (\nabla \times \mathbf{A}) = \nabla(\nabla \cdot \mathbf{A}) - \nabla^2 \mathbf{A}$ and the gauge condition, Eq. (II.A.11), we can simplify Eq. (II.A.9) to

$$\begin{aligned} -\nabla^2 \mathbf{A} + \frac{1}{c^2}\frac{\partial^2}{\partial t^2}\mathbf{A} &= \frac{1}{\epsilon_0 c^2}\mathbf{j} - \frac{1}{c^2}\nabla(\frac{\partial}{\partial t}\phi) && \text{(II.A.14)} \\ &= \frac{1}{\epsilon_0 c^2}\mathbf{j} - \frac{1}{4\pi\epsilon_0 c^2}\nabla\frac{\partial}{\partial t}\int d^3r' \frac{\rho(\mathbf{r}',t)}{|\mathbf{r}-\mathbf{r}'|} && \text{(II.A.15)} \\ &= \frac{1}{\epsilon_0 c^2}\mathbf{j} + \frac{1}{4\pi\epsilon_0 c^2}\nabla\int d^3r' \frac{\nabla\cdot\mathbf{j}(\mathbf{r}',t)}{|\mathbf{r}-\mathbf{r}'|} && \text{(II.A.16)} \\ &= \frac{1}{\epsilon_0 c^2}\mathbf{j} - \frac{1}{\epsilon_0 c^2}\mathbf{j}_L && \text{(II.A.17)} \\ &= \frac{1}{\epsilon_0 c^2}\mathbf{j}_T\,. && \text{(II.A.18)} \end{aligned}$$

Here, we used in the last steps first the equation of continuity and then Eq. (II.A.4). Thus in the Coulomb gauge the vector potential $\mathbf{A}$ is completely determined by the transverse part of the current

$$\mathbf{j}_T = \frac{1}{4\pi}\nabla\times\int d^3r' \frac{\nabla\times\mathbf{j}(\mathbf{r}')}{|\mathbf{r}-\mathbf{r}'|}\,. \qquad \text{(II.A.19)}$$

b) Standard Lagrangian and Minimal-Coupling Hamiltonian:

As can be shown [CTDRG89], the Maxwell-Lorentz equations arise naturally as the Lagrange equations for the so-called standard Lagrangian

$$\begin{aligned} L = &\underbrace{\frac{1}{2}\sum_\alpha m_\alpha \dot{\mathbf{r}}_\alpha^2(t)}_{L_P} + \underbrace{\frac{\epsilon_0}{2}\int d^3r\,\Big[\mathbf{E}^2(\mathbf{r},t) - c^2\mathbf{B}^2(\mathbf{r},t)\Big]}_{L_R} \\ &+ \underbrace{\sum_\alpha q_\alpha\Big[\dot{\mathbf{r}}_\alpha(t)\cdot\mathbf{A}(\mathbf{r}_\alpha(t),t) - \phi(\mathbf{r}_\alpha(t),t)\Big]}_{L_{\rm int}} \qquad \text{(II.A.20)} \end{aligned}$$

which consists of the Lagrangian for the particles, L_P, the Lagrangian of the electromagnetic field, L_R, and the interaction Lagrangian $L_{\rm int}$. Inserting Eq. (II.A.7) and using

$$\begin{aligned} \int d^3r\,(\nabla\phi(\mathbf{r}))^2 &= -\frac{1}{4\pi\epsilon_0}\int d^3r\phi(\mathbf{r})\int d^3r'\nabla^2_{\mathbf{r}}\frac{\rho(\mathbf{r}')}{|\mathbf{r}-\mathbf{r}'|} \\ &= \frac{1}{\epsilon_0}\int d^3r\phi(\mathbf{r})\rho(\mathbf{r}) = \frac{1}{\epsilon_0}\sum_\alpha q_\alpha\phi(\mathbf{r}_\alpha) \qquad \text{(II.A.21)} \end{aligned}$$

we obtain the Lagrangian in Coulomb gauge

$$\begin{aligned} L = &\frac{1}{2}\sum_\alpha m_\alpha\dot{\mathbf{r}}_\alpha^2(t) + \frac{\epsilon_0}{2}\int d^3r\,\Big[\mathbf{E}_T^2(\mathbf{r},t) - c^2\mathbf{B}^2(\mathbf{r},t)\Big] \\ &- \frac{1}{2}\frac{1}{4\pi\epsilon_0}\sum_{\alpha,\beta}\frac{q_\alpha q_\beta}{|\mathbf{r}_\alpha(t)-\mathbf{r}_\beta(t)|} + \sum_\alpha q_\alpha\dot{\mathbf{r}}_\alpha(t)\cdot\mathbf{A}(\mathbf{r}_\alpha(t),t) \\ &+ \epsilon_0\int d^3r\,\mathbf{E}_T(\mathbf{r},t)\cdot\mathbf{E}_L(\mathbf{r},t)\,. \qquad \text{(II.A.22)} \end{aligned}$$

With the help of the Parseval-Plancherel identity [CTDRG89]

$$\int d^3r\,F^*(\mathbf{r})G^*(\mathbf{r}) = \int d^3k\,\tilde{F}^*(\mathbf{k})\tilde{G}^*(\mathbf{k}) \qquad \text{(II.A.23)}$$

and Eq. (II.A.5) and Eq. (II.A.6), we see that the last term in Eq. (II.A.22) vanishes:

$$\int d^3r\, \mathbf{E}_T(\mathbf{r},t)\cdot\mathbf{E}_L(\mathbf{r},t) = \int d^3k\, \tilde{\mathbf{E}}_T(\mathbf{k},t)\cdot\tilde{\mathbf{E}}_L(\mathbf{k},t) = 0\,. \tag{II.A.24}$$

The Hamiltonian is defined by

$$H = \sum_\alpha \dot{x_\alpha} p_\alpha - L \tag{II.A.25}$$

where the summation goes over all variables x_α and their momentum conjugates $p_\alpha = \frac{\partial L}{\partial \dot{x}_\alpha}$. We insert the momentum conjugates for particle position $\mathbf{r}_\alpha$, vector potential $\mathbf{A}$ and scalar potential ϕ

$$\mathbf{p}_\alpha = \; m_\alpha \dot{\mathbf{r}}_\alpha(t) + q_\alpha \mathbf{A}(\mathbf{r}_\alpha(t),t) \tag{II.A.26a}$$
$$p_\phi = \; 0 \tag{II.A.26b}$$
$$\mathbf{p}_\mathbf{A}(\mathbf{r}) = -\epsilon_0 \mathbf{E}_T(\mathbf{r},t) \tag{II.A.26c}$$

and obtain the corresponding Hamilton-function

$$\begin{aligned}
H = \;& \sum_\alpha \mathbf{p}_\alpha\cdot\dot{\mathbf{r}}_\alpha + \int d^3r\, \mathbf{p}_\mathbf{A}(\mathbf{r})\cdot\dot{\mathbf{A}}(\mathbf{r}) - \frac{1}{2}\sum_\alpha m_\alpha \dot{\mathbf{r}}_\alpha^2 - \frac{\epsilon_0}{2}\int d^3r\, \Big[\mathbf{E}_T^2(\mathbf{r}) - c^2\mathbf{B}^2(\mathbf{r})\Big] \\
& + \frac{1}{2}\frac{1}{4\pi\epsilon_0}\sum_{\alpha,\beta}\frac{q_\alpha q_\beta}{|\mathbf{r}_\alpha - \mathbf{r}_\beta|} - \sum_\alpha q_\alpha \dot{\mathbf{r}}_\alpha\cdot\mathbf{A}(\mathbf{r}_\alpha) \\
= \;& \sum_\alpha \mathbf{p}_\alpha\cdot\frac{1}{m_\alpha}\Big[\mathbf{p}_\alpha - q_\alpha\mathbf{A}(\mathbf{r}_\alpha)\Big] + \epsilon_0\int d^3r\, \mathbf{E}_T^2(\mathbf{r}) - \frac{1}{2}\sum_\alpha \frac{1}{m_\alpha}\Big[\mathbf{p}_\alpha - q_\alpha\mathbf{A}(\mathbf{r}_\alpha)\Big]^2 \\
& - \frac{\epsilon_0}{2}\int d^3r\, \Big[\mathbf{E}_T^2(\mathbf{r}) - c^2\mathbf{B}^2(\mathbf{r})\Big] \\
& + \frac{1}{2}\frac{1}{4\pi\epsilon_0}\sum_{\alpha,\beta}\frac{q_\alpha q_\beta}{|\mathbf{r}_\alpha - \mathbf{r}_\beta|} - \sum_\alpha q_\alpha \frac{1}{m_\alpha}\Big[\mathbf{p}_\alpha - q_\alpha\mathbf{A}(\mathbf{r}_\alpha)\Big]\cdot\mathbf{A}(\mathbf{r}_\alpha) \\
= \;& \sum_\alpha \frac{1}{2m_\alpha}\Big[\mathbf{p}_\alpha - q_\alpha\mathbf{A}(\mathbf{r}_\alpha)\Big]^2 + \frac{1}{2}\frac{1}{4\pi\epsilon_0}\sum_{\alpha,\beta}\frac{q_\alpha q_\beta}{|\mathbf{r}_\alpha - \mathbf{r}_\beta|} \\
& + \frac{\epsilon_0}{2}\int d^3r\, \Big[\mathbf{E}_T^2(\mathbf{r}) + c^2\mathbf{B}^2(\mathbf{r})\Big]\,.
\end{aligned} \tag{II.A.27}$$

which yields the so-called minimal-coupling Hamiltonian [CT84]

$$\begin{aligned}
\hat{H} = \;& \sum_\alpha \frac{1}{2m_\alpha}\Big[\hat{\mathbf{p}}_\alpha^2 - 2q_\alpha\hat{\mathbf{A}}(\hat{\mathbf{r}}_\alpha)\cdot\hat{\mathbf{p}}_\alpha + q_\alpha^2\hat{\mathbf{A}}^2(\hat{\mathbf{r}}_\alpha)\Big] + \frac{1}{2}\frac{1}{4\pi\epsilon_0}\sum_{\alpha,\beta}\frac{q_\alpha q_\beta}{|\hat{\mathbf{r}}_\alpha - \hat{\mathbf{r}}_\beta|} \\
& + \frac{\epsilon_0}{2}\int d^3r\, \Big[\hat{\mathbf{E}}_T^2(\mathbf{r}) + c^2\hat{\mathbf{B}}^2(\mathbf{r})\Big]\,.
\end{aligned} \tag{II.A.28}$$

We here used that in Coulomb gauge $[\hat{\mathbf{p}}, \hat{\mathbf{A}}(\hat{\mathbf{r}})] = 0$, since $\nabla\cdot\mathbf{A} = 0$. The first part of the minimal-coupling Hamiltonian includes the kinetic energies of the charges and terms representing the interaction between the charges and the electromagnetic radiation, the second the Coulomb interaction between the charges and the last term the radiative energy. So far we did not specify the system of particles. Next, we want to adapt the Hamiltonian to the description of the dynamics of electrons in a semiconductor.

2. Semiconductor Hamiltonian

First, we divide the solid into background ion-cores (referred to as ions and denoted with upper-case letters N, M) and outer-shell electrons (referred to as electrons and denoted with lower-case letters

i, j) [Kno97]

$$\begin{aligned}\hat{H} = & \sum_N \frac{1}{2m_N}\Big[\hat{\mathbf{p}}_N^2 - 2q_N\hat{\mathbf{A}}(\hat{\mathbf{r}}_N)\cdot\hat{\mathbf{p}}_N + q_N^2\hat{\mathbf{A}}^2(\hat{\mathbf{r}}_N)\Big] \\ & + \sum_i \frac{1}{2m_i}\Big[\hat{\mathbf{p}}_i^2 - 2q_i\hat{\mathbf{A}}(\hat{\mathbf{r}}_i)\cdot\hat{\mathbf{p}}_i + q_i^2\hat{\mathbf{A}}^2(\hat{\mathbf{r}}_i)\Big] \\ & + \frac{1}{2}\frac{1}{4\pi\epsilon_0}\sum_{N,M}\frac{q_Nq_M}{|\hat{\mathbf{r}}_N - \hat{\mathbf{r}}_M|} + \frac{1}{4\pi\epsilon_0}\sum_{i,M}\frac{q_iq_M}{|\hat{\mathbf{r}}_i - \hat{\mathbf{r}}_M|} + \frac{1}{2}\frac{1}{4\pi\epsilon_0}\sum_{i,j}\frac{q_iq_j}{|\hat{\mathbf{r}}_i - \hat{\mathbf{r}}_j|} \\ & + \frac{\epsilon_0}{2}\int d^3r\,\Big[\hat{\mathbf{E}}_T^2(\mathbf{r}) + c^2\hat{\mathbf{B}}^2(\mathbf{r})\Big]\,. \end{aligned} \tag{II.A.29}$$

In the following, we assume the transverse field to have a negligible influence on the ionic motion and consider only the influence on the electrons. Furthermore, we invoke the Born-Oppenheimer approximation and consider that the ions cannot follow the motion of the electrons [YC99]. Thus, the ions are well localized around their lattice position $\hat{\mathbf{R}}_N$ and their time-dependent position can be expressed according to

$$\hat{\mathbf{r}}_M = \hat{\mathbf{R}}_M + \hat{\mathbf{u}}_M \tag{II.A.30}$$

where $\hat{\mathbf{u}}_M$ denotes the time-dependent elongation of ion M. Therewith the contributions containing ion coordinates can be expanded around the lattice positions of the ions which yields a decomposition of ion-ion interaction and electron-ion interaction in contributions as the static background charge contribution $V_{\mathrm{ii}}(\hat{\mathbf{R}}_N - \hat{\mathbf{R}}_M)$ (ion-ion interaction) and periodic lattice potential $V_{\mathrm{ei}}(\hat{\mathbf{r}}_i - \mathbf{R}_M)$ (static electron-ion interaction) for the propagating electrons, electron-phonon interaction (dynamic ion-electron interaction) and higher order contributions such as phonon-phonon interaction which shall be neglected in the following. Note, that from now on the hat "ˆ" denoting an operator is dropped.

In general, one could now proceed by transforming the resulting Hamiltonian into the language of second quantization. However, the present form of the carrier-field interaction Hamiltonian

$$H_{\mathrm{cf}} = \sum_i \frac{1}{2m_i}\Big[-2q_i\mathbf{A}(\mathbf{r}_i)\cdot\mathbf{p}_i + q_i^2\mathbf{A}^2(\mathbf{r}_i)\Big], \tag{II.A.31}$$

often known as the $\mathbf{p}\cdot\mathbf{A}$ form [Lou00] is not very convenient for the following calculation as the electromagnetic field appears via the transverse vector potential, which is not directly observable. Moreover, the interaction contains an $\mathbf{A}^2$ term. This term is often neglected even though it may affect the optical response in a significant way. For these reasons, we will here consider another form of the carrier-field Hamiltonian which can be obtained by performing a canonical transformation: the Power-Zienau transformation [CT84]. With the help of this transformation the $\mathbf{p}\cdot\mathbf{A}$ Hamiltonian is transformed into the so-called $\mathbf{r}\cdot\mathbf{E}_T$ Hamiltonian.

a) $\mathbf{r}\cdot\mathbf{E}_T$ Hamiltonian (Dipole-Approximation)

The Power-Zienau transformation changes any operator as

$$F' = \mathrm{e}^{\mathrm{i}\,S}F\mathrm{e}^{-\mathrm{i}\,S} \tag{II.A.32}$$

with [KJHK99]

$$S = -\frac{1}{\hbar}\sum_\alpha q_\alpha\mathbf{r}_\alpha\cdot\mathbf{A}(\mathbf{r}_\alpha)\,. \tag{II.A.33}$$

Therewith we transform particle and field operators where we assume that the spatial variations of the vector potential are small on the scale of an elementary unit cell of the semiconductor lattice, i.e. we use the dipole approximation. By performing the Power-Zienau transformation, the field and

material variables mix. The new field variables contain an "old matter" contribution and the new material variables contain an "old field" contribution.

However, it can be shown [Muk95] that in the semiclassical approximation where the field is treated classically and the material is described in its quantized form, the carrier-field Hamiltonian can be reduced to an effective semiclassical Hamiltonian of the form

$$H_{\mathrm{cf}} = -\int d^3r\, \mathbf{P}(\mathbf{r}) \cdot \mathbf{E}_T(\mathbf{r})\,. \tag{II.A.34}$$

Here $\mathbf{P}(\mathbf{r})$ is the dipole density operator [KJHK99]. This semiclassical Hamiltonian provides the basis for most theoretical treatments in the area of the linear or nonlinear response of semiconductors (cf. for example [Muk95, CK99, Kuh98]) and shall also be used in the scope of this work.

b) Hamiltonian in Second Quantization

Electrons

In order to express the Hamiltonian in the language of second quantization, we introduce the electron field operator [CK99]

$$\hat{\psi}(\mathbf{r},t) = \sum_{\lambda}\sum_{\mathbf{k}}\sum_{\sigma} a_{\lambda,\mathbf{k},\sigma}(t)\phi_{\lambda,\mathbf{k},\sigma}(\mathbf{r})\,, \tag{II.A.35}$$

where $\phi_{\lambda,\mathbf{k},\sigma}(\mathbf{r})$ is the single-particle eigenfunction for an electron in the semiconductor and $a_{\lambda,\mathbf{k},\sigma}(t)$ is the annihilation operator for the electron in the corresponding state. Namely, the state with band index $\lambda = c, v$ (conduction band, valence band), wave vector $\mathbf{k}$ and spin σ. The Hermitean adjoint $a^\dagger_{\lambda,\mathbf{k},\sigma}(t)$ is the corresponding creation operator. As Fermion operators, the electron creation and annihilation operators obey anti-commutation relations

$$[a_i^\dagger, a_j]_+ = \delta_{i,j}\,, \qquad [a_i^\dagger, a_j^\dagger]_+ = 0\,, \qquad [a_i, a_j]_+ = 0\,. \tag{II.A.36}$$

These relations are a direct consequence of the Pauli exclusion principle, stating that any given state can at most be occupied by one Fermion.

Phonons

The ion elongations $\mathbf{u}_M$ are expanded in terms of phonon creation and annihilation operators [Czy00]

$$\mathbf{u}_M = \frac{1}{\sqrt{N}}\sum_{\underline{\mathbf{q}},j}\sqrt{\frac{\hbar}{2m_M\omega_{j,\underline{\mathbf{q}}}}}(b_{j,\underline{\mathbf{q}}} + b^\dagger_{j,-\underline{\mathbf{q}}})\mathrm{e}^{\mathrm{i}\,\underline{\mathbf{q}}\mathbf{R}_M}\mathbf{e}_{j,\underline{\mathbf{q}}} \tag{II.A.37}$$

where the phonon energies $\omega_{j,\underline{\mathbf{q}}}$ depend on the $3D$ wave number $\underline{\mathbf{q}}$ of the j-th phonon mode with unit vector $\mathbf{e}_{j,\underline{\mathbf{q}}}$. Due to their bosonic nature the phonon operator obey the following commutation relations

$$[b_i^\dagger, b_j]_- = -\delta_{i,j}\,, \qquad [b_i^\dagger, b_j^\dagger]_- = 0\,, \qquad [b_i, b_j]_- = 0\,. \tag{II.A.38}$$

Photons

In the scope of this work, the interaction with the transverse electric is treated in the semiclassical approximation, i.e., the transverse field enters the Hamiltonian in its classical form.

With this background the Hamiltonian can be cast into

$$H = \quad H_{0,\mathrm{e/p}} + H_{\mathrm{cf}} + H_{\mathrm{cc}} + H_{\mathrm{cp}}\,. \tag{II.A.39}$$

where the different contributions are defined as follows:

- free-carrier and free-phonon Hamiltonian

$$H_{0,\mathrm{e}} = \int d^3r \hat{\psi}^\dagger(\mathbf{r}) \Big\{ -\frac{\hbar^2\nabla^2}{2m} + V_{\mathrm{L}}(\mathbf{r}) + \sum_{N,M} V_{\mathrm{ii}}(\mathbf{R}_N - \mathbf{R}_M) \Big\} \hat{\psi}(\mathbf{r}) \,, \tag{II.A.40}$$

$$H_{0,\mathrm{p}} = \sum_{\underline{\mathbf{q}},j} \hbar\,\omega_{j,\underline{\mathbf{q}}}\, b^\dagger_{j,\underline{\mathbf{q}}} b_{j,\underline{\mathbf{q}}} \tag{II.A.41}$$

- carrier-field Hamiltonian (in dipole approximation)

$$H_{\mathrm{cf}} = -e \int d^3r\, \hat{\psi}^\dagger(\mathbf{r}) \mathbf{r} \hat{\psi}^\dagger(\mathbf{r}) \cdot \mathbf{E}_T(\mathbf{r},t) \,. \tag{II.A.42}$$

- carrier-carrier Hamiltonian

$$H_{\mathrm{cc}} = \frac{1}{2}\frac{1}{4\pi\epsilon_0} \int d^3r \int d^3r'\, \hat{\psi}^\dagger(\mathbf{r}) \hat{\psi}^\dagger(\mathbf{r}') \frac{e^2}{|\mathbf{r}-\mathbf{r}'|} \hat{\psi}(\mathbf{r}) \hat{\psi}(\mathbf{r}') \tag{II.A.43}$$

- carrier-phonon Hamiltonian

$$H_{\mathrm{cp}} = \sum_M \int d^3r\, \hat{\psi}^\dagger(\mathbf{r}) (\mathbf{u}_M \cdot \nabla_{\mathbf{R}_M}) V_{\mathrm{ei}}(\mathbf{r} - \mathbf{R}_M) \hat{\psi}(\mathbf{r}) \tag{II.A.44}$$

In order to carry out specific calculations with the Hamiltonian given in Eq. (II.A.39), we have to determine the actual wave functions necessary for the determination of the required matrix elements. For this reason, we next take a closer look at the samples of interest, namely semiconductor quantum wells and the corresponding bandstructure.

3. Quantum Wells: Eigenfunctions and Energies

A quantum well is a heterostructure or in other words a double heterojunction. A heterojunction emerges, when two dissimilar semiconductors are placed adjacent to each other. The central feature of a heterojunction is that the bandgaps of the participating semiconductors are usually different. Thus, the energy of the carriers of at least one of the band edges must change as those carriers pass through the heterojunction. Most often, there will be discontinuities in both the conduction and valence band. These discontinuities are the origin of most of the useful properties of heterojunctions. Heterostructures are formed from multiple heterojunctions (cf. Fig. II.A.1).

If a thin layer with thickness L_W of a semiconductor material A with bandgap E^A_{gap} is sandwiched between two layers of another semiconductor B of equal thickness L_B with bandgap $E^B_{\mathrm{gap}} > E^A_{\mathrm{gap}}$, the result is a semiconductor quantum well. Due to the different bandgaps, the conduction and valence band edges of A and B do not align with each other. The difference between their band edges is known as the band offset and responsible for confining the electrons in layer A [YC99]. Thus the free-carrier Hamiltonian has to be extended by including the corresponding confinement potential which confines the electrons in the dimension perpendicular to the well layers[Kli95]:

$$H_{0,\mathrm{e}} = \int d^3r \hat{\psi}^\dagger(\mathbf{r}) \Big\{ -\frac{\hbar^2\nabla^2}{2m} + V_{\mathrm{L}}(\mathbf{r}) + \sum_{N,M} V_{\mathrm{ii}}(\mathbf{R}_N - \mathbf{R}_M) + V_{\mathrm{conf}}(z) \Big\} \hat{\psi}(\mathbf{r}) \,. \tag{II.A.45}$$

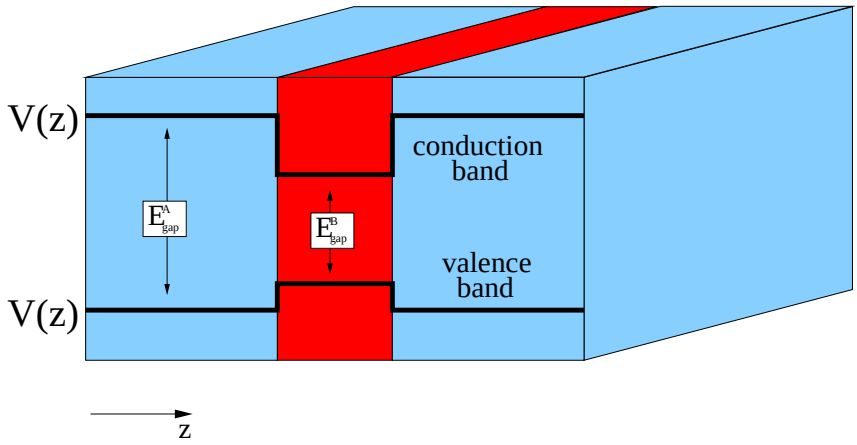

Figure II.A.1 — Double heterojunction: consisting of a thin layer of a narrower-bandgap material *A* sandwiched between two layers of a wider-bandgap material *B*.

More complex structures than the simple example given above, consist of several repeating units of the form $B/A/B/A/B/A...$ They either form a multiple quantum well (MQW) system or a super-lattice: if the barriers B are much thicker than the penetration depth of the wave functions into the barrier we speak about a MQW system, if the barriers are thin enough to allow overlap, one has a super-lattice [Kli95].

As has been shown in [Bas88], the eigenfunctions [cf. Eq. (II.A.35)] of the free-carrier Hamiltonian in Eq. (II.A.45) can - in effective mass approximation - be factorized according to

$$\phi_{\lambda,\mathbf{k},\sigma}(\mathbf{r}) = \frac{1}{\sqrt{A}} u_{\lambda,\mathbf{k}\approx 0,\sigma}(\mathbf{r}) \Phi_{\lambda,\mathbf{k},\sigma}(\mathbf{r}) \tag{II.A.46}$$

where $u_{\lambda,\mathbf{k}\approx 0,\sigma}(\mathbf{r})$ is the eigenfunction of the lattice periodic part and $\Phi_{\lambda,\mathbf{k},\sigma}(\mathbf{r})$ the wave function responding to the additional confinement potential V_{conf}. Note, that this expansion is valid only near the band edge, i.e., $\mathbf{k} \approx 0$.

The simplest theoretical approach to the confining potential caused by the band offset of a quantum well is the infinitely deep one-dimensional potential well. More sophisticated models account for the finite height of the confinement potential or effects of an external electric field [Har00].

a) Infinite Quantum Well

The infinitely deep one-dimensional quantum well is realized by the confinement potential

$$V_{\mathrm{conf}}(z) = \begin{cases} 0 & |z| < L/2 \\ \infty & |z| > L/2\,, \end{cases} \tag{II.A.47}$$

thus the electrons are completely confined in z-direction. The quantum-mechanical motion is described by the wave function $\Phi(\mathbf{r},t)$ which is the solution of the time-dependent Schrödinger equation

$$\mathrm{i}\,\hbar\,\frac{\partial}{\partial t}\Phi(\mathbf{r},t) = H\Phi(\mathbf{r},t) \tag{II.A.48}$$

where H is the corresponding Hamiltonian

$$H = -\frac{\hbar^2}{2m}\nabla^2 + V_{\mathrm{conf}}(z)\,. \tag{II.A.49}$$

As the Hamiltonian does not depend explicitly on time and furthermore, the confinement potential acts only on the z-component, the wave function can be factorized according to

$$\Phi(\mathbf{r},t) = \tilde{\Phi}(\mathbf{r}_{||})\zeta(z)\mathrm{e}^{-\mathrm{i}\,\frac{\epsilon}{\hbar}t}\,. \tag{II.A.50}$$

This yields decoupled equations for components perpendicular, $\mathbf{z}$, and parallel to the well layer, $\mathbf{r}_{||} = (x,y)$:

$$\left[-\frac{\hbar^2}{2m}\frac{d^2}{d_z^2} + V_{\mathrm{conf}}(z)\right]\zeta(z) = \epsilon_z\,\zeta(z) \tag{II.A.51}$$

$$-\frac{\hbar^2}{2m}\nabla^2_{r_{||}}\,\tilde{\Phi}(\mathbf{r}_{||}) = \epsilon_{||}\,\tilde{\Phi}(\mathbf{r}_{||})\,. \tag{II.A.52}$$

Considering the boundary conditions

$$\zeta(-\frac{L}{2}) = \zeta(\frac{L}{2}) = 0\,, \tag{II.A.53}$$

the z-dependent part of the wave function is obtained as

$$\zeta_n(z) = \sqrt{\frac{2}{L}}\cos(k_n z)\,, n \text{ even}\,, \tag{II.A.54}$$

$$\zeta_n(z) = \sqrt{\frac{2}{L}}\sin(k_n z)\,, n \text{ odd} \tag{II.A.55}$$

where the wave numbers k_n and the bound state energies are given by

$$k_n = \frac{n\pi}{L}\,, \qquad \epsilon_n = \frac{\pi^2\hbar^2 n^2}{2mL^2}\,. \tag{II.A.56}$$

In the (x,y)-plane, the particles can move freely and can therefore be described by plane waves

$$\tilde{\Phi}(\mathbf{r}_{||}) = \frac{1}{\sqrt{A}}\mathrm{e}^{\pm\mathrm{i}\,\mathbf{k}\cdot\mathbf{r}_{||}} \tag{II.A.57}$$

with area of the quantum well A, 2D wave numbers $\mathbf{k}$ and energies

$$\epsilon_{\mathbf{k}} = \frac{\hbar k^2}{2m}\,. \tag{II.A.58}$$

b) Finite Quantum Well

The finitely deep one-dimensional quantum well is realized by the confinement potential

$$V_{\mathrm{conf}}(z) = \begin{cases} 0 & |z| < L/2 \\ V_c & |z| > L/2\,, \end{cases} \tag{II.A.59}$$

thus the electrons are not completely confined in z-direction. Following Chapter II.A.3.a the wave function is again decoupled. But whereas the part $\tilde{\Phi}(\mathbf{r}_{||})$, which depends on $\mathbf{r}_{||}$, is unchanged, the z-dependent part, $\zeta(z)$, can no longer be determined analytically. For both $|z| < L/2$ and $|z| > L/2$, $\zeta(z)$ is the sum of two plane waves of opposite wave vectors: inside the well, $|z| < L/2$, the waves propagate; outside the well, $|z| > L/2$, the waves are evanescent. Introducing

$$\kappa = \sqrt{\frac{2m}{\hbar^2}(V_c - \epsilon_z)}\,, \qquad k_z = \sqrt{\frac{2m}{\hbar^2}\epsilon_z} \tag{II.A.60}$$

and considering the boundary conditions (and normalization condition) yields

$$\zeta_+(z) = \begin{cases} A\cos(k_z z) & |z| < L/2 \\ B\mathrm{e}^{-\kappa|z|} & |z| > L/2 \end{cases} \tag{II.A.61}$$

with the transcendental conditional equation

$$k_z \tan(k_z \frac{L}{2}) = \kappa \qquad \Leftrightarrow \qquad \sqrt{\epsilon_z} \tan(\sqrt{\frac{2m}{\hbar^2}\epsilon_z}\frac{L}{2}) = \sqrt{(V_c - \epsilon_z)} \tag{II.A.62}$$

for even states and

$$\zeta_-(z) = \begin{cases} C\sin(k_z z) & |z| < L/2 \\ -B\mathrm{e}^{\kappa z} & z < -L/2 \\ B\mathrm{e}^{-\kappa z} & z > L/2 \end{cases} \tag{II.A.63}$$

with the transcendental conditional equation

$$-k_z \cot(k_z \frac{L}{2}) = \kappa \qquad \Leftrightarrow \qquad -\sqrt{\epsilon_z} \cot(\sqrt{\frac{2m}{\hbar^2}\epsilon_z}\frac{L}{2}) = \sqrt{(V_c - \epsilon_z)} \tag{II.A.64}$$

for odd states. The constants A,B and C are given by

$$A = B\frac{\mathrm{e}^{-\kappa L/2}}{\cos(k_z L/2)}\,, \tag{II.A.65}$$

$$C = B\frac{\mathrm{e}^{-\kappa L/2}}{\sin(k_z L/2)}\,, \tag{II.A.66}$$

$$B = \mathrm{e}^{\kappa L/2}\left[\left(1+\frac{\kappa^2}{k_z^2}\right)\left(\frac{L}{2}+\frac{1}{\kappa}\right)\right]^{-\frac{1}{2}}\,. \tag{II.A.67}$$

In the scope of this work, in most cases, the finite height of the potential is taken into account, i.e. the wave functions are determined numerically by solving the transcendental equations given above. However, there is also the possibility to consider the impact of the finite height of the potential in a numerically less demanding way.

c) Effective Well-Width Approximation

The effective well-width approximation [Liu94] approximates the wave functions of a finite barrier well with physical well width L by infinite-barrier wave functions with an effective well width L_{eff}. The effective well with is thereby chosen so that the bound energy of the lowest subband is equal in both the infinite-barrier and the finite-barrier well. Together with an overview over the well-width dependence of the various Coulomb and Fröhlich matrix elements, the impact of this approximation on the matrix elements is shown in APP B. Generally, one can say, that the difference between a full calculation with the numerically determined wave functions of the finite-barrier well and the effective well-width approximation is in most cases negligibly small. Thus, if it is numerically too demanding to take the finite-barrer well functions into account, the effective well width offers a reasonable alternative. Considering an infinite-barrier well without effective well width can yield quite misleading results, since e.g. the depolarization effect depends very strongly on the actual well width. As the effective well width is usually larger than the physical well width (the electrons can leak into the barrier region when the barrier height of the well is finite), the infinite-barrier wave functions underestimate the depolarization effect if the well width is not adjusted to an effective one.

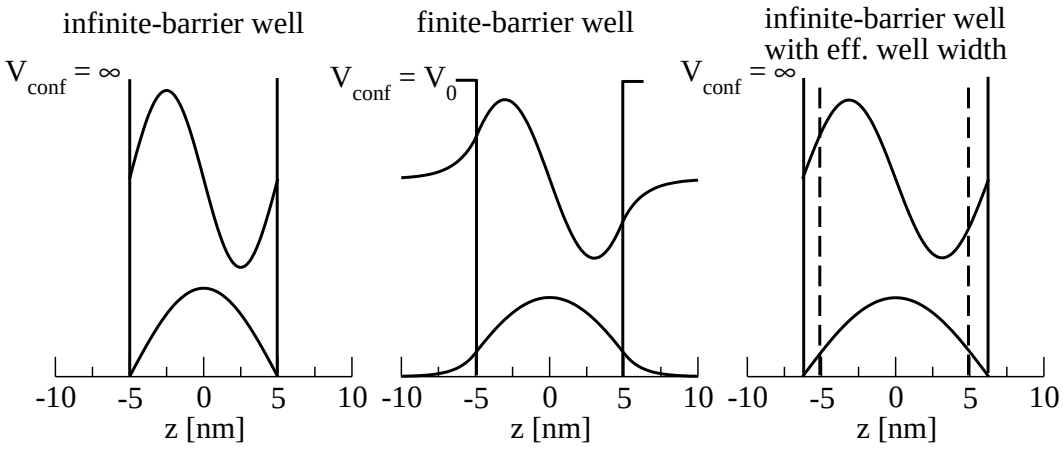

Figure II.A.2 — Wave functions for different quantum well modells: (infinite-barrier, finite-barrier and infinite-barrier well with effective well-width approximation) Example of a 10nm GaAs/AlGaAs quantum well with a finite potential of $V_0 = 360$ meV. Effective well-width $L_{\rm eff} = 12.56$ nm.

d) Nonparabolicity Effects

In narrow quantum wells the energy levels in the conduction band are of the order of 100 meV above the bulk conduction-band edge. Thus corrections due to the nonparabolicity of the conduction band, such as for example modifications of the energy dispersion parallel to the well layers, can be important. In the factorization used in Eq. (II.A.46) these effects are not included a priori. A common way to include nonparabolicity effects is to include a small number of bands in a matrix equation and treat the other bands in perturbation theory which modifies the effective masses. In the scope of this work, we follow the approach by Ekenberg [Eke89, Eke87] which is well suited not only for the idealized case with infinite barriers but also for the more realistic case with finite barriers. Starting point are the results from a 14-band $\mathbf{k} \cdot \mathbf{p}$ calculation done by Braun and Rössler [BR85], namely the conduction-band dispersion in the bulk of a direct-band-gap III-V compound semiconductor expanded up to fourth order in k. The obtained results are then used to determine numerically the bound state energies and the energy dispersion parallel to the layers. As in the "common" effective mass approximation, the obtained energy dispersions are expressed using effective masses for the subbands. In contrast to the parabolic approximation of the conduction band, the subbands are here characterized by different subband masses: $m_1 \neq m_2$. Thus, the subband dispersion derived in Eq. (II.A.58) is replaced according to:

$$\epsilon_{\mathbf{k}} = \frac{\hbar k^2}{2m} \rightarrow \epsilon_{i,\mathbf{k}} = \frac{\hbar k^2}{2m_i} \tag{II.A.68}$$

where i denotes the subband and m_i the corresponding mass numerically determined with the formula given in [Eke89]. The subband dependence of the in-plane dispersion results in an effectively wavenumber dependent transition energy

$$\epsilon_{i,\mathbf{k}} - \epsilon_{j,\mathbf{k}} = \frac{\hbar k^2}{2m_i} - \frac{\hbar k^2}{2m_j} \, . \tag{II.A.69}$$

For details see [Eke89, Eke87]. In the following, we will frequently compare the linear and nonlinear response of quantum wells with or without taking into account possible nonparabolicity effects. As the dominant impact of the nonparabolicity effects lies in the change of the effective subbands masses, i.e., the subband dispersion, we will mostly distinguish the different models by using the terminology *with equal subband dispersion* or *with different subband dispersion*. However, this shall not imply that only the impact on the subband masses is taken into account. The impact on bound state energy is also considered, the chosen terminology might be misleading in this case. In

order to get first insights on the impact of the nonparabolicity of the conduction band, we present in Fig. II.A.3 a comparison of the energy dispersion calculated with or without taking into account the nonparabolicity of the conduction band.

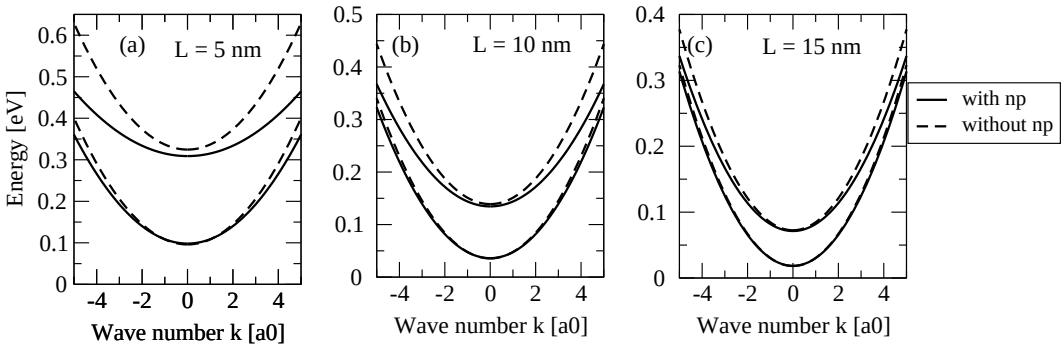

Figure II.A.3 — Energy Dispersion with/without regard to nonparabolicity effects: Taking into account the nonparabolicity of the conduction band according to the theory by [Eke89] for a GaAs/AlGaAs quantum well with $V_{\mathrm{conf}} = 350$ meV for different well width $L = 5, 10, 15$ nm. Whereas for wider quantum wells, the nonparabolicity of the conduction band is almost negligible, it causes a lowering of the upper bound state energy and larger effective masses for small wells.

4. Matrix Elements

Combining the results of Eq. (II.A.46) with Eq. (II.A.57) and Eq. (II.A.54), Eq. (II.A.63) respectively, the single particle functions are completely determined and thus the field operators are given by

$$\begin{aligned}\hat{\psi}(\mathbf{r},t) &= \sum_{\lambda,\mathbf{k},\sigma} a_{\lambda,\mathbf{k},\sigma}(t)\phi_{\lambda,\mathbf{k},\sigma}(\mathbf{r}) \\ &= \frac{1}{\sqrt{A}} \sum_{\lambda,\mathbf{k},\sigma,n,w} u_{\lambda,\mathbf{k}\approx 0,\sigma}(\mathbf{r})\, \zeta_{w,n}(\mathbf{r}_\perp)\, \mathrm{e}^{\mathrm{i}\,\mathbf{k}\cdot\mathbf{r}_{||}}\, a_{\lambda,\mathbf{k},\sigma,n,w}\ . \end{aligned} \tag{II.A.70}$$

Besides index λ for the band, $2D$ wave number $\mathbf{k}$ and spin σ we introduced furthermore the index n denoting the subband and with respect to a multiple quantum well system additionally the index w for the well number. In the following, only transitions between the subbands in the conduction band will be considered, i.e. $\lambda = c$. For convenience this index is dropped from now on and the other indices are absorbed into a compound index whenever possible:

$$\hat{\psi}(\mathbf{r},t) = \frac{1}{\sqrt{A}} \sum_i u_{\lambda,\mathbf{k}\approx 0,\sigma}(\mathbf{r})\, \zeta_{w_i,n_i}(\mathbf{r}_\perp)\, \mathrm{e}^{\mathrm{i}\,\mathbf{k}_i\cdot\mathbf{r}_{||}}\, a_i\ . \tag{II.A.71}$$

With Eq. (II.A.71) we can now derive the explicit formulas of the various matrix elements. For the sake of readability, the derivations are left to APP A and here only the final Hamiltonian is given.

Note, that as the focus of this works lies with heterostructures made from compound semiconductors, where the dominant electron-phonon interaction is with the longitudinal optical phonon (LO) phonon[Har00], we considered only these contributions. The LO phonon dispersion curve [see for example [YC99] p.110 et sqq.], is relatively flat. Therefore the LO phonon is almost dispersionless and the phonon energy $\hbar\omega_L$ can be approximated well with a constant value (taken as 36 meV in GaAs).

In total the Hamiltonian is given by

$$H_0 = \sum_i \epsilon_i \, a_i^\dagger \, a_i + \sum_{\underline{\mathbf{q}}} \hbar \, \omega_{LO} \, b_{\underline{\mathbf{q}}}^\dagger b_{\underline{\mathbf{q}}} \tag{II.A.72}$$

$$H_{\mathrm{cf}} = \; e \sum_{i',j'} \sum_{\mathbf{q},\mathbf{Q}} a^\dagger_{i',\mathbf{q}+\mathbf{Q}/2} a_{j',\mathbf{q}-\mathbf{Q}/2} \Big[F_{||}^{i',j'}(\mathbf{Q},t) + F_{\perp}^{i',j'}(\mathbf{Q},t) \Big] \delta_{\sigma_{i'},\sigma_{j'}} \tag{II.A.73}$$

$$H_{\mathrm{cc}} = \frac{1}{2} \sum_{a,b,c,d} V_{abcd} \, a_a^\dagger a_b^\dagger a_d a_c \tag{II.A.74}$$

$$H_{\mathrm{cp}} = \sum_{a,b,\mathbf{k},\underline{\mathbf{q}}} \left[g_{\underline{\mathbf{q}}}^{a,b} a^\dagger_{a,\mathbf{k}_a} b_{\underline{\mathbf{q}}} a_{b,\mathbf{k}_a - \underline{\mathbf{q}}_{||}} + g_{\underline{\mathbf{q}}}^{*a,b} a^\dagger_{b,\mathbf{k}_a - \underline{\mathbf{q}}_{||}} b^\dagger_{\underline{\mathbf{q}}} a_{a,\mathbf{k}_a} \right] \tag{II.A.75}$$

The introduced abbreviations in the carrier-field Hamiltonian read

$$F_{||}^{i',j'}(\mathbf{Q},t) = \mathrm{i} \int_{L_\perp} dR_\perp \zeta^*_{w_{i'},n_{i'}}(R_\perp) \zeta_{w_{j'},n_{j'}}(R_\perp) \nabla_{\mathbf{Q}} \cdot \mathbf{E}_{||}(\mathbf{Q},R_\perp,t) \tag{II.A.76}$$

$$F_{\perp}^{i',j'}(\mathbf{Q},t) = \int_{L_\perp} dR_\perp \zeta^*_{w_{i'},n_{i'}}(R_\perp) \zeta_{w_{j'},n_{j'}}(R_\perp) \, R_\perp E_\perp(\mathbf{Q},R_\perp,t) \tag{II.A.77}$$

with

$$\mathbf{E}(\mathbf{Q},\mathbf{R}_\perp) = \frac{1}{N_{||}} \sum_{\mathbf{R}_{||}} \mathrm{e}^{-\mathrm{i}\,\mathbf{Q}\cdot\mathbf{R}_{||}} \mathbf{E}(\mathbf{R}_{||},\mathbf{R}_\perp,t) \, . \tag{II.A.78}$$

Coulomb and Fröhlich matrix element are given by

$$V_{abcd} = \; \frac{1}{A} \frac{e^2}{2\epsilon_0} \int dz \int dz' \frac{\mathrm{e}^{-|\mathbf{k}_a - \mathbf{k}_c||z-z'|}}{|\mathbf{k}_a - \mathbf{k}_c|} \zeta^*_{w_a,n_a}(z) \zeta^*_{w_b,n_b}(z') \tag{II.A.79}$$

$$\times \, \zeta_{w_c,n_c}(z) \zeta_{w_d,n_d}(z') \delta_{\mathbf{k}_a+\mathbf{k}_b,\mathbf{k}_c+\mathbf{k}_d} \delta_{\sigma_a,\sigma_c} \delta_{\sigma_b,\sigma_d} \tag{II.A.80}$$

$$g_{\underline{\mathbf{q}}}^{ab} = -\mathrm{i} \sqrt{\frac{e^2 \hbar \omega_{LO}}{2\mathcal{V}} \left(\frac{1}{\varepsilon_\infty} - \frac{1}{\varepsilon_s} \right)} \frac{1}{|\underline{\mathbf{q}}|} \int \mathrm{d}z \phi_a(z) \phi_b(z) \mathrm{e}^{\mathrm{i}\,\underline{\mathbf{q}}_\perp z} \, . \tag{II.A.81a}$$

B. Microscopic/Macroscopic

Starting from the microscopic Maxwell-Lorentz Equations and corresponding standard Lagrangian we derived in the last sections the microscopic Hamiltonian for the quantum well system. The derived Hamiltonian is the starting point for the derivation of the microscopic equations of motions [cf. Chapter III], the backbone of the microscopic source calculation. Before actually immersing into the connected derivation, we first make the crossing to the so-called macroscopic equations which are the starting point of the field calculation.

1. Macroscopic Maxwell Equations

As a macroscopic sample contains of the order of $10^{23\pm5}$ electrons and nuclei [Jac98], which are all in incessant motion, the microscopic fields produced by these charges vary rapidly in space and time. However, macroscopic measuring devices used in experiments generally average over intervals in space and time longer than the fluctuations of the microscopic charges yielding relatively smooth

and slowly varying macroscopic quantities. The macroscopic electric and magnetic field quantities are thus defined as the averages of the microscopic fields

$$\overline{\mathbf{E}}(\mathbf{r},t) = \langle E(\mathbf{r},t)\rangle \tag{II.B.1}$$

$$\overline{\mathbf{B}}(\mathbf{r},t) = \langle B(\mathbf{r},t)\rangle\ . \tag{II.B.2}$$

Note that only a spatial average is necessary (for details see [Jac98]). The spatial average of a function $F(\mathbf{r},t)$ with respect to a test function $f(\mathbf{r})$ is defined as

$$\langle F(\mathbf{r},t)\rangle = \int d^3r' f(\mathbf{r}')F(\mathbf{r}-\mathbf{r}',t)\ . \tag{II.B.3}$$

This test function is real and normalized to unity over all space. Here the spatial average over one elementary cell with volume Ω_{EC} is sufficient [Kno97], thus we choose

$$f(\mathbf{r}) = \begin{cases} \frac{1}{\Omega_{\mathrm{EC}}} & \text{for } \mathbf{r}\in \mathrm{EC},\\ 0 & \text{for } \mathbf{r}\notin \mathrm{EC}. \end{cases}$$

Using that the operations of space and time differentiation commute with the averaging operation, we obtain the macroscopic Maxwell equations as the averages of the microscopic Maxwell equations (cf. Eq. (II.A.1)). For the here considered system they are given by

$$\nabla\cdot\overline{\mathbf{B}}(\mathbf{r},t) = 0 \tag{II.B.4}$$

$$\nabla\times\overline{\mathbf{E}}(\mathbf{r},t) = -\frac{\partial}{\partial t}\overline{\mathbf{B}}(\mathbf{r},t) \tag{II.B.5}$$

$$\epsilon_0\epsilon_b\nabla\cdot\overline{\mathbf{E}}(\mathbf{r},t) = -\nabla\cdot\overline{\mathbf{P}}(\mathbf{r},t) \tag{II.B.6}$$

$$\nabla\times\overline{\mathbf{B}}(\mathbf{r},t) = \mu_0\frac{\partial}{\partial t}\left[\epsilon_0\epsilon_b\overline{\mathbf{E}}(\mathbf{r},t)+\overline{\mathbf{P}}(\mathbf{r},t)\ .\right] \tag{II.B.7}$$

$\overline{\mathbf{P}}_t(\mathbf{r},t)$ denotes the total macroscopic polarization

$$\overline{\mathbf{P}}_t(\mathbf{r},t) = \overline{\mathbf{P}}(\mathbf{r},t)+\epsilon_0\chi_b\overline{\mathbf{E}}(\mathbf{r},t)\ . \tag{II.B.8}$$

composed of the polarization of the electrons

$$\overline{\mathbf{P}}(\mathbf{r},t) = \left\langle \mathbf{P}_{\mathrm{electrons}}(\mathbf{r},t)\right\rangle \tag{II.B.9}$$

and the polarization of the ions (approximated by a linear background polarisation)

$$\left\langle \mathbf{P}_{\mathrm{ions}}(\mathbf{r},t)\right\rangle \approx \epsilon_0\chi_b\overline{\mathbf{E}}(\mathbf{r},t)\ . \tag{II.B.10}$$

Combining Eq. II.B.4 - Eq. II.B.7 yields the wave equation for the macroscopic field $\overline{\mathbf{E}}(\mathbf{r},t)$

$$\nabla\times\nabla\times\overline{\mathbf{E}}(\mathbf{r},t) = -\nabla\times\frac{\partial}{\partial t}\overline{\mathbf{B}}(\mathbf{r},t)$$

$$\Leftrightarrow\left[\nabla^2-\frac{\epsilon_b}{c^2}\frac{\partial^2}{\partial t^2}\right]\overline{\mathbf{E}}(\mathbf{r},t)-\nabla(\nabla\cdot\overline{\mathbf{E}}(\mathbf{r},t)) = \mu_0\frac{\partial^2}{\partial t^2}\overline{\mathbf{P}}(\mathbf{r},t))\ . \tag{II.B.11}$$

The macroscopic field enters the microscopic Hamiltonian and therewith the microscopic equations. On the other hand, the microscopic equations yield the the macroscopic polarization, i.e. the source for the electromagnetic field. Thus macroscopic and microscopic equations of motion are coupled.

2. Macroscopic Polarization (Dipole Density)

As a last point we derive the explicit formula for the macroscopic polarization, the connection between microscopic and macroscopic equations for the here considered system. We start from the microscopic dipole density operator which in second quantization is given by

$$\mathbf{P}(\mathbf{r},t) = e\,\hat{\psi}^{\dagger}(\mathbf{r},t)\,\mathbf{r}\,\hat{\psi}(\mathbf{r},t)\,. \tag{II.B.12}$$

Similar to the derivation of carrier-field and carrier-carrier matrix elements given in APP A, we insert the expansion of the field operators in electron creation and annihilation operators [cf. Eq. (II.A.71)] which yields

$$\mathbf{P}(\mathbf{r},t) = \frac{e}{A}\sum_{i,j} \mathrm{e}^{-\mathrm{i}\,(\mathbf{k}_i-\mathbf{k}_j)\cdot\mathbf{r}_{||}}\zeta^{*}_{w_i,n_i}(\mathbf{r}_{\perp})\zeta_{w_j,n_j}(\mathbf{r}_{\perp})u^{*}_{\sigma_i,\mathbf{k}_i=0}(\mathbf{r})u_{\sigma_j,\mathbf{k}_j=0}(\mathbf{r})\,\mathbf{r}\,a^{\dagger}_i a_j\,. \tag{II.B.13}$$

Taking the quantum mechanically expectation value and averaging as described in Chapter II.B.1, we obtain the macroscopic polarization (dipole density)

$$\begin{aligned}\overline{\mathbf{P}}(\mathbf{r},t) = {} & \frac{e}{A}\sum_{\substack{n_i,n_j\\ \mathbf{Q}_{||},\mathbf{q}_{||}}} \mathrm{e}^{-\mathrm{i}\,\mathbf{Q}_{||}\cdot\mathbf{r}_{||}}\zeta^{*}_{n_i}(\mathbf{r}_{\perp})\zeta_{n_j}(\mathbf{r}_{\perp})\,\mathbf{r}_{\perp}\,\langle a^{\dagger}_{n_i,\mathbf{q}_{||}+\mathbf{Q}_{||}/2}a_{n_j,\mathbf{q}_{||}-\mathbf{Q}_{||}/2}\rangle \\ & -\frac{e}{A}\,\mathrm{i}\sum_{\substack{n_i,n_j\\ \mathbf{Q}_{||},\mathbf{q}_{||}}} \mathrm{e}^{-\mathrm{i}\,\mathbf{Q}_{||}\cdot\mathbf{r}_{||}}\zeta^{*}_{n_i}(\mathbf{r}_{\perp})\zeta_{n_j}\nabla_{\mathbf{Q}_{||}}\langle a^{\dagger}_{n_i,\mathbf{q}_{||}+\mathbf{Q}_{||}/2}a_{n_j,\mathbf{q}_{||}-\mathbf{Q}_{||}/2}\rangle\end{aligned} \tag{II.B.14}$$

where we have switched to centre of mass coordinates and relative coordinates:

$$\mathbf{q}_{||} = \frac{\mathbf{k}_{i||}+\mathbf{k}_{j||}}{2}\,, \qquad \mathbf{Q}_{||} = \mathbf{k}_{i||}-\mathbf{k}_{j||}\,. \tag{II.B.15}$$

As can be seen in Eq. (II.B.14), the macroscopic polarization is composed of both intrasubband drift contributions and contributions due to optical (intersubband) processes. According to the focus of this work, only the latter will be considered in the following.

In the next chapter, we will now derive the microscopic equations of motions for quantities $\langle a^{\dagger}_i a\ \rangle$, which determine the polarization and thus eventually drive the macroscopic fields.

CHAPTER III
Microscopic Equations of Motion: Source Calculation

As we have seen in Chapter II.B.2, the quantities of interest as polarization or population all depend on expectation values of the form $\langle a_k^\dagger a_l \rangle$, where indices k, l are compound indices, which contain the subband numbers n_k, n_l, 2D-wave numbers $\mathbf{k}_k, \mathbf{k}_l$ in the free propagation direction (xy-plane), spin σ_k, σ_l and well numbers w_k, w_l. For different indices, the expectation values yield coherences (for example $n_k \neq n_{k'}$: intersubband coherence), for equal indices, i.e., $k = k'$ they yield occupation numbers. The dynamics for the expectation values

$$\langle O \rangle = \mathrm{tr}(O\sigma) \tag{III..16}$$

reside either in the operator O (Heisenberg picture) or in the density operator σ (Schrödinger picture).

A. Introduction: Schrödinger Picture vs. Heisenberg Picture

In the Schrödinger picture, operators (observables) are time-independent if they do not dependent *explicitly* on the time (for example due to time-dependent external fields) and the density operator σ obeys the von-Neumann equation (Liouville equation)

$$\mathrm{i}\,\hbar\,\frac{\mathrm{d}}{\mathrm{d}t}\sigma = [H, \sigma]\,. \tag{III.A.1}$$

H denotes the total Hamiltonian and the commutator is given by

$$[A, B] = AB - BA\,. \tag{III.A.2}$$

With Eq. (III.A.1) expectation values of observables reads

$$\begin{aligned}\mathrm{i}\,\hbar\,\frac{\mathrm{d}}{\mathrm{d}t}\langle O\rangle &= \mathrm{i}\,\hbar\Big[\mathrm{tr}(\{\,\frac{\mathrm{d}}{\mathrm{d}t}O\}\sigma) + \mathrm{tr}(O\{\,\frac{\mathrm{d}}{\mathrm{d}t}\sigma\})\Big] = \mathrm{i}\,\hbar\langle\,\frac{\partial}{\partial t}O\rangle + \mathrm{tr}(O[H,\sigma]) \\ &= \mathrm{i}\,\hbar\langle\,\frac{\partial}{\partial t}O\rangle - \mathrm{tr}([O,H]\sigma]) = \mathrm{i}\,\hbar\langle\,\frac{\partial}{\partial t}O\rangle - \langle[H,O]\rangle\,,\end{aligned} \tag{III.A.3}$$

where in the last step the cyclic property of the trace has been used [cf. Eq. (III.C.6)].

In the Heisenberg picture, operators (observables) are time-dependent and obey the Heisenberg equation|seeequations, Heisenberg:

$$-\mathrm{i}\,\hbar\,\frac{\mathrm{d}}{\mathrm{d}t}O = [H, O] - \mathrm{i}\,\hbar\,\frac{\partial}{\partial t}O\,. \tag{III.A.4}$$

The states are time-independent and consequently the same applies for the density operator . This yields

$$-\mathrm{i}\,\hbar\,\frac{\mathrm{d}}{\mathrm{d}t}\langle O\rangle = \langle[H, O]\rangle - \mathrm{i}\,\hbar\langle\,\frac{\partial}{\partial t}O\rangle\,. \tag{III.A.5}$$

Thus both pictures give the same expectation values for the operator O. However, in the determination of the expectation values considered here, certain approximations have to be made. As we will see in the following, the Heisenberg picture is the more convenient approach in the many-body treatment. The Schrödinger picture is more difficult to handle, but does on the other hand give additional insight into the background of common approximations frequently used in the Heisenberg picture. Therefore, we will proceed as follows: we first derive the equations of motion in the Heisenberg picture using well-known approximations. After that, we revise the theory in the Schrödinger picture in the framework of the projector-operator theory and compare directly with the derivation performed in the Heisenberg picture. This will give more insight into the background of the applied approximations and therewith hopefully enhance the understanding.

B. Heisenberg Picture

In order to determine polarization and population, we derive the equation of motion for the density matrix elements $\langle a_k^\dagger a_l \rangle$. We start with the Heisenberg equation for $a_k^\dagger a_l$ and take the expectation value

$$\begin{aligned} -\mathrm{i}\,\hbar \frac{\mathrm{d}}{\mathrm{d}t}\langle a_k^\dagger a_l \rangle &= \langle [H, a_k^\dagger a_l] \rangle = \langle [H_0 + H_{\mathrm{cf}} + H_{\mathrm{cc}} + H_{\mathrm{cp}}, a_k^\dagger a_l] \rangle \\ &= -\mathrm{i}\,\hbar \frac{\mathrm{d}}{\mathrm{d}t}\langle a_k^\dagger a_l \rangle|_0 - \mathrm{i}\,\hbar \frac{\mathrm{d}}{\mathrm{d}t}\langle a_k^\dagger a_l \rangle|_{\mathrm{cf}} - \mathrm{i}\,\hbar \frac{\mathrm{d}}{\mathrm{d}t}\langle a_k^\dagger a_l \rangle|_{\mathrm{cc}} - \mathrm{i}\,\hbar \frac{\mathrm{d}}{\mathrm{d}t}\langle a_k^\dagger a_l \rangle|_{\mathrm{cp}} \,. \end{aligned} \tag{III.B.1}$$

For conciseness, in the following the contributions shall be derived for each Hamiltonian separately.

1. Free-Particle Hamiltonian

The free-particle Hamiltonian describes the motion of electrons of mass m_0 in the periodic lattice V_g with the superposed confinement potential V_{conf} (cf. Chapter II.A.3). Inserting the results of Eq. (APP E.1) we obtain

$$\frac{\mathrm{d}}{\mathrm{d}t}\langle a_k^\dagger a_l \rangle|_0 = \frac{\mathrm{i}}{\hbar}(\epsilon_k - \epsilon_l)\langle a_k^\dagger a_l \rangle \,, \tag{III.B.2}$$

where ϵ_i denotes the energy of an electron in subband i (of quantum well w_i) with wave number $\mathbf{k}_i$ and spin σ_i. This contribution thus directly reflects the bandstructure of the quantum well system. We can distinguish *bound state energy* or *subband energy* ϵ_{w_i,n_i} and *in-plane* energy dispersion, $\epsilon_{w_i,\mathbf{k}_i}$ [cf. Chapter II.A.3.a, II.A.3.b, II.A.3.d]. Dependent on the underlying bandstructure, or to be more exact, the curvature of the conduction band, the energy dispersion of different subbands (in one quantum well) can differ either only in the bound state energies, for example $\epsilon_{w_i,2} = \epsilon_{w_i,1} + \hbar\omega_G$ or additionally also in the in-plane energy dispersion. The latter being due to a non-parabolic curvature of the conduction band [cf. Chapter II.A.3.d].

2. Carrier-Field Hamiltonian

In the *semiclassical approach* the carrier-field Hamiltonian describes the interaction of the electrons with the *classical electromagnetic field*. Using the results of Eq. (APP E.11) and separating contributions due to optical transitions and electrical current, the contributions due to the interaction with the classical electromagnetic field read

$$\frac{\mathrm{d}}{\mathrm{d}t}\langle a_k^\dagger a_l \rangle|_{\mathrm{cf}} = \frac{\mathrm{d}}{\mathrm{d}t}\langle a_k^\dagger a_l \rangle|_{\mathrm{cf}}^{\mathrm{opt}} + \frac{\mathrm{d}}{\mathrm{d}t}\langle a_k^\dagger a_l \rangle|_{\mathrm{cf}}^{\mathrm{cur}} \tag{III.B.3}$$

with

$$\frac{\mathrm{d}}{\mathrm{d}t}\langle a_k^\dagger a_l\rangle|_{\mathrm{cf}}^{\mathrm{opt}} = e\frac{\mathrm{i}}{\hbar}\sum_i\int_L dz\Big\{d_{n_i,n_k}^{w_i,w_k}(z)\,\langle a_i^\dagger a_l\rangle\delta_{\sigma_i,\sigma_k}\,E_z(\mathbf{k}_i-\mathbf{k}_k,z,t) - d_{n_l,n_i}^{w_l,w_i}(z)\,\langle a_k^\dagger a_i\rangle\delta_{\sigma_l,\sigma_i}\,E_z(\mathbf{k}_l-\mathbf{k}_i,z,t)\Big\}, \tag{III.B.4}$$

$$\frac{\mathrm{d}}{\mathrm{d}t}\langle a_k^\dagger a_l\rangle|_{\mathrm{cf}}^{\mathrm{cur}} = -\frac{e}{\hbar}\sum_i\int_L dz\Big\{\Psi_{n_i,n_k}^{w_i,w_k}(z)\mathbf{E}_{||}(\mathbf{k}_i-\mathbf{k}_k,z,t)\cdot\nabla_{\mathbf{k}_k}\langle a_i^\dagger a_l\rangle\delta_{\sigma_i,\sigma_k} + \Psi_{n_l,n_i}^{w_l,w_i}(z)\mathbf{E}_{||}(\mathbf{k}_l-\mathbf{k}_i,z,t)\cdot\nabla_{\mathbf{k}_l}\langle a_k^\dagger a_i\rangle\delta_{\sigma_l,\sigma_i}\Big\}. \tag{III.B.5}$$

Whereas Eq. (III.B.5) describes the acceleration of carriers in the free directions, i.e., current in the x,y-plane, Eq. (III.B.4) describes optically induced transitions between the subbands [Kuh98]. In the scope of this work, the focus lies on the description of the latter and therefore only these contributions are considered in the following. Remember, that due to applying the Coulomb gauge in II.A.1.b, only the transverse part of the electromagnetic fields enters the equations of motion.

3. Carrier-Carrier Hamiltonian

Introducing carrier-carrier interaction, the electrons are no longer considered as non-interacting particles. Interaction between different electrons yields microscopic effects such as dephasing and screening.

With the results given in Eq. (APP E.16) we obtain

$$\frac{\mathrm{d}}{\mathrm{d}t}\langle a_k^\dagger a_l\rangle|_{\mathrm{cc}} = \frac{\mathrm{i}}{\hbar}\sum_{a,b,c}\Big[V_{abkc}\,\langle a_a^\dagger a_b^\dagger a_c a_l\rangle - V_{labc}\,\langle a_k^\dagger a_a^\dagger a_c a_b\rangle\Big]. \tag{III.B.6}$$

Regarding Eq. (III.B.6) it becomes obvious, that the system of equations does not close. Coulomb interaction couples the two-operator dynamics to four-operator terms which describe correlations between electrons. Thus, in order to solve Equation III.B.6, the four-operator terms have to be determined, which can be done using again the Heisenberg equation of motion. However, carrier-carrier interaction then couples the four-operator terms to six-operator terms, six-operator terms to eight-operator terms and so: Equation III.B.6 is the starting point of an infinite hierarchy involving higher-order density matrix elements. This so-called *hierarchy problem* is a common problem in many-particle physics. To obtain a solution, the hierarchy has to be truncated at some level. In the scope of this work, we use a correlation expansion based on the idea, that correlations, i.e., higher-order density matrix elements, involving an increasing number of carriers are of decreasing importance [Kuh98].

Therefore, we do the following: we factorize the foursome operators into products of two-operator terms,$\langle a_1^\dagger a_2^\dagger a_3 a_4\rangle_{\mathrm{f}}$, and a correction term, $\langle a_1^\dagger a_2^\dagger a_3 a_4\rangle_{\mathrm{c}}$, according to

$$\langle a_1^\dagger a_2^\dagger a_3 a_4\rangle = \langle a_1^\dagger a_2^\dagger a_3 a_4\rangle_{\mathrm{f}} + \langle a_1^\dagger a_2^\dagger a_3 a_4\rangle_{\mathrm{c}} \tag{III.B.7}$$

with

$$\langle a_1^\dagger a_2^\dagger a_3 a_4\rangle_{\mathrm{f}} = \langle a_1^\dagger a_4\rangle\langle a_2^\dagger a_3\rangle - \langle a_1^\dagger a_3\rangle\langle a_2^\dagger a_4\rangle. \tag{III.B.8}$$

This factorization is a common way to obtain a systematic hierarchy of equations [HK94, CK99] and as we will see later, the factorization according to Eq. (III.B.8), can be derived very neatly in the framework of projector-operator theory. Inserting Eq. (III.B.7) in Eq. (III.B.6), the equation of motion can be decomposed into *mean-field* or *Hartree-Fock* contributions (dependent on the factorized

contributions) and *collision* or *correlation* contributions (dependent on the correction contributions):

$$\frac{\mathrm{d}}{\mathrm{d}t}\langle a_k^\dagger a_l\rangle = \frac{\mathrm{d}}{\mathrm{d}t}\langle a_k^\dagger a_l\rangle|_{\mathrm{MF,cc}} + \frac{\mathrm{d}}{\mathrm{d}t}\langle a_k^\dagger a_l\rangle|_{\mathrm{corr,cc}} \tag{III.B.9}$$

with

$$\frac{\mathrm{d}}{\mathrm{d}t}\langle a_k^\dagger a_l\rangle|_{\mathrm{MF,cc}} = \frac{\mathrm{i}}{\hbar}\sum_{a,b,c}\left[V_{abkc}\,\langle a_a^\dagger a_b^\dagger a_c a_l\rangle_{\mathrm{f}} - V_{labc}\,\langle a_k^\dagger a_a^\dagger a_c a_b\rangle_{\mathrm{f}}\right], \tag{III.B.10}$$

$$\frac{\mathrm{d}}{\mathrm{d}t}\langle a_k^\dagger a_l\rangle|_{\mathrm{corr,cc}} = \frac{\mathrm{i}}{\hbar}\sum_{a,b,c}\left[V_{abkc}\,\langle a_a^\dagger a_b^\dagger a_c a_l\rangle_{\mathrm{c}} - V_{labc}\,\langle a_k^\dagger a_a^\dagger a_c a_b\rangle_{\mathrm{c}}\right]. \tag{III.B.11}$$

In general, the motion of the carriers is correlated because they interact, either directly or through the intermediary of other carriers in the system. As a first approximation, these correlations may be neglected, i.e., the carriers are assumed to propagate completely independently of each other. In this case, the equation of motion is approximated by Eq. (III.B.10), the mean-field contributions, only.

a) Carrier-Carrier Mean-Field Contributions (1st Order)

Inserting Eq. (III.B.8) in Eq. (III.B.6) yields the lowest order in the hierarchy, the mean-field contributions due to carrier-carrier interaction:

$$\begin{aligned}\frac{\mathrm{d}}{\mathrm{d}t}\langle a_k^\dagger a_l\rangle|_{\mathrm{MF,cc}} = \frac{\mathrm{i}}{\hbar}\sum_{a,b,c}\Big[&V_{abkc}\left(\langle a_a^\dagger a_l\rangle\langle a_b^\dagger a_c\rangle - \langle a_a^\dagger a_c\rangle\langle a_b^\dagger a_l\rangle\right)\\ &- V_{labc}\left(\langle a_k^\dagger a_b\rangle\langle a_a^\dagger a_c\rangle - \langle a_k^\dagger a_c\rangle\langle a_a^\dagger a_b\rangle\right)\Big].\end{aligned} \tag{III.B.12}$$

The expression *mean-field contributions* results from the fact, that the decomposition of the four-particle correlations in Eq. (III.B.6) leads to the same result as approximating H_{cc} by the one-particle Hamiltonian $H_{\mathrm{MF}}^{\mathrm{cc}}$:

$$H_{\mathrm{MF}}^{\mathrm{cc}} = \sum_{ab}\Big(\sum_{cd}\Big[V_{acbd} - V_{cabd}\Big]\langle a_c^\dagger a_d\rangle\Big)a_a^\dagger a_b\,. \tag{III.B.13}$$

Thus we see that the mean-field or Hartree-Fock approximation describes the many-particle system as a set of independent particles, each particle, however, moving through the average field produced by all particles - without possibility for collisions [KB89].

In the case of intersubband transitions, the mean-field contributions due to carrier-carrier interaction introduce three effects:

I. exchange shift: a renormalization of the free-carrier contributions,

II. excitonic contribution: a renormalization of the carrier-field interaction,

III. depolarization contribution: another renormalization of the carrier-field interaction, although of very different origin.

A detailed investigation of these contributions and their interplay is given in Chapter IV.

b) Carrier-Carrier Correlation Contributions (2nd Order)

The next step in the hierarchy is obtained by considering the correction terms to the mean-field factorization, i.e., Eq. (III.B.11). However, the correlation contributions are not determined as easily

as the mean-field contributions, since we have to derive equations of motion for the correction terms themselves. Using Eq. (III.A.5) we obtain

$$\begin{aligned}\frac{\mathrm{d}}{\mathrm{d}t}\langle a_1^\dagger a_2^\dagger a_3 a_4\rangle_\mathrm{c} = &\quad \frac{\mathrm{d}}{\mathrm{d}t}\langle a_1^\dagger a_2^\dagger a_3 a_4\rangle - \frac{\mathrm{d}}{\mathrm{d}t}\langle a_1^\dagger a_2^\dagger a_3 a_4\rangle_\mathrm{f} \\ = &\quad \frac{\mathrm{i}}{\hbar}\langle [H, a_1^\dagger a_2^\dagger a_3 a_4]\rangle - \frac{\mathrm{i}}{\hbar}\langle [H, a_1^\dagger a_4]\rangle\langle a_2^\dagger a_3\rangle - \frac{\mathrm{i}}{\hbar}\langle a_1^\dagger a_4\rangle\langle [H, a_2^\dagger a_3]\rangle \\ &+ \frac{\mathrm{i}}{\hbar}\langle [H, a_1^\dagger a_3]\rangle\langle a_2^\dagger a_4\rangle + \frac{\mathrm{i}}{\hbar}\langle a_1^\dagger a_3\rangle\langle [H, a_2^\dagger a_4]\rangle\,. \end{aligned} \tag{III.B.14}$$

In principle here the full Hamiltonian has to be considered, but in order to obtain a manageable theory, certain approximations have to be made. In the scope of this work, we neglect the contributions of transverse field and carrier-phonon interaction on the correction terms. Thus, we neglect that the correlations are also influenced by carrier-field and carrier-phonon interaction and focus on the more fundamental contributions due to free-particle and carrier-carrier Hamiltonian [Kuh98]:

$$\frac{\mathrm{d}}{\mathrm{d}t}\langle a_1^\dagger a_2^\dagger a_3 a_4\rangle_\mathrm{c} \approx \frac{\mathrm{d}}{\mathrm{d}t}\langle a_1^\dagger a_2^\dagger a_3 a_4\rangle_\mathrm{c}|_0 + \frac{\mathrm{d}}{\mathrm{d}t}\langle a_1^\dagger a_2^\dagger a_3 a_4\rangle_\mathrm{c}|_\mathrm{cc}\,. \tag{III.B.15}$$

Straightforward calculations yield

$$\frac{\mathrm{d}}{\mathrm{d}t}\langle a_1^\dagger a_2^\dagger a_3 a_4\rangle_\mathrm{c}|_0 = \frac{\mathrm{i}}{\hbar}(\epsilon_1 + \epsilon_2 - \epsilon_3 - \epsilon_4)\langle a_1^\dagger a_2^\dagger a_3 a_4\rangle_\mathrm{c}\,, \tag{III.B.16}$$

$$\begin{aligned}\frac{\mathrm{d}}{\mathrm{d}t}\langle a_1^\dagger a_2^\dagger a_3 a_4\rangle_\mathrm{c}|_\mathrm{cc} = &\quad \frac{\mathrm{i}}{\hbar}\sum_{a,b,c}\Big[V_{ab12}\langle a_a^\dagger a_b^\dagger a_3 a_4\rangle - V_{43cb}\langle a_1^\dagger a_2^\dagger a_b a_c\rangle\Big] \\ &+ \frac{\mathrm{i}}{\hbar}\sum_{a,b,c}\sum_{m,h}\Big[(\delta_{m,3}\delta_{h,4} - \delta_{m,4}\delta_{h,3}) \\ &\Big\{\Big(V_{ab1c}\langle a_a^\dagger a_b^\dagger a_c a_m\rangle - V_{amcb}\langle a_a^\dagger a_1^\dagger a_b a_c\rangle\Big)\langle a_2^\dagger a_h\rangle \\ &+ \Big(V_{ab2c}\langle a_a^\dagger a_b^\dagger a_c a_h\rangle - V_{habc}\langle a_a^\dagger a_2^\dagger a_b a_c\rangle\Big)\langle a_1^\dagger a_m\rangle\Big\} \\ &+ V_{abmc}(\delta_{m,2}\delta_{h,1} - \delta_{m,1}\delta_{h,2})\langle a_h^\dagger a_a^\dagger a_b^\dagger a_c a_3 a_4\rangle \\ &+ V_{macb}(\delta_{m,4}\delta_{h,3} - \delta_{m,3}\delta_{h,4})\langle a_1^\dagger a_2^\dagger a_a^\dagger a_h a_b a_c\rangle\Big]\,. \end{aligned} \tag{III.B.17}$$

As already announced before, carrier-carrier interaction couples the correction terms not only to four-operator terms and combinations of four and two-operator terms but also to six-operator terms. Again we factorize higher order terms in products of two-operator terms. Four-operator terms are factorized with Eq. (III.B.7) and Eq. (III.B.8), six-operator terms are factorized according to

$$\langle a_1^\dagger a_2^\dagger a_3^\dagger a_4 a_5 a_6\rangle = \langle a_1^\dagger a_2^\dagger a_3^\dagger a_4 a_5 a_6\rangle_\mathrm{f} + \langle a_1^\dagger a_2^\dagger a_3^\dagger a_4 a_5 a_6\rangle_\mathrm{c} \tag{III.B.18}$$

with

$$\begin{aligned}\langle a_1^\dagger a_2^\dagger a_3^\dagger a_4 a_5 a_6\rangle_\mathrm{f} = &\quad \langle a_1^\dagger a_4\rangle\left\{\langle a_2^\dagger a_6\rangle\langle a_3^\dagger a_5\rangle - \langle a_2^\dagger a_5\rangle\langle a_3^\dagger a_6\rangle\right\} \\ &+ \langle a_1^\dagger a_5\rangle\left\{\langle a_2^\dagger a_4\rangle\langle a_3^\dagger a_6\rangle - \langle a_2^\dagger a_6\rangle\langle a_3^\dagger a_4\rangle\right\} \\ &+ \langle a_1^\dagger a_6\rangle\left\{\langle a_2^\dagger a_5\rangle\langle a_3^\dagger a_4\rangle - \langle a_2^\dagger a_4\rangle\langle a_3^\dagger a_5\rangle\right\}\,. \end{aligned} \tag{III.B.19}$$

This factorization scheme can also be derived in the framework of projector-operator theory [cf. Appendix APP D]. Inserting the factorizations gives finally

$$\frac{\mathrm{d}}{\mathrm{d}t}\langle a_1^\dagger a_2^\dagger a_3 a_4\rangle_\mathrm{c}|_\mathrm{cc}$$

$$= \frac{\mathrm{i}}{\hbar}\sum_{a,b,c}\Bigg[\langle a_1^\dagger a_c\rangle\langle a_2^\dagger a_b\rangle\Big\{W_{4abc}\delta_{a,3} + \langle a_a^\dagger a_4\rangle W_{3abc} + \langle a_a^\dagger a_3\rangle W_{4acb}\Big\} \tag{III.B.20a}$$

$$+ \langle a_a^\dagger a_4\rangle\langle a_b^\dagger a_3\rangle\Big\{W_{abc2}\delta_{c,1} + \langle a_2^\dagger a_c\rangle W_{ba1c} + \langle a_1^\dagger a_c\rangle W_{4ab2c}\Big\}\Bigg] \tag{III.B.20b}$$

$$+ \frac{\mathrm{i}}{\hbar}\sum_{a,b}\Big[V_{ab12}\langle a_a^\dagger a_b^\dagger a_3 a_4\rangle_\mathrm{c} - V_{43ab}\langle a_1^\dagger a_2^\dagger a_b a_a\rangle_\mathrm{c}\Big] \tag{III.B.20c}$$

$$+ \frac{\mathrm{i}}{\hbar}\sum_{a,b,c}\sum_{m,h}\Big[(\delta_{m,3}\delta_{h,4} - \delta_{m,4}\delta_{h,3}) \tag{III.B.20d}$$

$$\Big\{\Big(V_{ab1c}\langle a_a^\dagger a_b^\dagger a_c a_m\rangle_\mathrm{c} - V_{amcb}\langle a_a^\dagger a_1^\dagger a_b a_c\rangle_\mathrm{c}\Big)\langle a_2^\dagger a_h\rangle \tag{III.B.20e}$$

$$+ \Big(V_{ab2c}\langle a_a^\dagger a_b^\dagger a_c a_h\rangle_\mathrm{c} - V_{habc}\langle a_a^\dagger a_2^\dagger a_b a_c\rangle_\mathrm{c}\Big)\langle a_1^\dagger a_m\rangle\Big\}\Big] \tag{III.B.20f}$$

$$+ \frac{\mathrm{i}}{\hbar}\sum_{a,b,c}\sum_{m,h}\Big[V_{abmc}(\delta_{m,2}\delta_{h,1} - \delta_{m,1}\delta_{h,2})\langle a_h^\dagger a_a^\dagger a_b^\dagger a_c a_3 a_4\rangle_\mathrm{c} \tag{III.B.20g}$$

$$+ V_{macb}(\delta_{m,4}\delta_{h,3} - \delta_{m,3}\delta_{h,4})\langle a_1^\dagger a_2^\dagger a_a^\dagger a_h a_b a_c\rangle_\mathrm{c}\Big]\,, \tag{III.B.20h}$$

where for conciseness the abbreviation $W_{1234} = V_{1234} - V_{2134}$ has been introduced. The simplest approximation to Eq. (III.B.20) is obtained by keeping only Eq. (III.B.20a)-Eq. (III.B.20b) and neglecting all higher contributions. In this case, the equation of motion for the correction terms is given by

$$\frac{\mathrm{d}}{\mathrm{d}t}\langle a_1^\dagger a_2^\dagger a_3 a_4\rangle_\mathrm{c}|_{0,\mathrm{cc}} = \frac{\mathrm{i}}{\hbar}\Delta\epsilon_0\,\langle a_1^\dagger a_2^\dagger a_3 a_4\rangle_\mathrm{c} + Q(t) \tag{III.B.21}$$

with the abbreviations

$$\Delta\epsilon_0 = \epsilon_1 + \epsilon_2 - \epsilon_3 - \epsilon_4\,, \tag{III.B.22}$$

$$Q(t) = \frac{\mathrm{i}}{\hbar}\sum_{a,b,c}\Bigg[\langle a_1^\dagger a_c\rangle\langle a_2^\dagger a_b\rangle\Big\{W_{4abc}\delta_{a,3} + \langle a_a^\dagger a_4\rangle W_{3abc} + \langle a_a^\dagger a_3\rangle W_{4acb}\Big\}$$
$$+ \langle a_a^\dagger a_4\rangle\langle a_b^\dagger a_3\rangle\Big\{W_{abc2}\delta_{c,1} + \langle a_2^\dagger a_c\rangle W_{ba1c} + \langle a_1^\dagger a_c\rangle W_{4ab2c}\Big\}\Bigg]\,. \tag{III.B.23}$$

With the intent to solve Eq. (III.B.21), we make a slight excursion and concentrate for a short while on the differential equation

$$\frac{\mathrm{d}}{\mathrm{d}t}S(t) = aB(t)S(t) + Q(t)\,, \tag{III.B.24}$$

where $S(t), B(T)$ and $Q(t)$ are complex valued functions depending explicitly on time. Formally integrating[1] Eq. (III.B.24) yields

$$\int_{t_0}^{t} dt_1 S(t_1) = \int_{t_0}^{t} dt_1 aB(t_1)S(t_1) + \int_{t_0}^{t} dt_1 Q(t_1) \tag{III.B.25a}$$

$$\Leftrightarrow S(t) - S(t_0) = a\int_{t_0}^{t} dt_1 B(t_1)S(t_1) + \int_{t_0}^{t} dt_1 Q(t_1) \tag{III.B.25b}$$

[1] We here use this lengthy derivation in order to underline the analogy to the calculations in Appendix APP C.

If we iterate Eq. (III.B.25b) twice, we obtain[2]

$$\begin{aligned} S(t) = & \left[1 + a\int_{t_0}^{t} dt_1 B(t_1) + a^2 \int_{t_0}^{t} dt_1 \int_{t_0}^{t_1} dt_2 B(t_1)B(t_2)\right] S(t_0) \\ & + \int_{t_0}^{t} dt_1 Q(t_1) + a\int_{t_0}^{t} dt_1 \int_{t_0}^{t_1} dt_2 B(t_1)Q(t_2) \\ & + a^2 \int_{t_0}^{t} dt_1 \int_{t_0}^{t_1} dt_2 \int_{t_0}^{t_2} dt_3 B(t_1)B(t_2)Q(t_3) \\ & + a^3 \int_{t_0}^{t} dt_1 \int_{t_0}^{t_1} dt_2 \int_{t_0}^{t_2} dt_3 B(t_1)B(t_2)B(t_3)S(t_3) \\ = & \left[1 + a\int_{t_0}^{t} dt_1 B(t_1) + \frac{1}{2}a^2 \iint_{t_0}^{t} dt_1 dt_2 B(t_1)B(t_2)\right] S(t_0) \\ & + \int_{t_0}^{t} dt_1 Q(t_1)\left[1 + a\int_{t_1}^{t} dt_2 B(t_2) + \frac{a^2}{2}\iint_{t_1}^{t} dt_2 dt_3 B(t_2)B(t_3)\right] \\ & + a^3 \int_{t_0}^{t} dt_1 \int_{t_0}^{t_1} dt_2 \int_{t_0}^{t_2} dt_3 B(t_1)B(t_2)B(t_3)S(t_3)\,. \end{aligned} \tag{III.B.29}$$

Keeping on reinserting Eq. (III.B.25b), we find the solution for Eq. (III.B.24) to be of the form

$$S(t) = \sum_{n=0}^{\infty} A^{(n)}(t)S(t_0) + \int_{t_0}^{t} dt_1 Q(t_1) \sum_{n=0}^{\infty} D^{(n)}(t)\,, \tag{III.B.30}$$

$$A^{(n)}(t) = \frac{a^n}{n!}\int_{t_0}^{t} .. \int_{t_0}^{t} dt_1 .. dt_n B(t_1) .. B(t_n)\,, \tag{III.B.31}$$

$$D^{(n)}(t) = \frac{a^n}{n!}\int_{t_1}^{t} .. \int_{t_1}^{t} dt_2 .. dt_n B(t_2) .. B(t_n) \tag{III.B.32}$$

which is equivalent to

$$S(t) = \mathrm{e}^{a\int_{t_0}^{t} dt_1 B(t_1)} S(t_0) + \int_{t_0}^{t} dt_1 Q(t_1) \mathrm{e}^{a\int_{t_1}^{t} dt_2 B(t_2)}\,. \tag{III.B.33}$$

With $t_0 \to -\infty$ and $\langle a_1^\dagger a_2^\dagger a_3 a_4\rangle_{\mathrm{c}}(-\infty) = 0$, we can use the obtained result to obtain the solution to Eq. (III.B.21):

$$\begin{aligned} \langle a_1^\dagger a_2^\dagger a_3 a_4\rangle_{\mathrm{c}}(t) &= \int_{-\infty}^{t} dt_1\, Q(t_1) \mathrm{e}^{\frac{\mathrm{i}}{\hbar}(t-t_1)\Delta\epsilon_0} \\ &= -\int_{\infty}^{0} ds\, Q(t-s)\mathrm{e}^{\frac{\mathrm{i}}{\hbar}\Delta\epsilon_0\, s} = \hbar\int_{0}^{\infty} ds'\, Q(t-\hbar s')\mathrm{e}^{\mathrm{i}\,\Delta\epsilon_0\, s'}\,. \end{aligned} \tag{III.B.34}$$

[2] In the last step of the iteration we used the following transformations

$$\int_{t_0}^{t} dt_1 \int_{t_0}^{t_1} dt_2 B(t_1)B(t_2) = \frac{a^2}{2}\iint_{t_0}^{t} dt_1 dt_2 B(t_1)B(t_2)\,, \tag{III.B.26}$$

$$\int_{t_0}^{t} dt_1 \int_{t_0}^{t_1} dt_2 B(t_1)Q(t_2) = \frac{a^2}{2}\int_{t_0}^{t}\int_{t_1}^{t} dt_1 dt_2 B(t_1)B(t_2)\,, \tag{III.B.27}$$

$$\int_{t_0}^{t} dt_1 \int_{t_0}^{t_1} dt_2 \int_{t_0}^{t_2} dt_3 B(t_1)B(t_2)Q(t_3) = \frac{a^2}{2}\int_{t_0}^{t} dt_1 Q(t_1) \iint_{t_1}^{t} dt_2 dt_3 B(t_2)B(t_3) \tag{III.B.28}$$

This shows that the correction term at time t depends on the past history, on the evolution of the system from $-\infty$ to t. This time dependence is the so-called Coulombic memory effect [CK99].

c) Memory effect and Markov approximation

Quantum mechanically, the wave functions of the carriers are smeared out so that there is always some overlap of wave functions and as a result the carriers retain some memory of the collisions they have experienced through the correlations with other particles in the system [KB89]. The memory of past behavior is greatly influenced by damping processes as damping destroys the memory. Within the scope of this work, we assume that the remaining memory is not very long and can be neglected, i.e., we make the Markov approximation [CK99, HK94, Kuh98][3]: $\langle a_i^\dagger a_k^\dagger\rangle(t-\hbar s') \approx \langle a_i^\dagger a_k^\dagger\rangle(t)\mathrm{e}^{-\mathrm{i}\,(\epsilon_i-\epsilon_k)s'}$. This yields

$$\begin{aligned}
\langle a_1^\dagger a_2^\dagger a_3 a_4\rangle_c(t) \quad &= \mathrm{i}\sum_{a,b,c}\int_0^\infty ds'\,\Bigg[\langle a_1^\dagger a_c\rangle(t)\langle a_2^\dagger a_b\rangle(t)\mathrm{e}^{-\mathrm{i}\,(\epsilon_1-\epsilon_c+\epsilon_2-\epsilon_b)s'}\Bigg\{W_{4abc}\delta_{a,3}\\
&\quad + \langle a_a^\dagger a_4\rangle(t)\mathrm{e}^{-\mathrm{i}\,(\epsilon_a-\epsilon_4)s'}W_{3abc} + \langle a_a^\dagger a_3\rangle(t)\mathrm{e}^{-\mathrm{i}\,(\epsilon_a-\epsilon_3)s'}W_{4acb}\Bigg\}\\
&\quad + \langle a_a^\dagger a_4\rangle(t)\langle a_b^\dagger a_3\rangle(t)\mathrm{e}^{-\mathrm{i}\,(\epsilon_a-\epsilon_4+\epsilon_b-\epsilon_3)s'}\Bigg\{W_{abc2}\delta_{c,1} + \langle a_2^\dagger a_c\rangle(t)\\
&\quad \mathrm{e}^{-\mathrm{i}\,(\epsilon_2-\epsilon_c)s'}W_{ba1c} + \langle a_1^\dagger a_c\rangle(t)\mathrm{e}^{-\mathrm{i}\,(\epsilon_1-\epsilon_c)s'}W_{ab2c}\Bigg\}\Bigg]\mathrm{e}^{\mathrm{i}\,(\epsilon_1+\epsilon_2-\epsilon_3-\epsilon_4)s'}\\
&= -\sum_{a,b,c}\Bigg[\langle a_1^\dagger a_c\rangle\langle a_2^\dagger a_b\rangle\Bigg\{\zeta(\epsilon_c+\epsilon_b-\epsilon_3-\epsilon_4)W_{4abc}\delta_{a,3}\\
&\quad + \langle a_a^\dagger a_4\rangle\zeta(\epsilon_c+\epsilon_b-\epsilon_a-\epsilon_3)W_{3abc} + \langle a_a^\dagger a_3\rangle\zeta(\epsilon_c+\epsilon_b-\epsilon_a-\epsilon_4)W_{4acb}\Bigg\}\\
&\quad + \langle a_a^\dagger a_4\rangle\langle a_b^\dagger a_3\rangle\Bigg\{\zeta(\epsilon_1+\epsilon_2-\epsilon_a-\epsilon_b)W_{abc2}\delta_{c,1} + \langle a_2^\dagger a_c\rangle\\
&\quad \zeta(\epsilon_1+\epsilon_c-\epsilon_a-\epsilon_b)W_{ba1c} + \langle a_1^\dagger a_c\rangle\zeta(\epsilon_c+\epsilon_2-\epsilon_a-\epsilon_b)W_{ab2c}\Bigg\}\Bigg]\,.
\end{aligned} \tag{III.B.35}$$

In the last step we have used the definition of the Heitler Zeta function [Hei84] given on page 69:

$$\zeta(x) = -\mathrm{i}\int_0^\infty ds\,\mathrm{e}^{\mathrm{i}\,as} = PV\left(\frac{1}{x}\right) - \mathrm{i}\,\pi\delta(x)\,, \tag{III.B.36}$$

[3] For an inclusion of Non-Markovian effects in the description of carrier-carrier scattering in the case of quantum wires see [Pre98].

where PV denotes the principal value and $\delta(x)$ the Dirac δ-function. Inserting the result in Eq. (III.B.11) we obtain the carrier-carrier correlation contributions

$$\begin{aligned}\frac{\mathrm{d}}{\mathrm{d}t}\langle a_k^\dagger a_l\rangle|_{\mathrm{corr,cc}} = \quad & \frac{\mathrm{i}}{\hbar}\sum_{\substack{a,b,c\\u,v,w}}\Big[V_{labc}\Big(\langle a_u^\dagger a_b\rangle\langle a_v^\dagger a_c\rangle - \langle a_v^\dagger a_b\rangle\langle a_u^\dagger a_c\rangle\Big)\Big\{\langle a_k^\dagger a_w\rangle V_{uvaw}\,\zeta_{wauv}\\ & + V_{uvka}\,\zeta_{wauv}\delta_{w,k} - \langle a_a^\dagger a_w\rangle V_{uvkw}\,\zeta_{kwuv}\Big\}\\ & + V_{abkc}\Big(\langle a_v^\dagger a_l\rangle\langle a_u^\dagger a_c\rangle - \langle a_u^\dagger a_l\rangle\langle a_v^\dagger a_c\rangle\Big)\Big\{\langle a_a^\dagger a_w\rangle V_{uvbw}\,\zeta_{wbuv}\\ & + V_{uvab}\,\zeta_{wbuv}\delta_{w,a} - \langle a_b^\dagger a_w\rangle V_{uvaw}\,\zeta_{awuv}\Big\}\\ & + V_{abkc}\Big(\langle a_a^\dagger a_w\rangle\langle a_b^\dagger a_v\rangle - \langle a_a^\dagger a_v\rangle\langle a_b^\dagger a_w\rangle\Big)\Big\{-\langle a_u^\dagger a_c\rangle V_{luwv}\,\zeta_{wvul}\\ & + V_{lcwv}\,\zeta_{wvcu}\delta_{u,l} - \langle a_u^\dagger a_l\rangle V_{cuvw}\,\zeta_{wvuc}\Big\}\\ & + V_{labc}\Big(\langle a_a^\dagger a_v\rangle\langle a_k^\dagger a_w\rangle - \langle a_a^\dagger a_w\rangle\langle a_k^\dagger a_v\rangle\Big)\Big\{\langle a_u^\dagger a_c\rangle V_{buwv}\,\zeta_{wvub}\\ & + V_{bcvw}\,\zeta_{wvcu}\delta_{u,b} - \langle a_u^\dagger a_b\rangle V_{cuvw}\,\zeta_{wvuc}\Big\}\Big]\,. \end{aligned} \tag{III.B.37}$$

For convenience, $\zeta(\epsilon_1+\epsilon_2+\epsilon_3-\epsilon_4)$ is abbreviated by ζ_{1234}. Inserting the definition of the ζ-function, we see that the correlation contributions derived above, account for dephasing effects (δ-function part) and renormalizations of the mean-field effects (principal value part). Next orders could be obtained by deriving an equation of motion for the correction terms $\langle a_1^\dagger a_2^\dagger a_3^\dagger a_4 a_5 a_6\rangle_{\mathrm{c}}$. Again carrier-carrier interaction would couple the correction terms to even higher contributions, at this point eight-operator expectation values. However, with increasing order the contributions are expected to become less important and are thus neglected in this work.

d) Screening

The derived scattering rates diverge for a bare Coulomb potential due to the long-range nature of the potential [Kuh98]. Usually this divergence is removed by replacing the unscreened Coulomb potential with a screened one. The question of the appropriate screening model is still controversial in the literature. For further details on appropriate screening models see for example [LG99, LG00] or recently [AK04, WAK03]. As we will also see in Chapter III.C.4.c, in the projector operator formalism the correlation contributions are in the simplest approximation screened via the Lindhard screening.

4. Carrier-Phonon Hamiltonian

The contribution due to carrier-phonon interaction, cf. Appendix APP E.4,

$$\begin{aligned}\frac{\mathrm{d}}{\mathrm{d}t}\langle a_{k,\mathbf{k}_k}^\dagger a_{l,\mathbf{k}_l}\rangle|_{\mathrm{cp}} = \quad & \frac{\mathrm{i}}{\hbar}\sum_{a,\underline{\mathbf{q}}}\Big\{g_{\underline{\mathbf{q}}}^{a,k}\langle a_{a,\mathbf{k}_k+\underline{\mathbf{q}}_{||}}^\dagger b_{\underline{\mathbf{q}}} a_{l,\mathbf{k}_l}\rangle - g_{\underline{\mathbf{q}}}^{l,a}\langle a_{k,\mathbf{k}_k}^\dagger b_{\underline{\mathbf{q}}} a_{a,\mathbf{k}_l-\underline{\mathbf{q}}_{||}}\rangle\\ & + g_{\underline{\mathbf{q}}}^{*k,a}\langle a_{a,\mathbf{k}_k-\underline{\mathbf{q}}_{||}}^\dagger b_{\underline{\mathbf{q}}}^\dagger a_{l,\mathbf{k}_l}\rangle - g_{\underline{\mathbf{q}}}^{*a,l}\langle a_{k,\mathbf{k}_k}^\dagger b_{\underline{\mathbf{q}}}^\dagger a_{a,\mathbf{k}_l+\underline{\mathbf{q}}_{||}}\rangle\Big\}\end{aligned} \tag{III.B.38}$$

couples the expectation values of two electron operators to expectation values of two electrons and a phonon, the latter often referred to as phonon assisted density matrix elements. These phonon

assisted density matrices in turn couple to higher elements and thus we are again facing a hierarchy problem. Similar to the treatment of the carrier-carrier interaction, we factorize the occurring matrix elements into elements of lower order and decompose the equation of motion in mean-field and correlation contributions

$$\frac{\mathrm{d}}{\mathrm{d}t}\langle a^\dagger_{k,\mathbf{k}_k} a_{l,\mathbf{k}_l}\rangle|_{\mathrm{cp}} = \frac{\mathrm{d}}{\mathrm{d}t}\langle a^\dagger_{k,\mathbf{k}_k} a_{l,\mathbf{k}_l}\rangle|_{\mathrm{MF,cp}} + \frac{\mathrm{d}}{\mathrm{d}t}\langle a^\dagger_{k,\mathbf{k}_k} a_{l,\mathbf{k}_l}\rangle|_{\mathrm{corr,cp}} \tag{III.B.39}$$

with

$$\begin{aligned}\frac{\mathrm{d}}{\mathrm{d}t}\langle a^\dagger_{k,\mathbf{k}_k} a_{l,\mathbf{k}_l}\rangle|_{\mathrm{MF,cp}} = \frac{\mathrm{i}}{\hbar}\sum_{a,\underline{\mathbf{q}}}\Big\{ & g^{a,k}_{\underline{\mathbf{q}}}\langle a^\dagger_{a,\mathbf{k}_k+\underline{\mathbf{q}}_{||}} b_{\underline{\mathbf{q}}} a_{l,\mathbf{k}_l}\rangle_{\mathrm{f}} - g^{l,a}_{\underline{\mathbf{q}}}\langle a^\dagger_{k,\mathbf{k}_k} b_{\underline{\mathbf{q}}} a_{a,\mathbf{k}_l-\underline{\mathbf{q}}_{||}}\rangle_{\mathrm{f}} \\ & + g^{*k,a}_{\underline{\mathbf{q}}}\langle a^\dagger_{a,\mathbf{k}_k-\underline{\mathbf{q}}_{||}} b^\dagger_{\underline{\mathbf{q}}} a_{l,\mathbf{k}_l}\rangle_{\mathrm{f}} - g^{*a,l}_{\underline{\mathbf{q}}}\langle a^\dagger_{k,\mathbf{k}_k} b^\dagger_{\underline{\mathbf{q}}} a_{a,\mathbf{k}_l+\underline{\mathbf{q}}_{||}}\rangle_{\mathrm{f}}\Big\}\end{aligned} \tag{III.B.40}$$

$$\begin{aligned}\frac{\mathrm{d}}{\mathrm{d}t}\langle a^\dagger_{k,\mathbf{k}_k} a_{l,\mathbf{k}_l}\rangle|_{\mathrm{corr,cp}} = \frac{\mathrm{i}}{\hbar}\sum_{a,\underline{\mathbf{q}}}\Big\{ & g^{a,k}_{\underline{\mathbf{q}}}\langle a^\dagger_{a,\mathbf{k}_k+\underline{\mathbf{q}}_{||}} b_{\underline{\mathbf{q}}} a_{l,\mathbf{k}_l}\rangle_{\mathrm{c}} - g^{l,a}_{\underline{\mathbf{q}}}\langle a^\dagger_{k,\mathbf{k}_k} b_{\underline{\mathbf{q}}} a_{a,\mathbf{k}_l-\underline{\mathbf{q}}_{||}}\rangle_{\mathrm{c}} \\ & + g^{*k,a}_{\underline{\mathbf{q}}}\langle a^\dagger_{a,\mathbf{k}_k-\underline{\mathbf{q}}_{||}} b^\dagger_{\underline{\mathbf{q}}} a_{l,\mathbf{k}_l}\rangle_{\mathrm{c}} - g^{*a,l}_{\underline{\mathbf{q}}}\langle a^\dagger_{k,\mathbf{k}_k} b^\dagger_{\underline{\mathbf{q}}} a_{a,\mathbf{k}_l+\underline{\mathbf{q}}_{||}}\rangle_{\mathrm{c}}\Big\}.\end{aligned} \tag{III.B.41}$$

and

$$\langle a^\dagger_{k,\mathbf{k}_k} b_{\underline{\mathbf{q}}} a_{a,\mathbf{k}_l-\underline{\mathbf{q}}_{||}}\rangle_{\mathrm{f}} = \langle a^\dagger_{k,\mathbf{k}_k} a_{a,\mathbf{k}_l-\underline{\mathbf{q}}_{||}}\rangle\langle b_{\underline{\mathbf{q}}}\rangle\,. \tag{III.B.42}$$

a) Carrier-Phonon Mean Field Contributions (1st Order)

Approximating the phonon assisted density matrix elements by the factorized part only, the 1st order in the hierarchy is obtained

$$\begin{aligned}\frac{\mathrm{d}}{\mathrm{d}t}\langle a^\dagger_{k,\mathbf{k}_k} a_{l,\mathbf{k}_l}\rangle|_{\mathrm{MF,cp}} = \frac{\mathrm{i}}{\hbar}\sum_{a,\underline{\mathbf{q}}}\Big\{ & g^{a,k}_{\underline{\mathbf{q}}}\langle a^\dagger_{a,\mathbf{k}_k+\underline{\mathbf{q}}_{||}} a_{l,\mathbf{k}_l}\rangle\langle b_{\underline{\mathbf{q}}}\rangle - g^{l,a}_{\underline{\mathbf{q}}}\langle a^\dagger_{k,\mathbf{k}_k} a_{a,\mathbf{k}_l-\underline{\mathbf{q}}_{||}}\rangle\langle b_{\underline{\mathbf{q}}}\rangle \\ & + g^{*k,a}_{\underline{\mathbf{q}}}\langle a^\dagger_{a,\mathbf{k}_k-\underline{\mathbf{q}}_{||}} a_{l,\mathbf{k}_l}\rangle\langle b^\dagger_{\underline{\mathbf{q}}}\rangle - g^{*a,l}_{\underline{\mathbf{q}}}\langle a^\dagger_{k,\mathbf{k}_k} a_{a,\mathbf{k}_l+\underline{\mathbf{q}}_{||}}\rangle\langle b^\dagger_{\underline{\mathbf{q}}}\rangle\Big\}\end{aligned} \tag{III.B.43}$$

In the bath approximation, where the phonon system acts as a thermal reservoir for the dynamical electronic system, no coherent phonons are created. Thus $\langle b_{\underline{\mathbf{q}}}\rangle = 0$ and the lowest order of the correlation expansion vanishes in this case.

b) Carrier-Phonon Correlation Contributions (2nd Order)

Analog the lines of III.B.3.b, we derive an equation of motion for the correction terms where we again focus on the dominant contributions, i.e., we neglect the influence of transverse field and Coulomb interaction on the phonon assisted density matrices

$$\frac{\mathrm{d}}{\mathrm{d}t}\langle a^\dagger_a b_{\underline{\mathbf{q}}} a_b\rangle_{\mathrm{c}} \approx \frac{\mathrm{i}}{\hbar}\langle[H_0+H_{\mathrm{cp}}, a^\dagger_a b_{\underline{\mathbf{q}}} a_b]\rangle - \frac{\mathrm{i}}{\hbar}\langle[H_0+H_{\mathrm{cp}}, a^\dagger_b a_b]\rangle\langle b_{\underline{\mathbf{q}}}\rangle - \frac{\mathrm{i}}{\hbar}\langle a^\dagger_b a_b\rangle\langle[H_0+H_{\mathrm{cp}}, b_{\underline{\mathbf{q}}}]\rangle\,. \tag{III.B.44}$$

With the results given in Chapter APP E, we obtain

$$\frac{\mathrm{d}}{\mathrm{d}t}\langle a^\dagger_a b_{\underline{\mathbf{q}}} a_b\rangle_{\mathrm{c}}|_0 = \frac{\mathrm{i}}{\hbar}(\epsilon_a - \epsilon_b - \hbar\omega_{L0})\langle a^\dagger_a b_{\underline{\mathbf{q}}} a_b\rangle_{\mathrm{c}} \tag{III.B.45}$$

and

$$\begin{aligned}\frac{\mathrm{d}}{\mathrm{d}t}\langle a_a^\dagger b_{\underline{\mathbf{q}}} a_b\rangle_{\mathrm{c}}|_{\mathrm{cp}} = \quad & \frac{\mathrm{i}}{\hbar}\sum_{f,\underline{\mathbf{q}}'}\Big(g_{\underline{\mathbf{q}}'}^{f,a}\langle a_{f,\mathbf{k}_a+\underline{\mathbf{q}}'_{||}}^\dagger a_b b_{\underline{\mathbf{q}}'} b_{\underline{\mathbf{q}}}\rangle - g_{\underline{\mathbf{q}}'}^{b,f}\langle a_a^\dagger a_{f,\mathbf{k}_b-\underline{\mathbf{q}}'_{||}} b_{\underline{\mathbf{q}}'} b_{\underline{\mathbf{q}}}\rangle \\ & + g_{\underline{\mathbf{q}}'}^{*af}\langle a_{f,\mathbf{k}_a-\underline{\mathbf{q}}'_{||}}^\dagger a_b b_{\underline{\mathbf{q}}'}^\dagger b_{\underline{\mathbf{q}}}\rangle - g_{\underline{\mathbf{q}}'}^{*fb}\langle a_a^\dagger a_{f,\mathbf{k}_b+\underline{\mathbf{q}}'_{||}} b_{\underline{\mathbf{q}}'}^\dagger b_{\underline{\mathbf{q}}}\rangle \\ & + \Big\{g_{\underline{\mathbf{q}}'}^{b,j}\langle a_a^\dagger a_{j,\mathbf{k}_b-\underline{\mathbf{q}}'_{||}}\rangle - g_{\underline{\mathbf{q}}'}^{j,a}\langle a_{j,\mathbf{k}_a+\underline{\mathbf{q}}'_{||}}^\dagger a_b\rangle\Big\}\langle b_{\underline{\mathbf{q}}'}\rangle\langle b_{\underline{\mathbf{q}}}\rangle \\ & + \Big\{g_{\underline{\mathbf{q}}'}^{*j,b}\langle a_a^\dagger a_{j,\mathbf{k}_b+\underline{\mathbf{q}}'_{||}}\rangle - g_{\underline{\mathbf{q}}'}^{*a,j}\langle a_{j,\mathbf{k}_a-\underline{\mathbf{q}}'_{||}}^\dagger a_b\rangle\Big\}\langle b_{\underline{\mathbf{q}}'}^\dagger\rangle\langle b_{\underline{\mathbf{q}}}\rangle\Big) \\ & - \frac{\mathrm{i}}{\hbar}\sum_{j,f,\mathbf{k}_j}\Big(g_{\underline{\mathbf{q}}}^{*jf}\langle a_a^\dagger a_b a_{f,\mathbf{k}_j-\underline{\mathbf{q}}_{||}}^\dagger a_{j,\mathbf{k}_j}\rangle - \langle a_a^\dagger a_b\rangle\langle a_{f,\mathbf{k}_j-\underline{\mathbf{q}}_{||}}^\dagger a_{j,\mathbf{k}_j}\rangle\Big)\,. \end{aligned} \tag{III.B.46}$$

The expectation values of two electron and two phonon operators are decomposed according to

$$\langle a_1^\dagger a_2 b_{\underline{\mathbf{q}}}^\dagger b_{\underline{\mathbf{q}}}\rangle = \langle a_1^\dagger a_2 b_{\underline{\mathbf{q}}}^\dagger b_{\underline{\mathbf{q}}}\rangle_{\mathrm{f}} + \langle a_1^\dagger a_2 b_{\underline{\mathbf{q}}}^\dagger b_{\underline{\mathbf{q}}}\rangle_{\mathrm{c}} \tag{III.B.47}$$

$$\langle a_1^\dagger a_2 b_{\underline{\mathbf{q}}}^\dagger b_{\underline{\mathbf{q}}}\rangle_{\mathrm{f}} = \langle a_1^\dagger a_2\rangle\langle b_{\underline{\mathbf{q}}}^\dagger b_{\underline{\mathbf{q}}}\rangle + \langle a_1^\dagger a_2\rangle\langle b_{\underline{\mathbf{q}}}^\dagger\rangle\langle b_{\underline{\mathbf{q}}}\rangle + \langle a_1^\dagger a_2 b_{\underline{\mathbf{q}}}^\dagger\rangle\langle b_{\underline{\mathbf{q}}}\rangle + \langle a_1^\dagger a_2 b_{\underline{\mathbf{q}}}\rangle\langle b_{\underline{\mathbf{q}}}^\dagger\rangle \tag{III.B.48}$$

which yields in bath approximation

$$\frac{\mathrm{d}}{\mathrm{d}t}\langle a_a^\dagger b_{\underline{\mathbf{q}}} a_b\rangle_{\mathrm{c}}|_{\mathrm{cp}} = \quad \frac{\mathrm{i}}{\hbar}\sum_{j,\underline{\mathbf{q}}'}\Big(g_{\underline{\mathbf{q}}'}^{*aj}\langle a_{j,\mathbf{k}_a-\underline{\mathbf{q}}'_{||}}^\dagger a_b\rangle\langle b_{\underline{\mathbf{q}}'}^\dagger b_{\underline{\mathbf{q}}}\rangle - g_{\underline{\mathbf{q}}'}^{*jb}\langle a_a^\dagger a_{j,\mathbf{k}_b+\underline{\mathbf{q}}'_{||}}\rangle\langle b_{\underline{\mathbf{q}}'}^\dagger b_{\underline{\mathbf{q}}}\rangle\Big) \tag{III.B.49a}$$

$$+ \frac{\mathrm{i}}{\hbar}\sum_{j,f,\mathbf{k}_j} g_{\underline{\mathbf{q}}}^{*jf}\langle a_a^\dagger a_{j,\mathbf{k}_j}\rangle\langle a_{f,\mathbf{k}_j-\underline{\mathbf{q}}_{||}}^\dagger a_b\rangle - \frac{\mathrm{i}}{\hbar}\sum_j g_{\underline{\mathbf{q}}}^{*jb}\langle a_a^\dagger a_{j,\mathbf{k}_b+\underline{\mathbf{q}}_{||}}\rangle \tag{III.B.49b}$$

$$+ \sum_{j,\underline{\mathbf{q}}'}\Big(g_{\underline{\mathbf{q}}'}^{j,a}\langle a_{j,\mathbf{k}_a+\underline{\mathbf{q}}'_{||}}^\dagger a_b b_{\underline{\mathbf{q}}'} b_{\underline{\mathbf{q}}}\rangle_{\mathrm{c}} - g_{\underline{\mathbf{q}}'}^{b,j}\langle a_a^\dagger a_{j,\mathbf{k}_b-\underline{\mathbf{q}}'_{||}} b_{\underline{\mathbf{q}}'} b_{\underline{\mathbf{q}}}\rangle_{\mathrm{c}} \tag{III.B.49c}$$

$$+ g_{\underline{\mathbf{q}}'}^{*aj}\langle a_{j,\mathbf{k}_a-\underline{\mathbf{q}}'_{||}}^\dagger a_b b_{\underline{\mathbf{q}}'}^\dagger b_{\underline{\mathbf{q}}}\rangle_{\mathrm{c}} - g_{\underline{\mathbf{q}}'}^{*jb}\langle a_a^\dagger a_{j,\mathbf{k}_b+\underline{\mathbf{q}}'_{||}} b_{\underline{\mathbf{q}}'}^\dagger b_{\underline{\mathbf{q}}}\rangle_{\mathrm{c}}\Big) \tag{III.B.49d}$$

$$- \sum_{j,f,\mathbf{k}_j} g_{\underline{\mathbf{q}}}^{*jf}\langle a_a^\dagger a_{f,\mathbf{k}_j-\underline{\mathbf{q}}_{||}}^\dagger a_b a_{j,\mathbf{k}_j}\rangle_{\mathrm{c}}\,. \tag{III.B.49e}$$

Similar to section III.B.3.b, we proceed in the simplest approximation. We consider only Eq. (III.B.49a)-Eq. (III.B.49b) of Eq. (III.B.49). Therewith the equation of motion for the correction terms is given by

$$\frac{\mathrm{d}}{\mathrm{d}t}\langle a_a^\dagger b_{\underline{\mathbf{q}}} a_b\rangle_{\mathrm{c}}|_{0,\mathrm{cp}} = \frac{\mathrm{i}}{\hbar}\Delta\epsilon_0\,\langle a_a^\dagger b_{\underline{\mathbf{q}}} a_b\rangle_{\mathrm{c}} + Q(t) \tag{III.B.50}$$

with the abbreviations

$$\Delta\epsilon_0 = \epsilon_a - \epsilon_b - \hbar\omega_{L0}\,, \tag{III.B.51}$$

$$\begin{aligned} Q(t) = \quad & \frac{\mathrm{i}}{\hbar}\sum_{j,\underline{\mathbf{q}}'}\Big(g_{\underline{\mathbf{q}}'}^{*aj}\langle a_{j,\mathbf{k}_a-\underline{\mathbf{q}}'_{||}}^\dagger a_b\rangle\langle b_{\underline{\mathbf{q}}'}^\dagger b_{\underline{\mathbf{q}}}\rangle - g_{\underline{\mathbf{q}}'}^{*jb}\langle a_a^\dagger a_{j,\mathbf{k}_b+\underline{\mathbf{q}}'_{||}}\rangle\langle b_{\underline{\mathbf{q}}'}^\dagger b_{\underline{\mathbf{q}}}\rangle\Big) \\ & + \frac{\mathrm{i}}{\hbar}\sum_{j,f,\mathbf{k}_j} g_{\underline{\mathbf{q}}}^{*jf}\langle a_a^\dagger a_{j,\mathbf{k}_j}\rangle\langle a_{f,\mathbf{k}_j-\underline{\mathbf{q}}_{||}}^\dagger a_b\rangle - \frac{\mathrm{i}}{\hbar}\sum_j g_{\underline{\mathbf{q}}}^{*jb}\langle a_a^\dagger a_{j,\mathbf{k}_b+\underline{\mathbf{q}}_{||}}\rangle\,. \end{aligned} \tag{III.B.52}$$

Analog the lines of sec. III.B.3.b we obtain

$$\langle a_a^\dagger b_{\underline{\mathbf{q}}} a_b\rangle_{\mathrm{c}}(t) = \int_0^\infty ds\, Q(t-s)\mathrm{e}^{\frac{\mathrm{i}}{\hbar}\Delta\epsilon_0\, s}\,. \tag{III.B.53}$$

In Markov approximation this can be cast into

$$\begin{aligned}\langle a_a^\dagger b_{\underline{\mathbf{q}}} a_b\rangle_{\mathrm{c}}(t) = -\sum_{j,\underline{\mathbf{q}}'}\Big(& g_{\underline{\mathbf{q}}'}^{*aj}\langle a_{j,\mathbf{k}_a-\underline{\mathbf{q}}'_{||}}^\dagger a_b\rangle\langle b_{\underline{\mathbf{q}}'}^\dagger b_{\underline{\mathbf{q}}}\rangle\zeta(\epsilon_{a,\mathbf{k}_a}-\epsilon_{j,\mathbf{k}_a-\underline{\mathbf{q}}_{||}}-\hbar\omega_{L0}) \\ & - g_{\underline{\mathbf{q}}'}^{*jb}\langle a_a^\dagger a_{j,\mathbf{k}_b+\underline{\mathbf{q}}'_{||}}\rangle(\langle b_{\underline{\mathbf{q}}'}^\dagger b_{\underline{\mathbf{q}}}\rangle+\delta_{\mathbf{q},\mathbf{q}'})\zeta(\epsilon_{j,\mathbf{k}_b+\underline{\mathbf{q}}_{||}}-\epsilon_{b,\mathbf{k}_b}-\hbar\omega_{L0})\Big) \\ & - \sum_{j,f,\mathbf{k}_j} g_{\underline{\mathbf{q}}}^{*jf}\langle a_a^\dagger a_{j,\mathbf{k}_j}\rangle\langle a_{f,\mathbf{k}_j-\underline{\mathbf{q}}_{||}}^\dagger a_b\rangle\zeta(\epsilon_{j,\mathbf{k}_j}-\epsilon_{f,\mathbf{k}_j-\underline{\mathbf{q}}_{||}}-\hbar\omega_{L0})\,.\end{aligned} \tag{III.B.54}$$

Inserting the obtained result in Eq. (III.B.41), the second order in the hierarchy is obtained. Again, the principal value part is associated with renormalizations of the energies while the δ-part describes scattering and dephasing processes [Kuh98].

C. Schrödinger Picture: The Projector-Operator Theory

Next, the equations of motions shall be derived in the Schrödinger picture, using projector-operator theory. Although, the Heisenberg picture is somewhat easier to handle, the Schrödinger picture has the advantage that some of the approximations connected with the treatment of the hierarchy problem come along more self-evidently.

Before applying the projector-operator formalism to the description of intersubband transitions in a multiple quantum well system, a short review of the underlying theory shall be given. A more detailed introduction into the projector-operator theory can be found in [FS90, BKP01].

1. The Density Operator

In a many particle system, only the expectation values of a certain set of observables $\{O\}$, the so-called observation level, are of interest. The observation level $\{O\}$, is typically not a complete system in the space of observables. Therefore, the knowledge of the true density operator $\sigma(t)$ of the system contains more information than necessary and it is possible to decompose the density operator with respect to the observables of interest, $O_\mu \in \{O\}$, into a relevant part, $\sigma_{\mathrm{rel}}(t)$, and an irrelevant part, $\sigma_{\mathrm{irr}}(t)$, with the properties:

$$\sigma(t) = \sigma_{\mathrm{rel}}(t) + \sigma_{\mathrm{irr}}(t)\,, \quad \mathrm{tr}(O_\mu\sigma(t)) = \mathrm{tr}(O_\mu\sigma_{\mathrm{rel}}(t))\,, \quad \mathrm{tr}(O_\mu\sigma_{\mathrm{irr}}(t)) = 0\,. \tag{III.C.1}$$

When t_0 is the switch-on time of the interaction, we assume in the following a Hartree-Fock ground-state, i.e.,

$$\sigma(t_0) = \sigma_{\mathrm{rel}}(t_0)\,. \tag{III.C.2}$$

Thus, the initial states under consideration, $\sigma(t_0)$ shall have no irrelevant part. The relevant part, $\sigma_{\mathrm{rel}}(t)$, is a mapping of the density operator $\sigma(t)$, i.e., $\sigma(t)$ and $\sigma_{\mathrm{rel}}(t)$ are related by a functional f:

$$\sigma_{\mathrm{rel}}(t) = f[\sigma(t)]\,. \tag{III.C.3}$$

For a differential variation of $\sigma_{\rm rel}(t)$, the variation of $f[\sigma(t)]$ defines an idempotent superoperator $\mathcal{P}[\sigma(t)]$ in Liouville space

$$\mathrm{d}\sigma_{\rm rel}(t) = \mathrm{d}\, f[\sigma(t)] = \mathcal{P}[\sigma(t)]\, \mathrm{d}\sigma(t) = \mathcal{P}[\sigma_{\rm rel}(t)]\, \mathrm{d}\sigma(t)\,, \tag{III.C.4}$$

where we claimed $\mathcal{P}[\sigma(t)] = \mathcal{P}[\sigma_{\rm rel}(t)]$.

a) Super-Operators and Liouville Space

As a super-operator we define the mapping of an operator F onto another operator G where the operators F, G are elements of the Hilbert space of quantum mechanical operators known as Liouville space. In the following, we denote super-operators with calligraphic letters, for expample $\mathcal{P}, \mathcal{L}, \mathcal{Q}$, in order to avoid confusion with general operators. For convenience, the suffix "super-" will dropped wherever possible. The unity super-operator is denoted by $\mathcal{I}$. If there exists a super-operator inverse to a given super-operator $\mathcal{A}$ it shall be denoted by $\mathcal{A}^{-1}$:

$$\mathcal{A}\mathcal{A}^{-1} = \mathcal{A}^{-1}\mathcal{A} = \mathcal{I}\,. \tag{III.C.5}$$

The most important super-operator is probably the so-called Liouville operator $\mathcal{L}(t)$, mediating the mapping of an element G of the Liouville space via the commutation $(1/\hbar)[H(t), G]$. Using the cyclic property of the trace we find the important rule

$$\begin{aligned} \mathrm{tr}(G \cdot \mathcal{L}F) = &\quad \mathrm{tr}(GHF - GFH) = \mathrm{tr}(GHF - HGF) = -\mathrm{tr}([H,G]F) \\ &= -\mathrm{tr}(\mathcal{L}G \cdot F)\,. \end{aligned} \tag{III.C.6}$$

Here the point indicates where the action of the Liouville operator ends. Another important relationship for the Liouville operator is

$$\mathrm{e}^{c\mathcal{L}}F = \mathrm{e}^{\frac{c}{\hbar}H} F \mathrm{e}^{-\frac{c}{\hbar}H} \tag{III.C.7}$$

which shows, that the superoperator $\mathrm{e}^{c\mathcal{L}}$ denotes the transformation of an operator F due to the linear operator $\mathrm{e}^{\frac{c}{\hbar}H}$[FS90].

2. The Relevant Part of the Density Operator

As we have stated before, the knowledge of the relevant part of the density operator, $\sigma_{\rm rel}$, is sufficient for the calculation of the expectation values $\langle O_\mu \rangle$ with $O_\mu \in \{O\}$. To derive an equation of motion for $\sigma_{\rm rel}(t)$ we start with the von Neumann-equation (Liouville equation) for the full density operator:

$$\frac{\mathrm{d}}{\mathrm{d}t}\sigma(t) = -\mathrm{i}\,\mathcal{L}(t)\,\sigma(t)\,. \tag{III.C.8}$$

In the following, the Hamiltonian $H(t)$ is assumed to be a many particle Hamiltonian including time-dependent external fields. Using Eq. (III.C.4) and Eq. (III.C.8) the time derivative of $\sigma_{\rm rel}(t)$ reads

$$\frac{\mathrm{d}}{\mathrm{d}t}\sigma_{\rm rel}(t) = \mathcal{P}[\sigma_{\rm rel}(t)]\frac{\mathrm{d}}{\mathrm{d}t}\sigma(t) = -\mathrm{i}\,\mathcal{P}[\sigma_{\rm rel}(t)]\mathcal{L}(t)\sigma(t) = -\mathrm{i}\,\mathcal{P}[\sigma_{\rm rel}(t)]\mathcal{L}(t)\big(\sigma_{\rm rel}(t) + \sigma_{\rm irr}(t)\big)\,. \tag{III.C.9}$$

In order to get a closed equation of motion for $\sigma_{\rm rel}(t)$ the irrelevant part of the density operator $\sigma_{\rm irr}$ in Eq. (III.C.9) is now related to $\sigma_{\rm rel}$. For this purpose, we introduce the superoperator $\mathcal{Q}[\sigma_{\rm rel}(t)]$:

$$\mathcal{Q}[\sigma_{\rm rel}(t)] + \mathcal{P}[\sigma_{\rm rel}(t)] = \mathcal{I}\,, \tag{III.C.10}$$

which we then use to decompose the Liouville operator $\mathcal{L}$ in relevant and irrelevant part, $\mathcal{L}(t) = \mathcal{L}_\mathcal{P}(t) + \mathcal{L}_\mathcal{Q}(t)$:

$$\mathcal{L}_{\rm rel}(t) := \mathcal{L}_\mathcal{P}(t) = \mathcal{P}[\sigma_{\rm rel}(t)]\,\mathcal{L}(t), \quad \mathcal{L}_{\rm irr}(t) := \mathcal{L}_\mathcal{Q}(t) = \mathcal{Q}[\sigma_{\rm rel}(t)]\,\mathcal{L}(t)\,. \tag{III.C.11}$$

Applying the operator identity

$$\mathcal{U}(t,t_0) = \mathcal{U}_\mathcal{Q}(t,t_0) - \mathrm{i}\int_{t_0}^{t} \mathrm{d}t'\,\mathcal{U}_\mathcal{Q}(t,t')\,\mathcal{L}_\mathcal{P}(t')\,\mathcal{U}(t',t_0)\,, \tag{III.C.12}$$

where $\mathcal{U}$ and $\mathcal{U}_\mathcal{Q} = \mathcal{Q}\mathcal{U}$ denote the time evolution operator for $\mathcal{L}$ and $\mathcal{L}_\mathcal{Q}$ (for details see Appendix APP C) and Eq. (III.C.9), the density operator can be written as:

$$\begin{aligned}\sigma(t) &= \mathcal{U}(t,t_0)\,\sigma(t_0) \\ &= \mathcal{U}_\mathcal{Q}(t,t_0)\,\sigma(t_0) + \int_{t_0}^{t}\mathrm{d}t'\,\mathcal{U}_\mathcal{Q}(t,t')\;\frac{d}{dt'}\sigma_{\rm rel}(t')\,.\end{aligned} \tag{III.C.13}$$

An integration by parts[1]

$$\begin{aligned}\sigma(t) &= \mathcal{U}_\mathcal{Q}(t,t_0)\,\sigma(t_0) + \sigma_{\rm rel}(t) - \mathcal{U}_\mathcal{Q}(t,t_0)\,\sigma_{\rm rel}(t_0) - \mathrm{i}\int_{t_0}^{t}\mathrm{d}t'\,\mathcal{U}_\mathcal{Q}(t,t')\mathcal{Q}[\sigma_{\rm rel}(t')]\,\mathcal{L}(t')\,\sigma_{\rm rel}(t') \\ &= \sigma_{\rm rel}(t) - \mathrm{i}\int_{t_0}^{t}\mathrm{d}t'\,\mathcal{U}_\mathcal{Q}(t,t')\mathcal{Q}[\sigma_{\rm rel}(t')]\,\mathcal{L}(t')\,\sigma_{\rm rel}(t')\end{aligned} \tag{III.C.14}$$

and comparison with Eq. (III.C.1) leads to the desired connection between irrelevant and relevant part of the density operator:

$$\sigma_{\rm irr}(t) = -\mathrm{i}\int_{t_0}^{t}\mathrm{d}t'\,\mathcal{U}_\mathcal{Q}(t,t')\mathcal{Q}[\sigma_{\rm rel}(t')]\,\mathcal{L}(t')\,\sigma_{\rm rel}(t')\,. \tag{III.C.15}$$

Inserting Eq. (III.C.15) into Eq. (III.C.9) one finally obtains a closed equation of motion for $\sigma_{\rm rel}$:

$$\begin{aligned}\frac{\mathrm{d}}{\mathrm{d}t}\sigma_{\rm rel}(t) &= -\mathrm{i}\,\mathcal{L}_\mathcal{P}(t)\sigma(t) = -\mathrm{i}\,\mathcal{L}_\mathcal{P}(t)(\sigma_{\rm rel}(t) + \sigma_{\rm irr}(t)) \\ &= -\mathrm{i}\,\mathcal{L}_\mathcal{P}(t)\sigma_{\rm rel}(t) - \mathcal{L}_\mathcal{P}(t)\int_{t_0}^{t}\mathrm{d}t'\;\mathcal{U}_\mathcal{Q}(t,t')\,\mathcal{L}_\mathcal{Q}(t')\sigma_{\rm rel}(t')\,.\end{aligned} \tag{III.C.16}$$

The expectation values of the observables of interest $O_n \in \{O\}$ can be calculated by using Eq. (III.C.1):

$$\begin{aligned}\frac{\mathrm{d}}{\mathrm{d}t}\langle O_n\rangle &= \frac{\mathrm{d}}{\mathrm{d}t}\mathrm{tr}(O_n\,\sigma(t)) = \frac{\mathrm{d}}{\mathrm{d}t}\mathrm{tr}(O_n\,\sigma_{\rm rel}(t)) \\ &= -\mathrm{i}\;\mathrm{tr}\big(O_n\,\mathcal{L}_\mathcal{P}(t)\sigma_{\rm rel}(t)\big) - \mathrm{tr}\big(O_n\,\mathcal{L}_\mathcal{P}(t)\;\underbrace{\int_{t_0}^{t}\mathrm{d}t'\,\mathcal{U}_\mathcal{Q}(t,t')\,\mathcal{L}_\mathcal{Q}(t')\sigma_{\rm rel}(t')}_{\mathrm{i}\,\sigma_{\rm irr}(t)}\big)\end{aligned} \tag{III.C.17}$$

$$= \frac{\mathrm{d}}{\mathrm{d}t}\langle O_n\rangle|_{\rm MF} + \frac{\mathrm{d}}{\mathrm{d}t}\langle O_n\rangle_{\rm corr}\,. \tag{III.C.18}$$

Equation Eq. (III.C.17) shows, that even though $\langle O_n\rangle = \mathrm{tr}(O_n\sigma_{\rm rel})$ depends only on the relevant part of the density operator, the equation of motion for $\langle O_n\rangle$ depends on both the relevant and the

[1] Here Eq. (III.C.2) and the following two properties of the time evolution operator have been used:

$$\frac{\partial}{\partial t'}\mathcal{U}_\mathcal{Q}(t,t') = \mathrm{i}\;\mathcal{U}_\mathcal{Q}(t,t')\;\mathcal{Q}[\sigma_{\rm rel}(t')]\;\mathcal{L}(t')\,, \quad \mathcal{U}_\mathcal{Q}(t,t) = 1$$

irrelevant part of the density matrix (although the latter can be expressed in terms of $\sigma_{\rm rel}$) and both relevant and irrelevant part have to be known in order to determine the time development of the expectation values. In anticipation of future results, the part dependent on $\sigma_{\rm rel}$ will be referred to as mean-field part $\frac{\rm d}{{\rm d}t}\langle O_n\rangle|_{\rm MF}$, the part dependent on $\sigma_{\rm irr}$ as correlation part $\frac{\rm d}{{\rm d}t}\langle O_n\rangle|_{\rm corr}$.

In order to use Eq. (III.C.17), the relevant density matrix operator has to be determined. As known from non-equilibrium statistical physics, the generalized canonical density operator

$$\sigma_{\rm can}(t) = \frac{{\rm e}^{-\sum_n \lambda_n(t) O_n}}{{\rm tr}({\rm e}^{-\sum_n \lambda_n(t) O_n})} \tag{III.C.19}$$

is the density operator which has the maximum uncertainty measure within a fixed set of observables. As can be found in textbooks [FS90], the mapping $\sigma(t)$ onto $\sigma_{\rm can}(t)$ has the required properties for the relevant density matrix operator Eq. (III.C.1). Thus, in the following we choose $\sigma_{\rm rel} = \sigma_{\rm can}$. Note that the expression for the canonical density operator does not imply a restriction to equilibrium processes, the full time dependence is included in the Lagrange parameters λ_n.

It can be shown that $\mathcal{P}$ is the Kawasaki-Gunton operator [FS90]

$$\mathcal{P}[\sigma_{\rm rel}(t)]Y = \left(\sigma_{\rm rel}(t) - \sum_{\nu=1}^{n} \frac{\partial\sigma_{\rm rel}(t)}{\partial\langle O_\nu\rangle(t)}\langle O_\nu\rangle(t)\right){\rm tr}(Y) + \sum_{\nu=1}^{n}\frac{\partial\sigma_{\rm rel}(t)}{\partial\langle O_\nu\rangle(t)}{\rm tr}(O_\nu Y)\,. \tag{III.C.20}$$

With this knowledge we can derive the useful identity

$${\rm tr}(O_\mu \mathcal{L}_{\mathcal{P}}\sigma_{\rm rel}) = {\rm tr}(O_\mu \mathcal{L}\sigma_{\rm rel}) \tag{III.C.21}$$

for an element O_μ of the observation level $\{O\}$:

$$\begin{aligned}
{\rm tr}(O_\mu \mathcal{P}\mathcal{L}\sigma_{\rm rel}) = \quad & \Big\{{\rm tr}(O_\mu\sigma_{\rm rel}(t)) - {\rm tr}\Big(O_\mu\sum_{\nu=1}^{n}\frac{\partial\sigma_{\rm rel}(t)}{\partial\langle O_\nu\rangle(t)}\Big)\langle O_\nu\rangle(t)\Big\}{\rm tr}(\mathcal{L}\sigma_{\rm rel}) \\
& + {\rm tr}\Big(O_\mu\sum_{\nu=1}^{n}\frac{\partial\sigma_{\rm rel}(t)}{\partial\langle O_\nu\rangle(t)}\Big){\rm tr}(O_\nu\mathcal{L}\sigma_{\rm rel}) \\
= \quad & \Big\{\langle O_\mu\rangle(t) - \sum_{\nu=1}^{n}\delta_{\mu\nu}\langle O_\nu\rangle(t)\Big\}{\rm tr}(\mathcal{L}\sigma_{\rm rel}) + \sum_{\nu=1}^{n}\delta_{\mu\nu}{\rm tr}(O_\nu\mathcal{L}\sigma_{\rm rel}) \\
= \quad & {\rm tr}(O_\mu\mathcal{L}\sigma_{\rm rel})\,,
\end{aligned} \tag{III.C.22}$$

where we have used

$${\rm tr}\Big(O_\mu\sum_{\nu=1}^{n}\frac{\partial\sigma_{\rm rel}(t)}{\partial\langle O_\nu\rangle(t)}\Big) = \sum_{\nu=1}^{n}\frac{\partial}{\partial\langle O_\nu\rangle(t)}{\rm tr}\Big(O_\mu\sigma_{\rm rel}(t)\Big) = \sum_{\nu=1}^{n}\frac{\partial\langle O_\mu\rangle(t)}{\partial\langle O_\nu\rangle(t)} = \sum_{\nu=1}^{n}\delta_{\mu\nu}\,. \tag{III.C.23}$$

Using Eq. (III.C.21), we rewrite the mean-field contributions:

$$\frac{\rm d}{{\rm d}t}\langle O_n\rangle|_{\rm MF} = -{\rm i}\ {\rm tr}\big(O_\mu\,\mathcal{P}(t)\mathcal{L}(t)\sigma_{\rm rel}(t)\big) \tag{III.C.24}$$

$$= -{\rm i}\ {\rm tr}\Big(O_\mu\mathcal{L}(t)\sigma_{\rm rel}(t)\Big)\,. \tag{III.C.25}$$

3. The Irrelevant Part of the Density Operator

As can be seen in Eq. (III.C.17), the equation of motion for the expectation value $\langle O_\mu\rangle$, with $O_\mu \in \{O\}$, depends not only on the relevant part but also on the irrelevant part of the density

operator

$$\frac{\mathrm{d}}{\mathrm{d}t}\langle O_\mu\rangle|_{\mathrm{corr}} = -\mathrm{i}\ \mathrm{tr}\big(O_\mu\ \mathcal{L}_{\mathcal{P}}(t)\sigma_{\mathrm{irr}}(t)\big) = -\mathrm{tr}\big(O_\mu\ \mathcal{L}_{\mathcal{P}}(t)\ \int_{t_0}^{t}\mathrm{d}t'\,\mathcal{U}_{\mathcal{Q}}(t,t')\ \mathcal{L}_{\mathcal{Q}}(t')\sigma_{\mathrm{rel}}(t')\big)\ . \tag{III.C.26}$$

In order to simplify the calculation of Eq. (III.C.26), we insert the Kawasaki-Gunton operator:

$$\begin{aligned}\frac{\mathrm{d}}{\mathrm{d}t}\langle O_n\rangle|_{\mathrm{corr}} &= -\mathrm{i}\ \mathrm{tr}\big(O_\mu\ \mathcal{P}(t)\mathcal{L}(t)\sigma_{\mathrm{irr}}(t)\big) \qquad\qquad (\text{III.C.27})\\ &= -\mathrm{i}\ \Big\{\langle O_\mu\rangle(t) - \sum_{\nu=1}^{n}\delta_{\mu\nu}\langle O_\nu\rangle(t)\Big\}\mathrm{tr}\Big(\mathcal{L}(t)\sigma_{\mathrm{irr}}(t)\Big) + \sum_{\nu=1}^{n}\delta_{\mu\nu}\mathrm{tr}\Big(O_\nu\mathcal{L}(t)\sigma_{\mathrm{irr}}(t)\Big)\\ &= -\mathrm{i}\ \mathrm{tr}\Big(O_\mu\mathcal{L}(t)\sigma_{\mathrm{irr}}(t)\Big)\ .\end{aligned}$$

Furthermore, we rewrite the irrelevant density operator,Eq. (III.C.15), using time ordering and anti-ordering operators (cf. Appendix APP C:Eq. (APP C.9) and Eq. (APP C.18))

$$\begin{aligned}\sigma_{\mathrm{irr}}(t) &= -\mathrm{i}\int_{t_0}^{t}\mathrm{d}t'\,\mathcal{U}_{\mathcal{Q}}(t,t')\ \mathcal{L}_{\mathcal{Q}}(t')\ \sigma_{\mathrm{rel}}(t')\\ &= -\mathrm{i}\int_{t_0}^{t}\mathrm{d}t'\,\mathcal{T}_{+}\mathrm{e}^{-\mathrm{i}\int_{t'}^{t}\mathrm{d}t''\mathcal{L}_{\mathcal{Q}}(t'')}\mathcal{L}_{\mathcal{Q}}(t')\,\mathcal{T}_{-}\mathrm{e}^{\mathrm{i}\int_{t'}^{t}\mathrm{d}t''\mathcal{L}_{\mathcal{P}}(t'')}(\sigma_{\mathrm{rel}}(t)+\sigma_{\mathrm{irr}}(t))\ . \qquad (\text{III.C.28})\end{aligned}$$

Next, we consider the case $t_0 \to -\infty$ and introduce the superoperator $\mathcal{X}(t)$

$$\mathcal{X}(t) = -\mathrm{i}\int_{-\infty}^{t}\mathrm{d}t'\mathcal{T}_{+}\mathrm{e}^{-\mathrm{i}\int_{t'}^{t}\mathrm{d}t''\mathcal{L}_{\mathcal{Q}}(t'')}\mathcal{L}_{\mathcal{Q}}(t')\,\mathcal{T}_{-}\mathrm{e}^{\mathrm{i}\int_{t'}^{t}\mathrm{d}t''\mathcal{L}_{\mathcal{P}}(t'')}\ , \tag{III.C.29}$$

which yields

$$\sigma_{\mathrm{irr}}(t) = (\mathcal{I}-\mathcal{X}(t))^{-1}\mathcal{X}(t)\sigma_{\mathrm{rel}}(t)\ . \tag{III.C.30}$$

Often, this expression for the irrelevant part of the density operator is a good starting point for approximation schemes to many particle correlations.

4. Equations of Motion for Quantum Well Excitations

In Chapter III.C.2 we have seen, that the expectation values of certain observables O_n, elements of a specific observation level $\{O\}$, depend only on the corresponding relevant part of the density operator whereas the equation of motion depends also on the irrelevant part suggesting a decomposition in mean-field and correlation contributions:

$$\begin{aligned}\frac{\mathrm{d}}{\mathrm{d}t}\langle O_n\rangle(t) &= \frac{\mathrm{d}}{\mathrm{d}t}\mathrm{tr}(O_n\,\sigma(t)) = \frac{\mathrm{d}}{\mathrm{d}t}\mathrm{tr}(O_n\,\sigma_{\mathrm{rel}}(t))\\ &= \frac{\mathrm{d}}{\mathrm{d}t}\langle O_n\rangle(t)|_{\mathrm{MF}} + \frac{\mathrm{d}}{\mathrm{d}t}\langle O_n\rangle(t)|_{\mathrm{corr}} \qquad (\text{III.C.31a})\end{aligned}$$

with

$$\frac{\mathrm{d}}{\mathrm{d}t}\langle O_n\rangle(t)|_{\mathrm{MF}} = -\mathrm{i}\ \mathrm{tr}\big(O_n\ \mathcal{L}(t)\sigma_{\mathrm{rel}}(t)\big) \tag{III.C.31b}$$

$$\begin{aligned}\frac{\mathrm{d}}{\mathrm{d}t}\langle O_n\rangle(t)|_{\mathrm{corr}} &= -\mathrm{i}\ \mathrm{tr}\big(O_n\ \mathcal{L}(t)\sigma_{\mathrm{irr}}(t)\big)\\ &= -\mathrm{tr}\big(O_n\ \mathcal{L}(t)\ \int_{t_0}^{t}\mathrm{d}t'\,\mathcal{U}_{\mathcal{Q}}(t,t')\ \mathcal{L}_{\mathcal{Q}}(t')\sigma_{\mathrm{rel}}(t')\big)\ . \qquad (\text{III.C.31c})\end{aligned}$$

We now want to apply this knowledge to the description of quantum well excitations.

a) Observation Level, Canonical Density Operator, Initial Conditions

In Section III.C.2, we have already chosen $\sigma_{\rm rel} = \sigma_{\rm can}$ with

$$\sigma_{\rm can}(t) = \frac{\mathrm{e}^{-\sum_n \lambda_n(t) O_n}}{\mathrm{tr}\big(\mathrm{e}^{-\sum_n \lambda_n(t) O_n}\big)} \,, \tag{III.C.32}$$

but did not specify the level of observation any further. As we have seen, in our case the quantities of interest as polarization or population all depend on expectation values of the form $\langle a_k^\dagger a_{k'} \rangle$, where indices k, k' are compound indices, which contain the subband number $n_k, n_{k'}$, 2D-wave number $\mathbf{k}_k, \mathbf{k}_{k'}$ in the free propagation direction (xy-plane), spin $\sigma_k, \sigma_{k'}$ and well number w, w'. For different indices, the expectation values yield coherences (for example $n_k \neq n_{k'}$: intersubband coherence), for equal indices, i.e. $k = k'$, they yield occupation numbers. Therefore, it seems reasonable to choose the observation level $\{O\} = \{a_k^\dagger a_{k'}\}$, since we are only interested in the expectation values of these operators. The corresponding canonical operator is thus given by

$$\sigma_{\rm can,e} = \frac{\mathrm{e}^{-\sum_{i,j} \lambda_{ij}(t) a_i^\dagger a_j}}{\mathrm{tr}\Big(\mathrm{e}^{-\sum_{i,j} \lambda_{i,j}(t) a_i^\dagger a_j}\Big)} \,. \tag{III.C.33}$$

This is a good starting point for the description of the dynamics of the electronic system Σ_e.

To incorporate the interaction of electronic system Σ_e and phonon system Σ_p, we assume in the following that Σ_p is not strongly influenced by the coupling to system Σ_e, i.e., the phonon system acts as a thermal reservoir (bath) described by the statistical operator

$$\sigma_{\rm can,p}(t) = \frac{\mathrm{e}^{-H_p/(k_B T)}}{\mathrm{tr}\big(\mathrm{e}^{-H_p/(k_B T)}\big)} \,. \tag{III.C.34}$$

This means, that the phonons are treated as a bath for the dynamical electronic system (phonon bath approximation) and the space of the whole system Σ is the product space of the two subspaces $\Sigma_{e,p}$ with the canonical operator

$$\sigma_{\rm rel}(t) = \sigma_{\rm can}(t) = \frac{\mathrm{e}^{-\sum_{i,j} \lambda_{ij}(t) a_i^\dagger a_j - \hbar/(k_B T) \sum_{\underline{\mathbf{q}}} \omega_{\underline{\mathbf{q}}} b_{\underline{\mathbf{q}}}^\dagger b_{\underline{\mathbf{q}}}}}{\mathrm{tr}\big(\mathrm{e}^{-\sum_{i,j} \lambda_{ij}(t) a_i^\dagger a_j - \hbar/(k_B T) \sum_{\underline{\mathbf{q}}} \omega_{\underline{\mathbf{q}}} b_{\underline{\mathbf{q}}}^\dagger b_{\underline{\mathbf{q}}}}\big)} \,. \tag{III.C.35}$$

With the chosen observation level, we can now calculate the expectation values of the observables $a_i^\dagger a_j$ by applying Eq. (III.C.31a):

$$\begin{aligned} \frac{\mathrm{d}}{\mathrm{d}t} \langle a_{w,k}^\dagger a_{w',k'} \rangle(t) = &-\mathrm{i}\ \mathrm{tr}\big(a_{w,k}^\dagger a_{w',k'}\ \mathcal{L}_{\mathcal{P}}(t) \sigma_{\rm rel}(t)\big) \\ &- \mathrm{tr}\big(a_{w,k}^\dagger a_{w',k'}\ \mathcal{L}_{\mathcal{P}}(t) \int_{t_0}^{t} \mathrm{d}t'\, \mathcal{U}_{\mathcal{Q}}(t,t')\, \mathcal{L}_{\mathcal{Q}}(t') \sigma_{\rm rel}(t')\big) \,. \end{aligned} \tag{III.C.36}$$

The equation can be decomposed into mean-field contributions (1st part) and correlation contributions (2nd part). For $n_k \neq n_l$, the temporal dynamics of field induced intersubband transitions, i.e. the destruction and creation of electrons in different subband, for $n_k = n_l$ the temporal dynamics of field induced intrasubband transitions are described. As initial conditions we assume that there exist no coherences at the switch-on time of the interaction:

$$\langle a_k^\dagger a_{k'} \rangle(t_0) = 0 \quad \text{if } k \neq k' \,. \tag{III.C.37}$$

If not otherwise stated, we will choose Fermi-Dirac quasi-equilibrium distributions as initial conditions for the occupation numbers $\langle a_k^\dagger a_k \rangle(t_0)$. The expectation values of the phonon number operators are given by the Bose-Einstein distribution.

In order to obtain a theory applicable to a range of different situations, we derive the equation of motion for the observable $\langle a_k^\dagger a_l \rangle$ and delay the assignation to special boundary conditions such as electronically uncoupled / coupled wells, weak / strong excitation, number of subbands etc ...

b) Mean-Field Contributions

On the basis of Eq. (III.C.31b), we obtain the equation of motion for the mean-field contributions in the form:

$$\begin{aligned}\frac{\mathrm{d}}{\mathrm{d}t}\langle a_k^\dagger a_l\rangle|_{\mathrm{MF}} &= \mathrm{i}\ \mathrm{tr}(\mathcal{L}(t)a_k^\dagger a_l\,\sigma_{\mathrm{rel}}(t)))\\ &= \frac{\mathrm{i}}{\hbar}\,\mathrm{tr}([H,a_k^\dagger a_l]\sigma_{\mathrm{rel}}(t)) \qquad \text{(III.C.38)}\\ &= \frac{\mathrm{i}}{\hbar}\,\mathrm{tr}([H_0+H_{\mathrm{cf}}+H_{\mathrm{cc}}+H_{\mathrm{cp}},a_k^\dagger a_l]\sigma_{\mathrm{rel}}(t))\,. \qquad \text{(III.C.39)}\end{aligned}$$

The evaluation of Eq. (III.C.38) is for conciseness performed for each Hamiltonian separately.

Free-Particle Hamiltonian and Carrier-Field Hamiltonian

Commutation with both free-particle Hamiltonian and carrier-field Hamiltonian yields elements which are again part of the specified observation level

$$[H_0+H_{\mathrm{cf}},O_\mu]\in\{O\} \qquad \text{with} \qquad \{O\}=\{a^\dagger_{w,k}a_{w',k'}\} \qquad \text{(III.C.40)}$$

and the corresponding equations are equivalent to their counterparts in the Heisenberg picture:

$$\begin{aligned}\frac{\mathrm{d}}{\mathrm{d}t}a_k^\dagger a_l\,|_{\mathrm{MF},0} &= \frac{\mathrm{i}}{\hbar}(\epsilon_k-\epsilon_l)a_k^\dagger a_l\ , \qquad \text{(III.C.41)}\\ \frac{\mathrm{d}}{\mathrm{d}t}\langle a_k^\dagger a_l\rangle|_{\mathrm{MF,cf}} &= \frac{\mathrm{d}}{\mathrm{d}t}\langle a_k^\dagger a_l\rangle|^{\mathrm{opt}}_{\mathrm{cf}}+\frac{\mathrm{d}}{\mathrm{d}t}\langle a_k^\dagger a_l\rangle|^{\mathrm{cur}}_{\mathrm{cf}}\ . \qquad \text{(III.C.42)}\end{aligned}$$

The optical and current contributions are given in Eq. (III.B.4) and Eq. (III.B.5).

Carrier-Carrier Hamiltonian

In contrast to free-carrier and carrier-field Hamiltonian, commutation with carrier-carrier Hamiltonian *does not* yield elements which are again part of the specified observation level

$$[H_{\mathrm{cc}},O_\mu]\notin\{O\} \qquad \text{(III.C.43)}$$

and thus the system of equations does not close:

$$\begin{aligned}\frac{\mathrm{d}}{\mathrm{d}t}\langle a_k^\dagger a_l\rangle|_{\mathrm{MF,cc}} = \ & \frac{\mathrm{i}}{\hbar}\sum_{a,b,c}\Big[V_{abkc}\,\mathrm{tr}\Big(a_a^\dagger a_b^\dagger a_c a_l\,\sigma_{\mathrm{rel}}(t)\Big)\\ & -V_{labc}\,\mathrm{tr}\Big(a_k^\dagger a_a^\dagger a_c a_b\sigma_{\mathrm{rel}}(t)\Big)\Big]\,. \qquad \text{(III.C.44)}\end{aligned}$$

Note, that we can here not replace $\mathrm{tr}(a_i^\dagger a_j^\dagger a_k a_l\,\sigma_{\mathrm{rel}}(t))$ *by* $\langle a_i^\dagger a_j^\dagger a_k a_l\rangle$ *since foursome operators do not lie in the chosen observation level* $\{O\}=\{a_k^\dagger a_{k'}\}$. Expectation values of the latter can be obtained according to

$$\langle O\rangle=\mathrm{tr}(O\sigma(t))=\mathrm{tr}(O\sigma_{\mathrm{rel}}(t)) \qquad \rightarrow\langle a_k^\dagger a_{k'}\rangle=\mathrm{tr}(a_k^\dagger a_{k'}\sigma(t))=\mathrm{tr}(a_k^\dagger a_{k'}\sigma_{\mathrm{rel}}(t)) \qquad \text{(III.C.45)}$$

due to

$$\mathrm{tr}(O\sigma_{\mathrm{irr}}(t))=0\,,$$

which does not hold for expectation values of operators beyond the observation level.

Mean-field Factorization

To simplify the calculation of $\mathrm{tr}(a_i^\dagger a_j^\dagger a_k a_l \sigma_{\mathrm{rel}}(t))$, we first diagonalize the electronic part of the relevant density operator given in Eq. (III.C.33). The matrix elements of the hermitian matrix λ with respect to a complete set of orthonormal functions, $\{\phi_n\}$, are given by $\lambda_{ij} = \langle\phi_i|\lambda|\phi_j\rangle$. Introducing a complete set of orthonormal functions,$\{\lambda_n\}$, with $\langle\lambda_n|\lambda|\lambda_m\rangle = \lambda_n\delta_{n,m}$ and matrix U with elements $U_{ni} = \langle\lambda_n|\phi_i\rangle$, we can rewrite λ according to

$$\lambda_{ij} = \sum_{n,m}\langle\phi_i|\lambda_n\rangle\langle\lambda_n|\lambda|\lambda_m\rangle\langle\lambda_m|\phi_j\rangle = \sum_n U_{ni}^*\lambda_n U_{nj}\,. \tag{III.C.46}$$

Therewith we obtain

$$\sigma_{\mathrm{rel,e}} = \frac{\mathrm{e}^{-\sum_n\lambda_n\sum_i U_{ni}^* a_i^\dagger\sum_j U_{nj}a_j}}{\mathrm{tr}\left(\mathrm{e}^{-\sum_n\lambda_n\sum_i U_{ni}^* a_i^\dagger\sum_j U_{nj}a_j}\right)} = \frac{\mathrm{e}^{-\sum_n\lambda_n d_n^\dagger d_n}}{\mathrm{tr}\left(\mathrm{e}^{-\sum_n\lambda_n d_n^\dagger d_n}\right)} \tag{III.C.47}$$

$$= \frac{\prod_n \mathrm{e}^{-\lambda_n\hat{n}_n}}{\sum_{\{n_\alpha\}}\langle\{n_\alpha\}|\prod_n \mathrm{e}^{-\lambda_n\hat{n}_n}|\{n_\alpha\}\rangle} = \prod_n\frac{\mathrm{e}^{-\lambda_n\hat{n}_n}}{1+\mathrm{e}^{-\lambda_n}} \tag{III.C.48}$$

where we first introduced new operators $d_i, d_i^\dagger$ with

$$d_i = \sum_j U_{ij}a_j\,,\quad (\rightarrow a_i = \sum_j U_{ji}^* d_j)\,,\quad d_i^\dagger = \sum_j U_{ij}^* a_j^\dagger\,,\quad (\rightarrow a_i^\dagger = \sum_j U_{ji} d_j^\dagger) \tag{III.C.49}$$

and for convenience then switched to number operators $\hat{n}_i = d_i^\dagger d_i$ with number states $|\{n_\alpha\}\rangle = |n_1,\ldots,n_\alpha,\ldots\rangle$ ($n_\alpha \in \{0,1\}$ due to the fermionic nature of electrons).

In order to determine $\mathrm{tr}(a_1^\dagger a_2^\dagger a_3 a_4\sigma_{\mathrm{rel,e}})$ we first insert the diagonalized electronic part of the relevant density operator and the new creation and annihilation operators:

$$\mathrm{tr}(a_1^\dagger a_2^\dagger a_3 a_4\sigma_{\mathrm{rel,e}}) = \sum_{\{n_\alpha\}}\sum_{a,b,c,d} U_{a1}U_{b2}U_{c3}^*U_{d4}^*\langle\{n_\alpha\}|d_a^\dagger d_b^\dagger d_c d_d\prod_n\frac{\mathrm{e}^{-\lambda_n\hat{n}_n}}{1+\mathrm{e}^{-\lambda_n}}|\{n_\alpha\}\rangle\,. \tag{III.C.50}$$

Having in mind

$$d_i^\dagger|N;..n_i..\rangle = (-1)^{N_i}\delta_{n_i,0}|N+1;..n_i+1..\rangle \tag{III.C.51}$$

$$d_i|N;..n_i..\rangle = (-1)^{N_i}\delta_{n_i,1}|N-1;..n_i-1..\rangle \tag{III.C.52}$$

$$\tag{III.C.53}$$

with $N_i = \sum_{j=1}^{i-1} n_j$, we can simply further

$$\begin{aligned}
\mathrm{tr}(a_1^\dagger a_2^\dagger a_3 a_4\sigma_{\mathrm{rel,e}}) = &\sum_{\{n_\alpha\}}\sum_{a,b} U_{a1}U_{b2}U_{a3}^*U_{b4}^*\langle\{n_\alpha\}|d_a^\dagger d_b^\dagger d_a d_b\prod_n\frac{\mathrm{e}^{-\lambda_n\hat{n}_n}}{1+\mathrm{e}^{-\lambda_n}}|\{n_\alpha\}\rangle\\
&+\sum_{\{n_\alpha\}}\sum_{a,b} U_{a1}U_{b2}U_{b3}^*U_{a4}^*\langle\{n_\alpha\}|d_a^\dagger d_b^\dagger d_b d_a\prod_n\frac{\mathrm{e}^{-\lambda_n\hat{n}_n}}{1+\mathrm{e}^{-\lambda_n}}|\{n_\alpha\}\rangle\\
=&-\sum_{\{n_\alpha\}}\sum_{a,b} U_{a1}U_{b2}U_{a3}^*U_{b4}^*\langle\{n_\alpha\}|n_a n_b\prod_n\frac{\mathrm{e}^{-\lambda_n\hat{n}_n}}{1+\mathrm{e}^{-\lambda_n}}|\{n_\alpha\}\rangle\\
&+\sum_{\{n_\alpha\}}\sum_{a,b} U_{a1}U_{b2}U_{b3}^*U_{a4}^*\langle\{n_\alpha\}|n_a n_b\prod_n\frac{\mathrm{e}^{-\lambda_n\hat{n}_n}}{1+\mathrm{e}^{-\lambda_n}}|\{n_\alpha\}\rangle\\
=&\sum_a\frac{U_{a1}U_{a4}^*}{1+\mathrm{e}^{\lambda_a}}\sum_b\frac{U_{b2}U_{b3}^*}{1+\mathrm{e}^{\lambda_b}} - \sum_a\frac{U_{a1}U_{a3}^*}{1+\mathrm{e}^{\lambda_a}}\sum_b\frac{U_{b2}U_{b4}^*}{1+\mathrm{e}^{\lambda_b}}\,.
\end{aligned} \tag{III.C.54}$$

For simplicity, we switched to number operators after using the commutator relations. A similar procedure yields

$$\mathrm{tr}(a_1^\dagger a_2 \sigma_{\mathrm{rel,e}}) = \sum_a \frac{U_{a1} U_{a2}^*}{1+\mathrm{e}^{\lambda_a}} \tag{III.C.55}$$

and therewith we obtain

$$\mathrm{tr}(a_1^\dagger a_2^\dagger a_3 a_4 \sigma_{\mathrm{rel,e}}) = \mathrm{tr}(a_1^\dagger a_4 \sigma_{\mathrm{rel,e}})\mathrm{tr}(a_2^\dagger a_3 \sigma_{\mathrm{rel,e}}) - \mathrm{tr}(a_1^\dagger a_3 \sigma_{\mathrm{rel,e}})\mathrm{tr}(a_2^\dagger a_4 \sigma_{\mathrm{rel,e}})\,. \tag{III.C.56}$$

Since the phonon part of the relevant density operator does - in the bath approximation - not change the number states of the whole system, $|\{n_\alpha\}\rangle|\{\tilde{n}_{\mathbf{Q}}\}\rangle$, we obtain

$$\mathrm{tr}(a_1^\dagger a_2^\dagger a_3 a_4 \sigma_{\mathrm{rel}}) = \langle a_1^\dagger a_4\rangle\langle a_2^\dagger a_3\rangle - \langle a_1^\dagger a_3\rangle\langle a_2^\dagger a_4\rangle \tag{III.C.57}$$

which is the so-called mean-field factorization for four-particle correlations. Note that in the same way the factorization of six-operator terms which has been used in Eq. (III.B.18) can be derived [cf. Chapter APP D].

Comparison with the Heisenberg picture Note that this is the same factorization we have used in Eq. (III.B.8) to factorize the occurring foursome operators. But whereas in Eq. (III.B.7), the foursome operator was split into factorized terms and correction/correlation contributions, the factorization of the four-particle correlations is exact here. This is due to the separation of the density operator in relevant and irrelevant part which yields the separation of mean-field and correlation contributions already on a earlier level. The division in Eq. (III.B.7) is thus the counterpart to

$$\langle a_1^\dagger a_2^\dagger a_3 a_4\rangle = \mathrm{tr}(a_1^\dagger a_2^\dagger a_3 a_4 \sigma) = \mathrm{tr}(a_1^\dagger a_2^\dagger a_3 a_4 \sigma_{\mathrm{rel}}) + \mathrm{tr}(a_1^\dagger a_2^\dagger a_3 a_4 \sigma_{\mathrm{irr}}) \tag{III.C.58}$$

Carrier-Phonon Hamiltonian

Commutation with the carrier-phonon Hamiltonian also yields elements which are not part of the specified observation level:

$$\begin{aligned}\frac{\mathrm{d}}{\mathrm{d}t}\langle a_{k,\mathbf{k}_k}^\dagger a_{l,\mathbf{k}_l}\rangle|_{\mathrm{MF,cp}} = \quad & \frac{\mathrm{i}}{\hbar}\sum_{a,\underline{\mathbf{q}}}\Big\{ g_{\underline{\mathbf{q}}}^{a,k}\mathrm{tr}\Big(a_{a,\mathbf{k}_k+\underline{\mathbf{q}}_{||}}^\dagger b_{\underline{\mathbf{q}}} a_{l,\mathbf{k}_l}\sigma_{\mathrm{rel}}(t)\Big) - g_{\underline{\mathbf{q}}}^{l,a}\mathrm{tr}\Big(a_{k,\mathbf{k}_k}^\dagger b_{\underline{\mathbf{q}}} a_{a,\mathbf{k}_l-\underline{\mathbf{q}}_{||}}\sigma_{\mathrm{rel}}(t)\Big) \\ & + g_{\underline{\mathbf{q}}}^{*k,a}\mathrm{tr}\Big(a_{a,\mathbf{k}_k-\underline{\mathbf{q}}_{||}}^\dagger b_{\underline{\mathbf{q}}}^\dagger a_{l,\mathbf{k}_l}\sigma_{\mathrm{rel}}(t)\Big) - g_{\underline{\mathbf{q}}}^{*a,l}\mathrm{tr}\Big(a_{k,\mathbf{k}_k}^\dagger b_{\underline{\mathbf{q}}}^\dagger a_{a,\mathbf{k}_l+\underline{\mathbf{q}}_{||}}\sigma_{\mathrm{rel}}(t)\Big)\Big\}\end{aligned} \tag{III.C.59}$$

and we have to deal with expectation values of the form $\mathrm{tr}(a_{a,\mathbf{k}+\underline{\mathbf{q}}'_{||}}^\dagger b_{\underline{\mathbf{q}}'} a_{b,\mathbf{k}}\sigma_{\mathrm{rel}})$. Using the diagonalized relevant density operator σ_{rel} for the full system we obtain

$$\begin{aligned}&\mathrm{tr}(a_a^\dagger b_{\underline{\mathbf{q}}_1} a_b \sigma_{\mathrm{rel}}) \\ &= \sum_{n_\alpha,\tilde{n}_{\underline{\mathbf{q}}}}\langle\{\tilde{n}_{\underline{\mathbf{q}}}\}|\langle\{n_\alpha\}|\sum_{i,j}U_{ia}U_{jb}^*\, d_i^\dagger d_j\, b_{\underline{\mathbf{q}}_1}\prod_n \frac{\mathrm{e}^{-\lambda_n\hat{n}_n - \sum_{\underline{\mathbf{q}}'}\hbar/(k_BT)\omega_{\underline{\mathbf{q}}'}\hat{n}_{\underline{\mathbf{q}}'}}}{(1+\mathrm{e}^{-\lambda_n})\mathrm{tr}(\mathrm{e}^{-\sum_{\underline{\mathbf{q}}'}\hbar/(k_BT)\omega_{\underline{\mathbf{q}}'}n_{\underline{\mathbf{q}}'}})}|\{n_\alpha\}\rangle|\{\tilde{n}_{\underline{\mathbf{q}}}\}\rangle \\ &= \sum_j \frac{U_{ja}U_{jb}^*}{1+\mathrm{e}^{\lambda_j}}\sum_{\tilde{n}_{\underline{\mathbf{q}}}}\langle\{\tilde{n}_{\underline{\mathbf{q}}}\}|b_{\underline{\mathbf{q}}_1}\frac{\mathrm{e}^{-\sum_{\underline{\mathbf{q}}'}\hbar/(k_BT)\omega_{\underline{\mathbf{q}}'}\hat{n}_{\underline{\mathbf{q}}'}}}{\mathrm{tr}(\mathrm{e}^{-\sum_{\underline{\mathbf{q}}'}\hbar/(k_BT)\omega_{\underline{\mathbf{q}}'}n_{\underline{\mathbf{q}}'}})}|\{\tilde{n}_{\underline{\mathbf{q}}}\}\rangle = \langle a_a^\dagger a_b\rangle\,\mathrm{tr}(b_{\underline{\mathbf{q}}_1}\sigma_{\mathrm{rel}}) \\ &= 0\,,\end{aligned} \tag{III.C.60}$$

and thus the electron-phonon mean-field contribution for the here considered phonon bath vanishes:

$$\frac{\mathrm{d}}{\mathrm{d}t}\langle a_{k,\mathbf{k}_k}^\dagger a_{l,\mathbf{k}_l}\rangle|_{\mathrm{MF,cp}} = 0\,. \tag{III.C.61}$$

This is consistent with the assumption that treating the phonons as a bath does not allow coherent phonon fields.

c) Correlation Contributions

Next, the correlation contributions, i.e., the part of the expectation value dependent on $\sigma_{\rm irr}$, have to be determined. As the complete derivation is very lengthy, only the most important steps are given below. The main purpose of this section is to illustrate that already with quite rigid approximations in the irrelevant part of the density operator, the correlation contributions can be derived in a form similar to the results obtained in the Heisenberg picture (the only difference is the self-consistently occurring Lindhard screening in the case of carrier-carrier scattering). The starting point of the derivation is given by

$$\begin{aligned}\frac{\mathrm{d}}{\mathrm{d}t}\langle a_k^\dagger a_l\rangle(t)|_{\rm corr} &= -\mathrm{i}\ \mathrm{tr}\big(a_k^\dagger a_l\ \mathcal{L}(t)\sigma_{\rm irr}(t)\big)\\ &= -\mathrm{tr}\big(a_k^\dagger a_l\ \mathcal{L}(t)\int_{t_0}^{t}\mathrm{d}t'\,\mathcal{U}_{\mathcal{Q}}(t,t')\,\mathcal{L}_{\mathcal{Q}}(t')\sigma_{\rm rel}(t')\big)\,. \end{aligned}\tag{III.C.62}$$

In Section III.C.4.b we have already seen, that only commutation with many-particle Hamiltonians, $H_{\rm cc}$ and $H_{\rm cp}$ yields elements which are not part of the specified observation level, i.e.,

$$[H_0+H_{\rm cf},O_\mu]\in\{O\},\qquad [H_{\rm cc}+H_{\rm cp},O_\mu]\notin\{O\}\tag{III.C.63}$$

with $\{O\}=\{a^\dagger_{w,k}a_{w',k'}\}$. Having in mind that elements of the observation level do yield only vanishing contributions to the expectation value with the irrelevant part, i.e., $\mathrm{tr}(O_\mu\sigma_{\rm irr}(t))=0$ [cf. Eq. (III.C.1)], we can thus restrict the Liouville operator $\mathcal{L}$ to the many particle Liouvillian $\mathcal{L}_{\rm mp}=\mathcal{L}_{\rm cc}+\mathcal{L}_{\rm cp}$. Assuming that the relevant and irrelevant Liouvillians depend only weakly on time (Markovian approximation), we approximate the integral kernels in Eq. (III.C.29) by:

$$\mathcal{T}_+\mathrm{e}^{-\mathrm{i}\int_{t'}^{t}\mathrm{d}t''\,\mathcal{L}_{\mathcal{Q}}(t'')}\approx\mathrm{e}^{-\mathrm{i}\,(t-t')\mathcal{L}_{\mathcal{Q}}}\,,\qquad \mathcal{T}_-\mathrm{e}^{\mathrm{i}\int_{t'}^{t}\mathrm{d}t''\,\mathcal{L}_{\mathcal{P}}(t'')}\approx\mathrm{e}^{\mathrm{i}\,(t-t')\mathcal{L}_{\mathcal{P}}}\tag{III.C.64}$$

and rewrite Eq. (III.C.29) by changing the integration variable:

$$\mathcal{X}=-\mathrm{i}\int_0^\infty\mathrm{d}s\,\mathrm{e}^{-\mathrm{i}\,\mathcal{L}_{\mathcal{Q}}s}\,\mathcal{L}_{\mathcal{Q}}\,\mathrm{e}^{\mathrm{i}\,\mathcal{L}_{\mathcal{P}}s}\,.\tag{III.C.65}$$

Since Eq. (III.C.65) contains an exponential of $\mathcal{L}_{\mathcal{Q}}$, we approximate $\mathcal{L}_{\mathcal{Q}}$ in the free-particle Liouvillian $\mathcal{L}_0$ and a correction $\mathcal{L}_C$ ($\mathcal{L}_{\mathcal{Q}}=\mathcal{L}_0+\mathcal{L}_{\rm MF}+\mathcal{L}_C\approx\mathcal{L}_0+\mathcal{L}_C$) and derive a perturbation series of the term $\mathrm{e}^{-\mathrm{i}\,\mathcal{L}_{\mathcal{Q}}s}$ with respect to $\mathcal{L}_0$ [Kno97], which is comparable to the approximation in Eq. (III.B.15). We rewrite Eq. (III.C.65)[2] by introducing the operator Ξ:

$$\mathcal{X}=-\mathrm{i}\int_0^\infty\mathrm{d}s\Xi(s)\mathcal{L}_{\mathcal{Q}}\mathrm{e}^{\mathrm{i}\,\mathcal{L}_0 s}\,,\tag{III.C.66}$$

$$\Xi(s)=(1+\int^s\mathrm{d}s'\mathrm{e}^{-\mathrm{i}\,(\mathcal{L}_0+\mathcal{Q}\mathcal{L}_{\mathcal{C}})s'}[-\mathrm{i}\,\mathcal{Q}\mathcal{L}_{\mathcal{C}}]\mathrm{e}^{\mathrm{i}\,\mathcal{L}_0 s'})\mathrm{e}^{-\mathrm{i}\,\mathcal{L}_0 s}\,,\tag{III.C.67}$$

$$\frac{\mathrm{d}}{\mathrm{d}s}(\Xi(s))=\mathcal{X}(s)[-\mathrm{i}\,\mathcal{Q}\mathcal{L}_{\mathcal{C}}]+\Xi(s)[-\mathrm{i}\,\mathcal{L}_0]\tag{III.C.68}$$

and use the Laplace-transformation $\tilde{\Xi}(z)=L(\Xi(s))$ for the operator $\mathcal{X}(s)$ to derive the homogeneous equation

$$\tilde{\mathcal{X}}(z)(z+\mathrm{i}\,\mathcal{L}_0)=\tilde{\Xi}(z)(-\mathrm{i}\,\mathcal{Q}\mathcal{L}_{\mathcal{C}})\,,\tag{III.C.69}$$

which can be solved by iteration (with $\Xi_0=1,\tilde{\Xi}_0=(z+\mathrm{i}\,\mathcal{L}_0)^{-1}$ as initial values):

$$\tilde{\mathcal{X}}(z)=(1-\mathcal{U}_0(z)[-\mathrm{i}\,\mathcal{Q}\mathcal{L}_{\mathcal{C}}])^{-1}\mathcal{U}_0(z),\quad \mathcal{U}_0(z)=(z+\mathrm{i}\,\mathcal{L}_0)^{-1}\,.\tag{III.C.70}$$

Therewith we rewrite $\mathcal{X}$:

$$\mathcal{X} = -\mathrm{i}\lim_{z\to 0}\int_0^\infty \mathrm{d}s\, \mathrm{e}^{-sz}\Xi(s)\mathrm{e}^{-\mathrm{i}\,\mathcal{L}_0 s}\mathcal{L}_\mathcal{Q}\mathrm{e}^{\mathrm{i}\,\mathcal{L}_0 s} \tag{III.C.71}$$

$$= -\mathrm{i}\lim_{z\to 0}(1-\mathcal{U}_1(z)[-\mathrm{i}\,\mathcal{Q}\mathcal{L}_\mathcal{C}])^{-1}\mathcal{U}_1(z)\mathcal{L}_\mathcal{Q}(2) \tag{III.C.72}$$

$$\mathcal{U}_1(z) = (z+\mathrm{i}\,\mathcal{L}_0(3)-\mathrm{i}\,\mathcal{L}_0(1))^{-1}\,. \tag{III.C.73}$$

Here the arguments in the operators denote the order of application to the right. Collecting all results, the electron-electron correlation part of the equations of motion can be cast into:

$$\frac{\mathrm{d}}{\mathrm{d}t}\langle a_k^\dagger a_l\rangle_{\mathrm{corr,cc}} = -\mathrm{tr}(\epsilon^{-1}\mathcal{L}_{\mathrm{MP}}a_k^{\dagger 1}a_k^2\epsilon^{-1}\mathcal{Q}\mathcal{L}_{\mathrm{MP}}(2)\zeta(\mathcal{L}_0(1)-\mathcal{L}_0(3))\sigma_{\mathrm{rel}}) \tag{III.C.74}$$

$$= -\mathrm{tr}(\epsilon^{-1}\sum_{abc}(V_{ab1c}a_a^\dagger a_b^\dagger a_c a_2 - V_{2abc}a_1^\dagger a_a^\dagger a_c a_b)\times \tag{III.C.75}$$

$$\times\,\epsilon^{-1}\mathcal{Q}\mathcal{L}_{\mathrm{MP}}(2)\zeta(\mathcal{L}_0(3)-\mathcal{L}_0(1))\sigma_{\mathrm{rel}}) \tag{III.C.76}$$

where we ζ denotes again the Heitler's zeta-function [Hei84] and the super-operator ϵ is given by

$$\epsilon = 1+\mathcal{L}_\mathcal{Q}(\mathcal{L}_0(3)-\mathcal{L}_0(1))^{-1}\,. \tag{III.C.77}$$

Equation Eq. (III.C.74) shows that the cc-correlations have to be calculated with many particle Liouvillianes screened by the operator ϵ, which in its simplest approximation contributes via the Lindhard screening of the Coulomb interaction matrix elements V_{abcd}. To show this, we have to calculate the action of ϵ on the 4-particle operator products, cf. Eq. (III.C.76). In order to apply ϵ as a whole to the 4-particle functions, we restrict to its eigenfunctions by choosing the index combinations which conserve the 4-particle function and find:

$$\epsilon^{-1}\sum_{abc}V_{ab1c}a_a^\dagger a_b^\dagger a_c a_2 = \langle\epsilon\rangle^{-1}\sum_{abc}V_{ab1c}a_a^\dagger a_b^\dagger a_c a_2$$

$$= \left(1 - V_q\sum_{a,\vec{k}_a}\frac{\sigma^{aa}_{\vec{k}_a}-\sigma^{aa}_{\vec{k}_a-\vec{q}}}{\varepsilon^a_{\vec{k}_a}-\varepsilon^a_{\vec{k}_a-\vec{q}}}\right)\sum_{abc}V_{ab1c}a_a^\dagger a_b^\dagger a_c a_2 \tag{III.C.78}$$

Then, by applying the second screening operator ϵ and the remaining superoperators ($\mathcal{Q}\mathcal{L}_{\mathrm{MP}} \approx \mathcal{L}_{\mathrm{MP}} - \mathcal{L}_0$) and using a similar treatment for the correlation contribution of the electron-phonon interaction, we finally obtain the correlation contributions already given in Eq. (III.B.37) and Eq. (III.B.54).

[2]Here we use a disentangling formula for superoperators [FS90] to decompose the exponential $\mathrm{e}^{-\mathrm{i}\,\mathcal{L}_\mathcal{Q}s}$:

$$\mathrm{e}^{\mathrm{i}\,(A+B)t} = \mathrm{e}^{\mathrm{i}\,At} + \int^t \mathrm{d}t'\mathrm{e}^{\mathrm{i}\,(A+B)t'}\,\mathrm{i}\,B\mathrm{e}^{\mathrm{i}\,A(t-t')}$$

$$\to \mathrm{e}^{-\mathrm{i}\,\mathcal{Q}(\mathcal{L}_0+\mathcal{L}_\mathcal{C})s} \approx \mathrm{e}^{-\mathrm{i}\,(\mathcal{L}_0+\mathcal{Q}\mathcal{L}_\mathcal{C})s} = (1+\int^s \mathrm{d}s'\mathrm{e}^{-\mathrm{i}\,(\mathcal{L}_0+\mathcal{Q}\mathcal{L}_\mathcal{C})s'}[-\mathrm{i}\,\mathcal{Q}\mathcal{L}_\mathcal{C}]\mathrm{e}^{\mathrm{i}\,\mathcal{L}_0 s'})\mathrm{e}^{-\mathrm{i}\,\mathcal{L}_0 s}\,.$$

After deriving the equations of motion for the observables of interest, we will now adapt them to different situations. In the scope of this work, we always consider only transitions between the two lowest subbands of the conduction band.

CHAPTER IV
Single Quantum Well with Homogeneous Electric Field

The aim of this chapter is to introduce all microscopic effects at the example of a very basic model system (single quantum well, homogenous electric field). Thereby, the impact of different microscopic contributions such as mean-field effects or correlation contributions and their interplay can be examined in its pure form, that is without mixing microscopic and macroscopic effects. In addition to this, the following chapter serves to familiarize with concepts or approximations frequently used in the scope of this work. All in all, the chapter provides the microscopic basis for the description of more complex systems, e.g., a multiple quantum well system embedded in a special geometry, - then also with respect to macroscopic effects.

In the following the microscopic theory derived above is applied to the case of a single quantum well where local field effects are negligible. We therefore assume that the local field is equivalent to the external applied field. For further simplification we take the field to be spatially homogenous which is a common approximation well justified for a wide range of applications [see for example [Kuh98]]. As we consider only a single quantum well, the index w denoting the well number is dropped in the following.

A. Initial Conditions and Approximations

1. Homogeneous Field

As stated above, we assume the electric field entering the microscopic equations of motion to be spatially homogeneous, i.e., we can replace the electric field in the equations according to

$$\mathbf{E}(\mathbf{Q}, z, t) \rightarrow \mathbf{E}(t)\, \delta_{\mathbf{Q},0}\,. \tag{IV.A.1}$$

Furthermore we concentrate on contributions describing optical processes i.e., we neglect current contributions in the framework of this work [cf. Chapter III.B.2]. Using that the wave functions of the two lowest subbands are orthonormal and have different parity, the contributions due to carrier-field interaction are reduced to

$$\frac{\mathrm{d}}{\mathrm{d}t}\sigma^{12}_{\substack{\mathbf{k},\mathbf{k}'\\ \sigma,\sigma'}}|_{\mathrm{cf}} = \mathrm{i}\,\Omega(t)\big(\sigma^{11}_{\substack{\mathbf{k},\mathbf{k}'\\ \sigma,\sigma'}} - \sigma^{22}_{\substack{\mathbf{k},\mathbf{k}'\\ \sigma,\sigma'}}\big)\,, \tag{IV.A.2a}$$

$$\frac{\mathrm{d}}{\mathrm{d}t}\sigma^{ii}_{\substack{\mathbf{k},\mathbf{k}'\\ \sigma,\sigma'}}|_{\mathrm{cf}} = \mathrm{i}\,\Omega(t)\big(\sigma^{ij}_{\substack{\mathbf{k},\mathbf{k}'\\ \sigma,\sigma'}} - \sigma^{ji}_{\substack{\mathbf{k},\mathbf{k}'\\ \sigma,\sigma'}}\big) \qquad [i,j=1,2,\ i\neq j]\,. \tag{IV.A.2b}$$

Here we have introduced the Rabi frequency

$$\Omega(t) = e\frac{D_{2,1}E_z(t)}{\hbar} \tag{IV.A.3}$$

with dipole matrix element

$$D_{n1,n2} = \int dz\, d_{n1,n2}(z) = \int dz \phi^*_{n1}(z)\, z\, \phi_{n2}(z)\,. \tag{IV.A.4}$$

As can be seen in Eq. (IV.A.2) a spatially homogenous field couples only density matrix elements with identical wave vectors $\mathbf{k}, \mathbf{k}'$ and spin σ, σ'. This means that in the case of homogeneous initial conditions, where no coherences exist at the switch-on time t_0, i.e.,

$$\sigma^{ij}_{\substack{\mathbf{k},\mathbf{k}'\\ \sigma,\sigma'}}(t_0) = 0 \qquad \text{if} \qquad i \neq j \ \wedge\ \mathbf{k} \neq \mathbf{k}' \ \wedge\ \sigma \neq \sigma'\,, \tag{IV.A.5}$$

coherences between different wave numbers and different spin are not driven by the electric field:

$$\frac{\mathrm{d}}{\mathrm{d}t}\sigma^{12}_{\substack{\mathbf{k},\mathbf{k}'\\ \sigma,\sigma'}}|_{\mathrm{cf}} \equiv \frac{\mathrm{d}}{\mathrm{d}t}\sigma^{ii}_{\substack{\mathbf{k},\mathbf{k}'\\ \sigma,\sigma'}}|_{\mathrm{cf}} \equiv 0 \quad \text{if} \quad \mathbf{k} \neq \mathbf{k}' \ \wedge\ \sigma \neq \sigma'\,. \tag{IV.A.6}$$

Hence, only equations of motion for the intersubband coherences, $p^{12}_{\mathbf{k},\sigma} = \sigma^{12}_{\substack{\mathbf{k},\mathbf{k}\\ \sigma,\sigma}}$, and occupation numbers, $f^{i}_{\mathbf{k},\sigma} = \sigma^{ii}_{\substack{\mathbf{k},\mathbf{k}\\ \sigma,\sigma}}$ will be solved in the following.

2. Matrix Elements

We restrict the analysis here to the description of a symmetric quantum well which reduces the number of non-vanishing Coulomb matrix elements considerably.

a) Coulomb Matrix Elements

For real wave functions the Coulomb matrix elements are given by [cf. Eq. (APP E.13)]

$$V_q^{n_a n_b n_c n_d} = \frac{1}{A}\frac{e^2}{2\epsilon_0}\int dz \int dz' \frac{\mathrm{e}^{-q|z-z'|}}{q}\phi_{n_a}(z)\phi_{n_b}(z')\phi_{n_a}(z)\phi_{n_b}(z') \tag{IV.A.7a}$$

$$= \frac{1}{A}\frac{e^2}{2\epsilon_0}\frac{1}{q}\mathcal{F}_q^{n_a n_b n_c n_d}\,. \tag{IV.A.7b}$$

Taking into account only the lowest two subbands in the conduction band, there exist thus only eight non-vanishing Coulomb form factors in a symmetric quantum well[1]:

I. V_{1111} and V_{2222} which describe purely intrasubband processes, i.e., two electrons interact in the same subband and remain in the initial subband (intrasubband interaction, intrasubband transitions)

II. V_{1212} and V_{2121} which describe an inter-intrasubband process, i.e., two electrons interact in different subbands and remain in the initial subband (intersubband interaction, intrasubband transitions)

III. V_{1221} and V_{2112} which describe purely inter-intersubband process, i.e., two electrons interact in different subbands and scatter to a different subband (intersubband interaction, intersubband transitions)

IV. V_{1122} and V_{2211} which describe an intra-intersubband process, i.e., two electrons interact in the same subbands and scatter to a different subband (intrasubband interaction, intersubband transitions) .

[1] Note, that in a symmetric quantum well all matrix elements corresponding to Auger processes are of zero value.

Because of the symmetry of the Coulomb matrix elements, we find that although they belong to different processes, the following matrix elements are the same

$$V_{1212} = V_{2121}\,, \qquad V_{1221} = V_{2112} = V_{1122} = V_{2211}\,. \tag{IV.A.8}$$

A sketch of the Coulomb matrix elements is given in Fig. IV.A.1. A detailed overview over the matrix elements and their dependence on wave vector and well width can be found in APP B.

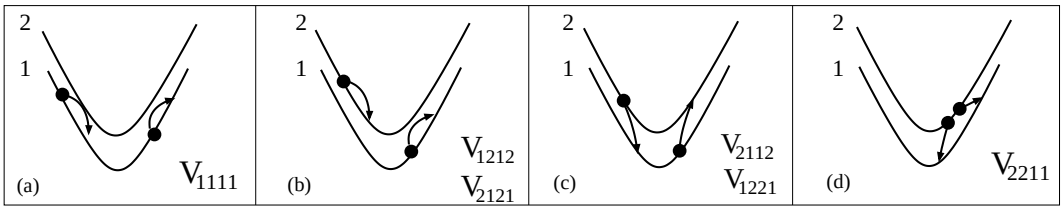

Figure IV.A.1 — Sketch of Coulomb Matrix Elements: The different matrix elements describe intrasubband, inter-intrasubband, inter-intersubband and intra-intersubband processes [cf. Chapter IV.A.2.a].

b) Fröhlich Matrix Elements

The Fröhlich matrix elements are given by

$$g^{ab}_{\underline{\mathbf{q}}} = -\mathrm{i}\sqrt{\frac{e^2\hbar\omega_{LO}}{2\mathcal{V}}\left(\frac{1}{\varepsilon_\infty}-\frac{1}{\varepsilon_s}\right)}\frac{1}{|\underline{\mathbf{q}}|}\int \mathrm{d}z\phi_a(z)\phi_b(z)\mathrm{e}^{\mathrm{i}\,\underline{\mathbf{q}}_\perp z}, \tag{IV.A.9a}$$

$$= -\mathrm{i}\sqrt{\frac{e^2\hbar\omega_{LO}}{2\mathcal{V}}\left(\frac{1}{\varepsilon_\infty}-\frac{1}{\varepsilon_s}\right)}\frac{1}{|\underline{\mathbf{q}}|}\mathcal{F}^{ab}_{\underline{\mathbf{q}}_\perp} \tag{IV.A.9b}$$

and taking into account the lowest two subbands we have intrasubband matrix elements $g^{11}_{\underline{\mathbf{q}}}, g^{22}_{\underline{\mathbf{q}}}$ and intersubband matrix elements $g^{12}_{\underline{\mathbf{q}}} = g^{*21}_{\underline{\mathbf{q}}}$. Note that in a symmetric quantum well products of inter- and intrasubband Fröhlich matrix elements vanish, $g^{ii}_{\underline{\mathbf{q}}} g^{ij}_{\underline{\mathbf{q}}} = 0$. Again an overview over the matrix elements and their dependence on wave vector and well width can be found in APP B. The underline below $\underline{\mathbf{q}}$ denotes, that this a $3D$ wave vector in contrast to $2D-$in-plane vectors $\mathbf{k}$.

B. Equations of motion

To proceed we evaluate Eq. (III.B.2), Eq. (III.B.4), Eq. (III.B.12), Eq. (III.B.37) and Eq. (III.B.41) with Eq. (III.B.54) for intersubband coherence $p^{12}_{\mathbf{k},\sigma}$ and occupation numbers $f^i_{\mathbf{k},\sigma}$. This is a very straightforward although lengthy task, therefore only the final result shall be given here. For the following analysis, it is convenient to distinguish different contributions of the equations of motion as done below

$$\begin{aligned}\frac{\mathrm{d}}{\mathrm{d}t}p^{12}_{\mathbf{k},\sigma} = &\left.\frac{\mathrm{d}}{\mathrm{d}t}p^{12}_{\mathbf{k},\sigma}\right|_0 + \left.\frac{\mathrm{d}}{\mathrm{d}t}p^{12}_{\mathbf{k},\sigma}\right|_{\mathrm{cf}} + \left.\frac{\mathrm{d}}{\mathrm{d}t}p^{12}_{\mathbf{k},\sigma}\right|^{\mathrm{mf},}_{A} + \left.\frac{\mathrm{d}}{\mathrm{d}t}p^{12}_{\mathbf{k},\sigma}\right|^{\mathrm{mf},}_{B} + \left.\frac{\mathrm{d}}{\mathrm{d}t}p^{12}_{\mathbf{k},\sigma}\right|^{\mathrm{mf},}_{C} \\ &+ \left.\frac{\mathrm{d}}{\mathrm{d}t}p^{12}_{\mathbf{k},\sigma}\right|_{\mathrm{cc-corr}} + \left.\frac{\mathrm{d}}{\mathrm{d}t}p^{12}_{\mathbf{k},\sigma}\right|_{\mathrm{cp-corr}}\,,\end{aligned} \tag{IV.B.1}$$

$$\begin{aligned}\frac{\mathrm{d}}{\mathrm{d}t}f^i_{\mathbf{k},\sigma} = &\left.\frac{\mathrm{d}}{\mathrm{d}t}f^i_{\mathbf{k},\sigma}\right|_{\mathrm{cf}} + \left.\frac{\mathrm{d}}{\mathrm{d}t}f^i_{\mathbf{k},\sigma}\right|^{\mathrm{mf},}_{B} + \left.\frac{\mathrm{d}}{\mathrm{d}t}f^i_{\mathbf{k},\sigma}\right|^{\mathrm{mf},}_{C} \\ &+ \left.\frac{\mathrm{d}}{\mathrm{d}t}f^i_{\mathbf{k},\sigma}\right|_{\mathrm{cc-corr}} + \left.\frac{\mathrm{d}}{\mathrm{d}t}f^i_{\mathbf{k},\sigma}\right|_{\mathrm{cp-corr}}\,.\end{aligned} \tag{IV.B.2}$$

The free-carrier, carrier-field and mean-field contributions read

$$\frac{\mathrm{d}}{\mathrm{d}t}p^{12}_{\mathbf{k},\sigma}|_0 = -\frac{\mathrm{i}}{\hbar}(\epsilon_{2,\mathbf{k}}-\epsilon_{1,\mathbf{k}})p^{12}_{\mathbf{k},\sigma} \tag{IV.B.3}$$

$$\frac{\mathrm{d}}{\mathrm{d}t}p^{12}_{\mathbf{k},\sigma}|_{\mathrm{cf}} = \mathrm{i}\,\Omega(t)\left[f^1_{\mathbf{k},\sigma}-f^2_{\mathbf{k},\sigma}\right] \tag{IV.B.4}$$

$$\frac{\mathrm{d}}{\mathrm{d}t}p^{12}_{\mathbf{k},\sigma}|_{\substack{\mathrm{mf},\\A}} = \frac{\mathrm{i}}{\hbar}\sum_{\mathbf{q}}\left[(V^{2222}_q-V^{2112}_q)\,f^2_{\mathbf{k}+\mathbf{q},\sigma}\;-(V^{1111}_q-V^{2112}_q)\,f^1_{\mathbf{k}+\mathbf{q},\sigma}\right]p^{12}_{\mathbf{k},\sigma} \tag{IV.B.5}$$

$$\frac{\mathrm{d}}{\mathrm{d}t}p^{12}_{\mathbf{k},\sigma}|_{\substack{\mathrm{mf},\\B}} = \frac{\mathrm{i}}{\hbar}\sum_{\mathbf{q}}\left[V^{1212}_q p^{12}_{\mathbf{k}-\mathbf{q},\sigma}+V^{2112}_q p^{21}_{\mathbf{k}-\mathbf{q},\sigma}\right](f^1_{\mathbf{k},\sigma}-f^2_{\mathbf{k},\sigma}) \tag{IV.B.6}$$

$$\frac{\mathrm{d}}{\mathrm{d}t}p^{12}_{\mathbf{k},\sigma}|_{\substack{\mathrm{mf},\\C}} = -\frac{\mathrm{i}}{\hbar}V^{2112}_0\sum_{\mathbf{k}_a,\sigma_a}\left[p^{12}_{\mathbf{k}_a,\sigma_a}+p^{21}_{\mathbf{k}_a,\sigma_a}\right](f^1_{\mathbf{k},\sigma}-f^2_{\mathbf{k},\sigma}) \tag{IV.B.7}$$

$$\frac{\mathrm{d}}{\mathrm{d}t}f^i_{\mathbf{k},\sigma}|_{\mathrm{cf}} = \mathrm{i}\;\Omega(t)\,p^{ij}_{\mathbf{k},\sigma}-c.c. \tag{IV.B.8}$$

$$\frac{\mathrm{d}}{\mathrm{d}t}f^i_{\mathbf{k},\sigma}|_{\substack{\mathrm{mf},\\B}} = \frac{\mathrm{i}}{\hbar}\sum_{\mathbf{q}}\left[V^{ijij}_q p^{ji}_{\mathbf{k}-\mathbf{q},\sigma}+V^{jiij}_q p^{ij}_{\mathbf{k}-\mathbf{q},\sigma}\right]p^{ij}_{\mathbf{k},\sigma}-c.c. \tag{IV.B.9}$$

$$\frac{\mathrm{d}}{\mathrm{d}t}f^i_{\mathbf{k},\sigma}|_{\substack{\mathrm{mf},\\C}} = -\frac{\mathrm{i}}{\hbar}V^{jiij}_0\sum_{\mathbf{k}_a,\sigma_a}\left[p^{ij}_{\mathbf{k}_a,\sigma_a}+p^{ji}_{\mathbf{k}_a,\sigma_a}\right]p^{ij}_{\mathbf{k},\sigma}+c.c.\,. \tag{IV.B.10}$$

Here, we already took into account that the divergent mean-field contributions

$$\frac{\mathrm{i}}{\hbar}(V^{1111}_0-V^{1212}_0)\,p^{12}_{\substack{\mathbf{k}\\\sigma}}\sum_{\mathbf{k}_a,\sigma_a}f^1_{\substack{\mathbf{k}_a\\\sigma_a}}+\frac{\mathrm{i}}{\hbar}(V^{1212}_0-V^{2222}_0)\,p^{12}_{\substack{\mathbf{k}\\\sigma}}\sum_{\mathbf{k}_a,\sigma_a}f^2_{\substack{\mathbf{k}_a\\\sigma_a}},$$

which occur in the equation of motion for the intersubband coherence, cancel with the ionic background [Kuh98, N$^+$97]. The three mean-field contributions A, B, C are exchange shift, excitonic contribution and depolarization effect, respectively, which will be discussed in separate sections in the following.

As we have seen in Chapter III.B.3.b and Chapter III.B.4.b, the correlation contributions consist of two parts: a principal value part and a δ-function part. Just like in interband transitions, the principal value part can be associated with second order renormalizations of the energies and the δ-function part with scattering and dephasing processes [BSP$^+$92, Kuh94]. As the first order renormalizations (mean-field effects) are expected to dominate the overall renormalizations [Kuh98], the second order renormalizations (principal value parts) are neglected in the following. The remaining correlation contributions for the intersubband coherence consist of diagonal terms, $\Xi_{\mathrm{d}}(p^{ij}_{\mathbf{k}})$, dependent on the intersubband coherence at same wavenumber, $p^{21}_{\mathbf{k}}$, non-diagonal terms, $\Xi_{\mathrm{nd}}(p^{ij}_{\mathbf{k}+\mathbf{k}''})$, which couple intersubband coherences at different wave vectors and terms nonlinear in the polarization Ξ_{nl}:

$$\frac{\mathrm{d}}{\mathrm{d}t}p^{21}_{\mathbf{k},\sigma}|_{\mathrm{cc/cp\text{-}corr}} = -\frac{\pi}{\hbar}\,\Xi_{\mathrm{d}}(p^{21}_{\mathbf{k}})+\frac{\pi}{\hbar}\sum_{\mathbf{k}''}\Xi_{\mathrm{nd}}(p^{ij}_{\mathbf{k}+\mathbf{k}''})+\frac{\pi}{\hbar}\Xi_{\mathrm{nl}}, \tag{IV.B.11}$$

(IV.B.12)

with

$$\Xi_{\mathrm{d}}(p^{21}_{\mathbf{k}}) = \Gamma_{\mathrm{d}}\,p^{21}_{\mathbf{k}} = \frac{1}{2}\sum_{i=1,2}(\Gamma^{i,\mathrm{cp}}_{\mathrm{d}}+\Gamma^{i,\mathrm{cc}}_{\mathrm{d}})\,p^{21}_{\mathbf{k}}, \tag{IV.B.13}$$

$$\sum_{\mathbf{k}''}\Xi_{\text{nd}}(p^{ij}_{\mathbf{k}+\mathbf{k}''}) = \sum_{i=1,2}\left[\sum_{\underline{\mathbf{q}}}\Gamma^{i,\text{cp}}_{\text{nd}}\; p^{21}_{\mathbf{k}+\underline{\mathbf{q}}_{||}} + \sum_{\mathbf{k}',\mathbf{q}}\Gamma^{i,\text{cc}}_{\text{nd1}}\; p^{21}_{\mathbf{k}'-\mathbf{q}} + \sum_{\mathbf{q}}\Gamma^{i,\text{cc}}_{\text{nd2}}\; p^{21}_{\mathbf{k}+\mathbf{q}} - \sum_{\mathbf{k}'}\Gamma^{i,\text{cc}}_{\text{nd3}}\; p^{21}_{\mathbf{k}'}\right] + \sum_{i=1,2}\left[\sum_{\underline{\mathbf{q}}}\tilde{\Gamma}^{i,\text{cp}}_{\text{nd}}\; \tilde{p}^{12}_{\mathbf{k}+\underline{\mathbf{q}}_{||}} + \sum_{\mathbf{k}',\mathbf{q}}\tilde{\Gamma}^{i,\text{cc}}_{\text{nd1}}\; \tilde{p}^{12}_{\mathbf{k}'-\mathbf{q}} + \sum_{\mathbf{q}}\tilde{\Gamma}^{i,\text{cc}}_{\text{nd2}}\; \tilde{p}^{12}_{\mathbf{k}+\mathbf{q}} - \sum_{\mathbf{k}'}\tilde{\Gamma}^{i,\text{cc}}_{\text{nd3}}\; \tilde{p}^{12}_{\mathbf{k}'}\right] . \tag{IV.B.14}$$

The explicit contributions and Ξ_{nl} are given in Chapter APP F. The corresponding equation for the occupation numbers read

$$\frac{\mathrm{d}}{\mathrm{d}t}f^{i}_{\mathbf{k},\sigma}|_{\text{cc/cp-corr}} = -\frac{\pi}{\hbar}f^{i}_{\mathbf{k},\sigma}\Gamma^{i,\text{out}}_{\text{d}} + \frac{\pi}{\hbar}(1-f^{i}_{\mathbf{k},\sigma})\Gamma^{i,\text{in}}_{\text{d}} + \Xi_{\text{nl},f_i} \qquad i,j=1,2;\; i\neq j\,. \tag{IV.B.15}$$

where $\Gamma^{i,\text{in}}_{\text{d}}$ denotes the diagonal in-scattering and $\Gamma^{i,\text{out}}_{\text{d}}$ the corresponding diagonal out-scattering rate ($\Gamma^{i}_{\text{d}} = \Gamma^{i,\text{in}}_{\text{d}} + \Gamma^{i,\text{out}}_{\text{d}}$). Ξ_{nl,f_i} denotes the contributions to the equation which are nonlinear in the polarization. In the following sections, the impact of the both mean-field and second order correlation contributions is investigated.

C. Preliminary Remarks

Before we really immerse into the application of the derived theory, some general remarks shall be made.

1. Linear versus Nonlinear Excitation: Absorption Spectra and Rabi Oscillations

Generally, we distinguish two regimes in which intersubband transitions are investigated: the linear and the nonlinear regime. The first denoting the response to a weak external field, the second to a strong field, respectively.

In the following, we generally assume, that the carriers are in equilibrium before the external excitation. In this case, the occupation numbers of the electrons are given by Fermi-Dirac distributions. While determining the actual Fermi-Dirac function, it has to be considered that even in equilibrium the electrons are not as a whole entirely located in the lowest subband. Depending on the gap-energy between the subbands, the actual carrier density and temperature, they can also be spread about the subbands [cf. Fig. IV.C.1].

a) Relaxation of a Non-Equilibrium Electron Distribution

The assumption of an initial equilibrium situation can be easily justified as any non-equilibrium carrier distribution, resulting for example from a previous external excitation, is rapidly modified by many-particle interactions so that it approaches the corresponding Fermi-Dirac distribution [CK99]. As an example, we show in Fig. IV.C.2, Fig. IV.C.3 and Fig. IV.C.4 the relaxation of an initially prepared non-equilibrium situation in the lowest subband - with respect to different many-particle interactions. The presented relaxations have been calculated using Eq. (IV.B.2). The lattice temperature has been taken as $T_L = 50$ Kelvin. In order to get some insight into the interplay of carrier-carrier and carrier-phonon interaction, we first consider carrier-carrier and carrier-phonon interaction separately and then include both mechanisms simultaneously. If *only* carrier-carrier or *only* carrier-phonon interaction is included in the calculation, the calculated distributions fail to reach the

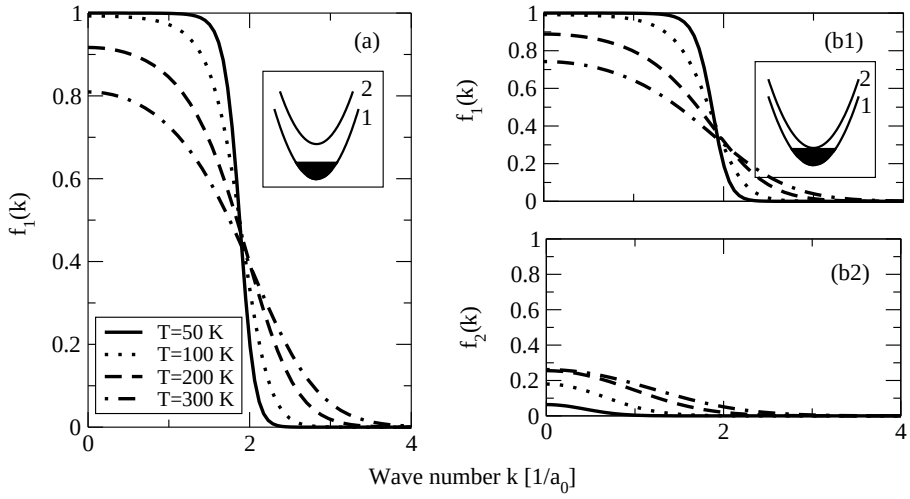

Figure IV.C.1 — Occupation Numbers (Equilibrium): Fermi-Dirac Distributions: Occupation numbers for quasi-equilibrium shown for carrier-density $n = 1.2^{12}\mathrm{cm}^{-2}$: (a) subbands are separated by large gap-energy (shown: 5 nm AlGaAs/GaAs quantum well); (b) subbands are separated by small gap-energy (shown: 15 nm AlGaAs/GaAs quantum well). At low temperature, the electrons tend to occupy the lowest available states. With increasing thermalization, the distributions broadens and for a small gap energy, fi gures (b), an increasing number of electrons populates the upper subband.

corresponding Fermi-Dirac distribution. Only including both dephasing mechanisms simultaneously yields satisfactory results.

In Fig. IV.C.2, we provide only carrier-phonon scattering as a relaxation mechanism. As carrier-phonon interaction is considered only semi-classically, i.e. in Markovian approximation, electrons can only scatter to lower energies by the emission of optical phonons with constant energy $\hbar\omega = 36$ meV. This results in a step-like distribution function, where the electrons have cooled down to roughly the lattice temperature. The occurring substructures are due to the completely dispersionless LO-phonons and the sharp energy conservation in the Markovian approximation. In [But04], it has been shown that including Non-Markovian scattering processes, the distribution function is able to relax into the correct Fermi-Dirac function.

In Fig. IV.C.3, only carrier-carrier interaction has been included in the theory. Although the occupation function does relax into a Fermi-Dirac distribution, the effective plasma temperature is in the range of $T = 370$ Kelvin which is well above the lattice temperature of $T_L = 50$ Kelvin.

In Fig. IV.C.4, we finally included both carrier-phonon and carrier-carrier interaction in the calculation. The combination of both scattering mechanisms obviously yields the desired result. After 3500 fs, the electron occupation is function almost identical to the Fermi-Dirac distribution of the corresponding density - although the lattice temperature has not been reached completely. The initially hot electrons have cooled down to a plasma temperature of roughly 70 Kelvin.

b) Linear Regime

In the case, of weak excitation, the change of occupation in the subbands is negligible small. Consequently, the initial occupation of the subbands can assumed to be constant for all times and the corresponding equations of motions (for the occupation numbers) do not have to be solved. Furthermore, diagonal correlation contributions can be calculated before the actual time wrap and thus only the non-diagonal contributions have to be computed in every time step, which does save cpu-time to a great extent. In addition to this, contributions nonlinear in the field, such as products of field-driven coherences, are also negligible [cf. Eq. (IV.B.11) and Eq. (IV.B.15)]. For weak excitation, the main focus lies on the investigation of linewidth and lineshape of absorption spectra. Within the scope of the approximations described above the absorption can be determined to be proportional to the

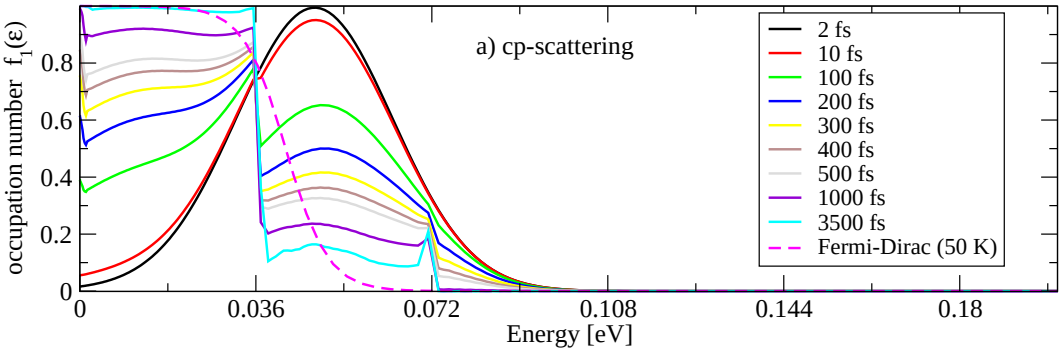

Figure IV.C.2 — Relaxation of Non-Equilibrium Electron Distribution through c-p scattering: The density is $n = 1.12 \times 10^{12}\mathrm{cm}^{-2}$, the lattice temperature is $T_L = 50$ Kelvin. Parameters taken for a quantum well with $L = 10$ nm. Electrons are cooled down to lattice temperature but substructures occur at energies $\epsilon = n\hbar\omega_{LO} = n36$ meV (n=1, 2, ...) as carrier-phonon scattering (LO) is included only semi-classically.

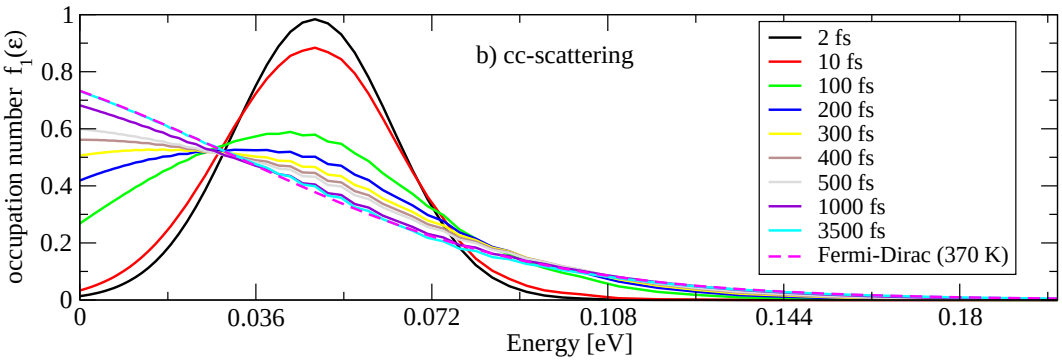

Figure IV.C.3 — Relaxation of Non-Equilibrium Electron Distribution through c-c scattering: Parameters as above. Carrier-carrier scattering effi ciently redistributes electrons, but fails in cooling down to lattice temperature.

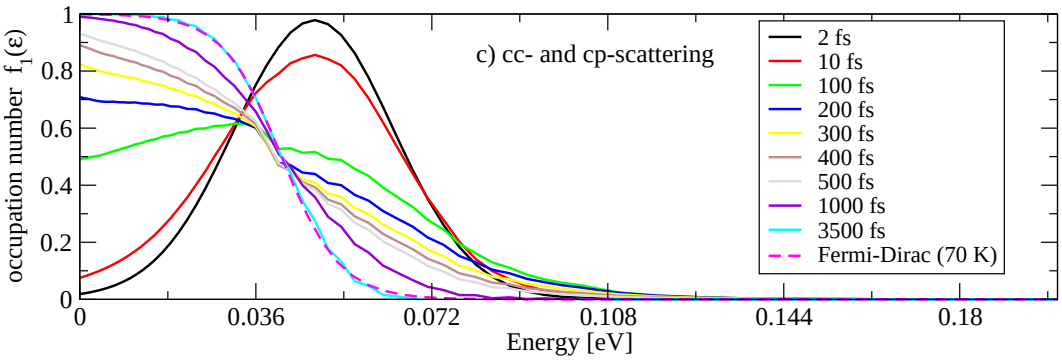

Figure IV.C.4 — Relaxation of Non-Equilibrium Electron Distribution through c-c & c-p scattering: Inclusion of both mechanisms yields redistribution without substructures and cooling down to (almost) lattice temperature. The missing 20 Kelvin might still be achieved in the future.

imaginary part of the susceptibility [for details cf. for example[CK99, HK94]]

$$\alpha(\omega) \propto \mathrm{Im}(\chi(\omega)) \tag{IV.C.1}$$

where the susceptibility connects the macroscopic polarization and the incident external field according to

$$\mathbf{P}(z,t) = \chi(\omega)\mathbf{E}(z,t)\,. \tag{IV.C.2}$$

c) Nonlinear Regime

In the case of nonlinear excitation, the occupations can not be assumed to be constant for all times. On the contrary, the investigation of the temporal behavior of the occupations or populations is one of the main focus points. The time-dependence of the occupation numbers yields a huge increase of the required cpu-time as not only additional equations of motion have to be solved, but also all correlation contributions have to be determined in each step.

The most dominant reason for the interest in the nonlinear excitation of matter in general is the prospect to observe Rabi oscillations. Since the beginning of ultrafast nonlinear optics, it is known, that coherently excited atomic systems exhibit Rabi oscillations: a driving field $E(t)$ couples the two energy levels with optical dipole moment d_{12} and induces sinusoidal oscillations of the population in the levels with Rabi frequency $\Omega(t) = E(t)d_{12}/\hbar$. Hereby resonant pulses with areas of $\pi, 2\pi, 3\pi$, and so on, are obviously particularly important as they have the power to invert the population $1, 2, 3$, and so on, times. As Rabi oscillations are important for a broad range of technical applications such as quantum information processing to name only one, there has been considerably interest in the investigation of possible Rabi oscillations in low-dimensional semiconductors. Up to this time the attention was mostly focused on *interband* Rabi oscillations in quantum dots [BLS$^+$02, FWDK03, Vas04, SMM$^+$04] and quantum wells [BKL$^+$90, CKF$^+$94, BHKP96, SBD$^+$99]. Recently, also *intersubband* Rabi flopping between subbands in the conduction band of quantum wells has been observed experimentally [LRW$^+$04] and first theoretical studies have been presented in [BC04, MVO03, SRW$^+$04]. Thereby it has been shown, that already first-level many-particle interactions can influence the ability to produce Rabi oscillations and therewith the coherent nonlinear control of populations in quantum wells considerably. Furthermore, the nonparabolicity of the conduction band can have a rather significant impact on the curvature of the subbands, strongest for small quantum wells [Eke89], yielding different subband dispersions and thus a variety of possible transition frequencies.

D. Applications

The general plan for the investigation of intersubband transitions in both linear and nonlinear regime is the following:

In the linear regime we will examine the impact of bandstructure (subband dispersion) and many-particle effects (mean-field effects and dephasing contributions) on lineshape and linewidth of the absorption spectra. Furthermore, the dependence on parameters such as lattice-temperature, well width and carrier density is investigated. The gained insights into the impact of the afore said contributions will then be used in order to control coherently the nonlinear excitation of the quantum well. That is, we try to take advantage of the information extracted in the linear regime in order to enhance the ability of the system to exhibit Rabi oscillations *in spite of many-particle interactions* which thwart the latter.

1. Comparison with Kohn's Theorem (Numerics Test)

It is always worthwhile performing convergence tests, i.e., taking the theoretical / computational model to established limits, which often have been derived analytically [Har00]. The idea is to increase confidence in the theory and to demonstrate that previous theories are limits of the new ones.

For this reason, before we now investigate the linear and nonlinear response of the quantum well in detail, we first concentrate on the special case of a quantum well sample, where the Coulomb and Fröhlich form factors can be approximated by

$$\mathcal{F}_q^{n_a n_b n_c n_d} \approx \delta_{n_a,n_c}\delta_{n_b,n_d}, \quad \mathcal{F}_{\underline{\mathbf{q}}_\perp}^{ab} \approx \delta_{a,b}\,. \tag{IV.D.1}$$

This means that the intersubband formfactors vanish and the intrasubband formfactors all have the same value. Considering the Coulomb and Fröhlich formfactors [cf. also Eq. (IV.A.7) and Eq. (IV.A.9)]

$$\begin{aligned} \mathcal{F}_q^{n_a n_b n_c n_d} &= \int \mathrm{d}z \phi_{n_a}(z)\phi_{n_c}(z) \int \mathrm{d}z' \phi_{n_b}(z')\phi_{n_d}(z')\mathrm{e}^{-|\mathbf{q}||z-z'|}\,, \\ \mathcal{F}_{\underline{\mathbf{q}}_\perp}^{ab} &= \int \mathrm{d}z \zeta_a^*(z)\zeta_b(z)\mathrm{e}^{\mathrm{i}\,Q_\perp z}, \end{aligned} \tag{IV.D.2}$$

we see that this approximation holds in the limit

$$\mathrm{e}^{-|\mathbf{q}||z-z'|} \approx 1 \quad \text{and} \quad \mathrm{e}^{\mathrm{i}\,Q_\perp z} \approx 1 \tag{IV.D.3}$$

i.e., in the limit of thin quantum wells and low densities [N$^+$97].

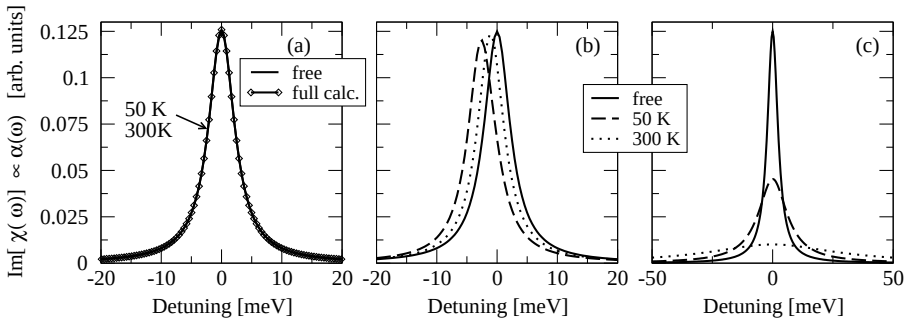

Figure IV.D.1 — Absorption in limit of thin wells and low carrier density: (a) including all contributions the spectra are identical to those of single-particle excitation, (b) neglecting the exchange contribution, (c) neglecting non-diagonal correlation contributions.

If we approximate the matrix elements using Eq. (IV.D.1), we neglect the three-dimensional character of the matrix elements. Taking the sum over all $\mathbf{k}$ contributions one can show by renumbering the summation indices in Eqs. (IV.B.3) to (IV.B.15), that within this approximation and in the case of equal subband dispersion ($m_1 == m_2$), the total contribution of the Coulomb interaction among the carriers and the total contribution of the electron-phonon interaction to the macroscopic polarization vanishes completely. Thus the linear susceptibility $\chi(\omega)$ is that of non-interacting single particle excitations, $\mathrm{Im}[\chi(\omega)] \propto \delta(\omega - \omega_0)$. This result can be compared to Kohn's Theorem [Koh61] which states that, for a parabolic potential or in the presence of a magnetic field, the absorption is independent of the electron-electron interaction. In contrast to Kohn's Theorem, however, which is valid for all strengths of the parabolic potential and for all carrier densities, the approximation for the formfactors used above is justified only for $(-|\mathbf{q}||z-z'|) \approx 0$ and $(\mathrm{i}\,Q_\perp z) \approx 0$, i.e., in the limit of thin wells and low densities.[N$^+$97]. Nevertheless, an investigation of this limit can be used to scrutinize the credibility of common approximations concerning the equations of

motions and additionally, the numerics used to solve the very. As can be seen in Fig. IV.D.1 (a) solving the full equations of motions yields indeed absorption spectra completely identical to those of non-interacting single particle excitations. Note, that this finding does not mean, that the specific contributions vanish on their own, only contributions connected with intersubband transitions vanish, the other contributions cancel. This is demonstrated in Fig. IV.D.1 (b) where one mean-field effect (exchange contribution) has been excluded from the theory. Finally, in Fig. IV.D.1 (b), we avail ourselves of the frequently used relaxation rate approximation, i.e., we approximate the correlation contribution by the diagonal contributions (the inverse of the T_2 time) only. In this case, the corresponding spectra show a strong temperature-dependent broadening. This demonstrates clearly the cancellation effects between diagonal and non-diagonal terms. *Disregarding the non-diagonal terms completely neglects possible interference effects between various scattering events and yields a strong overestimation of the linewidth.*

In the following sections, the optical response of a single quantum well shall now be investigated - with respect to the three dimensional character of the matrix elements.

2. Single Particle Excitation

To begin with, we include only contributions due to free-particle Hamiltonian and carrier-field Hamiltonian explicitly in the equations of motion and neglect many-particle contributions due to carrier-carrier and carrier-phonon interaction. To include dephasing, which is indispensable for the calculation of absorption spectra, a phenomenological dephasing constant γ_p is introduced in the equation for the intersubband coherence. Note, that we choose $\gamma_p \neq 0$ only if the sample is excitated in the linear regime, i.e., only for the calculation of absorption spectra. At this level, the microscopic equations describe simply the excitation of non-interacting electrons by an external applied field - with respect to the considered bandstructure: The corresponding equations of motion are given by

$$\frac{\mathrm{d}}{\mathrm{d}t} p^{12}_{\mathbf{k},\sigma} \approx \left.\frac{\mathrm{d}}{\mathrm{d}t} p^{12}_{\mathbf{k},\sigma}\right|_0 + \left.\frac{\mathrm{d}}{\mathrm{d}t} p^{12}_{\mathbf{k},\sigma}\right|_{\mathrm{cf}} - \gamma_p p^{12}_{\mathbf{k},\sigma} \tag{IV.D.4}$$

$$\frac{\mathrm{d}}{\mathrm{d}t} f^{1}_{\mathbf{k},\sigma} \approx \left.\frac{\mathrm{d}}{\mathrm{d}t} f^{1}_{\mathbf{k},\sigma}\right|_{\mathrm{cf}} \tag{IV.D.5}$$

To bring up the impact of the considered bandstructure, we investigate first an idealized quantum well, where a possible nonparabolicity of the conduction band is a priori neglected. We then consider a more realistic quantum well model which takes the nonparabolicity of the bandstructure into account. As we have seen in Chapter II.A.3.d, the nonparabolicity of the conduction band yields mainly a difference in subband dispersion: in effective mass approximation the subbands have different effective masses. Additionally, the bound state energies are also shifted to some degree. As the impact on the subband masses is the dominating effect, we will mostly refer to the neglect of nonparabolicity as a quantum well with *equal subband dispersion* in contrast to a quantum well with *different subband dispersion.* Note that this denotation shall not indicate that the difference in bound state energies is not taken into account.

a) Equal Subband Dispersion

If the in-plane dispersion is identical in both subbands, the transition frequency is independent of the in-plane vector $\mathbf{k}$, $\epsilon_{2,\mathbf{k}} - \epsilon_{1,\mathbf{k}} = \omega_G$. The excitation of electrons between the two subbands is comparable with an atomic two-level system oscillating at frequency ω_G.

Linear Regime

Due to the phenomenological dephasing introduced in Eq. (IV.D.4), the spectral width of the corresponding linear absorption spectra is not infinitely sharp. The shape of the absorption spectrum

is pure Lorentzian with the finite linewidth $\hbar\gamma_p$ (here $\hbar\gamma_p = 1$ meV). The absorption of a single quantum well with equal subband dispersion is plotted in Fig. IV.D.2 for different well width L and temperatures T. The carrier density is $n = 1.2^{12}\mathrm{cm}^{-2}$. The absorption peak is located at the gap-energy (or transition energy). The lineshape is neither influenced by the well width nor the temperature, which enters through the Fermi-Dirac distribution determining the occupance of the subbands. The well width does only influence the peak position, as the bound state energies are directly connected with the gap energy, $\hbar\omega_G = \epsilon_{2,\mathbf{k}=0} - \epsilon_{1,\mathbf{k}=0}$ [cf. Chapter II.A.3.a and Chapter II.A.3.b]. Note, however, that the absolute height of the spectrum is - for the high carrier density considered here - dependent on well width and temperature. For wide quantum wells which have a small gap energy electrons may occupy the upper subband depending on the temperature and density. If this is the case, the number of electrons in the lower subband is reduced which results consequently in a reduced absorption. Apart from this, no further temperature dependency can be observed.

Nonlinear Regime

For strong excitation, the population oscillates between the subbands. Here, again, the strong resemblance to an atomic two-level system is visible. Excited resonantly with a pulse with pulse area $\Theta = n\pi$, the population will make $0.5n$ Rabi flops, i.e., for pulse areas with odd multiples of π the system is inverted, for even multiples of π the system is in the initial condition again. No matter how temporally broad the pulse (and therewith spectrally small), electrons at all energies will exhibit perfect Rabi flops, since the excitation frequency is **k**-independent. These general statements hold, however, only, if a possible dephasing of the system is on a time-scale much longer than the external excitation. Otherwise, the oscillations will be suppressed as we will see later when considering dephasing due to carrier-carrier and carrier-phonon interaction. For the present, we neglect dephasing, whenever we excite the system nonlinearly.

In Fig. IV.D.3 we investigate the nonlinear response of the quantum well considered in Fig. IV.C.1 (b) ($L = 10$nm, $n = 1.2^{12}\mathrm{cm}^{-2}$) for temperature $T = 50$ Kelvin. Particularly with respect to later results, we show the results of excitation by two different Gaussian pulse: a short ($\tau = 100$ fs, solid lines) and a longer ($\tau = 100$ fs, dashed lines) one, both resonant to the transition energy. The energy spectrum of the two pulses is given in Fig. IV.D.3 (a2). As an example of the time-resolved incident field, the short pulse is shown in Fig. IV.D.3 (a1). As can be seen, the relative population in the upper subband, i.e. the time-dependent population in the upper subband divided by the carrier density, oscillates exactly as a two-level system. For a pulse area of $\Theta = 1\pi$ the system is inverted, for $\Theta = 2\pi$ the electrons are all in the lower subband again, and so on. As the transition energy is **k**-independent, all electrons (independent of their wave vector) have the same excitation frequency. In this case the temporal pulse duration does not influence the number of excited electrons.

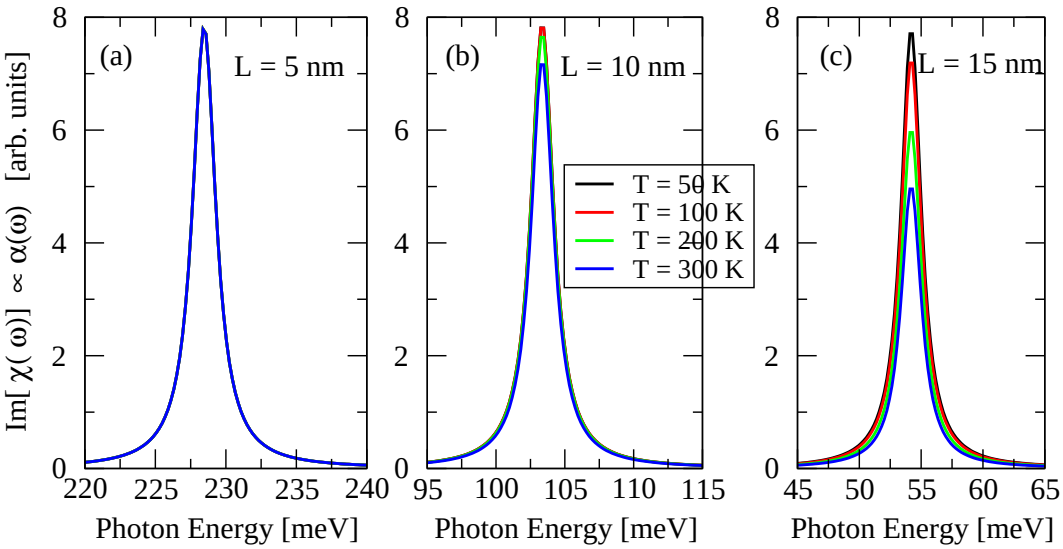

Figure IV.D.2 — Free-Carrier Absorption (Equal Subband Dispersion): Absorption of a quantum well with carrier density $n = 1.2 \times 10^{12}\mathrm{cm}^{-2}$ and well width (a) $L = 5$ nm, (b) $L = 10$ nm, (c) $L = 15$ nm assuming equal subband dispersion. With increasing temperature the height of the absorption spectra in (b) and (c) decreases which is due to the increase of population in the upper subband. In (a) this effect does not occur, since the transition energy is very high in this case and the upper subband is not populated in equilibrium.

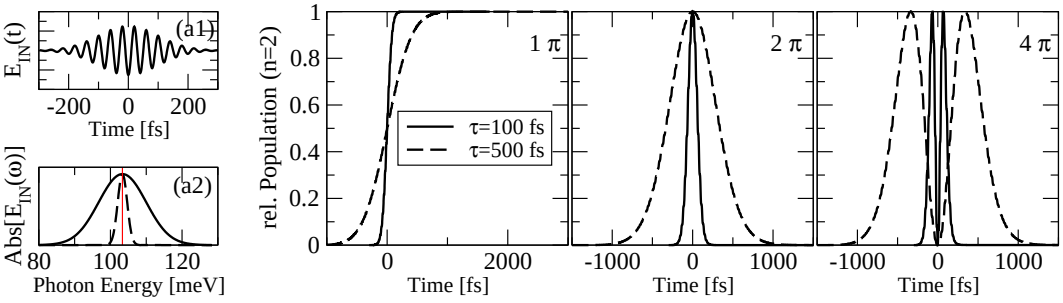

Figure IV.D.3 — Rabi Flops in Free-Carrier Model (Equal Subband Dispersion): Relative population in the upper subband (carrier density $n = 1.2^{12}\mathrm{cm}^{-2}$, well width $L = 10$ nm, temperature $T = 50$ Kelvin, $\gamma_p \equiv 0$) excited by a Gaussian pulse with pulse area $\Theta = 1\pi, 2\pi, 4\pi$ for two different pulse durations $\tau = 100$ fs (solid lines) and$\tau = 500$ fs (dashed lines). (a1) shows the time-resolved incident pulse ($\tau = 100$ fs), (a2) shows the energy spectrum for both pulse durations. As the transition energy is **k**-independent, the pulse duration does only influence the time in which the oscillations of the population take place and does not have any influence on the overall number of excited electrons.

b) Different Subband Dispersion: Inhomogeneous Broadening

A difference in subband dispersion yields a variety of excitation frequencies. In this case the absorption spectrum is the superposition of a large number of Lorentzian lines, each with linewidth $\hbar\gamma$ and each with a distinct frequency ω_G. The spectrum is said to be *inhomogeneously* broadened.

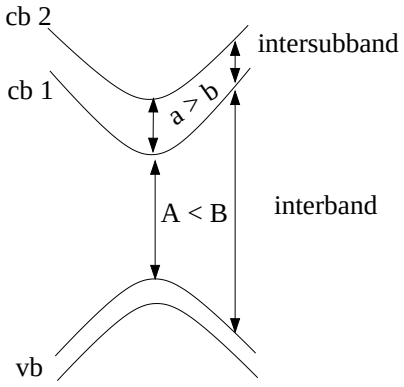

Figure IV.D.4: **Interband vs. Intersubband Transitions:** In contrast to interband transitions, for intersubband transitions the transition energy is largest at $\mathbf{k} = 0$. Consequently, the absorption spectrum covers energies equivalent to or smaller as the subband-gap energy.

The term "inhomogenous" originates from the description of atomic dipole oscillations. Here the origin of the different effective resonance frequencies possessed by otherwise identical oscillators can be traced back to slightly different environments (random dislocation, impurities, strain fields) in which the resonant atoms find themselves [AE87]. With increasing temperature, the electron distribution broadens and a range of energies exist in which the states are partially filled [cf. Fig. IV.C.1]. With the increasing occupation of energetically higher states the impact of the different subband dispersion, i.e., of the **k**-dependent transition energy, increases. Note that the smallest transition energy exists for $\mathbf{k} = 0$, with increasing wave vector **k** the transition energy decreases. Thus, absorption can be observed only at frequencies *equivalent to* or *smaller* as the subband-gap energy. Due to the different subband dispersion, the corresponding absorption spectrum covers thus the range of energies equivalent to or smaller than the gap-energy.

This is different from interband transitions between conduction and valence band, two bands with opposite curvature, where absorption can take place only at frequencies *equivalent to* or *larger* as the band-gap energy.

Linear Regime

The impact of the **k**- dependent difference in subband dispersion is investigated for six different single quantum wells in Fig. IV.D.5. The parameters of the individual wells are given by (a1) carrier density $n = 1.2 \times 10^{12}\mathrm{cm}^{-2}$, well width $L = 5$ nm, (a2) $n = 5.0 \times 10^{10}\mathrm{cm}^{-2}$, $L = 5$, (b1) $n = 1.2{\times}10^{12}\mathrm{cm}^{-2}$, $L = 10$, (b2) $n = 5.0{\times}10^{10}\mathrm{cm}^{-2}$, $L = 10$, (b1) $n = 1.2{\times}10^{12}\mathrm{cm}^{-2}$, $L = 15$, (b2) $n = 5.0 \times 10^{10}\mathrm{cm}^{-2}$, $L = 15$. In all cases the absorption is calculated for $T = 50, 100, 200$ and 300 Kelvin. The difference in subband dispersion is due to the nonparabolicity of the conduction band, which is strongly dependent on the well width of the quantum well. Consequently, absorption spectra of small quantum wells [cf. Fig. IV.D.5 (a1, a2)] are strongly inhomogeneously broadened and the lineshape has no alikeness with a Lorentzian. For wider quantum wells [cf. Fig. IV.D.5 (c1, c2)] nonparabolicity effects are almost neglectable, the corresponding spectra are comparable to those of Fig. IV.D.2 where the nonparabolicity of the conduction band has not been taken into account.

Nonlinear Regime

Similar to Chapter IV.D.2.a.2 we focus on the 10 nm quantum well considered in Fig. IV.D.5 (b1) with $T = 50$ Kelvin. Due to the **k**-dependent transition energy, the pulse duration now has a strong influence on the number of electrons excited to the upper subband (in contrast to Fig. IV.D.3). Whereas a temporally short pulse ($\tau = 100$ fs, solid lines) is spectrally wide enough to cover the variety of transition energies and thus can excite a large amount of electrons to the second subband,

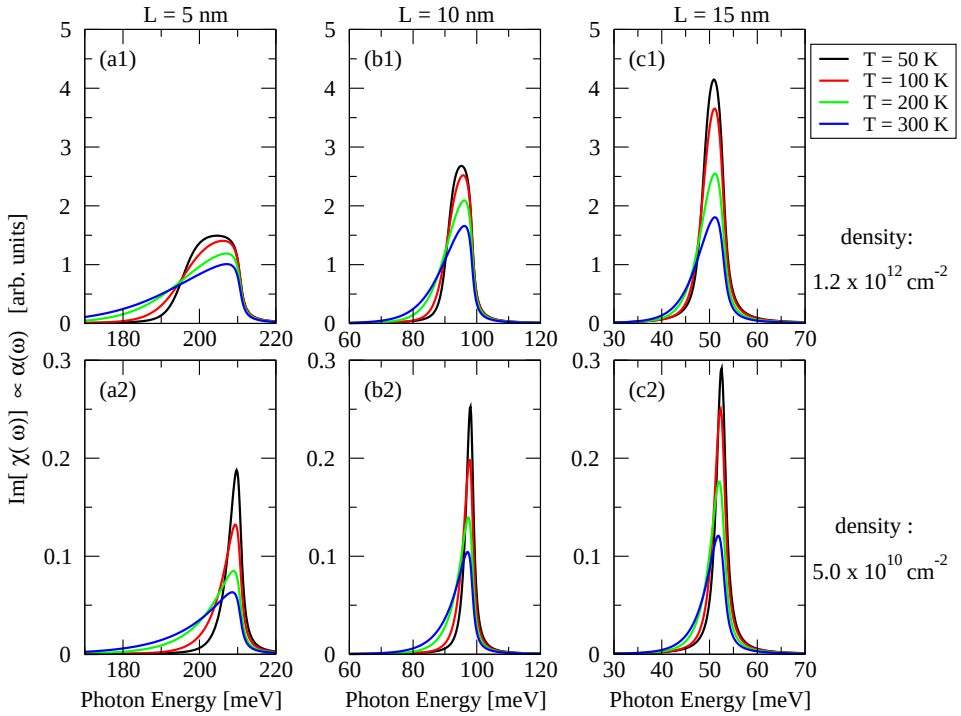

Figure IV.D.5 — Free-Carrier Absorption (Equal Subband Dispersion): Absorption of a quantum well with carrier density $n = 1.2^{12}\mathrm{cm}^{-2}$ and well width (a) $L = 5$ nm, (b) $L = 10$ nm, (c) $L = 15$ nm taking into account the different subband dispersions due to the nonparabolicity of the conduction band.

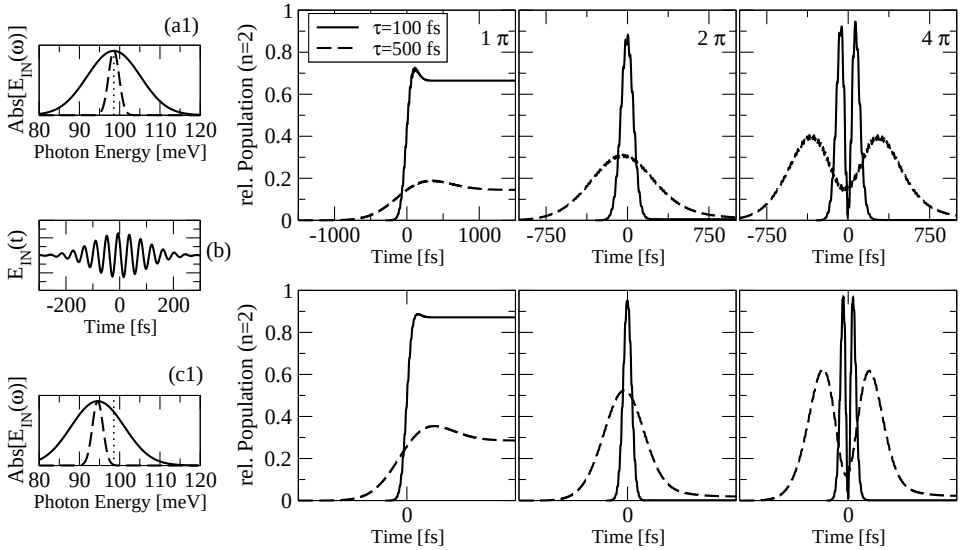

Figure IV.D.6 — Rabi Flops in Free-Carrier Model (Different Subband Dispersion): Relative population in the upper subband (carrier density $n = 1.2^{12}\mathrm{cm}^{-2}$, well width $L = 10$ nm, temperature $T = 50$ Kelvin, $\gamma_p \equiv 0$) excited by a Gaussian pulse with pulse area $\Theta = 1\pi, 2\pi, 4\pi$ for two different pulse durations $\tau = 100$ fs (solid lines) and $\tau = 500$ fs (dashed lines). (a1) shows the time-resolved incident pulse ($\tau = 100$ fs), (a2) shows the energy spectrum for both pulse durations. Due to the **k**-dependent transition energy, the number of excited electrons is strongly dependent on the pulse duration. Whereas the shorter pulse is still spectrally wide enough to excite most electrons, only a small number of electrons is excited by the longer pulse. The number of excitations can be enhanced, if the sample is excited at a slightly detuned frequency.

the frequency spectrum of the longer pulse ($\tau = 500$ fs, dashed lines) does not cover same amount of the transition range and is thus too small to excite the same number of electrons. The number of excitations can be enhanced, if the sample is excited at a slightly detuned frequency. Thereby, a wider range of transition frequencies is covered by the pulse (remember that the absorption spectrum is not Lorentzian).

3. Inclusion of Mean-Field Contributions [1]

In the following sections, the impact of the different mean-field contributions is taken into account. As we will see, these contributions introduce wave vector dependent renormalizations of single-particle energies and Rabi frequency and thus we expect a strong influence on the ability of the system to produce Rabi oscillations.

a) Exchange Contribution

If we regard the exchange contribution together with the free-carrier contribution

$$\begin{aligned}\frac{\mathrm{d}}{\mathrm{d}t}p^{12}_{\mathbf{k},\sigma}|_0 + \left.\frac{\mathrm{d}}{\mathrm{d}t}p^{12}_{\mathbf{k},\sigma}\right|_{\substack{\mathrm{mf},\\ A}} = & \frac{\mathrm{i}}{\hbar}\Big\{-(\epsilon_{2,k}-\epsilon_{1,k}) \\ & + \sum_{\mathbf{q}}\left[(V^{2222}_{\mathbf{q}} - V^{2112}_{q})\, f^{2}_{\mathbf{k}+\mathbf{q},\sigma} - (V^{1111}_{q} - V^{2112}_{q})\, f^{1}_{\mathbf{k}+\mathbf{q},\sigma}\right]\Big\}\, p^{12}_{\mathbf{k},\sigma} \\ = & -\frac{\mathrm{i}}{\hbar}\,\tilde{\mathcal{E}}^{21}_{\mathbf{k},\sigma}\, p^{12}_{\mathbf{k},\sigma}\,, \end{aligned} \tag{IV.D.6}$$

we see immediately that this contribution renormalizes the single-particle energies and consequently the transition energies. The renormalization depends on the occupation in the subbands and the relation between the different Coulomb matrix elements. As matrix elements V_q^{iiii} are always larger than matrix element V_q^{2112} [cf. APP B], the transition energy is thus shifted to higher energies if all electrons are in the lower subband. The energy is shifted to lower energies, if all electrons are in the upper subband. Due to the **k**-dependence of the Coulomb matrix elements and much more important the occupation numbers, the shift is strongly **k**-dependent. This means, that even if the initial transition energy can be considered as almost (or completely) **k**-independent, the actual transition energy is **k**-dependent due to Coulomb interaction. Besides the **k**-dependence the renormalized transition energy is dependent on well width, temperature, carrier density and - depending on the excitation strength - also on time. Including the exchange contribution in the theory, we thus consider that due to the interaction of electrons inside one subband, the electrons can occupy energetically more favorable states which yields a lowering of the corresponding energy subband. If the interacting electrons are in the lower subband, the energy difference of the two subbands is thus increased, if they occupy the upper subband, the transition energy is decreased. The whole process is slightly reduced by the possibility of electrons interacting in different subbands. In the following, the impact of the exchange shift is investigated. Therefore, we expand the theory for single-particle excitations by including additionally the exchange contribution in equations of motion for the intersubband coherence

$$\frac{\mathrm{d}}{\mathrm{d}t}p^{12}_{\mathbf{k},\sigma} \approx \frac{\mathrm{d}}{\mathrm{d}t}p^{12}_{\mathbf{k},\sigma}|_0 + \frac{\mathrm{d}}{\mathrm{d}t}p^{12}_{\mathbf{k},\sigma}|_{\mathrm{cf}} + \left.\frac{\mathrm{d}}{\mathrm{d}t}p^{12}_{\mathbf{k},\sigma}\right|_{\substack{\mathrm{mf},\\ A}} - \gamma_p p^{12}_{\mathbf{k},\sigma}\,, \tag{IV.D.7}$$

$$\frac{\mathrm{d}}{\mathrm{d}t}f^{1}_{\mathbf{k},\sigma} \approx \frac{\mathrm{d}}{\mathrm{d}t}f^{1}_{\mathbf{k},\sigma}|_{\mathrm{cf}}\,. \tag{IV.D.8}$$

Linear Regime

In the linear regime, where the populations in the subbands do not change with time, the renormalization is constant in time. In Fig. IV.D.8 and Fig. IV.D.9, we show a comparison of original and renormalized transition energy. In order to visualize the dependencies of the exchange contribution on well width and carrier density, the corresponding values are given for six different quantum well samples: (a) well width $L = 5$nm, (b) $L = 10$nm and (c) $L = 15$nm with carrier densities of $n = 1.2 \times 10^{12}\mathrm{cm}^{-2}$ and $n = 5.0 \times 10^{10}\mathrm{cm}^{-2}$ - always for temperatures $T = 50$ Kelvin (dashed

[1] The impact of mean-fi eld contributions on the *linear gain spectrum* has already been published in [Wal02], some results of the impact on the linear absorption spectra in [FÖ4, WFL$^+$04, WFK04]

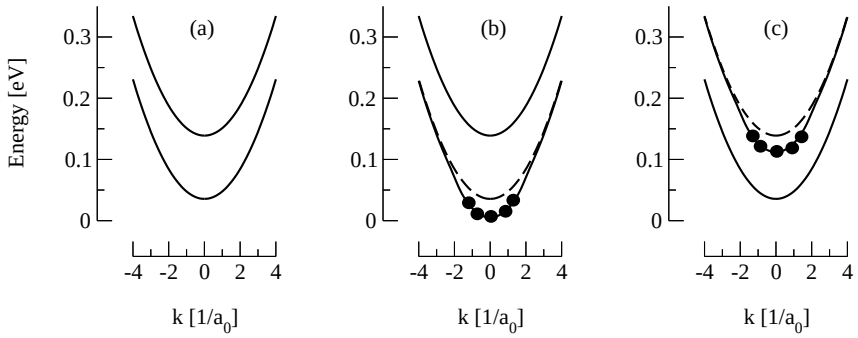

Figure IV.D.7 — Impact of Exchange Contribution: Coulomb interaction renormalizes the initial subband dispersion as the electrons can occupy energetically more favorable states which yields a lowering of the corresponding energy subband. (a) initial subband dispersion, (b, c) effective subband dispersion (solid lines) compared to initial subband dispersion (dashed lines) for (b) all electrons located in the lower subband, (c) all electrons located in the upper subband.

lines) and $T = 300$ Kelvin (dotted lines). In Fig. IV.D.8, the subband dispersion is calculated without respect to nonparabolicity effects (equal subband dispersion), in Fig. IV.D.9 nonparabolicity effects are taken into account (different subband dispersion). Whether nonparabolicity effects are considered or not, does have almost no impact on the shift of transition energy at $\mathbf{k} = 0$. In both cases, the shift is weakest for the wide quantum well and strongest for the small well. For the low temperature of $T = 50$ Kelvin, the shift ranges from about $16 - 17$ meV to $23 - 24$ meV for the high density and only $2 - 3$ meV for the low density. For the higher temperature of $T = 300$ Kelvin, it ranges from 9 meV to 19.3 for the high density and from $0.06 - 0.1$ meV for the low density. In addition to this, the $\mathbf{k}$-dependence of the renormalization is almost the same, although it does appear to preponderate more strongly when the subband dispersions are initially the same. Knowing of the effects of the exchange shift, the consequences for the linear absorption spectra are near at hand. In all cases, the spectra will be overall shifted to higher energies. Furthermore, not only the spectra of quantum wells with *initially different* subband dispersion but also the spectra of quantum wells with *initially equal* subband dispersion will be broadened inhomogeneously. The effects will be strongest for small wells with high carrier density and low temperature. The corresponding spectra are given in Fig. IV.D.11 and Fig. IV.D.10. For comparison the corresponding free-carrier spectra are plotted as well.

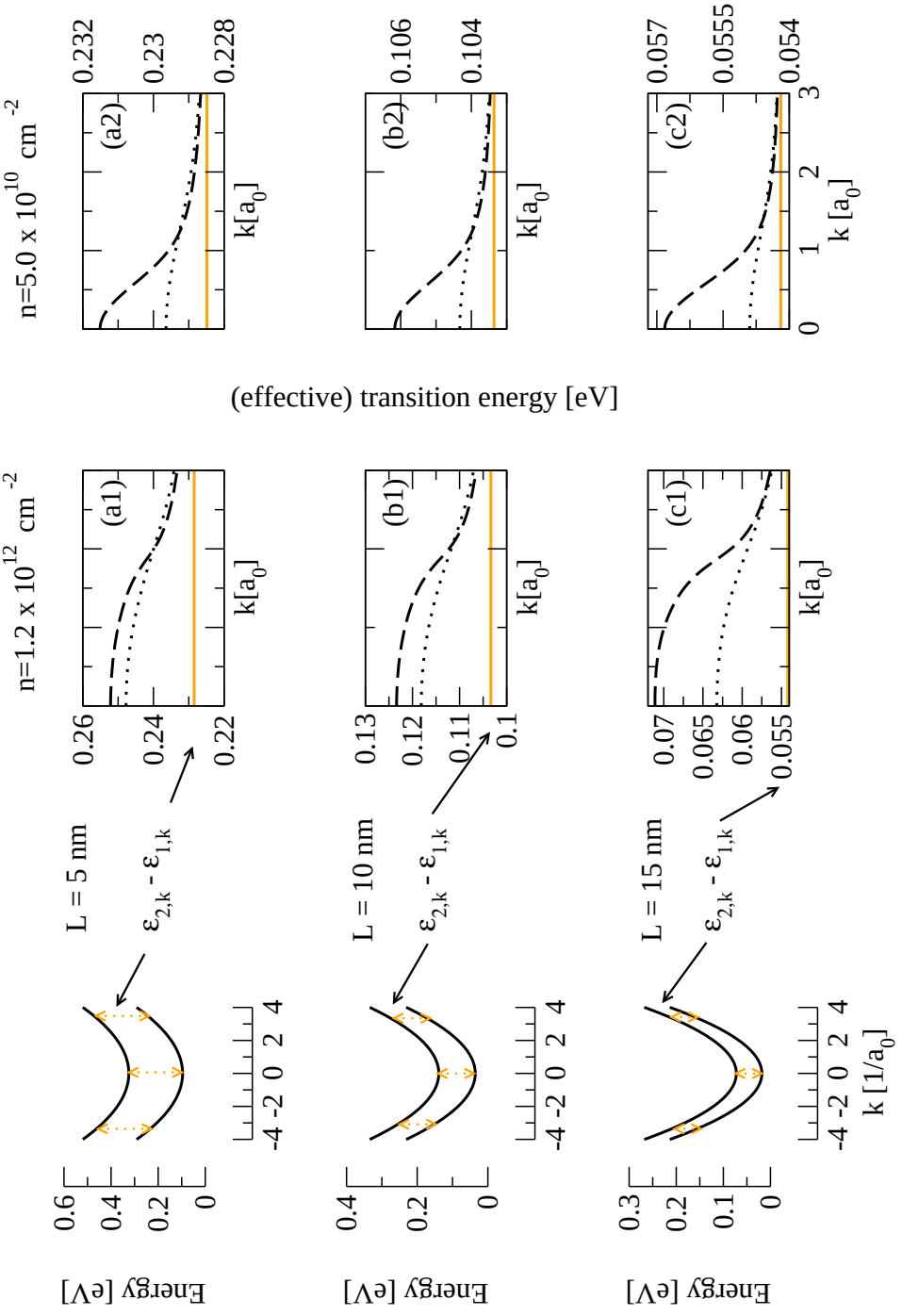

Figure IV.D.8 — Effective transition energy (Equal Subband Dispersion): **k**-dependent renormalization of transition energy due to exchange-energy for different carrier density n and well width L: (a) $L = 5$ nm,(b) $L = 10$ nm, (c) $L = 15$ nm. The dashed lines show the original transition energy, $\epsilon_{2,k} - \epsilon_{1,k}$, due to the considered bandstructure. Neglecting possible nonparabolicity effects, as done here, the original transition energy is **k**-independent. The dashed and dotted lines show the effective transition energy, which results, when the exchange contribution is included in the theory for $T = 50$ Kelvin (dashed) and $T = 300$ Kelvin (dotted). Note, that due to the exchange contribution the effective transition energy is now **k**-dependent.

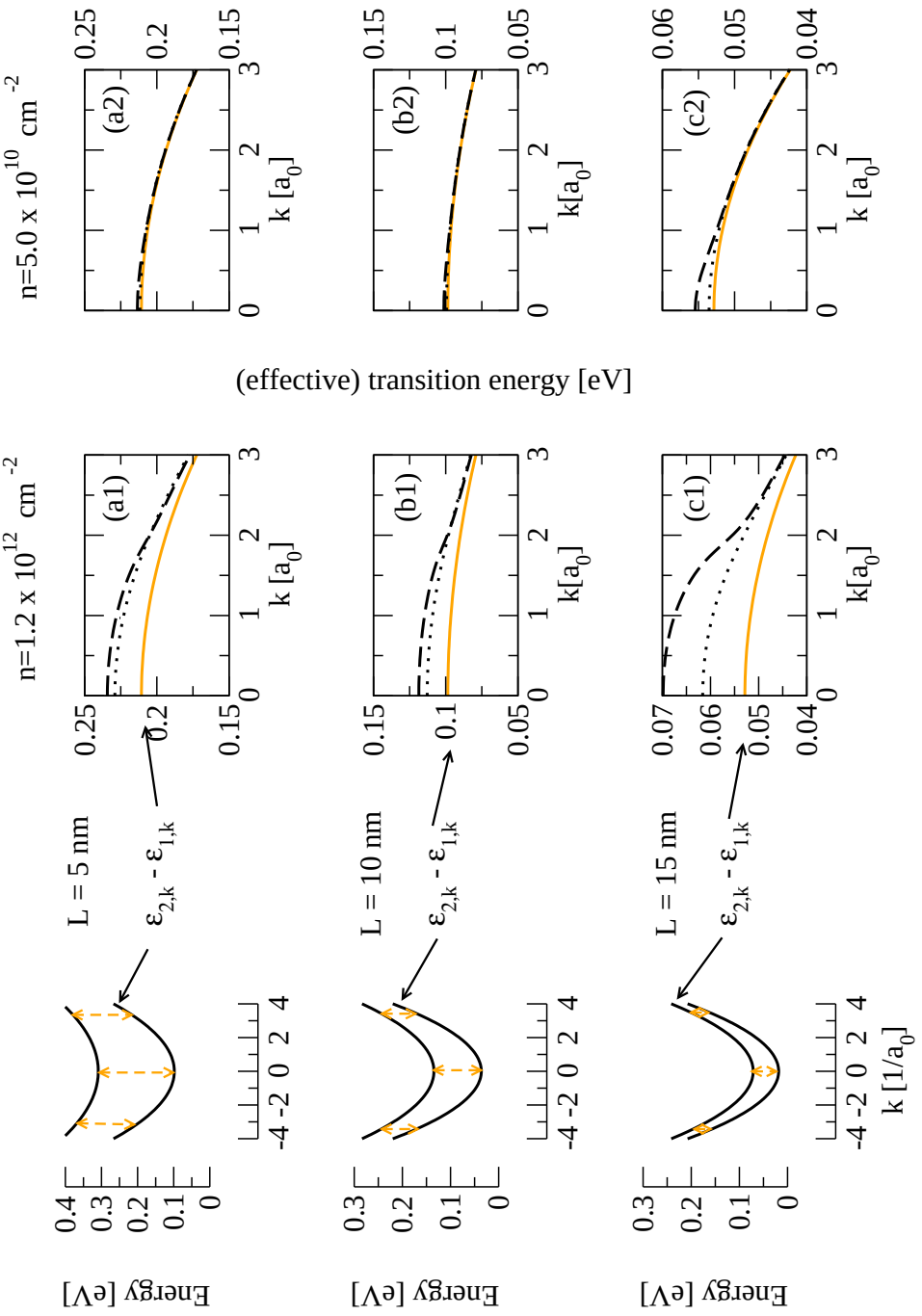

Figure IV.D.9 — Effective transition energy (different subband dispersion): **k**-dependent renormalization of transition energy due to exchange-energy for different carrier density n and well width L: (a) $L = 5$ nm,(b) $L = 10$ nm, (c) $L = 15$ nm. The red, solid lines show the original transition energy, $\epsilon_{2,k} - \epsilon_{1,k}$, due to the considered bandstructure. Considering possible nonparabolicity effects, as done here, the original transition energy is **k**-dependent, strongest for small quantum wells. The dashed and dotted lines show the effective transition energy, which results, when the exchange contribution is included in the theory for $T = 50$ Kelvin (dashed) and $T = 300$ Kelvin (dotted).

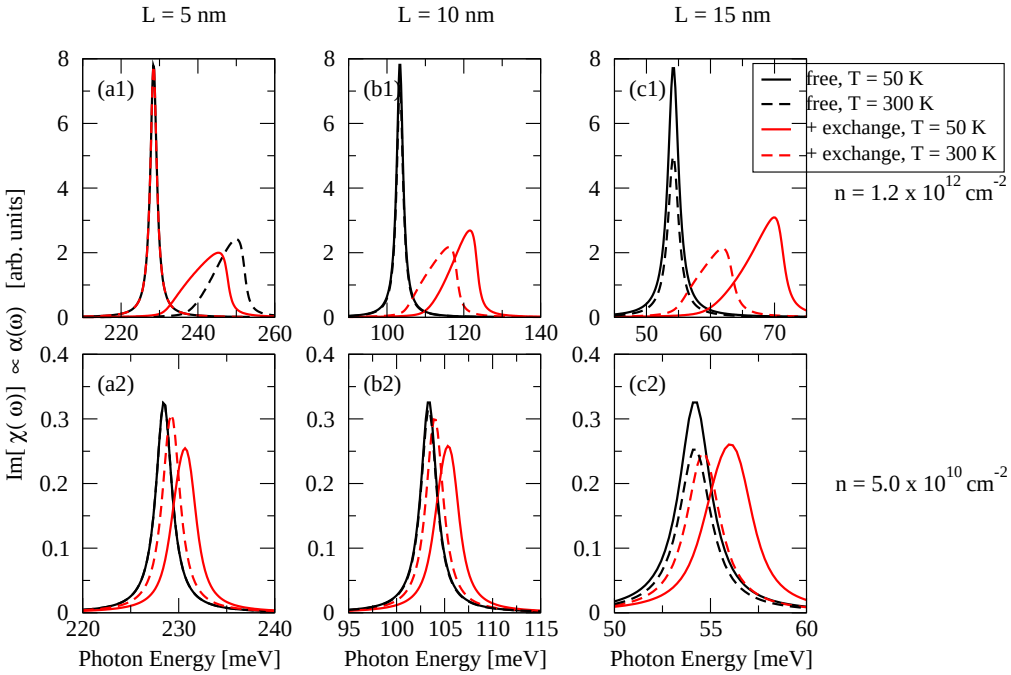

Figure IV.D.10 — Absorption: Inclusion of Exchange Shift (Equal Subband Dispersion): Absorption of a quantum well with carrier density (a1, b1, c1) $n = 1.2 \times 10^{12}\mathrm{cm}^{-2}$, (a2, b2, c2) $n = 5.0 \times 10^{10}\mathrm{cm}^{-2}$ and well width (a) $L = 5$ nm, (b) $L = 10$ nm, (c) $L = 15$ nm assuming equal subband dispersion - without (free) and with inclusion of exchange shift. Due to the **k**-dependent renormalizations of the transition energy (cf. Fig. IV.D.8) the spectra are now inhomogeneously broadened. Furthermore, the absorption peaks are shifted to higher energies.

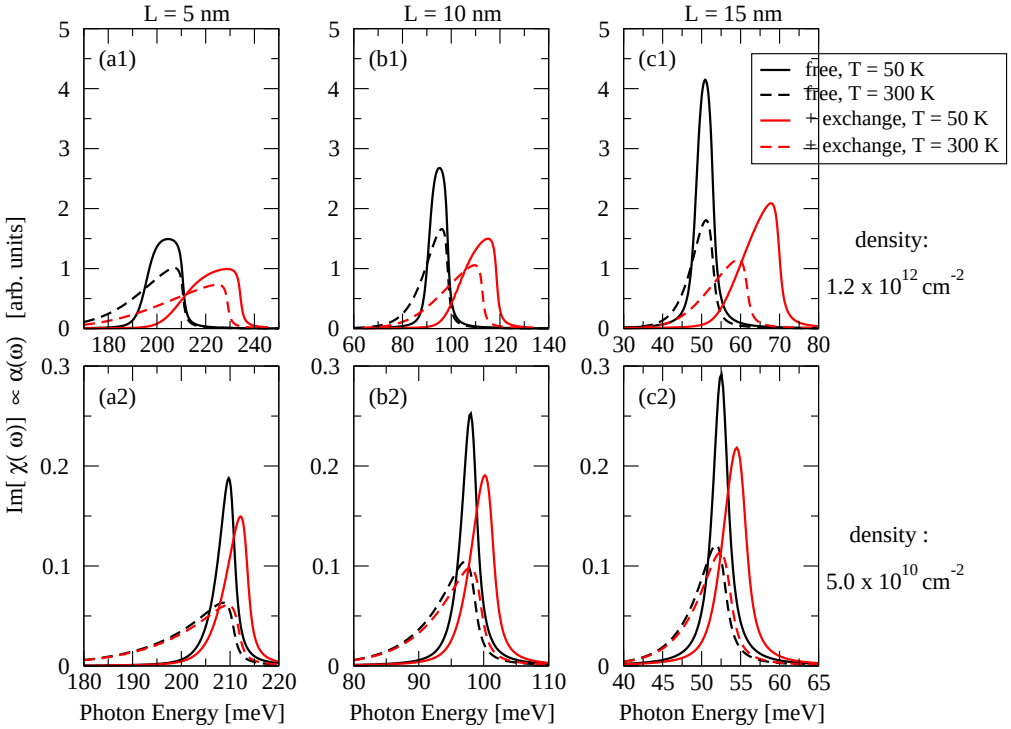

Figure IV.D.11 — Absorption: Inclusion of Exchange Shift (Different Subband Dispersion): Same as in Fig. IV.D.11, but with regard to nonparabolicity effects (different subband dispersion)

Nonlinear Regime

In the nonlinear regime, the impact of the exchange contribution is a little more complicated. Whereas in the linear regime the exchange shift yields a *time-independent* renormalization of the transition energy, since the occupation numbers remain constant by weak excitation, this is not the case in the nonlinear regime. Together with the occupation numbers, the exchange shift is now strongly dependent on time. Thus, the system has a *time-dependent* transition energy and therewith it seems to be impossible to excite resonantly at all times while using a laser field with a time-independent laser frequency ω_L. In addition to this, the $\mathbf{k}$-dependence of the effective transition energy also complicates the excitation of complete Rabi oscillations. To illustrate this, we investigate first the artificial case where the exchange shift is still time-independent, i.e. we approximate the mean-field contribution by

$$\frac{\mathrm{d}}{\mathrm{d}t} p^{12}_{\mathbf{k},\sigma}|^{\mathrm{mf},}_{A} \approx \quad \frac{\mathrm{i}}{\hbar}\Big\{ \sum_{\mathbf{q}} \big[(V^{2222}_{\mathbf{q}} - V^{2112}_{q})\, f^{2}_{\mathbf{k}+\mathbf{q},\sigma}(t_0) \; - (V^{1111}_{q} - V^{2112}_{q})\, f^{1}_{\mathbf{k}+\mathbf{q},\sigma}(t_0) \,\big] \Big\}\, p^{12}_{\mathbf{k},\sigma} \tag{IV.D.9}$$

where t_0 denotes a time before the external excitation sets in.

This is a very rigid approximation and shall only demonstrate that even a time-independent but $\mathbf{k}$-dependent renormalization does change to ability to excite complete Rabi oscillations to some extent. In Fig. IV.D.12, we show the corresponding numerical results for a 10 nm quantum well with carrier density $n = 1.2 \times 10^{12}\mathrm{cm}^{-2}$ and temperature $T = 50$ Kelvin without or with taking into account different subband dispersion. As can be seen in Fig. IV.D.10 (b1) and Fig. IV.D.11 (b1), the linear absorption spectra are in both cases inhomogeneously broadened and the lineshapes differ strongly from a Lorentzian. This is reflected in the oscillations of the population presented in Fig. IV.D.12. Similar to the free-carrier excitation of a quantum well system with subband dispersion, the best oscillation is achieved for excitation slightly detuned to the peak frequency of the linear absorption spectrum. The artificial situation of a time-independent exchange shift, is completely comparable to a quantum well system with initial different subband dispersion. We only have to take into account, that the actual transition energy differs from the initial one.

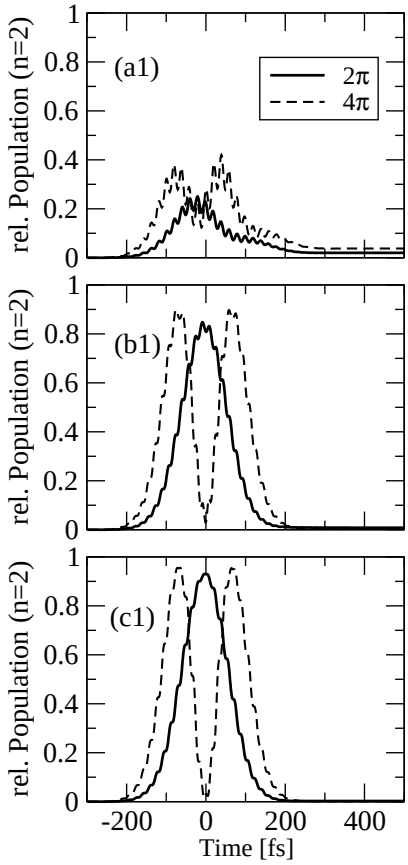

Figure IV.D.12: **Rabi Oscillation with constant exchange contribution:** Artificial situation of a constant exchange contribution [cf. Eq. (IV.D.9)] is comparable to the excitation of a quantum well with initial different subband dispersion.

However, the exchange shift is not time-independent. The occupation numbers are changing with time. The strength of the change of the occupation numbers is strongly connected with the degree of excitation: the change is strongest for strong and resonant excitation. The impact of the exchange shift is therefore connected with the laser frequency or more specific the actual detuning and the pulse duration. Consider the following scenario (we focus on a

quantum well with equal subband dispersion, $n = 1.2 \times 10^{12}\mathrm{cm}^{-2}$, $L = 10$ nm, $T = 50$ K, $\tau = 100$ fs):

- Fig. IV.D.13 (a) we excite the quantum well with a 2π pulse resonant to the *initial transition energy*, i.e. $\hbar\omega_L \approx 0.1036$. Due to the interaction of the electrons in their initial allocation, the actual transition energy at $\mathbf{k} = 0$ is $\hbar\omega_L \approx 0.123$. Thus, we start the external excitation with a detuning of about 20 meV.
- Fig. IV.D.13 (b) we excite the quantum well with a 2π pulse resonant to the *actual transition energy at the beginning of the external excitation*, i.e. $\hbar\omega_L \approx 0.123$. At the beginning of the external excitation, the system is thus excited resonantly.
- Fig. IV.D.13 (c) we excite the quantum well with a 2π pulse with $\hbar\omega_L \approx 0.1105$, thus we start the excitation with a detuning of ≈ 7 meV.

Dependent on the initial detuning and the spectral width of the pulse, the occupation in the upper subband is increased thus yielding a decrease of the actual, effective transition energy. With all electrons in the upper subband, the effective transition energy reaches the minimum value. With increasing depopulation of the upper subband, the transition energy increases again. Thus, the actual transition energy oscillates - the strength of the oscillation is dependent on the oscillations of the population which in turn dependent on the extent of (resonant) excitation. In order to observe complete oscillations of the population, most preferably Rabi oscillations which follow the area theorem, we have in principle to excite the system with a time-dependent laser frequency which balances the associated oscillations of the effective transition energy. If this is not the case, best results are achieved, if the system is excited with a laser frequency settled in the intermediate region of initially transition energy and effective transition energy due to exchange shift at $t = t_0$. In the case of ultrashort excitation, where the exciting pulse is spectrally wide enough to cover a substantial area of the transition range, we thereby can excite almost complete oscillations which are consistent with the area theorem [cf. the oscillations due to exciting with a 4π pulse in Fig. IV.D.13].

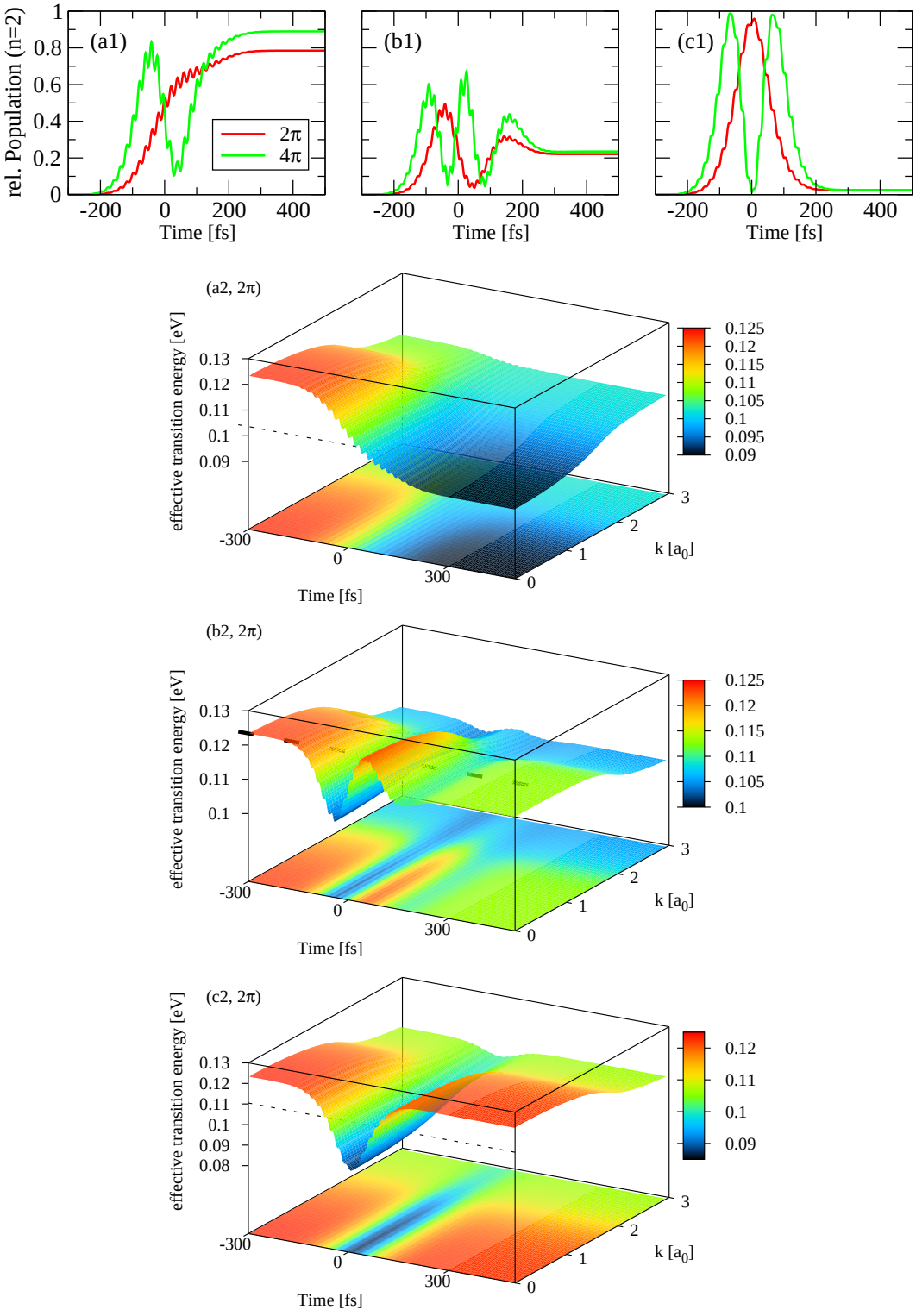

Figure IV.D.13 — Density Oscillations and Time-Dependent Renormalized Transition Energy: (Equal Subband Dispersion) Absorption of a quantum well with carrier density $n = 1.2 \times 10^{12}\mathrm{cm}^{-2}$, well width $L = 10$ nm assuming equal subband dispersion. Same external fi eld as in Fig. IV.D.3 with $\tau = 100$ fs but with different laser frequencies (a1) resonant to the original transition energy, $\hbar\omega_L \approx 0.1036$, (b1) resonant to the renormalized transition energy at $t = t_0$, $\hbar\omega_L \approx 0.123$, (c) intermediate value $\hbar\omega_L \approx 0.1105$

b) Excitonic Contribution

Next, we investigate the impact of the excitonic contribution. Grouping this mean-field contribution together with the carrier-field interaction, we see immediately that the Rabi frequency is renormalized:

$$\begin{aligned}\frac{\mathrm{d}}{\mathrm{d}t}p^{12}_{\mathbf{k},\sigma}|_{\mathrm{cf}} + \left.\frac{\mathrm{d}}{\mathrm{d}t}p^{12}_{\mathbf{k},\sigma}\right|_{\substack{\mathrm{mf},\\ B}} &= \mathrm{i}\Big\{\Omega(t) \\ &\quad + \frac{1}{\hbar}\sum_{\mathbf{q}}\Big[V^{1212}_{q}p^{12}_{\mathbf{k}-\mathbf{q},\sigma} + V^{2112}_{q}p^{21}_{\mathbf{k}-\mathbf{q},\sigma}\Big]\Big\}\,(f^{1}_{\mathbf{k},\sigma} - f^{2}_{\mathbf{k},\sigma}) \\ &= \mathrm{i}\Big\{\Omega(t) + \Omega_{\mathrm{exc}}(t)\Big\}\,(f^{1}_{\mathbf{k},\sigma} - f^{2}_{\mathbf{k},\sigma}) \\ &= \mathrm{i}\,\Omega_{\mathrm{ren}}(t)\,(f^{1}_{\mathbf{k},\sigma} - f^{2}_{\mathbf{k},\sigma}) \qquad \text{(IV.D.10)}\end{aligned}$$

The excitonic contribution yields an internal field, $\Omega_{\mathrm{exc}}(t)$, which renormalizes the external field. The dominant contribution of the internal field is due to inter-intrasubband processes, i.e. two electrons interact in different subbands and remain in the initial subband (intersubband interaction, intrasubband transitions). If an electron is excited from the initially filled lower subband to the upper subband, a "hole" is created in the lower subband. Note that the denotation "hole" is in most cases only applied to the descriptions of carriers in the valence band (electron-hole description). The use of this denotation shall here simply underline, that the excitonic contribution is due to the interaction of electrons in one subband with empty states between electrons in the other subband. Therewith this mean-field contribution is comparable to the interband-exciton [CK99, HK94]. In contrast to interband transitions, which take place between the opposed-curved valence and conduction band, the subbands in the conduction have similar curvature, the subband of the upper band being slightly *larger* than the mass of the lower subband. Consequently, the reduced mass of the "exciton" is negative, the interaction is repulsive [N^{+}97, NIS99]. The repulsive interaction results in a strong redistribution of the oscillator strength, strongest for small quantum wells where the overlap of the wave functions reaches maximal values. With increasing well width, the overlap of the wave functions is reduced, thus the corresponding matrix elements and therewith the impact of the excitonic contribution decrease.

Linear Regime

Similar to the investigation of the exchange contribution, we first examine the impact in the linear regime before exciting the quantum well nonlinearly. Before concentrating on actual absorption spectra, we focus on the strength of the excitonic contribution in Fig. IV.D.14 and Fig. IV.D.15. At the example of a 10 nm quantum well (without nonparabolicity effects in Fig. IV.D.14, with nonparabolicity effects in Fig. IV.D.15) with carrier density $n = 1.2 \times 10^{12}\mathrm{cm}^{-2}$ and temperature $T = 50$ Kelvin, we show the actual impact of the internal field which results from the redistribution of the carriers. For comparison we present in Fig. IV.D.14 (a) the slowly-varying envelope of the initial Rabi frequency in time-domain and in (b) the absolute value of the Fourier transformed Rabi frequency. The real-part of the time-resolved internal field due to the excitonic contribution is given in Fig. IV.D.14 (c). Note that due to the dependence on the complex intersubband coherence p^{ij}_{q}, the local field has also a small imaginary part. However, the real part is the dominant contribution. In congruence with the intersubband coherence, the local field is strongly dependent on the time and the wave vector. For the example presented here, the actual magnitude is similar to that of the initial Rabi frequency. In Fig. IV.D.14 (d), the Fourier transformation of the resulting effective Rabi frequency $\Omega_{\mathrm{ren}}(t)$ shows, that the initial field is almost unaltered for higher in-plane wave vectors $\mathbf{k}$. For wave vectors near the subband edge, where the excitonic contribution is the most effective, the shape of the initial frequency is strongly redistributed. Now a much stronger contribution can be found slightly below the laser frequency [cf. Fig. IV.D.14 (a)] and a second (weaker) contribution located around $\hbar\omega = 85$ meV. Figure IV.D.15 shows the same comparison for a quantum well with different subband dispersion. Similar to IV.D.14 the initial Rabi frequency is almost unaltered

for large wave numbers. For wave number around the subband edge, we again, observe a strong renormalization.

The corresponding linear absorption spectra are presented in Fig. IV.D.16 and Fig. IV.D.17. A comparison of absorption spectra for a variety of quantum wells (well width $L = 5$ nm, 10 nm, 15 nm, carrier density $n = 1.2 \times 10^{12}\mathrm{cm}^{-2}$ and $n = 5.0 \times 10^{10}$) shows that the excitonic contribution is strongest for high carrier densities and low temperatures. Furthermore, the initially very different absorption spectra of quantum wells with or without different subband dispersion have become more akin. Note the small second absorption peak in Fig. IV.D.16 (a1, b1, c1).

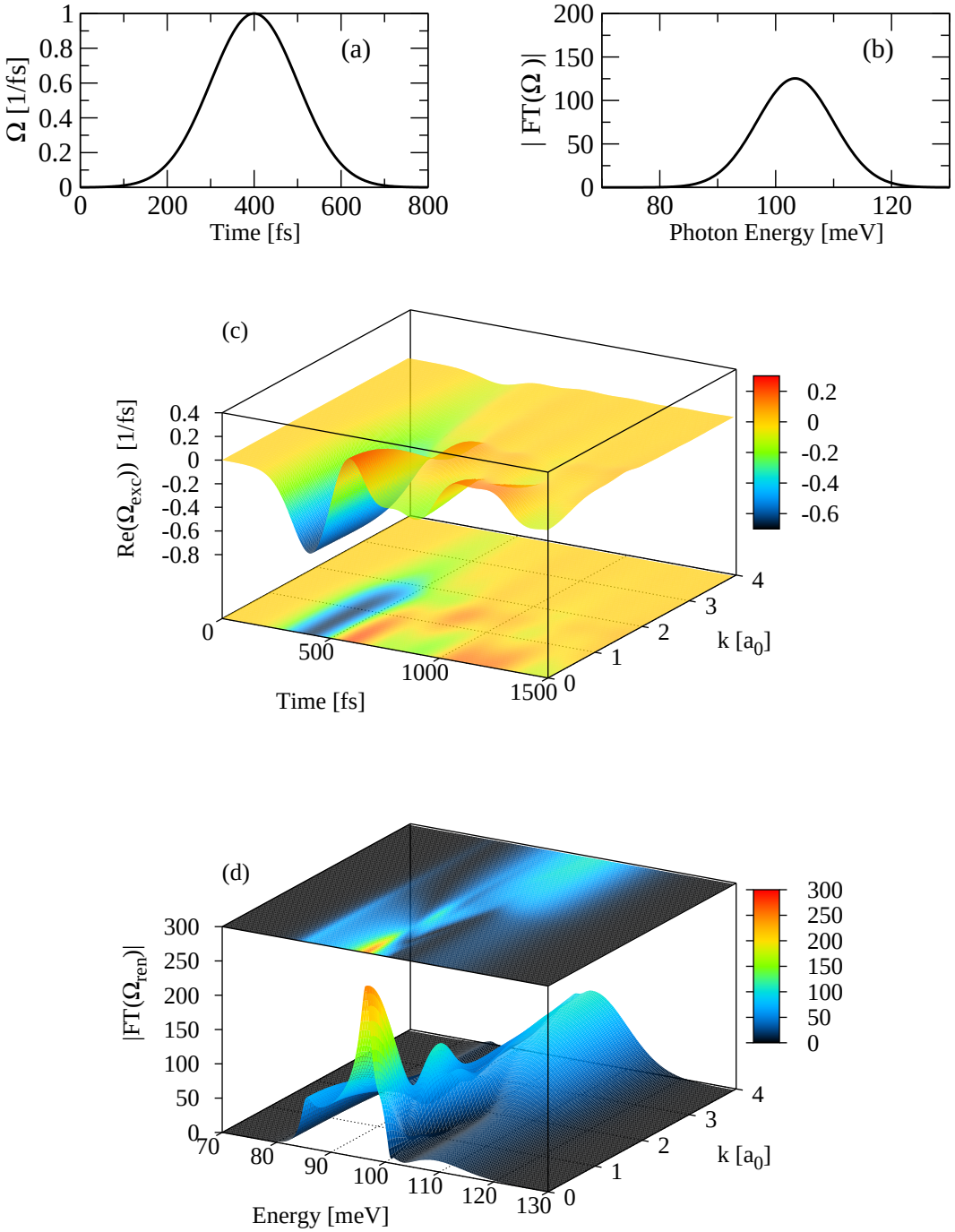

Figure IV.D.14 — Renormalization of Rabi Frequency (Equal Subband Dispersion): (Excitonic Contribution) The excitonic contribution yields a renormalization of the external applied Rabi frequency. Here shown for a quantum well with $n = 1.2\times10^{12}\mathrm{cm}^{-2}$, $L = 10$ nm, $T = 50$ Kelvin with equal subband dispersion. Top: external Rabi frequency $\Omega(t)$ [resonant to the gap-energy]: (a) time-resolved (slowly-varying envelope), (b) in Fourier domain. Middle: (c) time-resolved $\mathbf{k}$-dependent change of Rabi frequency due to excitonic contribution $\Omega_{\mathrm{exc}}(t,\mathbf{k})$. Bottom: (d) Fourier Transform of renormalized $\mathbf{k}$-dependent Rabi frequency $\mathrm{FT}(\Omega_{\mathrm{ren}}(t,\mathbf{k}))$ with $\Omega_{\mathrm{ren}}(t,\mathbf{k}) = \Omega(t) + \Omega_{\mathrm{exc}}(t,\mathbf{k})$

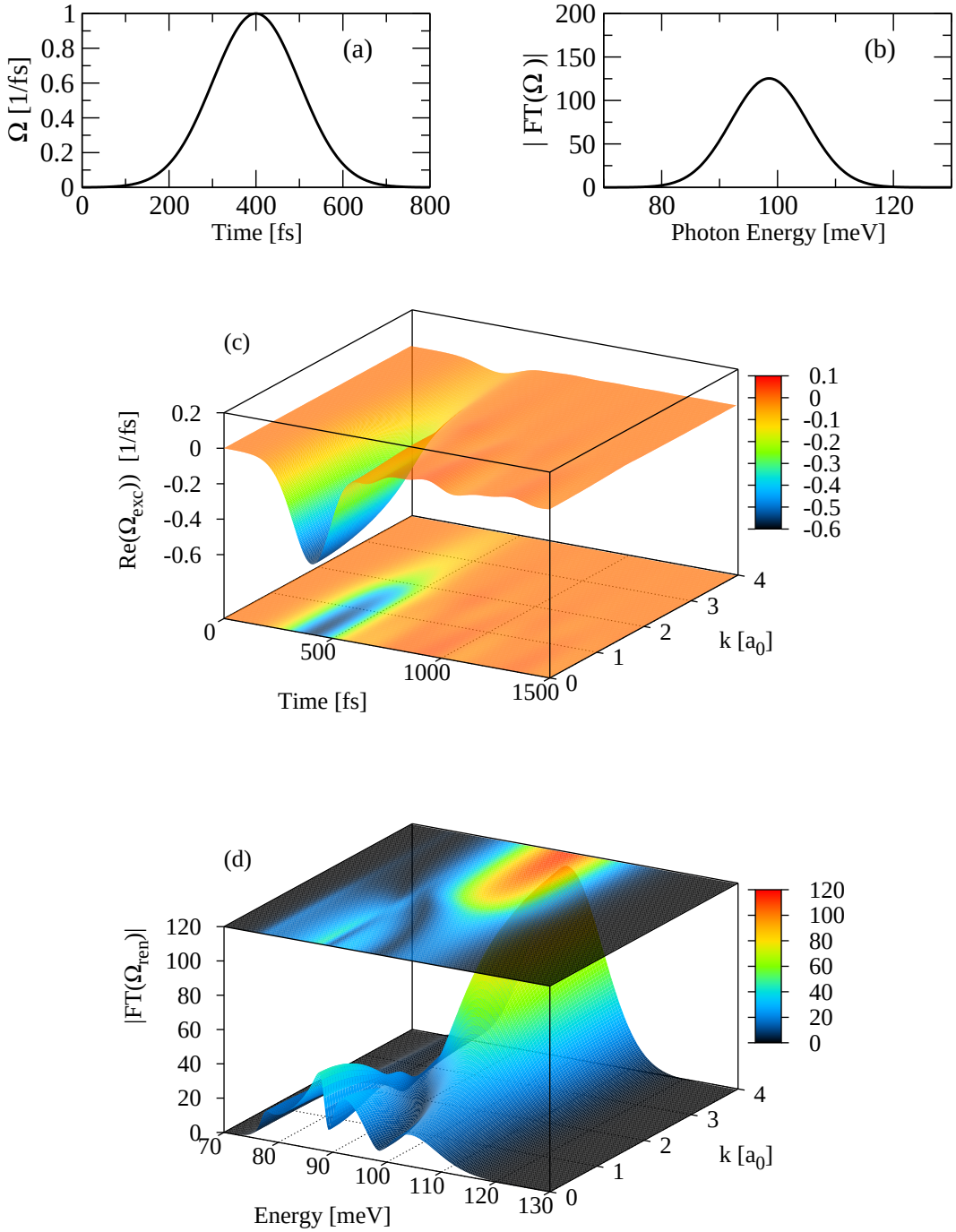

Figure IV.D.15 — Renormalization of Rabi Frequency (Different Subband Dispersion): (Excitonic Contribution) The excitonic contribution yields a renormalization of the external applied Rabi frequency. Here shown for a quantum well with $n = 1.2 \times 10^{12}\mathrm{cm}^{-2}$, $L = 10$ nm, $T = 50$ Kelvin with equal subband dispersion. Top: external Rabi frequency $\Omega(t)$ [resonant to the gap-energy]: (a) time-resolved (slowly-varying envelope), (b) in Fourier domain. Middle: (c) time-resolved $\mathbf{k}$-dependent change of Rabi frequency due to excitonic contribution $\Omega_{\mathrm{exc}}(t, \mathbf{k})$. Bottom: (d) Fourier Transform of renormalized $\mathbf{k}$-dependent Rabi frequency $FT(\Omega_{\mathrm{ren}}(t, \mathbf{k}))$ with $\Omega_{\mathrm{ren}}(t, \mathbf{k}) = \Omega(t) + \Omega_{\mathrm{exc}}(t, \mathbf{k})$

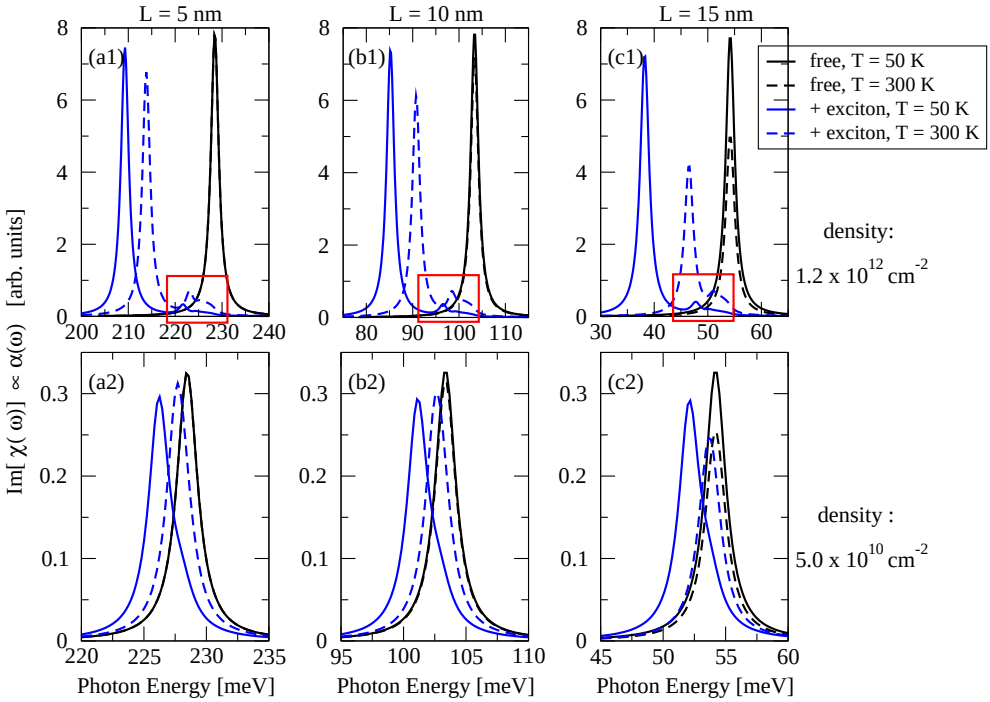

Figure IV.D.16 — Absorption: Inclusion of Excitonic Contribution (Equal Subband Dispersion): Absorption of a quantum well with carrier density (a1, b1, c1) $n = 1.2 \times 10^{12}\mathrm{cm}^{-2}$, (a2, b2, c2) $n = 5.0 \times 10^{10}\mathrm{cm}^{-2}$ and well width (a) $L = 5$ nm, (b) $L = 10$ nm, (c) $L = 15$ nm with equal subband dispersion - without (free) and with inclusion of excitonic contribution.

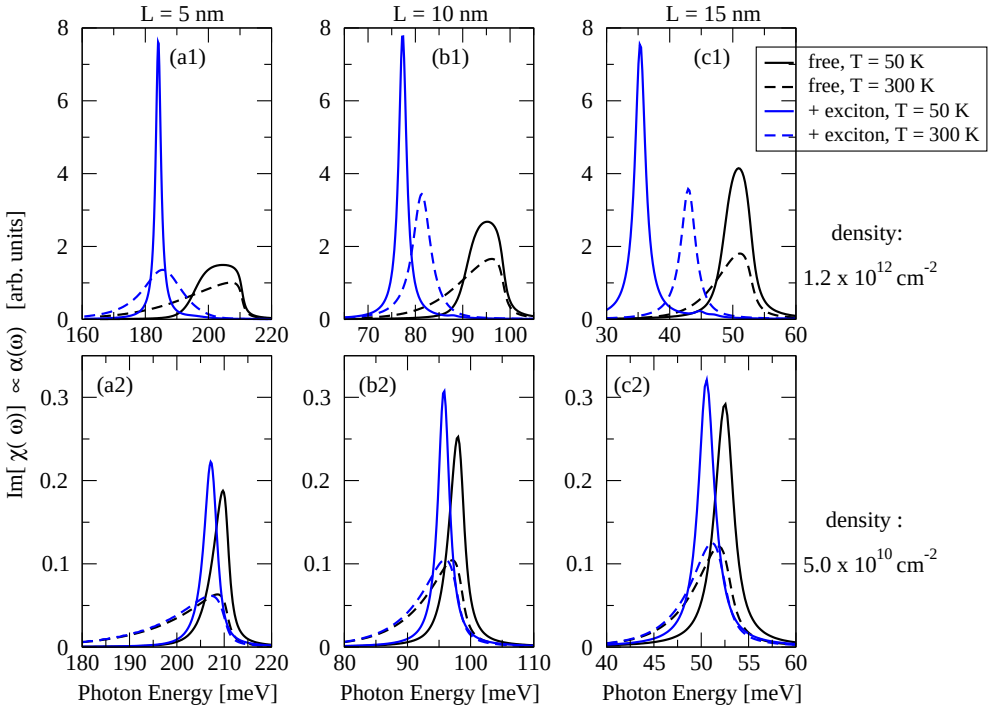

Figure IV.D.17 — Absorption: Inclusion of Excitonic Contribution (Different Subband Dispersion): Absorption of a quantum well with carrier density (a1, b1, c1) $n = 1.2 \times 10^{12}\mathrm{cm}^{-2}$, (a2, b2, c2) $n = 5.0 \times 10^{10}\mathrm{cm}^{-2}$ and well width (a) $L = 5$ nm, (b) $L = 10$ nm, (c) $L = 15$ nm with different subband dispersion - without (free) and with inclusion of excitonic contribution.

Nonlinear Regime

For the case of nonlinear excitation, the excitonic contribution now yields oscillating internal fields. Analogous to the lines of Chapter IV.D.3.a.2, we try nevertheless to excite the quantum well in the aspiration to detect Rabi oscillations - despite the excitonic contributions. As we have already seen in the linear regime, the internal field is dependent on both wave vector and time. Due to the dependence of the excitonic contribution on the intersubband coherence which in turn is driven by the Rabi frequency, the renormalized Rabi frequency now also depends on the laser frequency and the pulse duration of the incident field. Similar to the investigation of the exchange contribution, we first examine the relative population if the system is excited resonant to the initial transition frequency, i.e, $\hbar\omega_L \approx 0.103$ eV. In this case, the renormalized Rabi frequency is almost bisected at wave vectors near the subband edge, which are the most populated ones for the low temperature considered here. The bisected Rabi frequency can also be seen in the bisected Rabi oscillations presented in Fig. IV.D.18 (a1). Second, we excite resonantly to the peak position of the corresponding linear absorption spectrum, i.e., $\hbar\omega_L \approx 0.085$ eV, which yields almost the opposed result: a strongly enhanced Rabi frequency and more, albeit suppressed, density oscillations [cf. Fig. IV.D.18 (b1, b2)]. Again, excitation at an intermediate frequency ($\hbar\omega_L \approx 0.096$ eV) yields almost perfect Rabi oscillations - despite the inclusion of the collective excitonic contribution.

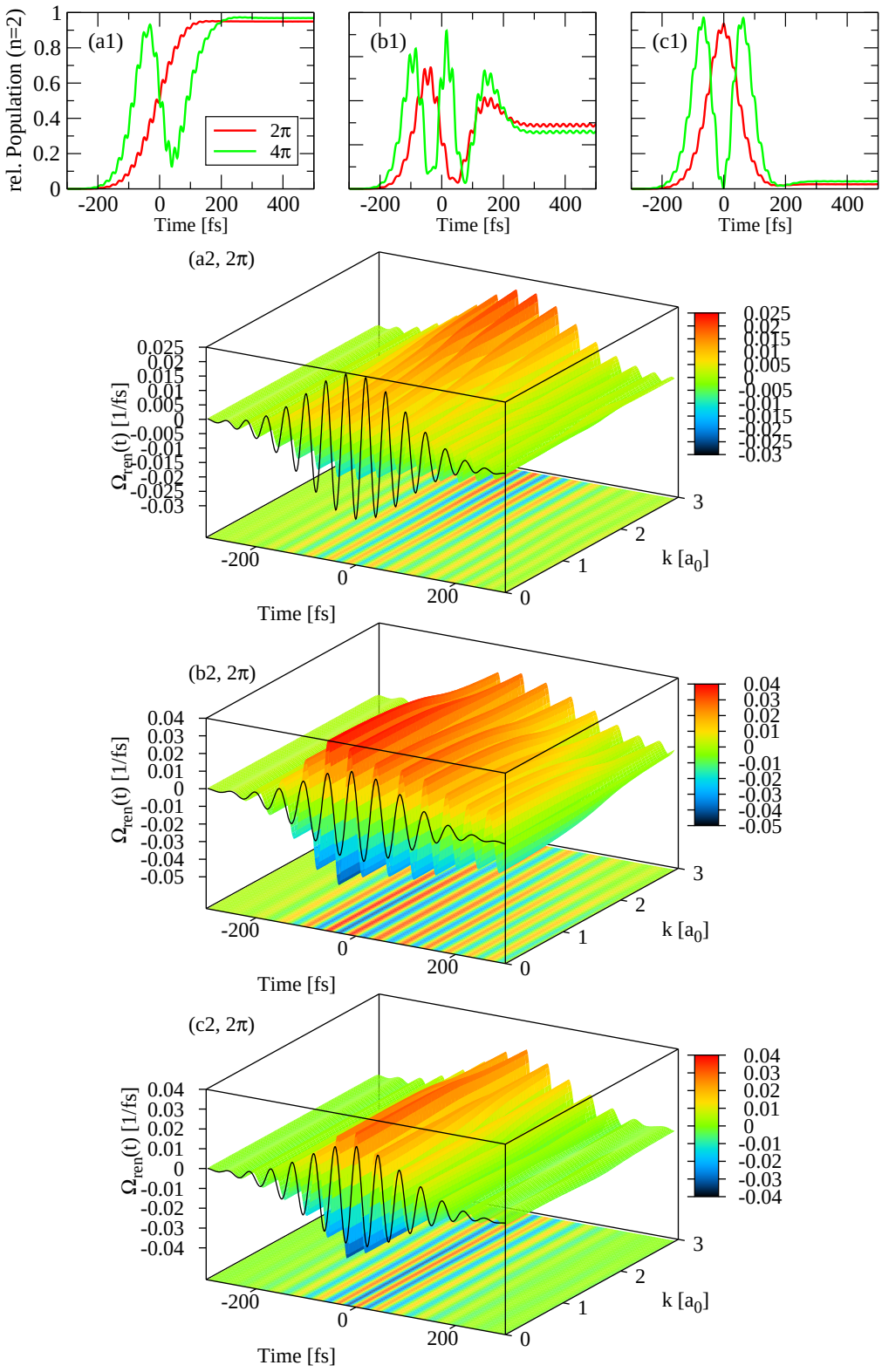

Figure IV.D.18 — Impact of Exc. Contribution in Nonlinear Regime (Equal Subband Dispersion): Density Oscillations of a quantum well with $n = 1.2 \times 10^{12}\mathrm{cm}^{-2}$, $L = 10$ nm, $T = 50$ K. Top: relative population in upper subband for excitation with 2π and 4π pulse and different laser frequencies (a1) resonant to the original transition energy, $\hbar\omega_L \approx 0.10336$ eV, (b1) resonant to the linear absorption spectrum [cf. Fig. IV.D.2], $\hbar\omega_L \approx 0.085$ eV [cf. Fig. IV.D.16], (c) $\hbar\omega_L \approx 0.096$ eV. For the 2π pulse the corresponding renormalized Rabi frequencies and the initial Rabi frequency (thin black line in front) are plotted below.

c) Depolarization

Last, the impact of the depolarization effect shall be examined. Grouping this mean-field contribution together with the carrier-field interaction, we see immediately that here also the Rabi frequency is renormalized by the carrier-carrier interaction:

$$\begin{aligned}\frac{\mathrm{d}}{\mathrm{d}t}p^{12}_{\mathbf{k},\sigma}|_{\mathrm{cf}} + \frac{\mathrm{d}}{\mathrm{d}t}p^{12}_{\mathbf{k},\sigma}|_{\underset{C}{\mathrm{mf},}} &= \mathrm{i}\Big\{\Omega(t) \\ &\quad - \frac{1}{\hbar}V_0^{2112}\sum_{\mathbf{k}_a,\sigma_a}\left[p^{12}_{\mathbf{k}_a,\sigma_a} + p^{21}_{\mathbf{k}_a,\sigma_a}\right]\Big\}(f^1_{\mathbf{k},\sigma} - f^2_{\mathbf{k},\sigma}) \\ &= \mathrm{i}\Big\{\Omega(t) + \Omega_{\mathrm{dep}}(t)\Big\}(f^1_{\mathbf{k},\sigma} - f^2_{\mathbf{k},\sigma}) \\ &= \mathrm{i}\ \Omega_{\mathrm{ren}}(t)(f^1_{\mathbf{k},\sigma} - f^2_{\mathbf{k},\sigma}) \end{aligned} \tag{IV.D.11}$$

Although the effective impact, namely a renormalization of the Rabi frequency, is comparable to that of the excitonic contribution, the background of this contribution is a very different one [N$^+$97, Zal91, LN03]. The depolarization effect is caused by the inhomogeneous carrier distribution in the semiconductor and the overall contribution is therefore directly proportional to the difference of the carrier population in the lower subband, n_1, and the upper subband n_2:

$$\begin{aligned}\sum_{\mathbf{k},\sigma}\frac{\mathrm{d}}{\mathrm{d}t}p^{12}_{\mathbf{k},\sigma}|_{\underset{C}{\mathrm{mf},}} &= -\frac{\mathrm{i}}{\hbar}V_0^{2112}\sum_{\mathbf{k}_a,\sigma_a}\left[p^{12}_{\mathbf{k}_a,\sigma_a} + p^{21}_{\mathbf{k}_a,\sigma_a}\right]\sum_{\mathbf{k},\sigma}(f^1_{\mathbf{k},\sigma} - f^2_{\mathbf{k},\sigma}) \\ &= -\frac{\mathrm{i}}{\hbar}V_0^{2112}\sum_{\mathbf{k}_a,\sigma_a}\left[p^{12}_{\mathbf{k}_a,\sigma_a} + p^{21}_{\mathbf{k}_a,\sigma_a}\right](n_1 - n_2)\,. \end{aligned} \tag{IV.D.12}$$

It can be shown, that the depolarization contribution is equivalent to the longitudinal part of the electric field [cf. Chapter V] [WFK04, WFL$^+$04]. In contrast to the excitonic contribution, the impact of the depolarization contribution increases with increasing well width [GSKB00, TRN$^+$00] and does yield an internal field *independent* of the wave number.

Linear Regime

An example of the renormalization of the Rabi frequency due to the depolarization contribution is given in Fig. IV.D.19 for a 10 nm quantum well with equal subband dispersion and in Fig. IV.D.20 for a well with different subband dispersion. As can be seen by direct comparison of the resulting contributions, the impact of the depolarization is strongest for quantum wells with different subband dispersion and counteracts the otherwise dominating inhomogeneous broadening [WGW$^+$96, Zal84]. The overall effect can best be observed by comparison of the Fourier transformation of the initial and the renormalized Rabi frequency [cf. Fig. IV.D.19 (b, d) and Fig. IV.D.20 (b, d)], which demonstrates the resulting shift to higher frequencies and in the case of a quantum well with subband dispersion, additionally, the almost trebled maximum value. The resulting absorption spectra are presented in Fig. IV.D.21 and Fig. IV.D.23, showing clearly the dependence on well width, carrier density and subband dispersion.

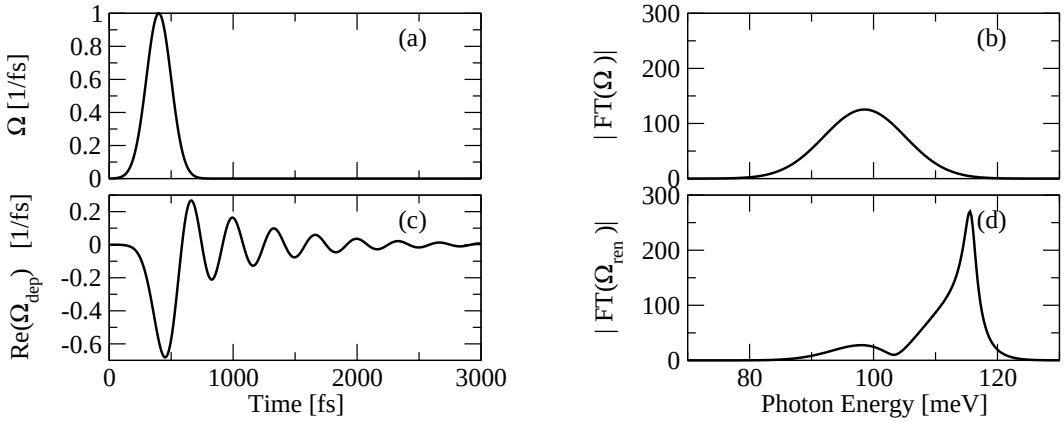

Figure IV.D.19 — Renormalization of Rabi Frequency (Equal Subband Dispersion): (Depolarization) Renormalization of the external applied Rabi frequency due to depolarization effect. Here shown for a quantum well with $n = 1.2 \times 10^{12}\mathrm{cm}^{-2}$, $L = 10$ nm, $T = 50$ Kelvin with equal subband dispersion. Top: external Rabi frequency $\Omega(t)$ [resonant to the gap-energy]: (a) time-resolved (slowly-varying envelope), (b) in Fourier domain. Middle: (c) time-resolved $\mathbf{k}$-dependent change of Rabi frequency due to depolarization $\Omega_{\mathrm{dep}}(t, \mathbf{k})$. Bottom: (d) Fourier Transform of renormalized $\mathbf{k}$-dependent Rabi frequency $\mathrm{FT}(\Omega_{\mathrm{ren}}(t, \mathbf{k}))$ with $\Omega_{\mathrm{ren}}(t, \mathbf{k}) = \Omega(t) + \Omega_{\mathrm{dep}}(t, \mathbf{k})$

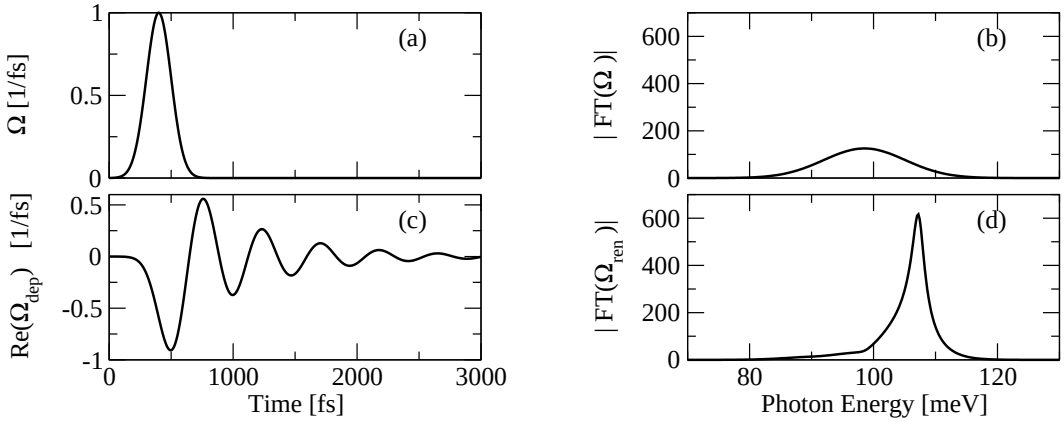

Figure IV.D.20 — Renormalization of Rabi Frequency (Different Subband Dispersion): (Depolarization) Renormalization of the external applied Rabi frequency due to depolarization effect. Here shown for a quantum well with $n = 1.2 \times 10^{12}\mathrm{cm}^{-2}$, $L = 10$ nm, $T = 50$ Kelvin with different subband dispersion. Top: external Rabi frequency $\Omega(t)$ [resonant to the gap-energy]: (a) time-resolved (slowly-varying envelope), (b) in Fourier domain. Middle: (c) time-resolved $\mathbf{k}$-dependent change of Rabi frequency due to depolarization $\Omega_{\mathrm{dep}}(t, \mathbf{k})$. Bottom: (d) Fourier Transform of renormalized $\mathbf{k}$-dependent Rabi frequency $\mathrm{FT}(\Omega_{\mathrm{ren}}(t, \mathbf{k}))$ with $\Omega_{\mathrm{ren}}(t, \mathbf{k}) = \Omega(t) + \Omega_{\mathrm{dep}}(t, \mathbf{k})$

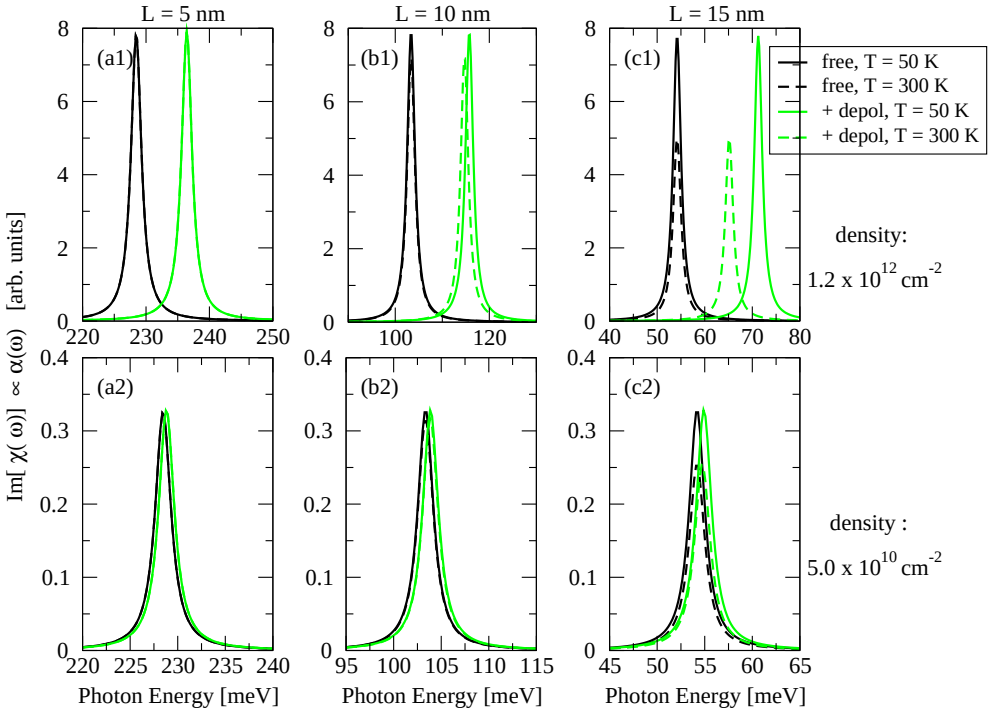

Figure IV.D.21 — Absorption: Inclusion of Depolarization (Equal Subband Dispersion): Absorption of a quantum well with carrier density (a1, b1, c1) $n = 1.2 \times 10^{12}\mathrm{cm}^{-2}$, (a2, b2, c2) $n = 5.0 \times 10^{10}\mathrm{cm}^{-2}$ and well width (a) $L = 5$ nm, (b) $L = 10$ nm, (c) $L = 15$ nm with equal subband dispersion - without (free) and with inclusion of depolarization.

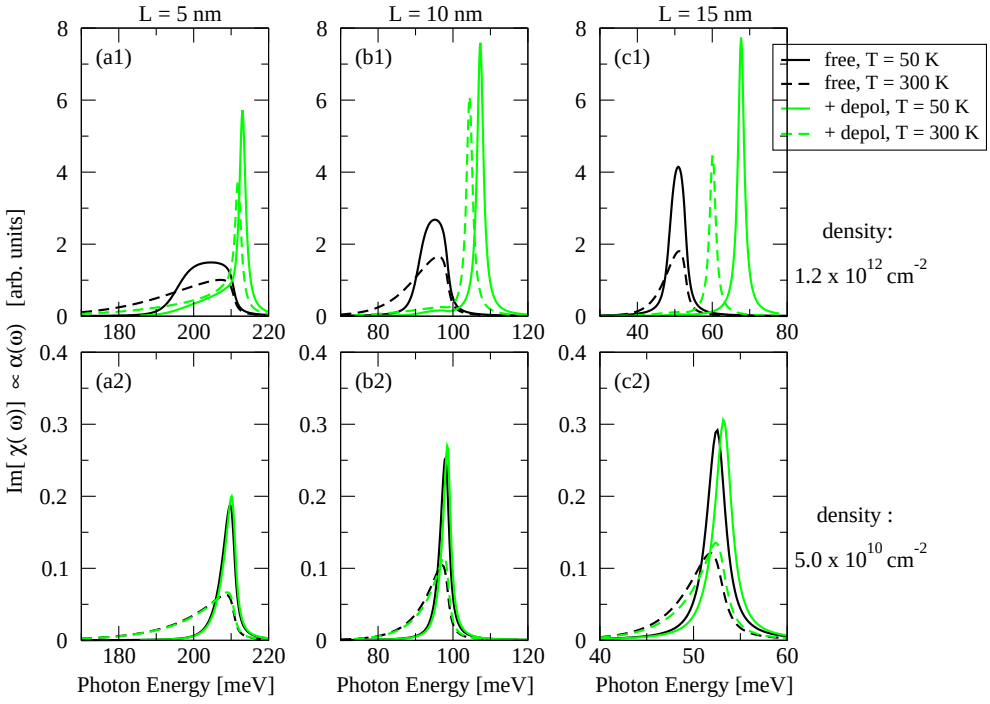

Figure IV.D.22 — Absorption: Inclusion of Depolarization (Different Subband Dispersion): Absorption of a quantum well with carrier density (a1, b1, c1) $n = 1.2 \times 10^{12}\mathrm{cm}^{-2}$, (a2, b2, c2) $n = 5.0 \times 10^{10}\mathrm{cm}^{-2}$ and well width (a) $L = 5$ nm, (b) $L = 10$ nm, (c) $L = 15$ nm with different subband dispersion - without (free) and with inclusion of depolarization.

Nonlinear Regime

Considering a double quantum well structure with equal subband dispersion, Batista et. al. showed very recently [cf. [BC04]] the impact of the depolarization effect on density oscillations excited by pulses with a pulse duration of roughly 15 ps. They showed, that even for excitation with comparatively long pulses Rabi oscillations can in principle be detected the oscillations of the internal field are balanced by using chirped excitation pulses. As we can see in Fig. IV.D.23, for the parameter range considered here, i.e. excitation pulses with pulse duration $\tau \approx 100$ fsec, that the impact of the depolarization contribution can - similar to the other mean-field contributions - already be balanced by using a detuned pulse.

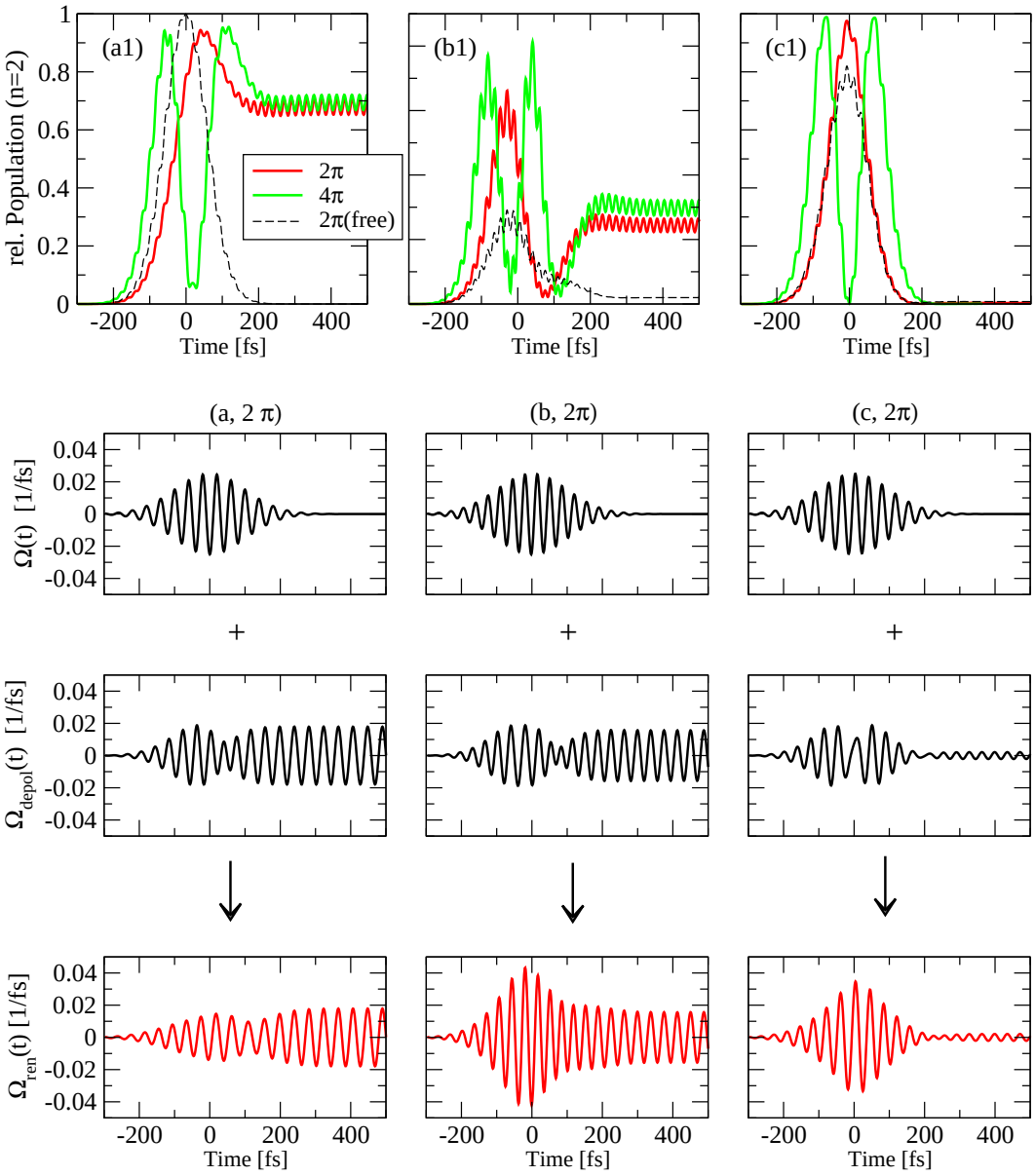

Figure IV.D.23 — Impact of Depol. Effect in Nonlinear Regime (Equal Subband Dispersion): Density Oscillations of a quantum well with $n = 1.2 \times 10^{12}\mathrm{cm}^{-2}$, $L = 10$ nm, $T = 50$ K. Top: relative population in upper subband for excitation with 2π and 4π pulses and different laser frequencies (a1) resonant to the original transition energy, $\hbar\omega_L \approx 0.10336$, (b1) resonant to the linear absorption spectrum, $\hbar\omega_L \approx 0.118$, (c) $\hbar\omega_L \approx 0.109$. The dashed line show the population for a 2π pulse without considering the depolarization effect. For the 2π pulse the initial Rabi frequency, the contribution due to the depolarization effect and the corresponding renormalized Rabi frequency are plotted below.

d) All Mean-Field Contributions

The impact of the simultaneously inclusion of all mean-field contributions is strongly depend on well width, temperature and carrier density, as can already be anticipated from the dependencies of the various contributions.

Linear Regime

For a quantum well with equal subband dispersion, the actual impact of exchange and excitonic contribution almost completely compensate each other [cf. also the limit considered in Chapter IV.D.1] and the spectra are dominated by the depolarization effect [cf. Fig. IV.D.24]. The same applies for wide quantum wells, where the nonparabolicity of the conduction band has been taken into account [cf. Fig. IV.D.25 (b, c)]. Thus, for this parameter range, the impact of nonparabolicity effects and exchange and excitonic contribution, respectively, on the absorption spectra is almost negligible. For small quantum wells, where the depolarization effects is generally less pronounced and the nonparabolicity effects are getting more important, the resulting absorption spectra differ (a) from absorption spectra including only depolarization effect and (b) also from absorption spectra neglecting nonparabolicity effects [cf. Fig. IV.D.24 (a) and Fig. IV.D.25 (a)].

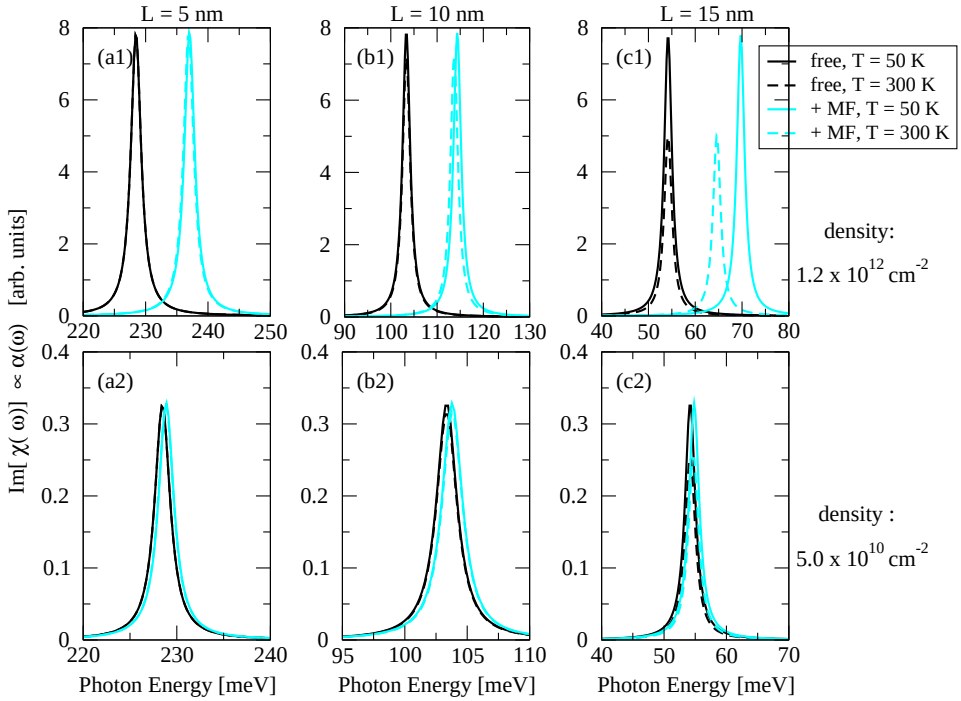

Figure IV.D.24 — Absorption: Inclusion of all Mean-Field Contrib. (Equal Subband Dispersion): Absorption of a quantum well with carrier density (a1, b1, c1) $n = 1.2 \times 10^{12}\mathrm{cm}^{-2}$, (a2, b2, c2) $n = 5.0 \times 10^{10}\mathrm{cm}^{-2}$ and well width (a) $L = 5$ nm, (b) $L = 10$ nm, (c) $L = 15$ nm with equal subband dispersion - without (free) and with inclusion of all mean-fi eld contributions.

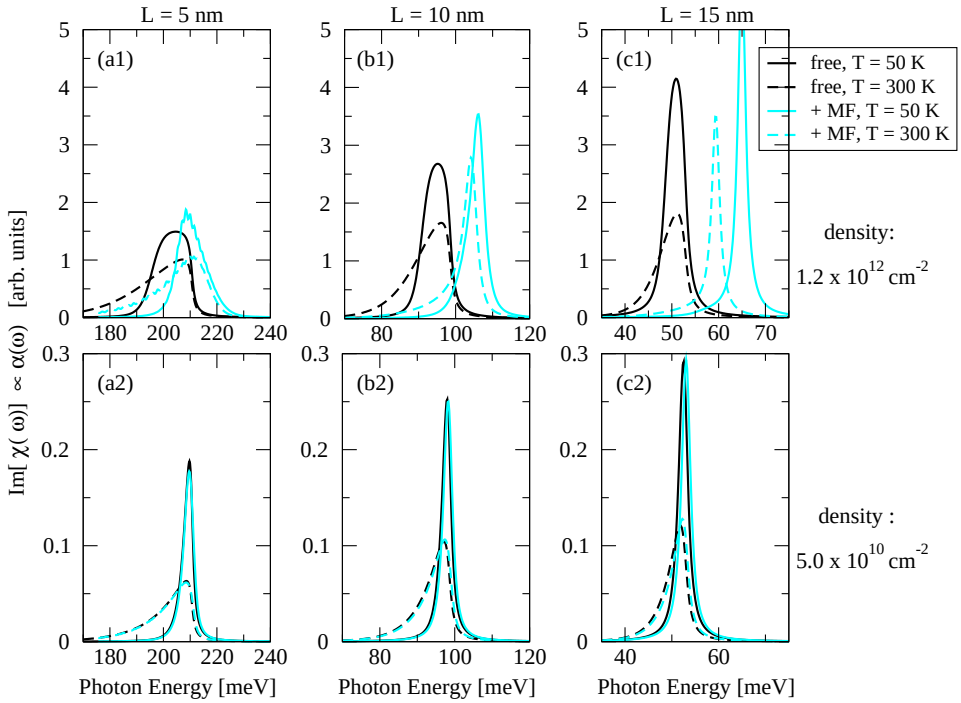

Figure IV.D.25 — Absorption: Inclusion of all Mean-Field Contrib. (Different Subband Dispersion): Absorption of a quantum well with carrier density (a1, b1, c1) $n = 1.2 \times 10^{12}\mathrm{cm}^{-2}$, (a2, b2, c2) $n = 5.0 \times 10^{10}\mathrm{cm}^{-2}$ and well width (a) $L = 5$ nm, (b) $L = 10$ nm, (c) $L = 15$ nm with different subband dispersion - without (free) and with inclusion of all mean-fi eld contributions.

Nonlinear Regime

As in the preceding sections, we want to excite Rabi oscillations of the carrier populations. Preferably, deep Rabi flops, comparable to those observed in the simplified system of non-interacting particles. In the preceding sections, we have seen that we are able to obtain coherent control over Rabi oscillation of electrons as long as they can be considered as non-interacting particles and their transition energy does not depend too strongly on their wave vector. Furthermore, we saw, that we could - under certain conditions - enhance the ability to excite Rabi oscillations even to the situation of interacting particles (in lowest order). However, so far we considered the occurring mean-field contributions only separately. Simply by detuning the laser frequency from the resonance of the corresponding linear absorption spectrum, we could in all occasions recover completely or (almost completely) the Rabi oscillations of the free-carrier model. Even, if the considered mean-field contribution introduced a strong wave vector dependence of either transition energy or Rabi frequency. Admittedly, we should in this context remember that we excited with ultrashort pulses, which still have a considerably spectral width. For longer pulses, which are thus spectrally smaller, the oscillations will be suppressed to some degree. On the other hand, the considered pulse durations are of comparable magnitude to those recently applied in [LRW$^+$04]. Thus, we next include all mean-field contributions simultaneously. This implies, that

- the effective transition energy of the electrons is time and wave-vector dependent
- and simultaneously the effective Rabi frequency is also time and wave-vector dependent.

The linear absorption spectra presented in Fig. IV.D.25 and Fig. IV.D.24 demonstrate that mean-field contributions cancel to some extent and the resulting absorption spectra are less different from the free-carrier absorption if all mean-field effects are included simultaneously than if the contributions are considered separately. However, this does not necessarily mean, that the outcome will be the same in the nonlinear regime. In Fig. IV.D.26 we excite in (a) resonant to the free-carrier absorption and in (b) resonant to the absorption of the corresponding mean-field calculation. Complete oscillations can not be observed. Similar to the results achieved for separate inclusion of the various mean-field contributions, the time and wave vector dependence of renormalized transition energy and effective Rabi frequency is strongly dependent on the laser frequency. Consequently, the strength of the observed oscillations is quite different.

In (c) we then present the results of excitation at the intermediate frequency $\omega_L = 0.1085$ eV. The inclusion of nonparabolicity effects yields only a small suppression of the observed flops, if the sample is again excited with a well-chosen detuning. In conclusion, we can thus state, that it is indeed possible to excite (almost) complete Rabi oscillations, which follow the area theorem - even in the high-carrier regime where (first-order) many-particle effects are in principle dominantly influencing the linear and nonlinear response. The key to the successful excitation can be found in the combination of short pulse duration and deliberately introduced detuning.

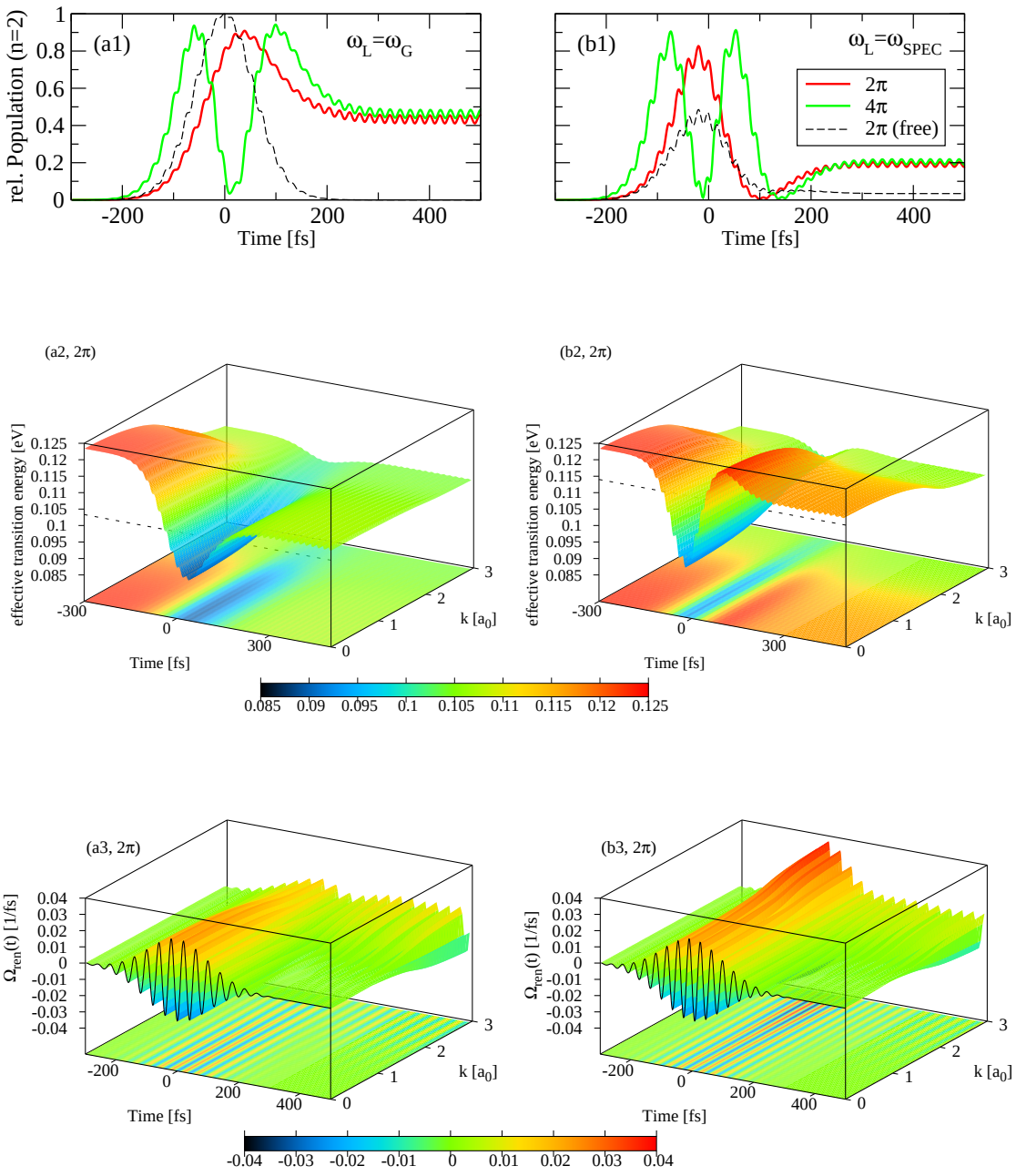

Figure IV.D.26 — Incl. of all Mean-Field Effects (Nonlinear Regime, Equal Subband Dispersion): Nonlinear excitation of a quantum well with $n = 1.2 \times 10^{12}\mathrm{cm}^{-2}$, $L = 10$ nm, $T = 50$ K. Top: relative population in upper subband for excitation with 2π and 4π pulses and different laser frequencies (a1) resonant to the original transition energy, $\hbar\omega_L \approx 0.10336$ eV [cf. Fig. IV.D.2], (b1) resonant to the linear absorption spectrum, $\hbar\omega_L \approx 0.114$ eV [cf. Fig. IV.D.24]. For comparison the free-carrier excitation is plotted for a 2π as well (dashed line). For the 2π pulse the renormalized transition energy and Rabi frequency are plotted in a2(b2) and a3(b3), respectively.

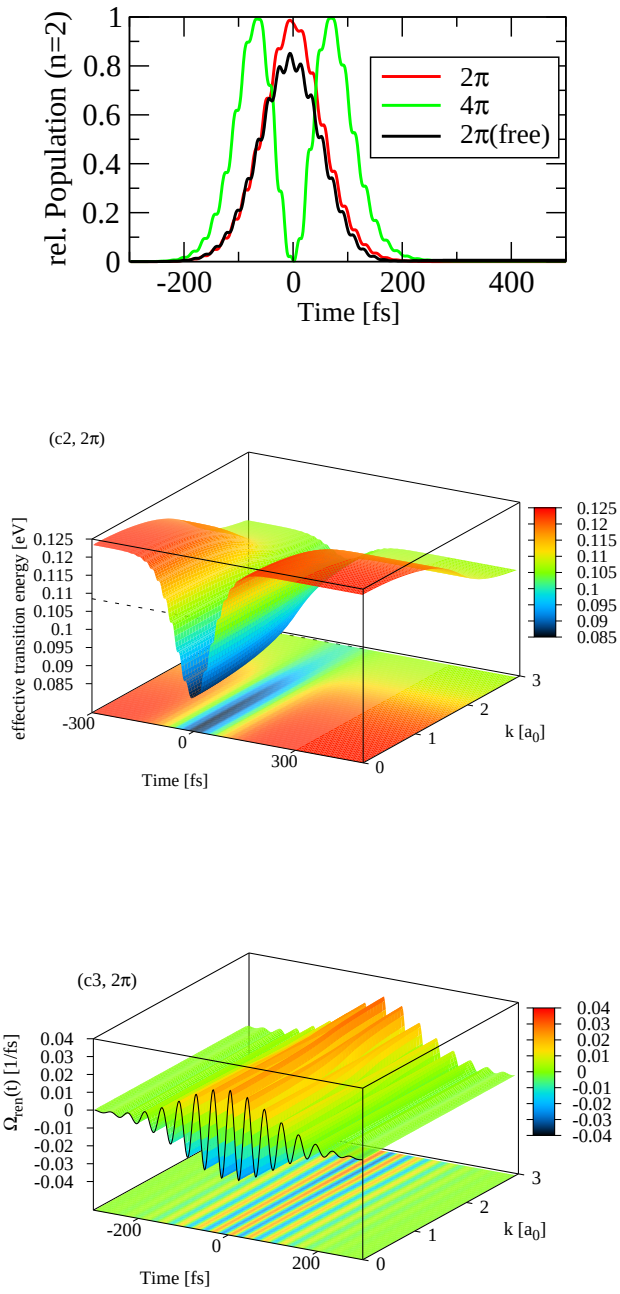

Figure IV.D.27 — Incl. of all Mean-Field Effects (Nonlinear Regime, Equal Subband Dispersion): Same situation as in Fig. IV.D.26, but for excitation at the intermediate frequency $\omega_L = 0.1085$ eV. For comparison the free-carrier excitation is plotted for a 2π as well (dashed line). For the 2π pulse the renormalized transition energy and Rabi frequency are plotted below.

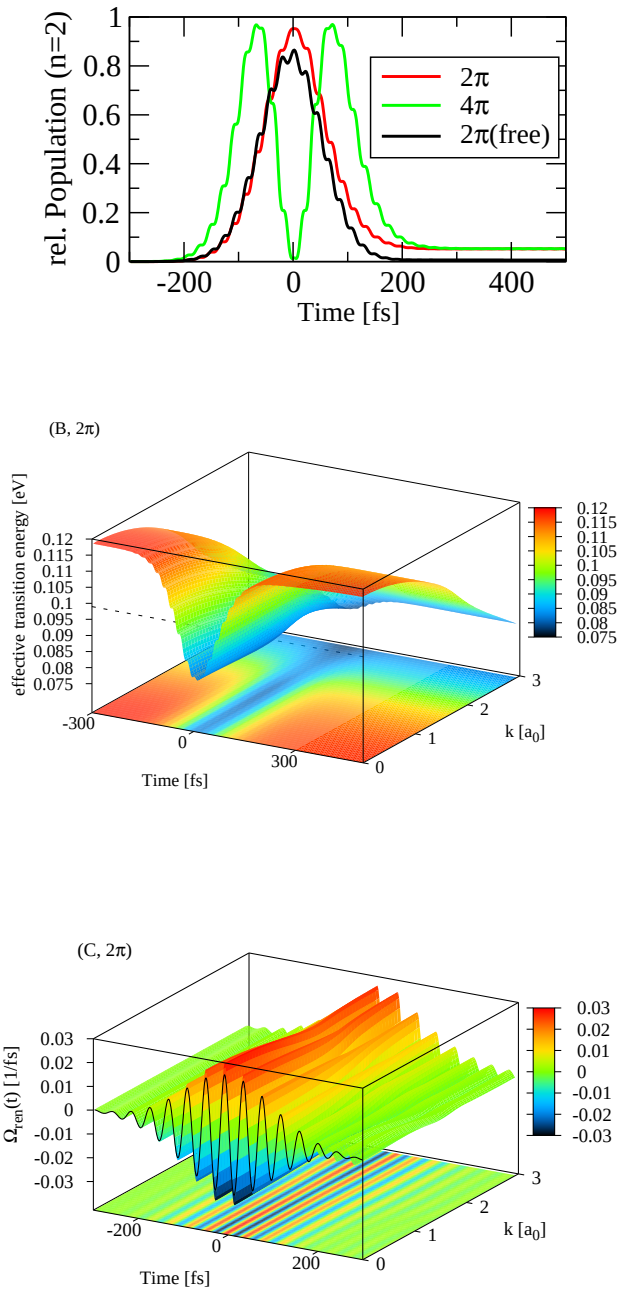

Figure IV.D.28 — Incl. of all Mean-Field Effects (Nonlinear Regime, *Different Subband Disp.*): Same situation as in Fig. IV.D.26, i.e., for excitation at an intermediate frequency (for different subband dispersion the intermediate frequency is $\omega_L = 0.099$ eV). For comparison the free-carrier excitation is plotted for a 2π as well (dashed line). For the 2π pulse the renormalized transition energy and Rabi frequency are plotted below.

4. Correlation Contributions: Carrier-Carrier and Carrier-Phonon Scattering

Up to this moment, we concentrated on the impact of first order correlation contributions. Hence, we either approximated second order contributions by a phenomenological dephasing constant γ_p ($\gamma_p = 1$ meV, linear regime/ absorption spectra) or excluded second order contributions completely from the theory ($\gamma_p = 0$, nonlinear regime/ density oscillations). In the following, these contributions shall now be investigated. As has already been mentioned shortly in Chapter IV B, the correlation contributions in the equation of motion for the intersubband coherence can be divided in three different parts similar to the description of interband transitions [JKK97, BSP$^+$92]

$$\frac{\mathrm{d}}{\mathrm{d}t} p^{21}_{\mathbf{k},\sigma}|_{\text{cc/cp-corr}} = -\frac{\pi}{\hbar}\,\Xi_{\text{d}}(p^{21}_{\mathbf{k}}) + \frac{\pi}{\hbar}\sum_{\mathbf{k}''}\,\Xi_{\text{nd}}(p^{ij}_{\mathbf{k}+\mathbf{k}''}) + \frac{\pi}{\hbar}\Xi_{\text{nl}}, \tag{IV.D.13}$$

namely

- diagonal contributions,

$$\Xi_{\text{d}}(p^{21}_{\mathbf{k}}) = \Gamma_{\text{d}}\, p^{21}_{\mathbf{k}} = \frac{1}{2}\sum_{i=1,2}(\Gamma^{i,\text{cp}}_{\text{d}} + \Gamma^{i,\text{cc}}_{\text{d}})\, p^{21}_{\mathbf{k}}, \tag{IV.D.14}$$

  dependent on the intersubband coherence at same wavenumber, $p^{21}_{\mathbf{k}}$,

- nondiagonal contributions,

$$\begin{aligned}\sum_{\mathbf{k}''}\Xi_{\text{nd}}(p^{ij}_{\mathbf{k}+\mathbf{k}''}) = \quad & \sum_{i=1,2}\left[\sum_{\underline{\mathbf{q}}}\Gamma^{i,\text{cp}}_{\text{nd}}\; p^{21}_{\mathbf{k}+\underline{\mathbf{q}}_{||}} + \sum_{\mathbf{k}',\mathbf{q}}\Gamma^{i,\text{cc}}_{\text{nd1}}\; p^{21}_{\mathbf{k}'-\mathbf{q}} + \sum_{\mathbf{q}}\Gamma^{i,\text{cc}}_{\text{nd2}}\; p^{21}_{\mathbf{k}+\mathbf{q}} - \sum_{\mathbf{k}'}\Gamma^{i,\text{cc}}_{\text{nd3}}\; p^{21}_{\mathbf{k}'}\right] \\ & + \sum_{i=1,2}\left[\sum_{\underline{\mathbf{q}}}\tilde{\Gamma}^{i,\text{cp}}_{\text{nd}}\; \tilde{p}^{12}_{\mathbf{k}+\underline{\mathbf{q}}_{||}} + \sum_{\mathbf{k}',\mathbf{q}}\tilde{\Gamma}^{i,\text{cc}}_{\text{nd1}}\; \tilde{p}^{12}_{\mathbf{k}'-\mathbf{q}} + \sum_{\mathbf{q}}\tilde{\Gamma}^{i,\text{cc}}_{\text{nd2}}\; \tilde{p}^{12}_{\mathbf{k}+\mathbf{q}} - \sum_{\mathbf{k}'}\tilde{\Gamma}^{i,\text{cc}}_{\text{nd3}}\; \tilde{p}^{12}_{\mathbf{k}'}\right],\end{aligned} \tag{IV.D.15}$$

  which couple intersubband coherences at different wave vectors,

- contributions nonlinear in the polarization Ξ_{nl}, which are thus important under nonlinear excitation, where a large induced intersubband polarization is present.

The corresponding equation for the occupation numbers reads

$$\frac{\mathrm{d}}{\mathrm{d}t} f^{i}_{\mathbf{k},\sigma}|_{\text{cc/cp-corr}} = -\frac{\pi}{\hbar} f^{i}_{\mathbf{k},\sigma}\Gamma^{i,\text{out}}_{\text{d}} + \frac{\pi}{\hbar}(1 - f^{i}_{\mathbf{k},\sigma})\Gamma^{i,\text{in}}_{\text{d}} + \Xi_{\text{nl},f_i} \qquad i,j = 1,2;\; i \neq j\,. \tag{IV.D.16}$$

where $\Gamma^{i,\text{in}}_{\text{d}}$denotes the diagonal in-scattering and $\Gamma^{i,\text{out}}_{\text{d}}$ the corresponding diagonal out-scattering rate ($\Gamma^{i}_{\text{d}} = \Gamma^{i,\text{in}}_{\text{d}} + \Gamma^{i,\text{out}}_{\text{d}}$). Ξ_{nl,f_i} denotes the contributions to the equation which are nonlinear in the polarization. The complete diagonal and non-diagonal contributions and the nonlinear contributions Ξ_{nl} and Ξ_{nl,f_i} are given in APP F.

a) Scattering Rates

As an example for the general form of scattering rates we discuss a typical intrasubband rate, taken form the diagonal contribution Γ^{i}_{d}, first for carrier-phonon and afterwards for carrier-carrier scattering.

Carrier-Phonon Scattering Rates

The intrasubband carrier-phonon rate

$$\begin{aligned}\Gamma^{\text{cp}} = \quad & 2\sum_{\underline{\mathbf{q}}}\Big[\delta(-\epsilon^i_{\mathbf{k}}+\epsilon^i_{\mathbf{k}+\underline{\mathbf{q}}_{||}}-\hbar\omega_{LO})|g^{ii}_{\underline{\mathbf{q}}}|^2\left\{n_{\underline{\mathbf{q}}}(1-f^i_{\mathbf{k}+\underline{\mathbf{q}}_{||}})+\left(n_{\underline{\mathbf{q}}}+1\right)f^i_{\mathbf{k}+\underline{\mathbf{q}}_{||}}\right\}\\ & +\delta(-\epsilon^i_{\mathbf{k}}+\epsilon^i_{\mathbf{k}+\underline{\mathbf{q}}_{||}}+\hbar\omega_{LO})|g^{ii}_{\underline{\mathbf{q}}}|^2\left\{\left(n_{\underline{\mathbf{q}}}+1\right)(1-f^i_{\mathbf{k}+\underline{\mathbf{q}}_{||}})+n_{\underline{\mathbf{q}}}f^i_{\mathbf{k}+\underline{\mathbf{q}}_{||}}\right\}\Big]\end{aligned} \tag{IV.D.17}$$

describes scattering events where an electron is scattered in or out a state with vector $\mathbf{k}$ in subband i - either by absorption or emission of a LO-phonon with $3D$ wave vector $\underline{\mathbf{q}}$. In detail, the terms proportional to $(1-f^i_{\mathbf{k}+\underline{\mathbf{q}}_{||}})$ describe the transition from state $\mathbf{k}$ into state $\mathbf{k}+\underline{\mathbf{q}}_{||}$ (out- scattering rate), the terms proportional to $f^i_{\mathbf{k}+\underline{\mathbf{q}}_{||}}$ the transition from state $\mathbf{k}+\underline{\mathbf{q}}_{||}$ into $\mathbf{k}$ (in- scattering rate) -always under emission or absorption of a phonon. As before, $n_{\underline{\mathbf{q}}}$ denotes the phonon population which in bath approximation is given by the Bose function

$$n_{\underline{\mathbf{q}}} = \frac{1}{\mathrm{e}^{\beta\hbar\omega_{LO}-1}}\,. \tag{IV.D.18}$$

The probability for the scattering processes is given by the corresponding Fröhlich matrix elements, which are strongly dependent on wave vector and well width [cf. APP B]. Note, that although the Fröhlich matrix elements are divergent for $\mathbf{q}_{||}=0$, it is not necessary to consider screened matrix elements, as the corresponding contributions cancel. Therefore, the matrix elements will remain unscreened in the scope of this work. An investigation of the impact of static or dynamic screening on the carrier-phonon scattering rates is given in [PAL00, Ahn94]. Due to the Markovian approximation performed in Chapter III.B.4.b, only scattering events which obey strict energy conservation are taken into account. First results of recently performed investigations of carrier-phonon scattering in intersubband transitions with regard to non-Markovian results can be found in [BFWK04, But04, FÖ4]. A small comparison of intrasubband scattering rates, where the electron stays in its initial subband and intersubband scattering rates where the subband is changed, is given in Fig. IV.D.29. These scattering rates are often calculated on the basis of Fermis golden rule [AW97, Har00] and frequently used to introduce dephasing due to carrier-phonon scattering in the framework of a relaxation rate approximation. As we will see in Chapter IV.D.4.b.1 an approximation of this kind overestimates the actual dephasing to a large extent. Note, that these contributions are time-independent only in the linear regime, where for all times the occupation functions f_i can be approximated by Fermi-Dirac distributions. In the nonlinear regime, the electronic occupation functions are time-dependent and thus the scattering rates for the examples presented in Fig. IV.D.29 also vary with time.

Carrier-Carrier Scattering Rates

The diagonal intrasubband carrier-carrier scattering rate for scattering in subband i

$$\begin{aligned}\Gamma^{\text{cc}} = \quad & 2\sum_{\mathbf{k}',\mathbf{q}}\Big[\delta(\epsilon^i_{\mathbf{k}}+\epsilon^i_{\mathbf{k}'}-\epsilon^i_{\mathbf{k}'-\mathbf{q}}-\epsilon^i_{\mathbf{k}+\mathbf{q}})V^{iiii}_{\mathbf{q}}(2V^{iiii}_{\mathbf{q}}-V^{iiii}_{\mathbf{k}'-\mathbf{k}-\mathbf{q}})\\ & \left\{f^i_{\mathbf{k}'}(i-f^i_{\mathbf{k}'-\mathbf{q}})(1-f^i_{\mathbf{k}+\mathbf{q}})+f^i_{\mathbf{k}'-\mathbf{q}}f^i_{\mathbf{k}+\mathbf{q}}(1-f^i_{\mathbf{k}'})\right\}\Big].\end{aligned} \tag{IV.D.19}$$

describes scattering processes of two electrons between states $\mathbf{k},\mathbf{k}',\mathbf{k}+\mathbf{q},\mathbf{k}'-\mathbf{q}$ due to carrier-carrier interaction. Again, the total contributions consists of in- and out-scattering contributions: whereas terms proportional to $(1-f^i_{\mathbf{k}'-\mathbf{q}})(1-f^i_{\mathbf{k}+\mathbf{q}})$ describe scattering from states $\mathbf{k}$ and $\mathbf{k}'$

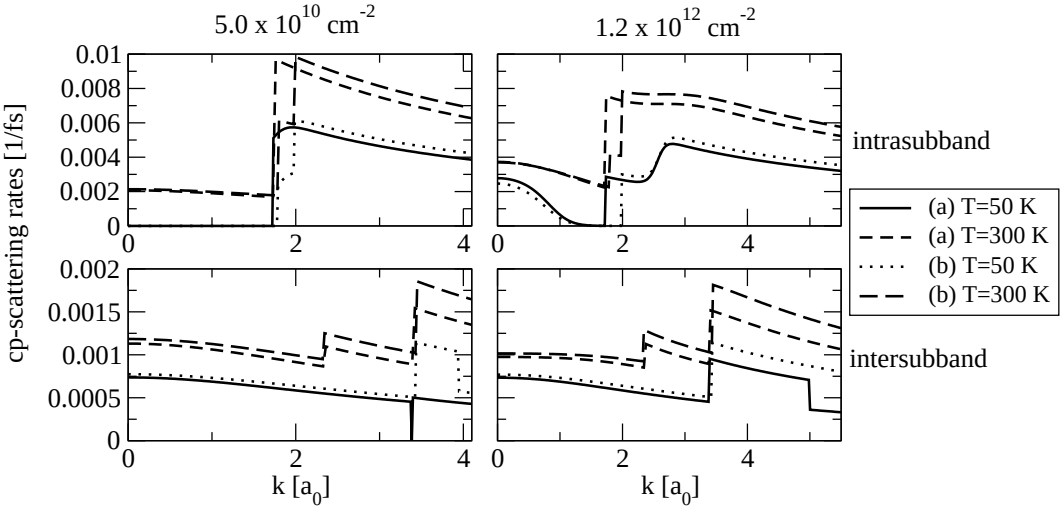

Figure IV.D.29 — Intra- vs intersubband carrier-phonon scattering rates (Linear Regime): Diagonal scattering contributions of a 10nm GaAs/AlGaAs quantum well without (a) or with (b) respect to nonparabolicity effects for carrier density $n = 5.0 \times 10^{10}\mathrm{cm}^{-2}$ or $n = 1.2 \times 10^{12}\mathrm{cm}^{-2}$ and temperatures $T = 50, 300$ Kelvin. The upper row shows intrasubband rates (terms with $\delta(-\epsilon^i_{\mathbf{k}} + \epsilon^i_{\mathbf{k}+\mathbf{q}_{||}} \pm \hbar\omega_{LO}),\ i = 1, 2$), the lower row intrasubband rates (terms with $\delta(-\epsilon^i_{\mathbf{k}} + \epsilon^j_{\mathbf{k}+\mathbf{q}_{||}} \pm \hbar\omega_{LO}),\ i, j = 1, 2$ and $i \neq j$). The explicit scattering rates are given in APP F

into states $\mathbf{k}+\mathbf{q}$ and $\mathbf{k}'-\mathbf{q}$, terms proportional to $f^i_{\mathbf{k}'-\mathbf{q}} f^i_{\mathbf{k}+\mathbf{q}}$ describe scattering from states $\mathbf{k}+\mathbf{q}$ and $\mathbf{k}'-\mathbf{q}$ into states $\mathbf{k}$ and $\mathbf{k}'$. Non-Markovian events are again excluded, only scattering processes which obey the strict energy conservation are taken into account. A detailed investigation of non-Markovian effects of carrier-carrier scattering in semiconductor *quantum wires* is given in [Pre98, PS99]. Besides the direct scattering contributions, i.e., contributions with Coulomb matrix elements $\propto 2|V^{iiii}_{\mathbf{q}}|^2$, we find exchange contributions with Coulomb matrix elements $\propto V^{iiii}_{\mathbf{q}} V^{iiii}_{\mathbf{k}-\mathbf{k}'-\mathbf{q}}$ which effectively reduce the scattering rates [cf. also [LG00]] similar to interband transitions [JKK$^+$96]. In Chapter IV.D.4.b.1 we will see however, that even though the diagonal scattering rates are decreased by the exchange contributions, the effective linewidth remains almost completely unchanged due to large compensating effects between diagonal and non-diagonal correlation contributions. A comparison of carrier-carrier scattering rates with / without inclusion of exchange contributions is given in Fig. IV.D.30 for the example of a 10 nm quantum well with carrier densities (a) $n = 1.2 \times 10^{12}\mathrm{cm}^{-2}$ and (b) $n = 5.0 \times 10^{10}\mathrm{cm}^{-2}$.

b) Dephasing Rate Approximation

The inverse of the diagonal correlation contributions Γ_d can be identified with the T_2 time known from atomic two-level systems [HK94], i.e., $(\Gamma_d)^{-1} = T_2$ [cf. Eq. (IV.B.15)]. Therefore, the diagonal scattering rates are frequently used to approximate the microscopic dephasing on the basis of the relaxation or dephasing rate approximation. In this approximation the dephasing is so strong, that almost all differences which could initially be observed in the absorption spectra (on the level of mean-field calculations) are damped out. The corresponding absorption spectra show almost no dependence on well width or subband dispersion. As we have already seen in the special limit considered in Chapter IV.D.1 at the beginning of this chapter, the dephasing rate approximation overestimates the actual dephasing to a large extent. If we exclude mean-field contributions and consider a quantum well with equal subband dispersion, i.e. without inhomogeneous broadening, the linewidth due to carrier-carrier and carrier-phonon scattering is completely additive. As can already be seen at the structure of the corresponding equations, the linewidth of the absorption spectra including both carrier-carrier and carrier-phonon interaction simultaneously is in this case identical

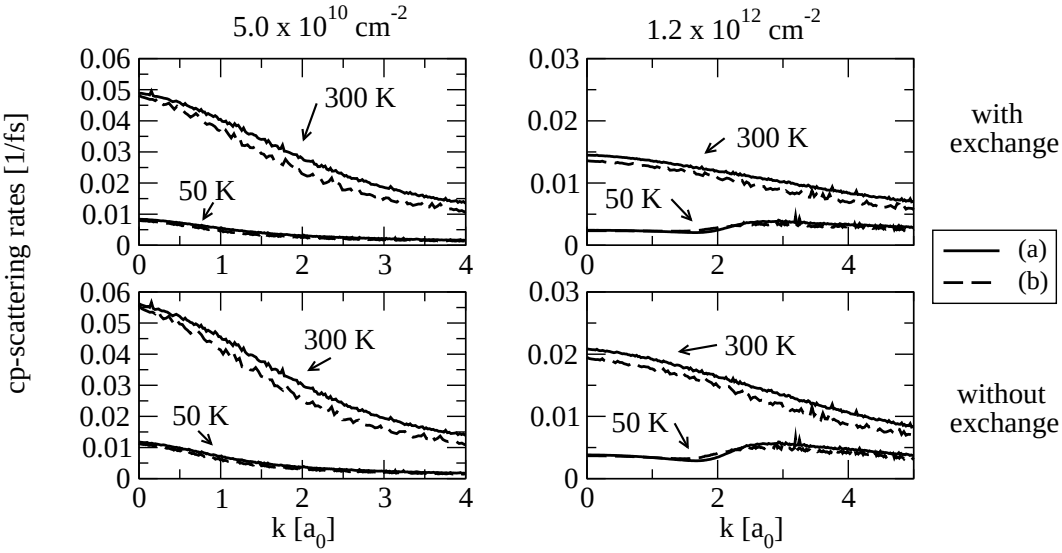

Figure IV.D.30 — Carrier-carrier scattering rates (Linear Regime): Diagonal scattering contributions of a 10nm GaAs/AlGaAs quantum well without (a) or with (b) respect to nonparabolicity effects for carrier density $n = 5.0 \times 10^{10}\mathrm{cm}^{-2}$ or $n = 1.2 \times 10^{12}\mathrm{cm}^{-2}$ and temperatures $T = 50, 300$ Kelvin. The upper row shows diagonal scattering rates with inclusion of exchange scattering contributions, the lower row intrasubband rates terms without inclusion of exchange scattering contributions. The explicit scattering rates are given in APP F.

to the linewidth of the absorption spectra where these contributions have been considered separately. Due to excitonic contribution and depolarization effect, two mean-field contributions which couple intersubband coherences at different wave vectors, the complete additive-ness is lost. The inclusion of inhomogeneous broadening naturally reduces the additive-ness even further. However, the difference in linewidth is small compared to the overall linewidth in the dephasing rate approximation.

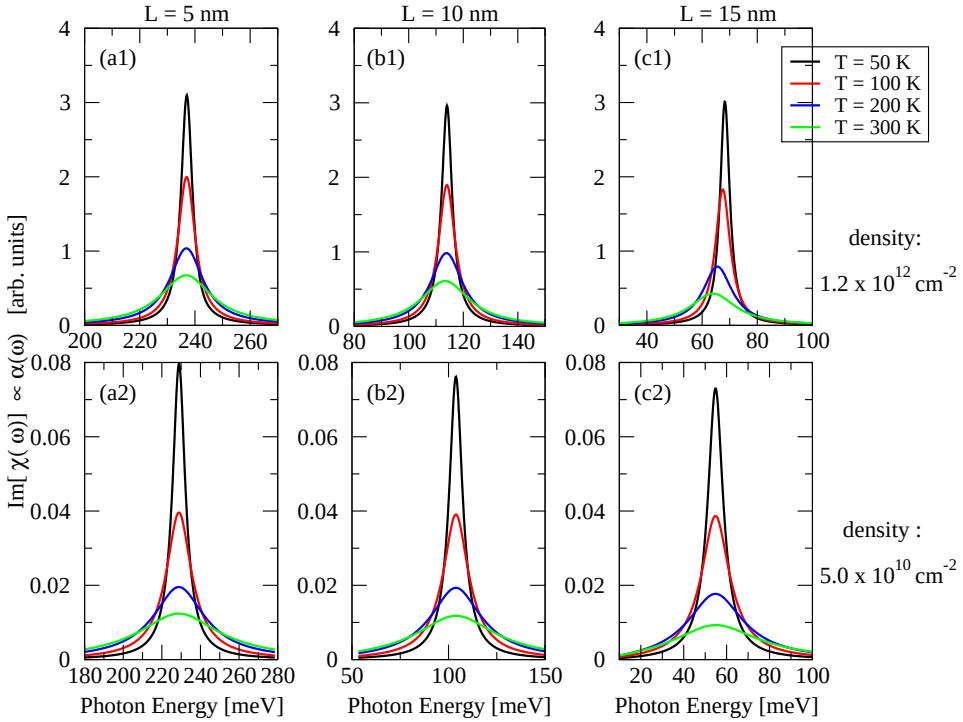

Figure IV.D.31 — Absorption in Dephasing Rate Approximation (Equal Subband Dispersion): of a quantum well with carrier density (a1, b1, c1) $n = 1.2 \times 10^{12}\mathrm{cm}^{-2}$, (a2, b2, c2) $n = 5.0 \times 10^{10}\mathrm{cm}^{-2}$ and well width (a) $L = 5$ nm, (b) $L = 10$ nm, (c) $L = 15$ nm. The initially observed differences due to mean-field effects [cf. Fig. IV.D.24] are completely damped out.

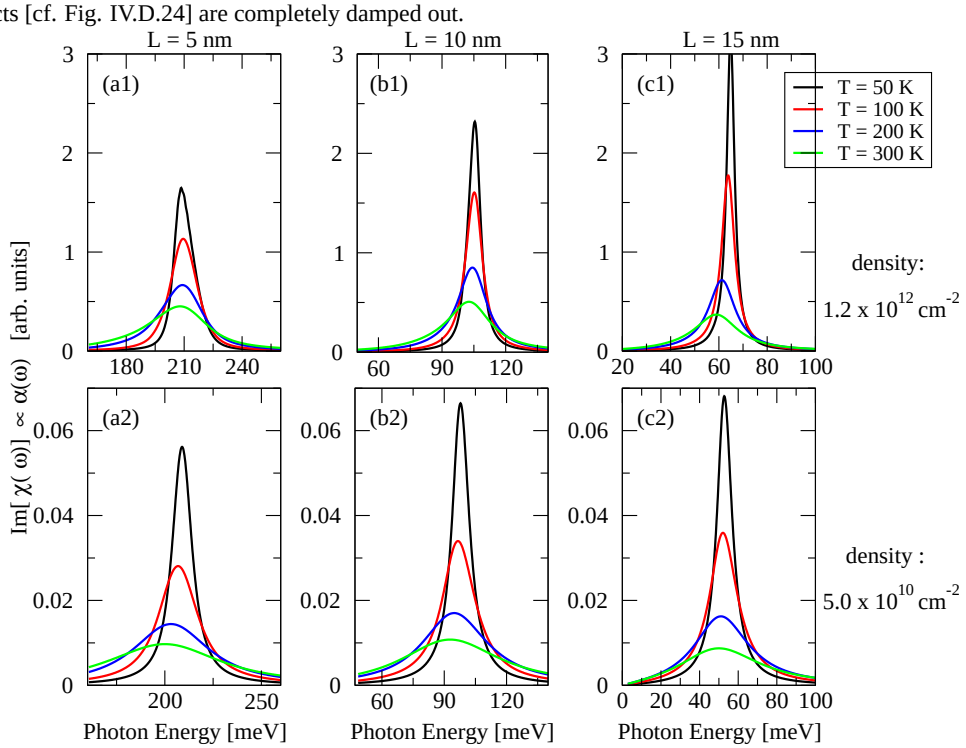

Figure IV.D.32 — Absorption in Dephasing Rate Approximation (Different Subband Dispersion): for the parameters given above. The spectra are almost identical to those in Fig. IV.D.31 in contrast to the differences in Fig. IV.D.24 / Fig. IV.D.25.

Full Microscopic Theory

Last, we now include all contributions in the theory, i.e., all mean-field contributions and all correlation contributions. As can be seen in Fig. IV.D.33 and Fig. IV.D.34 the corresponding linear absorption spectra are quite different from those calculated within the dephasing rate approximation [cf. Fig. IV.D.31 and Fig. IV.D.32]. The most striking difference being the very small linewidths. Whereas in the dephasing rate approximation, the linewidth of the absorption spectra was in the range of up to 60 meV, we here encounter linewidth in all cases smaller than 10 meV. This clearly shows, the enormous cancellation effects between diagonal and non-diagonal correlation contributions which are even stronger than in the interband case [LK88, JKK$^+$96, IR01, HKK$^+$96, WFK04, LN04]. Furthermore, investigating the additive-ness of the various scattering mechanisms as done in Chapter IV.D.4.b, we see that including non-diagonal correlation contributions, the dephasing contributions are not-additive, not even in the simplified case, where the non-diagonal mean-field contributions (excitonic contribution and depolarization effect) and inhomogeneous broadening are excluded. This is because including the non-diagonal correlation contributions as done in Fig. IV.D.33 and Fig. IV.D.34 takes into account the interference phenomena between various scattering mechanisms which are completely left out on the basis of a diagonal dephasing rate approximation [WFL$^+$04].

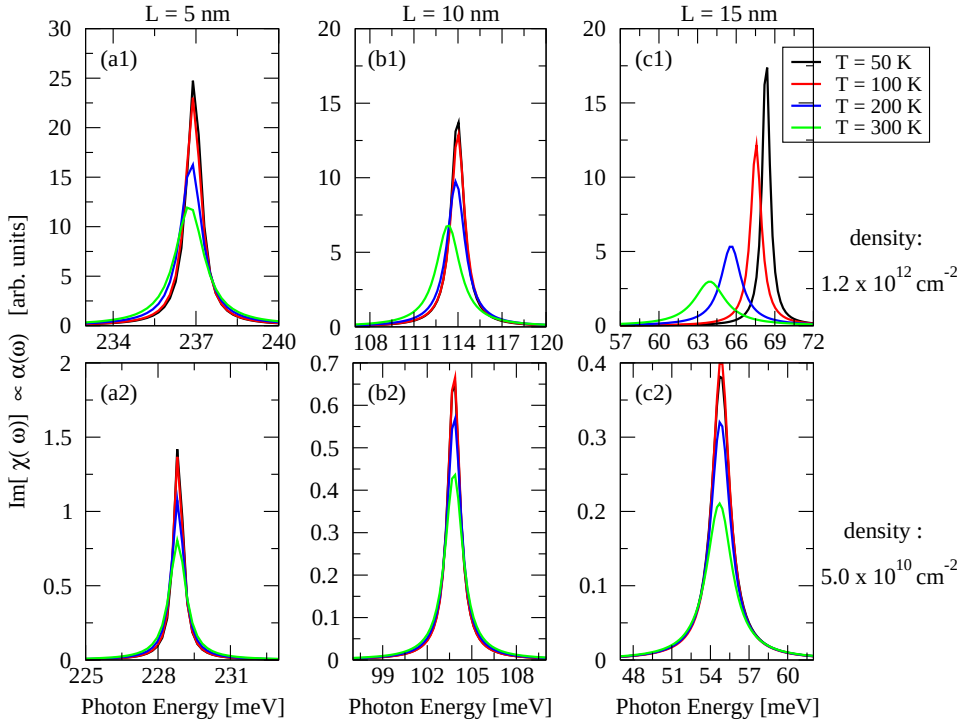

Figure IV.D.33 — Absorption: Incl. of Mean-Field and Corr. Contrib. (Equal Subband Dispersion): Absorption of a quantum well with carrier density (a1, b1, c1) $n = 1.2 \times 10^{12}\mathrm{cm}^{-2}$, (a2, b2, c2) $n = 5.0 \times 10^{10}\mathrm{cm}^{-2}$ and well width (a) $L = 5$ nm, (b) $L = 10$ nm, (c) $L = 15$ nm with equal subband dispersion. Note the different y-scales of (a1, b1, c1).

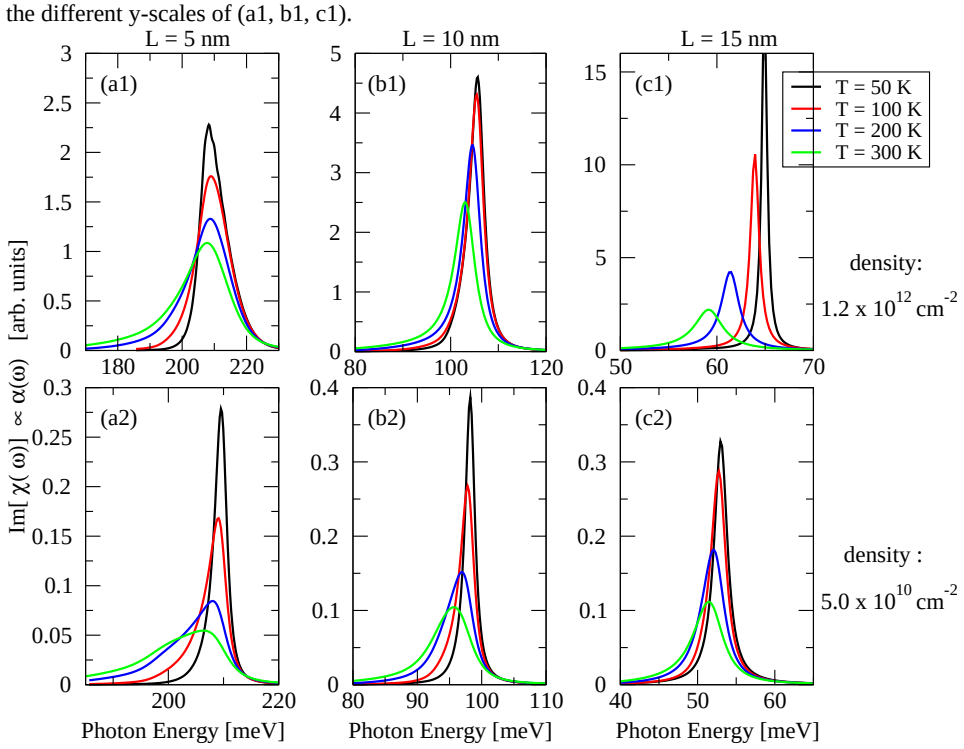

Figure IV.D.34 — Absorption: Incl. of Mean-Field and Corr. Contrib. (Different Subband Disp.): Absorption of a quantum well with carrier density (a1 ,b1 ,c1) $n = 1.2 \times 10^{12}\mathrm{cm}^{-2}$, (a2, b2, c2) $n = 5.0 \times 10^{10}\mathrm{cm}^{-2}$ and well width (a) $L = 5$ nm, (b) $L = 10$ nm, (c) $L = 15$ nm with different subband dispersion. Note the different y-scales of (a1, b1, c1).

c) Nonlinear Regime

To conclude the investigations of the impact of the various microscopic many-particle contributions on the ability of the system to experience Rabi oscillations, we finally investigate the influence of second order correlation contributions on the nonlinear response of intersubband transitions. As the occupation numbers are time-dependent in the nonlinear regime, now *all* correlation contributions have to be calculated *completely anew* in every time step. The corresponding extension of the required cpu-time is consequently very huge - especially for carrier-carrier scattering.

In Fig. IV.D.35 and Fig. IV.D.36, we present the density oscillations in a quantum well sample with different subband dispersion and the following parameters: well width $L = 10$ nm, carrier density $n = 1.2 \times 10^{12}\mathrm{cm}^{-2}$ and temperature $T = 50, 300$ Kelvin. The sample is excited by a Gaussian pulse with $\tau = 100$ fs and pulse areas as indicated in the figures. We compare the actual oscillations calculated for inclusion of carrier-carrier and carrier-phonon scattering first separately and finally simultaneously. As can be seen in the examples presented above, for the here considered parameters, the impact of carrier-carrier scattering on the actual density oscillations is actually very small.

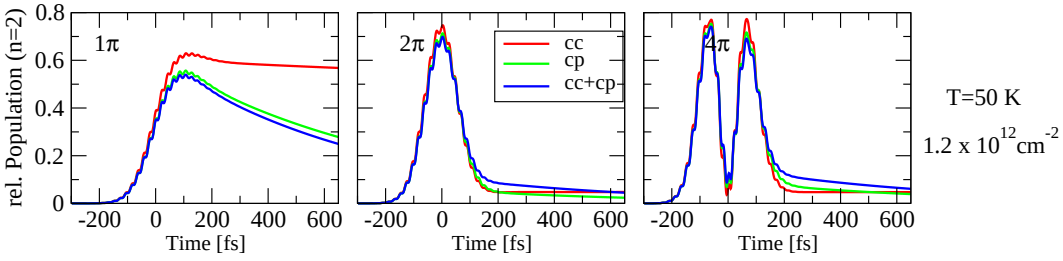

Figure IV.D.35 — Impact of correlation contributions on Density Oscillations: Comparison of density oscillations with respect to different correlation contributions for a single quantum well with $T = 50K, n = 1.2e12, L = 10$nm

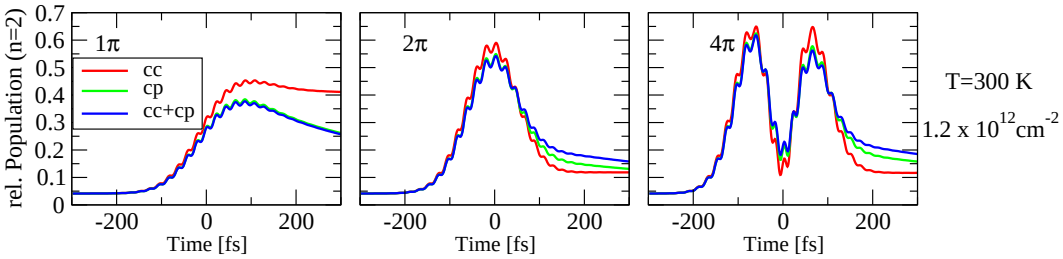

Figure IV.D.36 — Impact of correlation contributions on Density Oscillations: Comparison of density oscillations with respect to different correlation contributions for a single quantum well with $T = 300K, n = 1.2e12, L = 10$nm

CHAPTER V
Macroscopic Equations of Motion: Field Calculation

In the previous chapters we derived the microscopic equations for the quantum well system. We started with the microscopic Maxwell-Lorentz Equations and corresponding standard Lagrangian and derived the Hamiltonian and the equations of motion for the quantities of interest (intersubband coherence and occupation). Although we already made the crossover to the macroscopic equations of motion and commented on their connection to the microscopic equations, we did not actually consider the coupling in practice.

A. Multiple Quantum Well Systems

In Chapter IV we applied the derived microscopic theory in order to investigate the linear and nonlinear response of a single quantum well, where local field effects and thus the coupling to the macroscopic equations are neglectable. In this chapter we concentrated on the microscopic aspect of intersubband transitions, i.e. we examined in great detail the impact and interplay of the various many-particle effects such as mean-field contributions and correlation contributions. In the following, we will now focus on quantum well samples where the coupling of microscopic and macroscopic equations can not a priori be neglected. With respect to experimental setups and measurements, we aim to adapt the derived theory to the description of multiple quantum well samples as the one presented in Fig. V.A.1. At the end of this chapter we want to be able to determine the actual macroscopic fields emitted by a multiple quantum well system - with respect to

- the radiative coupling between the wells
- special effects due to the sample geometry, for example total reflection at a prism base
- different dielectric constants of barrier and well material.

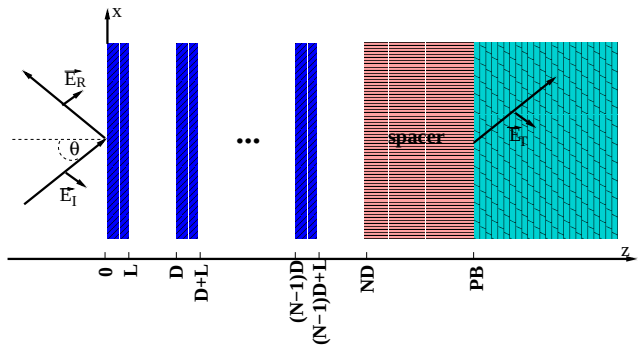

Figure V.A.1 — General Setup of Arbitrary MQW-Sample: Sketch of a MQW with respect to different dielectric constants of barrier and well material. Additionally added layers can be used to simulate effects due to spacer layer or reflection at a prism base.

Generally spoken, the theory shall be able to determine the local fields in a MQW system like the one given in Fig. V.A.1: a sample consisting of N quantum wells followed by layers of two -so far- unspecified materials. In principle this is nothing else than a multi-layer geometry with sheets of polarization in the well areas and the following dielectric constants:

$$\epsilon_b = \begin{cases} \epsilon_B, & \text{if} \quad -\infty < z < 0 \quad \vee \quad (n-1)D + L < z < nD\,; \\ \epsilon_W, & \text{if} \quad (n-1)D < z < (n-1)D + L\,; \\ \epsilon_S, & \text{if} \quad ND < z < PB\,; \\ \epsilon_{PB}, & \text{if} \quad PB < z < \infty\,. \end{cases} \tag{V.A.1}$$

Thereby, we can then investigate the linear and nonlinear response of multiple quantum wells systems - with respect to both microscopic and macroscopic effects - for a variety of realistic experimental setups.

The coarse outline of this chapter is the following: Adapting the Greens function approach presented in [Sip87], we first derive the fields generated by a sheet of polarization embedded in a medium with dielectric constant ϵ_b. If a possible mismatch of dielectric constants in barrier and well is neglected, the obtained results can easily be generalized to describe the fields generated by a number of quantum wells. At this level the theory concentrates on the contributions due to the polarization of the wells, effects due to material and sample parameters are not included. Therefore we will in the following refer to this level as the description of a *simplified multiple quantum well sample*. In order to account for reflection effects due to a mismatch of dielectric constants, we revise shortly the basic concept of the transfer matrix approach, which we then combine with the results of the Greens function approach. Thereby a "mismatch of dielectric constants" can refer to different permittivities of well and barrier material but also to a basic reflection at an interface as in the case of a single-pass-prism geometry where total reflection at an interface effectively enhances the local field. A sketch of the outline of this chapter is given in Fig. V.A.2.

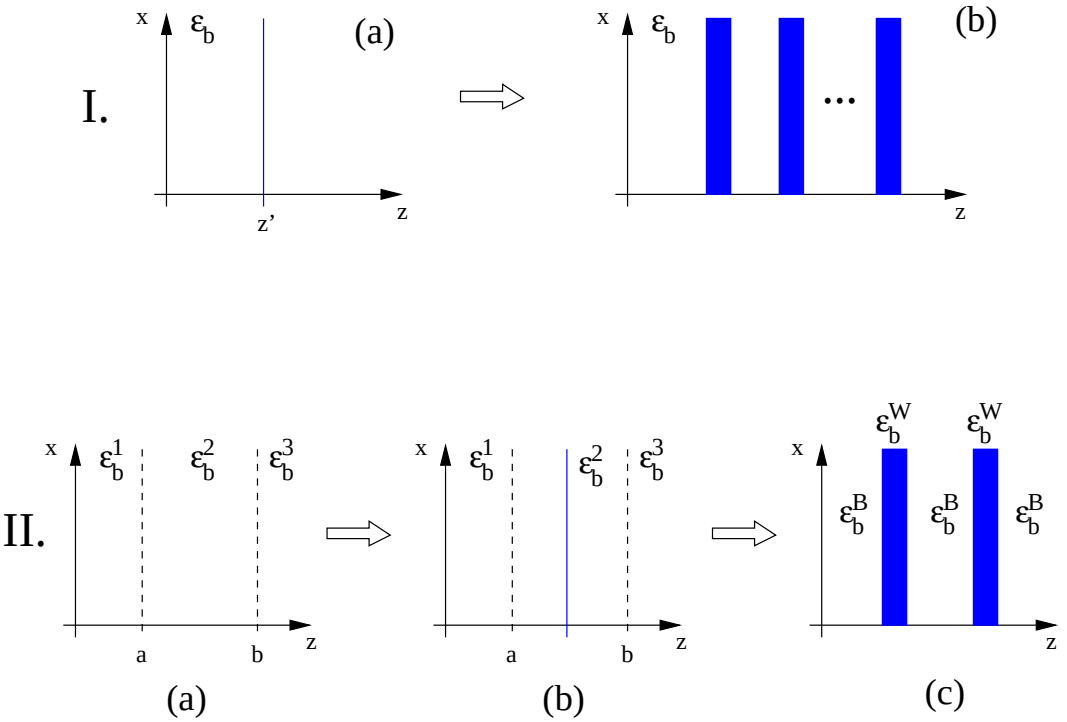

Figure V.A.2 — Basic Outline of Build-Up of Field Derivation: I. Greens function formalism to derive fields generated by (a) a sheet of polarisation or (b) a number of quantum wells, II. Combination of transfer matrix formalism for the description of multiple reflections in a multi-layer geometry (a) with the results of the Greens function formalism to determine the fields generated by a (b) sheet of polarization or (c) multiple quantum wells with respect to a mismatch of barrier and well dielectric constants.

B. Field Calculation for Monochromatic Stationary Fields

For convenience, we consider first only stationary fields, monochromatic $\mathbf{F}(\mathbf{r},t)$ with a frequency ω,

$$\mathbf{F}(\mathbf{r},t) = \hat{\mathbf{F}}(\mathbf{r})\, e^{-\mathrm{i}\ \omega\, t}\,. \tag{V.B.1}$$

From the basic solutions for the monochromatic fields, we can afterwards build general solutions by Fourier superposition. We start with a derivation of the fields generated by a sheet of polarization at $z = z'$ with a spatial variation in the plane characterized by a wave vector $\mathbf{q}_{||}$ [Sip87]:

$$\mathbf{P}(\mathbf{r}) = \mathbf{P}\delta(z - z')\, \mathrm{e}^{\mathrm{i}\ \mathbf{q}_{||}\cdot\mathbf{r}_{||}}\,. \tag{V.B.2}$$

and generalize the result later to account for the polarization of a single quantum well or a MQW system.

1. Fields Generated by a Single Sheet of Polarization

First, we derive the solution of the homogeneous wave equation (i.e. we set $\mathbf{P}(\mathbf{r}) = 0$):

$$\left[\nabla^2 + \frac{\epsilon_b \omega^2}{c^2}\right]\mathbf{E}(\mathbf{r}) - \nabla(\nabla\cdot\mathbf{E}(\mathbf{r})) = \quad 0\,. \tag{V.B.3}$$

a) Homogeneous Equation

Bearing in mind, that the sheet of polarization is parallel to the (x,y) plane, we divide the fields in right- and leftward propagating waves

$$\mathbf{E}_+(\mathbf{r}) = \mathbf{E}_+\mathrm{e}^{\mathrm{i}\ \mathbf{q}_+\cdot\mathbf{r}}\,, \quad \mathbf{E}_-(\mathbf{r}) = \mathbf{E}_-\mathrm{e}^{\mathrm{i}\ \mathbf{q}_-\cdot\mathbf{r}}, \tag{V.B.4}$$

where

$$\mathbf{q}_\pm = q_x\hat{\mathbf{x}} + q_y\hat{\mathbf{y}} \pm q_\perp\hat{\mathbf{z}} = q_{||}\hat{\mathbf{q}}_{||} \pm q_\perp\hat{\mathbf{z}} \tag{V.B.5}$$

lies in the plane of incidence spanned by unit vectors $\hat{\mathbf{q}}_{||}$ and $\hat{\mathbf{z}}$. The wave-vector projection parallel to the well layers, $q_{||} = \sqrt{q_x^2 + q_y^2}$, is chosen to be real and the projection perpendicular to the well layers is given by

$$q_\perp = \sqrt{q^2 - q_{||}^2} = \sqrt{\frac{\omega^2}{c^2}\epsilon_b - q_{||}^2} \tag{V.B.6}$$

and can also take on complex values. Next, we introduce a unit vector perpendicular to the plane of incidence

$$\hat{\mathbf{s}} = \hat{\mathbf{q}}_{||}\times\hat{\mathbf{z}} = q_{||}^{-1}\,(q_y\hat{\mathbf{x}} - q_x\hat{\mathbf{y}})\,. \tag{V.B.7}$$

Considering that the solution of the homogeneous wave equation must be transverse ($\nabla\cdot\mathbf{E} = 0 \rightarrow \mathbf{q}_\pm \perp \mathbf{E}$), it is convenient to introduce two vectors perpendicular to $\mathbf{q}_\pm$ that span the possible $\mathbf{E}$ [Sip87]. One of these vectors can obviously be taken as the unit vector $\hat{\mathbf{s}}$, the other can be taken as

$$\hat{\mathbf{p}}_\pm = \frac{1}{q}\,(q_{||}\,\hat{\mathbf{z}} \mp q_\perp\,\hat{\mathbf{q}_{||}}) = \frac{1}{q}(q_{||}\,\hat{\mathbf{z}} \mp \frac{q_\perp}{q_{||}}[q_x\hat{\mathbf{x}} + q_y\hat{\mathbf{y}}])\,. \tag{V.B.8}$$

It is clear that while choosing $\mathbf{q}_\pm$ as the wave vector, $\mathbf{E}$ can have only $\hat{\mathbf{s}}$ and $\hat{\mathbf{p}}_\pm$ components:

$$\mathbf{E}_+(\mathbf{r}) = (E_{s+}\,\hat{\mathbf{s}} + E_{p+}\,\hat{\mathbf{p}}_+)\,\mathrm{e}^{\mathrm{i}\,\mathbf{q}_+\cdot\mathbf{r}}\,, \qquad \mathbf{E}_-(\mathbf{r}) = (E_{s-}\,\hat{\mathbf{s}} + E_{p-}\,\hat{\mathbf{p}}_-)\,\mathrm{e}^{\mathrm{i}\,\mathbf{q}_-\cdot\mathbf{r}}\,. \tag{V.B.9}$$

An electric field with only $E_{p\pm}$ components is often referred to as a $p\pm$-polarized, parallel polarized or transverse magnetic (*TM*) field, with only $E_{s\pm}$ components a s-polarized, perpendicular polarized or transverse electric (*TE*) field. Once $\mathbf{E}(\mathbf{r})$ is specified, $\mathbf{B}(\mathbf{r})$ follows from $\nabla\times\mathbf{E} = \mathrm{i}\,\omega\mathbf{B}$

$$\mathbf{B}_+(\mathbf{r}) = \frac{\sqrt{\epsilon_b}}{c}(E_{p+}\hat{\mathbf{s}} - E_{s+}\hat{\mathbf{p}}_+)\mathrm{e}^{\mathrm{i}\,\mathbf{q}_+\cdot\mathbf{r}}, \qquad \mathbf{B}_-(\mathbf{r}) = \frac{\sqrt{\epsilon_b}}{c}(E_{p-}\hat{\mathbf{s}} - E_{s-}\hat{\mathbf{p}}_-)\mathrm{e}^{\mathrm{i}\,\mathbf{q}_-\cdot\mathbf{r}}. \tag{V.B.10}$$

b) Inhomogeneous Equation

Next, we determine the field in the presence of the polarization given in Eq. (V.B.2). Therefore we have to solve

$$\left[\nabla^2 + \frac{\epsilon_b\omega^2}{c^2}\right]\mathbf{E}(\mathbf{r}) - \nabla(\nabla\cdot\mathbf{E}(\mathbf{r})) = \quad -\omega^2\mu_0\mathbf{P}(\mathbf{r})\,. \tag{V.B.11}$$

Since for $z \neq z'$ the solutions of Eq. (V.B.11) also fulfill the homogenous wave equation, we make the ansatz

$$\mathbf{E}(\mathbf{r}) = \mathbf{E}_+(\mathbf{r})\,\mathrm{e}^{-\mathrm{i}\,q_\perp\,z'}\,\Theta(z-z') + \mathbf{E}_-(\mathbf{r})\,\mathrm{e}^{\mathrm{i}\,q_\perp\,z'}\,\Theta(z'-z) + \mathcal{E}\,\delta(z-z')\,\mathrm{e}^{\mathrm{i}\,\mathbf{q}_{||}\cdot\mathbf{r}_{||}} \tag{V.B.12}$$

with

$$\mathcal{E} = \mathcal{E}_s\,\hat{\mathbf{s}} + \mathcal{E}_{q_{||}}\,\hat{\mathbf{q}}_{||} + \mathcal{E}_z\,\hat{\mathbf{z}}\,. \tag{V.B.13}$$

To ensure physically reasonable behavior for $z\to\infty$ and $z\to-\infty$, we choose here a rightward wave for $z > z'$ and a leftward wave for $z < z'$. The factors $\mathrm{e}^{-\mathrm{i}\,q_\perp\,z'}$, $\mathrm{e}^{\mathrm{i}\,q_\perp\,z'}$ are included for convenience [Sip87]. Inserting the ansatz, Eq. (V.B.12), into the inhomogeneous wave equation, Eq. (V.B.11), the unknown coefficients E_i and $\mathcal{E}_i$ can be determined. Using

$$\frac{d}{dx}\Theta(\pm x) = \pm\delta(x)\,, \qquad \delta(x-x')\,f(x) = \delta(x-x')\,f(x') \tag{V.B.14}$$

which yields

$$\frac{\partial^2}{\partial z^2}\mathrm{e}^{\mathrm{i}\,q_\perp\,(z-z')}\,\Theta(z-z') = -q_\perp^2\Theta(z-z')\mathrm{e}^{\mathrm{i}\,q_\perp\,(z-z')} + \mathrm{i}\;q_\perp\delta(z-z') + \delta'(z-z')\,,$$
$$\frac{\partial^2}{\partial z^2}\mathrm{e}^{-\mathrm{i}\,q_\perp\,(z-z')}\,\Theta(z'-z) = -q_\perp^2\Theta(z'-z)\mathrm{e}^{-\mathrm{i}\,q_\perp\,(z-z')} + \mathrm{i}\;q_\perp\delta(z-z') - \delta'(z-z')$$

we find three equations

$$
\begin{array}{lll}
(-\mathrm{i}\, q \frac{q_x}{q_{||}}\,(E_{p+}-E_{p-}) + \mathcal{E}_{q_{||}} q^2 \frac{q_x}{q_{||}} + \mathrm{i}\,\frac{q_\perp}{q_{||}} q_y (E_{s+}+E_{s-}) + \mathcal{E}_s\,\frac{q_\perp^2}{q_{||}} q_y + \omega^2\,\mu_0\,P_x) & \delta(z-z') & \\
+ \quad (-\frac{q_\perp q_x}{q_{||} q}\,(E_{p+}+E_{p-}) + \frac{q_y}{q_{||}}(E_{s+}-E_{s-}) - \mathcal{E}_z\,\mathrm{i}\,q_x) & \delta'(z-z') & \\
+ \quad (\frac{q_y}{q_{||}}\mathcal{E}_s + \frac{q_x}{q_{||}}\mathcal{E}_{q_{||}}) & \delta''(z-z') & = 0 \\
 & & \\
(-\mathrm{i}\, q \frac{q_y}{q_{||}}\,(E_{p+}-E_{p-}) - \mathrm{i}\, q_\perp \frac{q_x}{q_{||}}\,(E_{s+}+E_{s-}) + \mathcal{E}_{q_{||}}\, q^2 \frac{q_y}{q_{||}} + \mathcal{E}_s\,\frac{q_\perp^2}{q_{||}} q_x + \omega^2\,\mu_0\,P_y) & \delta(z-z') & \\
+ \quad (-\frac{q_\perp q_y}{q_{||} q}\,(E_{p+}+E_{p-}) - \frac{q_x}{q_{||}}(E_{s+}-E_{s-}) - \mathcal{E}_z\,\mathrm{i}\,q_y) & \delta'(z-z') & \\
+ \quad (\frac{q_y}{q_{||}}\mathcal{E}_{q_{||}} - \frac{q_x}{q_{||}}\mathcal{E}_s) & \delta''(z-z') & = 0 \\
 & & \\
(\mathrm{i}\,\frac{q_{||}\, q_\perp}{q}\,(E_{p+}+E_{p-}) + \mathcal{E}_z\, q_\perp^2 + \omega^2\,\mu_0\,P_z) & \delta(z-z') & \\
- \quad \mathrm{i}\; q_{||}\, E_{q_{||}} & \delta'(z-z') & = 0\,.
\end{array}
\qquad \text{(V.B.15)}
$$

Since the different orders of singularities in Eq. (V.B.15) must vanish separately, the coefficients are obtained as

$$\mathcal{E}_{q_{||}} = \mathcal{E}_s = 0,\ \mathcal{E}_z = -\frac{c^2\,\mu_0}{\epsilon_b}\,P_z,\ E_{s\pm} \quad = -\frac{\omega^2\,\mu_0}{2\,\mathrm{i}\ q_\perp}\,\hat{\mathbf{s}}\cdot\mathbf{P},\ E_{p\pm} = -\frac{\omega^2\,\mu_0}{2\,\mathrm{i}\ q_\perp}\,\hat{\mathbf{p}}_\pm\cdot\mathbf{P}\,. \quad \text{(V.B.16)}$$

The field generated by the sheet of polarization at $z = z'$ is thus given by

$$\mathbf{E}(\mathbf{r}) = \quad -\omega^2\,\mu_0\,\overleftrightarrow{\mathcal{G}}\,(z,z')\,\mathbf{P}\,\mathrm{e}^{\mathrm{i}\ \mathbf{q}_{||}\cdot\mathbf{r}_{||}} \quad \text{(V.B.17)}$$

where we introduced the retarded Green's function tensor in dyadic form

$$\overleftrightarrow{\mathcal{G}}\,(z,z') = \frac{\mathrm{e}^{\mathrm{i}\ q_\perp\,|z-z'|}}{2\,\mathrm{i}\ q_\perp}[(\hat{\mathbf{s}}\hat{\mathbf{s}}+\hat{\mathbf{p}}_+\hat{\mathbf{p}}_+)\Theta(z-z')+(\hat{\mathbf{s}}\hat{\mathbf{s}}+\hat{\mathbf{p}}_-\hat{\mathbf{p}}_-)\Theta(z'-z)]+\frac{c^2}{\omega^2\,\epsilon_b}\delta(z-z')\,\hat{\mathbf{z}}\hat{\mathbf{z}}\,. \quad \text{(V.B.18)}$$

Thus we are now able to determine the fields generated by a sheet of polarization - embedded in an infinite medium of dielectric constant ϵ_b.

2. Generalization to the Polarization of Multiple Quantum Wells

Next, we generalize the derived results to describe the fields generated by the polarization of a single quantum well or a system of quantum wells. Therefore, we express the polarization of a single quantum well through its Fourier transform

$$\mathbf{P}_{\mathrm{QW}}(\mathbf{r}) = \quad \frac{1}{(2\pi)^2}\int d^2\mathbf{q}_{||}\mathbf{P}_{\mathrm{QW}}(\mathbf{q}_{||},z)\mathrm{e}^{\mathrm{i}\,\mathbf{q}_{||}\cdot\mathbf{r}_{||}} \quad \text{(V.B.19)}$$

$$= \quad \frac{1}{(2\pi)^2}\int d^2\mathbf{q}_{||}\int dz'\{\mathbf{P}_{\mathrm{QW}}(\mathbf{q}_{||},z')\delta(z-z')\mathrm{e}^{\mathrm{i}\,\mathbf{q}_{||}\cdot\mathbf{r}_{||}}\} \quad \text{(V.B.20)}$$

with

$$\mathbf{P}_{\mathrm{QW}}(\mathbf{q}_{||},z) = \int d^2r_{||}\mathbf{P}_{\mathrm{QW}}(\mathbf{r})\mathrm{e}^{-\mathrm{i}\,\mathbf{q}_{||}\cdot\mathbf{r}_{||}} \quad \text{(V.B.21)}$$

and find immediately that Eq. (V.B.2) is nothing else than a Fourier component of Eq. (V.B.20). Thus, we obtain the fields generated by the polarization of a single quantum well by adding up the fields generated by sources of the form of Eq. (V.B.2) with different z' and $q_{||}$, i.e. by summing up the different Fourier components:

$$\mathbf{E}(\mathbf{r}) = \quad \frac{1}{(2\pi)^2}\int d^2\mathbf{q}_{||}\mathbf{E}(\mathbf{q}_{||},z)\mathrm{e}^{\mathrm{i}\,\mathbf{q}_{||}\cdot\mathbf{r}_{||}} \quad \text{(V.B.22)}$$

with

$$\mathbf{E}(\mathbf{q}_{||},z) = \quad \int dz'\mathbf{E}(\mathbf{q}_{||},z')\,. \quad \text{(V.B.23)}$$

Here $\mathbf{E}(\mathbf{q}_{||},z')$ denotes the field generated by the corresponding Fourier component of the polarization and is equivalent to the field derived in Eq. (V.B.17). Inserting the result in Eq. (V.B.23) yields

$$\mathbf{E}(\mathbf{q}_{||},z) = \quad -\omega^2\,\mu_0\int dz'\,\overleftrightarrow{\mathcal{G}}\,(z,z')\mathbf{P}_{\mathrm{QW}}(\mathbf{q}_{||},z') \quad \text{(V.B.24)}$$

for a single quantum well or

$$\mathbf{E}(\mathbf{q}_{||},z) = \quad -\omega^2\,\mu_0\sum_{m=1}^{N}\int dz'\,\overleftrightarrow{\mathcal{G}}\,(z,z')\mathbf{P}^{(m)}_{\mathrm{QW}}(\mathbf{q}_{||},z') \quad \text{(V.B.25)}$$

for a system of N electronically uncoupled quantum wells. The Green's function tensor is given in Eq. (V.B.18).

a) Coupling of Microscopic and Macroscopic Equations: Distinction of Longitudinal and Transverse Field

If we actually want to couple microscopic and macroscopic equations by inserting the local field in the microscopic equations of motions derived in Chapter III we have to consider that only the transverse part of the field enters the carrier-field Hamiltonian. In Chapter A we used *Helmholtz's theorem* [Nol97] to divide the field in the Hamiltonian in longitudinal and transverse part, $\mathbf{a}(\mathbf{r},t) = \mathbf{a}_L(\mathbf{r},t) + \mathbf{a}_T(\mathbf{r},t)$, with

$$\begin{aligned} \mathbf{a}_L(\mathbf{r},t) = &\quad -\frac{1}{4\pi}\nabla\int d^3r'\frac{\nabla\cdot\mathbf{a}(\mathbf{r}',t)}{|\mathbf{r}-\mathbf{r}'|} = \nabla\alpha(\mathbf{r})\,, \\ \mathbf{a}_T(\mathbf{r},t) = &\quad \frac{1}{4\pi}\nabla\times\int d^3r'\frac{\nabla\times\mathbf{a}(\mathbf{r}',t)}{|\mathbf{r}-\mathbf{r}'|} = \nabla\times\beta(\mathbf{r})\,. \end{aligned} \tag{V.B.26}$$

Using the Coulomb gauge, we incorporated the longitudinal field in the Coulomb interaction. If we now inserte the complete field in the microscopic equations, we would double count the longitudinal part.

Therefore, the field in the layer of the polarization (cf. Eq. (V.B.56)) shall next be decomposed in transverse and longitudinal part. The divergence of this field is given by

$$\nabla\cdot\mathbf{E}(\mathbf{r}) = (v_{p+}-v_{p-})\frac{q_{||}}{q}\mathrm{e}^{\mathrm{i}\,\mathbf{q}_{||}\cdot\mathbf{r}_{||}}\delta(z-z') - \frac{c^2\mu_0}{\epsilon_b}P_z\delta'(z-z')\mathrm{e}^{\mathrm{i}\,\mathbf{q}_{||}\cdot\mathbf{r}_{||}} \tag{V.B.27}$$

and thus $\alpha(\mathbf{r})$ is obtained as

$$\begin{aligned} \alpha(\mathbf{r}) = &\quad -\frac{1}{4\pi}\int d^3r''\frac{1}{|\mathbf{r}-\mathbf{r}''|}\Big[(v_{p+}-v_{p-})\frac{q_{||}}{q}\delta(z''-z') - \frac{c^2\mu_0}{\epsilon_b}P_z\delta'(z''-z')\Big]\mathrm{e}^{\mathrm{i}\,\mathbf{q}_{||}\cdot\mathbf{r}''_{||}} \\ = &\quad -\frac{1}{4\pi}\mathrm{e}^{\mathrm{i}\,\mathbf{q}_{||}\cdot\mathbf{r}_{||}}\int dz''\,\Big[(v_{p+}-v_{p-})\frac{q_{||}}{q}\delta(z''-z') - \frac{c^2\mu_0}{\epsilon_b}P_z\delta'(z''-z')\Big] \\ &\int_0^\infty d\hat{r}\,\hat{r}\int_0^{2\pi}d\phi\,\frac{\mathrm{e}^{\mathrm{i}\,q_{||}\hat{r}\cos(\phi)}}{r^2+|z-z''|^2} \\ = &\quad -\frac{1}{2}\mathrm{e}^{\mathrm{i}\,\mathbf{q}_{||}\cdot\mathbf{r}_{||}}\int dz''\,\mathrm{e}^{-|z-z''|q_{||}}\Big[(v_{p+}-v_{p-})\frac{q_{||}}{q}\delta(z''-z') - \frac{c^2\mu_0}{\epsilon_b}P_z\delta'(z''-z')\Big] \\ = &\quad -\frac{1}{2}\mathrm{e}^{\mathrm{i}\,\mathbf{q}_{||}\cdot\mathbf{r}_{||}}\Big[(v_{p+}-v_{p-})\frac{q_{||}}{q} + \frac{c^2\mu_0}{\epsilon_b}P_z[\Theta(z-z')-\Theta(z'-z)]\Big]\mathrm{e}^{-|z-z'|q_{||}} \end{aligned} \tag{V.B.28}$$

where in the last step we used the identity

$$\begin{aligned} \mathrm{e}^{-|z-z''|q_{||}}\frac{\partial}{\partial z''}\delta(z''-z') = &\quad \delta(z''-z')\frac{\partial}{\partial z'}\mathrm{e}^{-|z-z'|q_{||}} \\ = &\quad -\delta(z''-z')\,q_{||}\,\mathrm{e}^{-|z-z'|q_{||}}[\Theta(z-z')-\Theta(z'-z)]\,. \end{aligned} \tag{V.B.29}$$

The longitudinal field can therewith be written as

$$\mathbf{E}_L^{(m)}(\mathbf{r}) = \Big(-\frac{c^2\mu_0}{\epsilon_b}P_z\delta(z-z')\,\hat{\mathbf{z}} - \frac{1}{2}\mathbf{E}_{pL}^{(m)}(z)\Big)\mathrm{e}^{-|z-z'|q_{||}}\,\mathrm{e}^{\mathrm{i}\,\mathbf{q}_{||}\cdot\mathbf{r}_{||}} \tag{V.B.30}$$

with

$$\mathbf{E}_{pL}^{(m)}(z) = \begin{pmatrix} \mathrm{i}\,q_x\{(v_{p+}-v_{p-})\frac{q_{||}}{q} + \frac{c^2\mu_0}{\epsilon_b}P_z[\Theta(z-z')-\Theta(z'-z)]\} \\ \mathrm{i}\,q_y\{(v_{p+}-v_{p-})\frac{q_{||}}{q} + \frac{c^2\mu_0}{\epsilon_b}P_z[\Theta(z-z')-\Theta(z'-z)]\} \\ (v_{p-}-v_{p+})\frac{q_{||}^2}{q}[\Theta(z-z')-\Theta(z'-z)] - q_{||}\frac{c^2\mu_0}{\epsilon_b}P_z[\Theta(z-z')+\Theta(z'-z)] \end{pmatrix}. \tag{V.B.31}$$

Note, that the longitudinal part of the field derived in Eq. (V.B.30) is identical to the depolarization effect investigated in Chapter IV. For a coupling of micro- and macroscopic equations we can now either insert only the transverse part of the local field, $\mathbf{E}_T^{(m)}(z) = \mathbf{E}^{(m)}(z) - \mathbf{E}_L^{(m)}(z)$, in the carrier-field contribution or exclude the depolarization contribution from the microscopic equations.

As a last step, the theory is expanded in order to account for effects due to the presence of a multi-layer geometry. To do so, we first neglect the sheet of polarization and concentrate on the effects of interfaces on the propagation of fields in general - by employing the transfer matrix formalism.

3. Transfer Matrix Formalism for Propagation in Multi-Layer Structures

The basic idea of the transfer matrix formalism [Kni76] is to calculate the propagation of fields through structures composed of layers which are linear with a scalar dielectric constant by expressing

I. the fields in each layer with the help of so-called *matrices of the separated field*,

II. the transformation of the fields upon penetration through the boundary of two adjoining layers with different refractive index in form of *transfer matrices*

III. the propagation inside one layer with *propagation matrices*.

Therewith, the series of reflections and transmissions connected with a multi-layer geometry can be easily obtained by matrix multiplication.

In the following, we focus on multi-layer geometries composed of layers parallel to the xy-plane. As the boundary conditions connect only fields with the same polarization, s and p-polarized light can be considered separately. First, we divide the field in the m-th layer into left- and rightward propagating waves according to

$$\mathbf{E}_s^{(m)}(\mathbf{r}) = E_{s+}^{(m)}\,\hat{\mathbf{s}}_m\,\mathrm{e}^{\mathrm{i}\,\mathbf{q}_{m+}\cdot\mathbf{r}} + E_{s-}^{(m)}\,\hat{\mathbf{s}}_m\,\mathrm{e}^{\mathrm{i}\,\mathbf{q}_{m-}\cdot\mathbf{r}}\,, \tag{V.B.32}$$

$$\mathbf{E}_p^{(m)}(\mathbf{r}) = E_{p+}^{(m)}\,\hat{\mathbf{p}}_{m+}\,\mathrm{e}^{\mathrm{i}\,\mathbf{q}_{m+}\cdot\mathbf{r}} + E_{p-}^{(m)}\,\hat{\mathbf{p}}_{m-}\,\mathrm{e}^{\mathrm{i}\,\mathbf{q}_{m-}\cdot\mathbf{r}}\,. \tag{V.B.33}$$

Vectors $\hat{\mathbf{p}}_{m\pm}, \hat{\mathbf{s}}$ and $\mathbf{q}_{m\pm}$ are given again by Eq. V.B.5 - Eq. V.B.8 but with ϵ_b replaced by the corresponding value of the m-th layer $\epsilon_b^{(m)}$. As already announced above, the fields in the m-th layer are now expressed in form of single-column matrices of the separated field (separated in the sense that one knows the components of the right- and leftward propagating waves of the field)

$$\mathbf{e}_s^{(m)}(z) = \begin{pmatrix} E_{s+}^{(m)}\,\mathrm{e}^{\mathrm{i}\,q_\perp^{(m)}z} \\ E_{s-}^{(m)}\,\mathrm{e}^{-\mathrm{i}\,q_\perp^{(m)}z} \end{pmatrix}\,, \qquad \mathbf{e}_p^{(m)}(z) = \begin{pmatrix} E_{p+}^{(m)}\,\mathrm{e}^{\mathrm{i}\,q_\perp^{(m)}z} \\ E_{p-}^{(m)}\,\mathrm{e}^{-\mathrm{i}\,q_\perp^{(m)}z} \end{pmatrix}\,. \tag{V.B.34}$$

The transformation of the field matrices upon penetration through the boundary of two adjoining layers, m and $m+1$, with $\epsilon_b^{(m)}$ and $\epsilon_b^{(m+1)}$ can be expressed as

$$\mathbf{e}_s^{(m)}(z_{m,m+1}) = \mathbf{M}_{m,m+1}^s \mathbf{e}_s^{(m+1)}(z_{m,m+1})\,, \qquad \mathbf{e}_p^{(m)}(z_{m,m+1}) \quad = \mathbf{M}_{m,m+1}^p \mathbf{e}_p^{(m+1)}(z_{m,m+1}) \tag{V.B.35}$$

where $z_{m,m+1}$ denotes the position of the boundary or interface between layer m and layer $m+1$ and $\mathbf{M}_{m,m+1}^{s,p}$ are the corresponding *transfer matrices*

$$\mathbf{M}_{m,m+1}^s = \frac{1}{t_{m,m+1}^s}\begin{pmatrix} 1 & r_{m,m+1}^s \\ r_{m,m+1}^s & 1 \end{pmatrix}\,, \qquad \mathbf{M}_{m,m+1}^p = \frac{1}{t_{m,m+1}^p}\begin{pmatrix} 1 & r_{m,m+1}^p \\ r_{m,m+1}^p & 1 \end{pmatrix}\,. \tag{V.B.36}$$

$r^{s,p}_{m,m+1}$ and $t^{s,p}_{m,m+1}$ are the Fresnel coefficients for s- and p-polarized light

$$r^{s}_{m,m+1} = \frac{q_\perp^{(m)} - q_\perp^{(m+1)}}{q_\perp^{(m)} + q_\perp^{(m+1)}}\,, \qquad t^{s}_{m,m+1} = \frac{2\,q_\perp^{(m)}}{q_\perp^{(m)} + q_\perp^{(m+1)}}\,, \tag{V.B.37}$$

$$r^{p}_{m,m+1} = \frac{q_\perp^{(m)}\,\epsilon_b^{(m+1)} - q_\perp^{(m+1)}\,\epsilon_b^{(m)}}{q_\perp^{(m)}\,\epsilon_b^{(m+1)} + q_\perp^{(m+1)}\,\epsilon_b^{(m)}}\,, \qquad t^{p}_{m,m+1} = \frac{2\,\sqrt{\epsilon_b^{(m)}}\,\sqrt{\epsilon_b^{(m+1)}}\,q_\perp^{(m)}}{q_\perp^{(m)}\,\epsilon_b^{(m+1)} + q_\perp^{(m+1)}\,\epsilon_b^{(m)}} \tag{V.B.38}$$

with

$$q_\perp^{(m)} = \sqrt{(q^{(m)})^2 - (q_{||}^{(m)})^2}\,, \qquad q_\perp^{(m+1)} = \sqrt{(q^{(m+1)})^2 - (q_{||}^{(m)})^2}\,. \tag{V.B.39}$$

Propagation inside one layer is expressed with the *propagation matrix*

$$\mathbf{M}_m(z) = \begin{pmatrix} \mathrm{e}^{\mathrm{i}\,q_\perp z} & 0 \\ 0 & \mathrm{e}^{-\mathrm{i}\,q_\perp z} \end{pmatrix} \tag{V.B.40}$$

according to

$$\mathbf{e}^{(m)}_{s,p}(z_a) = \mathbf{M}_m(z_a - z_b)\mathbf{e}^{m}_{s,p}(z_b)\,. \tag{V.B.41}$$

With these definitions, the propagation of fields in a multi-layer geometry can be obtained easily and includes already multiple reflections.

As an example, the propagation of a p-polarized field in the multi-layer geometry sketched in Fig. V.B.1 is determined in the following.

Using Eq. V.B.35 - Eq. V.B.41, we first relate the field matrices of layer 0 and 2 according to

$$\begin{aligned} \mathbf{e}^{(0)}_p(z_{0,1}) &= \mathbf{M}^p_{0,1}\mathbf{e}^{(1)}_p(z_{0,1}) \\ &= \mathbf{M}^p_{0,1}\mathbf{M}_1(z_{0,1} - z_{1,2})\mathbf{e}^{(1)}_p(z_{1,2}) \\ &= \mathbf{M}^p_{0,1}\mathbf{M}_1(z_{0,1} - z_{1,2})\mathbf{M}^p_{1,2}\mathbf{e}^{(2)}_p(z_{1,2})\,. \end{aligned} \tag{V.B.42}$$

Next, we consider the boundary conditions of the situation of interest in order to determine the field matrices from medium 0 and medium 2. Here, they are given by (cf. Fig. V.B.1)

$$\mathbf{e}^{(0)}_p(z) = \begin{pmatrix} E_0\,\mathrm{e}^{\mathrm{i}\,q_\perp^{(0)} z} \\ E_R\,\mathrm{e}^{-\mathrm{i}\,q_\perp^{(0)} z} \end{pmatrix}\,, \qquad \mathbf{e}^{(2)}_p(z) = \begin{pmatrix} E_T\,\mathrm{e}^{\mathrm{i}\,q_\perp^{(2)} z} \\ 0 \end{pmatrix}, \tag{V.B.43}$$

where we took into account that there is no wave incident from $z = \infty$ and denoted $E^{(0,2)}_{p\pm}$ analog to Fig. V.B.1. The unknown amplitudes E_R and E_T can be determined by inserting Eq. (V.B.43) in Eq. (V.B.42) and once they are known, Eq. (V.B.42) can also be used to determine the field in layer 1.

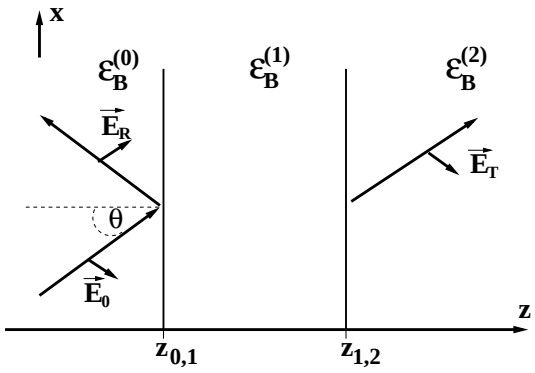

Figure V.B.1 — Propagation through a Multi-Layer Geometry: Example of a propagation through a multi-layer geometry for the case of an incident p-polarized fi eld with amplitude E_0.

4. Combination of Transfer Matrix Formalism and Green-Function Formalism

In order to investigate the effect of the presence of a multilayer structure on the fields generated by the sheet of polarization, the Green-function formalism is now combined with the transfer matrix formalism as done in [Sip87]. From chapter V.B.1.b we know that the field generated by a sheet of polarization at $z = z'$, i.e. $\mathbf{P}(\mathbf{r}) = \mathbf{P}\delta(z - z')\mathrm{e}^{\mathrm{i}\ \mathbf{q}_{||}\cdot\mathbf{r}_{||}}$, is given by

$$\mathbf{E}(\mathbf{r}) = -\omega^2\,\mu_0\Bigg\{\frac{\mathrm{e}^{\mathrm{i}\ q_\perp\,|z-z'|}}{2\,\mathrm{i}\ q_\perp}[(\hat{\mathbf{s}}\hat{\mathbf{s}} + \hat{\mathbf{p}}_+\hat{\mathbf{p}}_+)\Theta(z - z') + (\hat{\mathbf{s}}\hat{\mathbf{s}} + \hat{\mathbf{p}}_-\hat{\mathbf{p}}_-)\Theta(z' - z)] + \frac{c^2}{\omega^2\,\epsilon_b}\delta(z - z')\hat{\mathbf{z}}\hat{\mathbf{z}}\Bigg\}\mathbf{P}\ \mathrm{e}^{\mathrm{i}\ \mathbf{q}_{||}\cdot\mathbf{r}_{||}}\ . \tag{V.B.44}$$

Using Eq. (V.B.34), we find that we can connect the field matrices left and right from the discontinuity at $z = z'$ according to

$$\mathbf{e}_{s,p}(z'_+) = \quad \mathbf{e}_{s,p}(z'_-) + \mathbf{v}_{s,p}\ , \tag{V.B.45}$$

where $z'_+(z'_-)$ is infinitesimal larger (smaller) than z' and $\mathbf{v}_{s,p}$ is defined as

$$\mathbf{v}_{s,p} = \quad \begin{pmatrix} v_{s,p+} \\ -v_{s,p-} \end{pmatrix}\ , \qquad v_s = -\frac{\omega^2\,\mu_0}{2\,\mathrm{i}\ q_\perp}\hat{\mathbf{s}}\cdot\mathbf{P}\ , \qquad v_{p\pm} = -\frac{\omega^2\,\mu_0}{2\,\mathrm{i}\ q_\perp}\hat{\mathbf{p}}_\pm\cdot\mathbf{P}\ . \tag{V.B.46}$$

In contrast to the generated field, reflections of the generated fields due to the presence of interfaces will not be discontinuous at $z = z'$. Thus the generated fields in the presence of a multi-layer geometry can be derived by simply combining Eq. (V.B.45) with Eq. V.B.35 - Eq. V.B.41. As an example, we again consider the multi-layer geometry given in Fig. V.B.1 but add the polarization $\mathbf{P}(\mathbf{r}) = \mathbf{P}\delta(z - z')\mathrm{e}^{\mathrm{i}\ \mathbf{q}_{||}\cdot\mathbf{r}_{||}}$ with $z' = 0.5(z_{1,2} - z_{0,1})$, i.e. we now have a sheet of polarization in the middle of layer 1. This yields

$$\begin{aligned}
\mathbf{e}_p^{(0)}(z_{0,1}) = &\quad \mathbf{M}_{0,1}^p\mathbf{e}_p^{(1)}(z_{0,1}) && \text{(V.B.47)}\\
= &\quad \mathbf{M}_{0,1}^p\mathbf{M}_1(z_{0,1} - z')\mathbf{e}_p^{(1)}(z'_-) && \text{(V.B.48)}\\
= &\quad \mathbf{M}_{0,1}^p\mathbf{M}_1(z_{0,1} - z'_-)[\mathbf{e}_p^{(1)}(z'_+) - \mathbf{v}_p] && \text{(V.B.49)}\\
= &-\mathbf{M}_{0,1}^p\mathbf{M}_1(z_{0,1} - z'_-)\mathbf{v}_p + \mathbf{M}_{0,1}^p\mathbf{M}_1(z_{0,1} - z_{1,2})\mathbf{e}_p^{(1)}(z_{1,2}) && \text{(V.B.50)}\\
= &-\mathbf{M}_{0,1}^p\mathbf{M}_1(z_{0,1} - z'_-)\mathbf{v}_p + \mathbf{M}_{0,1}^p\mathbf{M}_1(z_{0,1} - z_{1,2})\mathbf{M}_{1,2}^p\mathbf{e}_p^{(2)}(z_{1,2})\ . && \text{(V.B.51)}
\end{aligned}$$

The boundary conditions are still the same, thus the field matrices from medium 0 and medium 2 are given by

$$\mathbf{e}_p^{(0)}(z) = \begin{pmatrix} E_0\ \mathrm{e}^{\mathrm{i}\ q_\perp^{(0)}z} \\ E_R\ \mathrm{e}^{-\mathrm{i}\ q_\perp^{(0)}z} \end{pmatrix}\ , \qquad \mathbf{e}_p^{(2)}(z) = \begin{pmatrix} E_T\ \mathrm{e}^{\mathrm{i}\ q_\perp^{(2)}z} \\ 0 \end{pmatrix}\ . \tag{V.B.52}$$

The only difference to Eq. (V.B.52) lies in the definition of E_R and E_T. Whereas in Eq. (V.B.52), E_R, E_T consist only of the reflected/transmitted parts of the incident field, here also contributions of the generated fields (including their multiple reflections) are included. The amplitudes, $E_{p+}^{(1)}$, $E_{p-}^{(1)}$, of the fields in layer 1 can again be determined when E_R, E_T are known. The easiest way is probably to express the field in layer 1 according to

$$\mathbf{E}_p^{(1)}(\mathbf{r}) = \quad [E_{p+}^{(1)} + v_{p+}\mathrm{e}^{-\mathrm{i}\ q_\perp^1 z'}\Theta(z - z')]\ \hat{\mathbf{p}}_{1+}\ \mathrm{e}^{\mathrm{i}\ \mathbf{q}_{1+}\cdot\mathbf{r}} + [E_{p-}^{(1)} + v_{p-}\mathrm{e}^{\mathrm{i}\ q_\perp^1 z'}\Theta(z' - z)]\ \hat{\mathbf{p}}_{1-}\ \mathrm{e}^{\mathrm{i}\ \mathbf{q}_{1-}\cdot\mathbf{r}} - \frac{c^2\mu_0}{\epsilon_b}\delta(z - z')(\hat{\mathbf{z}}\cdot\mathbf{P})\hat{\mathbf{z}}\,\mathrm{e}^{\mathrm{i}\ \mathbf{q}_{||}\cdot\mathbf{r}_{||}}\ . \tag{V.B.53}$$

Here, the amplitudes $E_{p+}^{(1)}$ and $E_{p-}^{(1)}$ contain all contributions, which are continuous at $z = z'$ (incident field and all reflections). The direct contributions of the generated fields, which are discontinuous at $z = z'$, are added explicitly. Thus, $E_{p+}^{(1)}$ should be determined using the equation for $z_{0,1} < z < z'$, i.e. Eq. (V.B.48), as in this area the rightward contribution of the field does not contain direct contributions of the generated field (only reflected ones, which are thus continuous at $z = z'$). Respectively, $E_{p-}^{(1)}$ should be determined using the equation for $z' < z < z_{1,2}$:

$$\mathbf{e}_p^{(2)}(z_{1,2}) = \mathbf{M}_{2,1}^p \mathbf{M}_1(z_{1,2} - z'_+)\mathbf{e}_p^{(1)}(z'_+) \,. \tag{V.B.54}$$

To summarize, in a multi-layer structure, the fields in layers n without sources can always be written according to

$$\mathbf{E}^{(n)}(\mathbf{r}) = \quad (E_{s+}^{(n)}\,\hat{\mathbf{s}}_n + E_{p+}^{(n)}\,\hat{\mathbf{p}}_{n+})\mathrm{e}^{\mathrm{i}\ \mathbf{q}_{n+}\cdot\mathbf{r}} + (E_{s-}^{(n)}\,\hat{\mathbf{s}}_n + E_{p-}^{(n)}\,\hat{\mathbf{p}}_{n-})\mathrm{e}^{\mathrm{i}\ \mathbf{q}_{n-}\cdot\mathbf{r}} \tag{V.B.55}$$

in layer $m \neq n$ which contains a sheet of polarization at $z = z'$ (and therewith is discontinuous) according to

$$\begin{aligned}
\mathbf{E}^{(m)}(\mathbf{r}) = \quad & [E_{p+}^{(m)} + v_{p+}\mathrm{e}^{-\mathrm{i}\ q_\perp^m z'}\Theta(z - z')]\,\hat{\mathbf{p}}_{m+}\,\mathrm{e}^{\mathrm{i}\ \mathbf{q}_{m+}\cdot\mathbf{r}} \\
& + [E_{p-}^{(m)} + v_{p-}\mathrm{e}^{\mathrm{i}\ q_\perp^m z'}\Theta(z' - z)]\,\hat{\mathbf{p}}_{m-}\,\mathrm{e}^{\mathrm{i}\ \mathbf{q}_{m-}\cdot\mathbf{r}} \\
& + [E_{s+}^{(m)} + v_s\mathrm{e}^{-\mathrm{i}\ q_\perp^m z'}\Theta(z - z')]\,\hat{\mathbf{s}}_m\,\mathrm{e}^{\mathrm{i}\ \mathbf{q}_{m+}\cdot\mathbf{r}} \\
& + [E_{s-}^{(m)} + v_s\mathrm{e}^{\mathrm{i}\ q_\perp^m z'}\Theta(z' - z)]\,\hat{\mathbf{s}}_m\,\mathrm{e}^{\mathrm{i}\ \mathbf{q}_{m-}\cdot\mathbf{r}} \\
& - \frac{c^2\mu_0}{\epsilon_b}\delta(z - z')(\hat{\mathbf{z}}\cdot\mathbf{P})\hat{\mathbf{z}}\,\mathrm{e}^{\mathrm{i}\ \mathbf{q}_{||}\cdot\mathbf{r}_{||}} \,.
\end{aligned} \tag{V.B.56}$$

To this point, we are now able to derive the macroscopic fields generated by a *given sheet of polarization*, in the presence of a multi-layer geometry. If the polarization of the MQW system would be known, the generalization of the obtained results could be achieved by adding up the fields generated by different sheets of polarization. However, the polarization of the MQW system is not known beforehand as it is dependent on the local field (which in turn is dependent on the polarization) and leads back to the coupling of microscopic and macroscopic equations.

CHAPTER VI
Coupling of Microscopic and Macroscopic Equations of Motion: Multiple Quantum Well Samples

In the following, the derived macroscopic equations are coupled to the microscopic equations which have been derived in Chapter III and already analyzed for the case of a single quantum well in Chapter IV. Consequently, the derived theory is enhanced to the description of multiple quantum well samples. For convenience, we focus on the description of multiple quantum well samples composed of N electronically uncoupled - in principle identical - quantum wells. Note, however, that the theory can be easily adjusted to the description of quantum well samples composed of different quantum wells.

Due to the different dependence on the electric field, the distinction between linear and nonlinear excitation is stronger than before. In Chapter IV, the theoretical approach was mainly the same in linear and nonlinear regime. The only differences being (a) a reduction of the required cpu-time due to simplified equations of motion (time-independent occupation numbers) and (b) different quantities of interest (absorption spectra vs. density oscillations). However, the actual numerical implementation was (apart from the recently addressed difference in cpu-requirements) completely the same. As we will see in the following, the coupling of macroscopic and microscopic equations is quite different in linear and nonlinear regime. Thereby, the investigation of the nonlinear regime is again the challenging one and certain approximations have to be made in order to obtain an applicable theory.

A. Application to the Linear Regime

In the case of linear absorption, the Fourier transformation of the equation of motion for the intersubband coherence (which gives the macroscopic polarization[1]) yields an equation linear in $\int \mathrm{d}z\, \mathbf{d}_{ab}(z) \cdot \mathbf{E}(z,\omega)$:

$$p^{(n)}(\omega) = \chi^{(n)}(\omega) \int \mathrm{d}z\, \mathbf{d}_{ab}^{(n)}(z) \cdot \mathbf{E}^{(n)}(z,\omega), \tag{VI.A.1}$$

where $\chi^{(n)}$ denotes the general linear susceptibility in quantum well n (see Chapter IV) which is defined in terms of the intersubband coherences and can be evaluated once the latter are determined [WFK04, WFL$^+$04]. $p^{(n)}(\omega)$ denotes the sum over the intersubband coherences in Fourier domain $p^{(n)}(\omega) = \sum_{\mathbf{k}} p_{\mathbf{k}}^{(n)}(\omega)$. In the linear regime $\chi^{(n)}$ is independent of the electric field. This can be used to simplify the determination of the susceptibility according to

$$\chi^{(n)}(\omega) = \frac{p^{(n)21}(\omega)}{\frac{1}{\hbar}\int \mathrm{d}z\, \mathbf{d}_{ab}^{(n)}(z) \cdot \mathbf{E}^{(n)}(z,\omega)}, \tag{VI.A.2}$$

$$= \frac{\hat{p}^{(n)21}(\omega)}{\frac{1}{\hbar}\mathbf{E}^{(n)}(z_0,\omega)\int \mathrm{d}z\, \mathbf{d}_{ab}^{(n)}(z)}\ . \tag{VI.A.3}$$

[1] Note that the overline indicating the macroscopic nature is dropped in the following.

In this notation $\hat{p}^{(n)21}(\omega)$ denotes the IS coherence obtained by approximating

$$\int \mathrm{d}z\, \mathbf{d}_{ab}^{(n)}(z) \cdot \mathbf{E}^{(n)}(z,\omega) \approx \mathbf{E}^{(n)}(z_0,\omega) \int \mathrm{d}z\, \mathbf{d}_{ab}^{(n)}(z) \tag{VI.A.4}$$

in the corresponding equation of motion. z_0 denotes the center of quantum well n. Thus, we can here resort to the susceptibilities calculated in Chapter IV. Using Eq. (VI.A.1) we obtain the dipole density $\mathbf{P}^{(n)}(z',\omega)$ as a function of the local field $\mathbf{E}^{(n)}(z,\omega)$

$$\mathbf{P}^{(n)}(z,\omega) = \int_{(n)} \overleftrightarrow{\chi}_{z,z'}^{(n)}(\omega) \cdot \mathbf{E}^{(n)}(z',\omega)\, dz', \tag{VI.A.5a}$$

where $\overleftrightarrow{\chi}_{z,z'}^{(n)}(\omega)$ is the nonlocal susceptibility tensor in dyadic form

$$\overleftrightarrow{\chi}_{z,z'}^{(n)}(\omega) := \frac{1}{\mathcal{A}\hbar}\, \chi^{(n)}(\omega)\, \mathbf{d}_{21}^{(n)}(z)\, \mathbf{d}_{21}^{(n)}(z')\,. \tag{VI.A.6}$$

For the case of identical quantum wells, which have thus the same linear susceptibility, this can be further simplified according to

$$\overleftrightarrow{\chi}_{z,z'}^{(n)}(\omega) = \frac{1}{\mathcal{A}\hbar}\, \chi(\omega)\, \mathbf{d}_{21}^{(n)}(z)\, \mathbf{d}_{21}^{(n)}(z')\,. \tag{VI.A.7}$$

In a nutshell this means, that we can - in the linear regime - account for the coupling of macroscopic and microscopic separately. We can first determine the linear susceptibility of a single quantum well excited by a homogenous external field and can then use the determined susceptibility to investigate the linear response of a multiple quantum well sample (with respect to a variety of geometrical or material parameters) by solving the corresponding macroscopic equations of motions, namely Eq. (V.B.56) or a modification of this equation.

1. Absorption of a Simplified MQW System Sample

To elucidate the general procedure, we discuss in the following the very basic example of a MQW without respect to any geometrical complications such as different dielectric constants or additional layers. A coarse sketch of the considered geometry is given in Fig. VI.A.1.

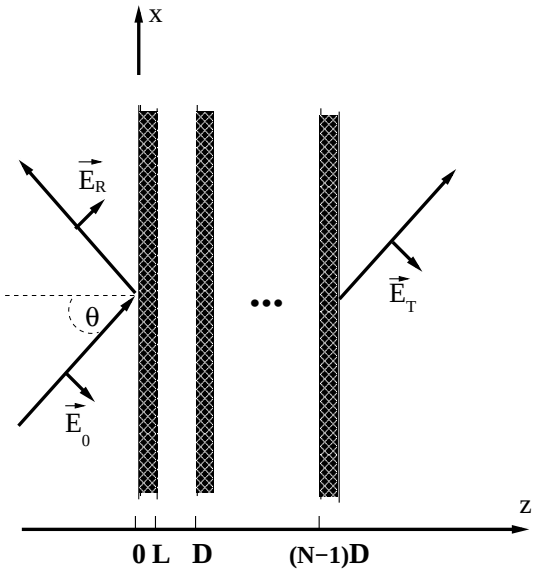

Figure VI.A.1 — Example of a Simplified MQW System Sample: A possible mismatch of dielectric constants of barrier and well layers is neglected. The sample consists of N electronically uncoupled (identical) quantum wells. $\mathbf{E}_0$ denotes the incident (p-polarized) field, $\mathbf{E}_T$ and $\mathbf{E}_R$ the transmitted and reflected fields.

In this case, we insert Eq. (VI.A.6) and Eq. (V.B.18) in Eq. (V.B.17) (which we have generalized according to section V.B.2). This yields

$$E_x^{(n)}(z) = -E_0 \frac{q_\perp}{q} \mathrm{e}^{\mathrm{i}\ q_\perp\ z} - \mu_0\,\omega^2\,\frac{1}{\mathcal{A}\hbar}\,\chi(\omega)\,\frac{e^2\,q_\perp\,q_{||}}{2\,\mathrm{i}\ q_\perp\,q^2}\sum_{m=1}^{N}\Gamma_z^{(m)} \tag{VI.A.8}$$
$$\times \int_{(m)} \mathrm{d}z'\, d_{21}^{(m)}(z')\,[\mathrm{e}^{\mathrm{i}\ q_\perp|z-z'|}(\Theta(z'-z)-\Theta(z-z'))],$$

$$E_z^{(n)}(z) = E_0 \frac{q_{||}}{q} \mathrm{e}^{\mathrm{i}\ q_\perp\ z} - \mu_0\,\omega^2\,\frac{1}{\mathcal{A}\hbar}\,\chi(\omega)\,e^2\sum_{m=1}^{N}\Gamma_z^{(m)} \tag{VI.A.9}$$
$$\times \int_{(m)} \mathrm{d}z'\, d_{21}^{(m)}(z')\,[\frac{q_{||}^2}{2\,\mathrm{i}\ q_\perp\,q^2}\mathrm{e}^{\mathrm{i}\ q_\perp|z-z'|}(\Theta(z'-z)+\Theta(z-z'))$$
$$+\frac{c^2}{\omega^2\,\epsilon_b}\delta(z-z')]\,.$$

Here we have applied

$$\Gamma_z^{(m)} = \int_{(m)} \mathrm{d}z''\, d_{21}^{(m)}(z'')\,E_z^{(m)}(z'')\,. \tag{VI.A.10}$$

In order to determine the unknown quantity $\Gamma_z^{(m)}$, Eq. (VI.A.9) is multiplied with the dipole moment $d_{21}^{(n)}(z)$ and the resulting equation is integrated over z across the *n*-th quantum well [Liu94] leading to

$$\Gamma_z^{(n)} = \quad E_0 \frac{q_{||}}{q} \int_{(n)} \mathrm{d}z\,\mathrm{e}^{\mathrm{i}\ q_\perp\ z}\,d_{21}^{(n)}(z) \tag{VI.A.11}$$
$$-\,\mu_0\,\omega^2\ \frac{1}{\mathcal{A}\hbar}\,\chi(\omega)\ e^2\sum_{m=1}^{N}\Gamma_z^{(m)}\int_{(n)}\mathrm{d}z\,d_{21}^{(n)}(z)(\int_{(m)}\mathrm{d}z'\,d_{21}^{(m)}(z')\frac{q_{||}^2}{2\,\mathrm{i}\ q_\perp\,q^2}$$
$$[\mathrm{e}^{\mathrm{i}\ q_\perp|z-z'|}(\Theta(z'-z)+\Theta(z-z'))+\frac{c^2}{\omega^2\,\epsilon_b}\delta(z-z')]).$$

Equation VI.A.11 forms a system of N linear equations which can be solved numerically. The calculation of $\Gamma_z^{(n)}$ yields the determination of the local field which in turns yields the transmitted and reflected fields and therewith the absorbance (optical absorption strength):

$$A = 1 - R - T = 1 - |\mathbf{E}^R|^2/|\mathbf{E}_0|^2 - |\mathbf{E}^T|^2/|\mathbf{E}_0|^2\,. \tag{VI.A.12}$$

In the same way, the absorption of more complicated multiple quantum well systems can be determined. Combining transfer matrix formalism and Green's function formalism as described in Section V.B.4, we can not only take into account reflections at a prism base and a possible mismatch of dielectric constants but also consider the existence of polarization in the barriers in the case of a finite potential. Once, an expression for the considered structure has been derived (which can be done in a very general way for example for the structure sketched in Fig. V.A.1), the local fields can be determined in the same way as described for the simplified example in Section VI.A.1.

2. Numerical Results

In the following, we investigate the influence of radiative coupling on the linear absorption spectra. First, we focus on the simplified MQW sample [cf. Fig. VI.A.1], we considered in the preceding section. The sample shall consist of N GaAs quantum wells each with well width L, and separated by $Al_{0.35}Ga_{0.65}As$ barriers, each with a thickness of $D = 2L$ nm. In order to directly demonstrate the dependence of radiative coupling on well width and carrier density, we consider quantum wells with (A) carrier density $n = 1.2 \times 10^{12}\text{cm}^{-2}$ and (B) $n = 5.0 \times 10^{10}\text{cm}^{-2}$. The temperature is $T = 50$ Kelvin. As can be seen, the impact of radiative coupling is strongly dependent on the carrier density. Whereas for a small carrier density an increase in well number yields mainly a proportional enhancement of the absorption, for the high density, increasing the well number yields only first an enhancement. Further increasing yields an effective lower but more strongly broadened absorption. The same difference can be seen for a variation of the angle of incidence. For the low carrier density a larger angle of incidence yields a larger overall absorption, as the coupling to the electric field is increased. For the high density the overall absorption is first enhanced and then reduced as the light is reflected to a large extent at the high susceptibility.

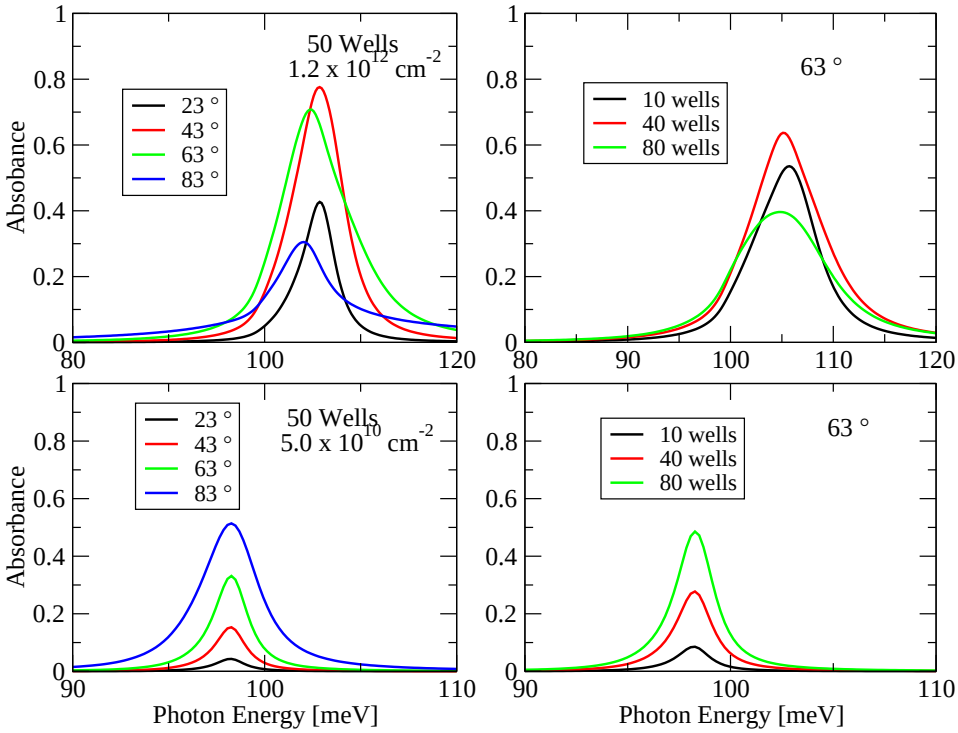

Figure VI.A.2 — Absorption in Multiple Quantum Well System: Absorption in different MQWs. Upper row: carrier density $n = 1.2 \times 10^{12}\text{cm}^{-2}$, lower row: carrier density $n = 5.0 \times 10^{10}\text{cm}^{-2}$ with different well number and different angle of incidence

Next, we vary the geometry of the sample, by including total reflection at an interface located behind the wells, similar to Fig. V.A.1 but without taking into account different dielectric constants for well and barrier material. The spacing between wells and interface and angle of incidence is chosen so that the sample is excited in a total-reflection geometry - with the center of the quantum wells located in the middle of the resulting standing wave. The corresponding spectra are given in Fig. VI.A.3. Due to the standing wave effect, the radiative coupling is enhanced. Although the lineshape is in some cases differently shaped and the maximum absorption is altered, the tendencies are the same as in Fig. VI.A.2.

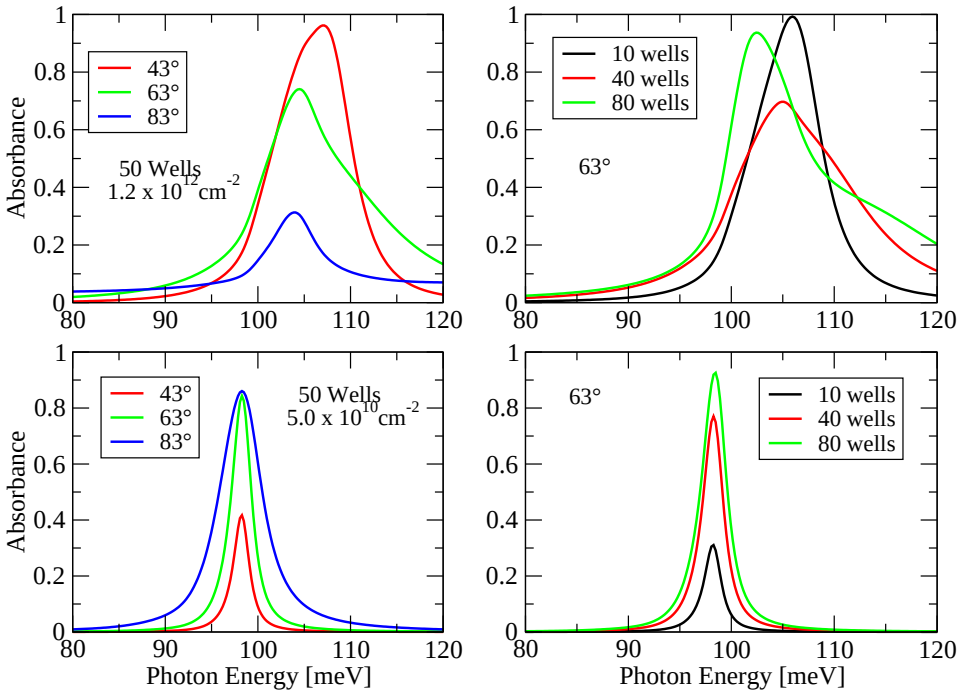

Figure VI.A.3 — Absorption of MQW in total reflection geometry: Absorption in different MQWs. Upper row: carrier density $n = 1.2 \times 10^{12}\mathrm{cm}^{-2}$, lower row: carrier density $n = 5.0 \times 10^{10}\mathrm{cm}^{-2}$ with different well number and different angle of incidence. The distance from the interface is chosen so that *in all cases* the center of the wells is located in the middle of the standing wave

Last, we investigate the impact of a dismatch of the dielectric constants of well and barrier material. As can be seen in Fig. VI.A.4 the inclusion of different dielectric constants yields, for the here considered example [50 quantum wells in total reflection geometry], a slight change in the lineshape, but the overall impression does not change. In conclusion one can say, that linewidth and lineshape can be altered strongly by changing macroscopic quantities or parameters. Whereas for low densities, the main effect is simply an enhancement of the overall absorption, the response is more complex for quantum well samples with higher carrier densities. Thus for a successful comparison with experimental results or more general for a valuable prediction of lineshape and linewidth of linear absorption spectra especially of highly doped multiple quantum well samples, the actual geometry of the sample should be taken into account.

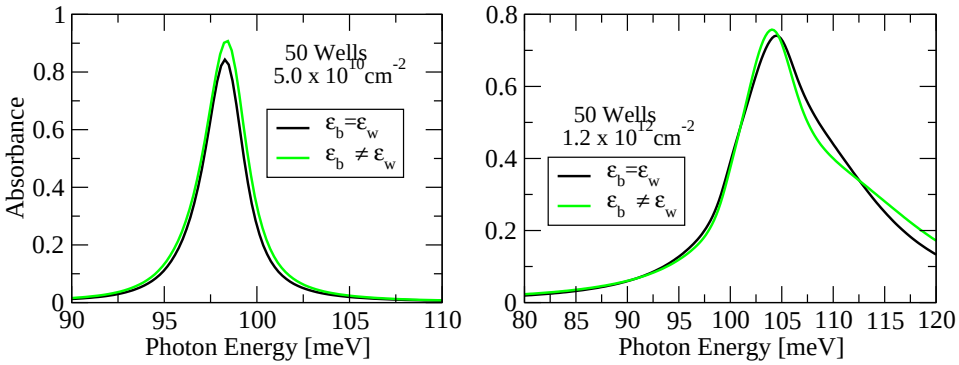

Figure VI.A.4 — Absorption of MQW in total reflection geometry with $\epsilon_B = \epsilon_W$ or $\epsilon_B \neq \epsilon_W$: Absorption in different MQWs. Upper row: carrier density $n = 1.2 \times 10^{12}\mathrm{cm}^{-2}$, lower row: carrier density $n = 5.0 \times 10^{10}\mathrm{cm}^{-2}$ with different well number and different angle of incidence. The distance from the interface is again chosen so that *in all cases* the center of the wells is located in the middle of the standing wave

B. Application to the Nonlinear Regime

To account for the impact of radiative coupling/dephasing in the nonlinear regime, i.e. the interaction with reemitted photons, the solution of Maxwell's Equations has to be combined with the equation for the polarization density in time domain: in the microscopic equations of motion the *actual local* field consisting of external field and fields generated by the polarization in the MQW-sample has to be considered while solving the equations of motion. Thus, both macroscopic and microscopic equations have to be solved simultaneously.

In the preceding chapter, we derived the fields generated by the monochromatic polarization

$$\mathbf{P}(\mathbf{r},t) = \mathbf{P}(\mathbf{r})\mathrm{e}^{-\mathrm{i}\,\omega t}\,. \tag{VI.B.1}$$

which is a Fourier component of the arbitrary polarization given by

$$\mathbf{P}(\mathbf{r},t) = \frac{1}{2\pi}\int_{-\infty}^{\infty} d\omega \mathbf{P}(\mathbf{r},\omega)\mathrm{e}^{-\mathrm{i}\,\omega t}\,. \tag{VI.B.2}$$

Based on the solutions of Maxwell's Equations in Fourier domain we can thus obtain the desired z-component of the field generated by the polarization density of the quantum wells by Fourier superposition. In the following, we again consider the simplest possible multiple quantum well system for explaining the derivation [cf. Fig. VI.A.1]):

$$\begin{aligned} E_z(\mathbf{r},t) = \frac{1}{\sqrt{2\pi}^3}\int d^2Q_{||}\int_{-\infty}^{\infty} d\omega \mathrm{e}^{\mathrm{i}\,(\mathbf{Q}_{||}\cdot\mathbf{r}_{||}-\omega t)}\sum_{m=1}^{N}\int_{(m)} dz'\,\mathbf{P}^{(m)}(\mathbf{Q}_{||},z',\omega) \\ \times\left\{\frac{\mathrm{i}\,\mu_0\omega^2}{2Q_\perp}\frac{Q_{||}^2}{Q^2}\mathrm{e}^{\mathrm{i}\,Q_\perp|z-z'|}\big[\Theta(z-z')+\Theta(z'-z)\big]-\frac{1}{\epsilon_\infty}\delta(z-z')\right\}. \end{aligned} \tag{VI.B.3}$$

In contrast to the linear regime, we can here not consider a homogenous field while solving the microscopic equations of motion as done in the previous section, as the intersubband coherence is not linearly dependent on the exciting field. Thus, if we want to include the radiative coupling in the theory, we now have to consider the actual space-dependent field in the microscopic equations

of motion. However, in the parameter range considered here, we can simplify the actual space-dependence to a large extent. Therefore we rewrite the macroscopic polarization according to

$$\mathbf{P}(\mathbf{r},t) = \sum_{\mathbf{Q}} \mathbf{P}(\mathbf{Q},z,t)\mathrm{e}^{\mathrm{i}\,\mathbf{Q}\cdot\mathbf{r}_{||}} \tag{VI.B.4}$$

with

$$\mathbf{P}(\mathbf{Q},z,t) = \frac{1}{A}\sum_{\mathbf{q}} \Big\{\langle a^{\dagger}_{1,\mathbf{q}-\mathbf{Q}/2}a_{2,\mathbf{q}+\mathbf{Q}/2}\rangle + c.c.\Big\}\mathbf{d}_{12}(z) \tag{VI.B.5}$$

$$= \frac{1}{A}\sum_{\mathbf{k}} \Big\{\langle a^{\dagger}_{1,\mathbf{k}-\mathbf{Q}}a_{2,\mathbf{k}}\rangle + c.c.\Big\}\mathbf{d}_{12}(z)\,. \tag{VI.B.6}$$

Next, we focus on a simplified equation of motion for the intersubband coherence. Simplified in the sense, that we consider only free-carrier and carrier-field contributions and neglect the many-particle contributions for a while.

$$\frac{\mathrm{d}}{\mathrm{d}t}\langle a^{\dagger}_{1,\mathbf{k}-\mathbf{Q}}a_{2,\mathbf{k}}\rangle = \frac{\mathrm{i}}{\hbar}(\epsilon_{1,\mathbf{k}-\mathbf{Q}} - \epsilon_{2,\mathbf{k}})\langle a^{\dagger}_{1,\mathbf{k}-\mathbf{Q}}a_{1,\mathbf{k}}\rangle \\ - e\frac{\mathrm{i}}{\hbar}\sum_{\mathbf{q}}\int dz d_{12}(z)E_z(\mathbf{q},z,t)\Big\{\langle a^{\dagger}_{1,\mathbf{k}-\mathbf{Q}+\mathbf{q}}a_{1,\mathbf{k}}\rangle - \langle a^{\dagger}_{2,\mathbf{k}-\mathbf{Q}}a_{2,\mathbf{k}-\mathbf{q}}\rangle\Big\}\,. \tag{VI.B.7}$$

As can be seen, in the case of initial homogenous electron distributions:

$$\langle a^{\dagger}_{1,\mathbf{k}-\mathbf{Q}+\mathbf{q}}a_{1,\mathbf{k}}\rangle(t_0) = \langle a^{\dagger}_{1,\mathbf{k}}a_{1,\mathbf{k}}\rangle(t_0)\delta_{\mathbf{k}-\mathbf{Q}+\mathbf{q},\mathbf{k}}$$

only for intersubband coherences with $\mathbf{Q} = \mathbf{q}$ the dynamics is driven directly by the field. In the following, we consider the external field (only the $z-$component is important here) to be of the form

$$E_z^{\mathrm{ext}}(\mathbf{r},t) \propto \mathrm{Cos}(\omega_{\mathrm{L}}\mathrm{t} - \mathrm{k}_{\mathrm{x}}^{\mathrm{L}}\mathrm{x} - \mathrm{k}_{\mathrm{z}}^{\mathrm{L}}\mathrm{z})\mathrm{e}^{-\frac{(\mathrm{t}-\mathrm{t}_0-\mathrm{k}_{\mathrm{x}}^{\mathrm{L}}/\omega_{\mathrm{L}}\mathrm{x}-\mathrm{k}_{\mathrm{z}}^{\mathrm{L}}/\omega_{\mathrm{L}}\mathrm{z})^2}{2\tau^2}} \tag{VI.B.8}$$

where ω_L is the laser frequency and $\mathbf{k}_L = (k_x^L, 0, k_z^L)$ is the corresponding wave vector. The Fourier transform of Eq. (VI.B.8) with respect to in-plane space coordinates and time can be expressed according to

$$\tilde{E}_z^{\mathrm{ext}}(\mathbf{q},z,\omega) = \hat{E}_z^{\mathrm{ext}}(\mathbf{q},z,\omega)\delta(q_x - \frac{\omega}{\omega_L}k_x^L)\delta(q_y)\,. \tag{VI.B.9}$$

Note, that $\hat{E}_z^{\mathrm{ext}}(\mathbf{q},z,\omega)$ is only an abbreviation for the explicit function as we here are mainly interested in the part with the delta-function. Inserting Eq. (VI.B.9) in the (time) Fourier Transform of Eq. (VI.B.7), we find that thus only intersubband coherences with $\mathbf{Q}' = \frac{\omega}{\omega_L}k_x^L\mathbf{e}_x$ are driven directly by the external field. Assuming that these contributions are the dominant ones and having in mind the parameter range considered here, we thus approximate the macroscopic polarization according to

$$\mathbf{P}(\mathbf{r},t) \;\approx\; \frac{1}{\sqrt{2\pi}}\int_{-\infty}^{\infty}d\omega\sum_{\mathbf{Q}}\mathbf{P}(z,\omega)\mathrm{e}^{\mathrm{i}\,(\mathbf{Q}\cdot\mathbf{r}_{||}-\omega t)}\delta_{\mathbf{Q},\frac{\omega}{\omega_L}k_x^L\mathbf{e}_x}$$

with

$$\mathbf{P}(z,\omega) \;=\; \frac{1}{A}\sum_{\mathbf{k},m}\Big\{p^{(m)}_{\mathbf{k}-\frac{\omega}{\omega_L}k_x^L\mathbf{e}_x,\mathbf{k}}(\omega) + c.c.\Big\}\mathbf{d}_{12}(z)\,. \tag{VI.B.10}$$

As for the parameter range considered here $k_x^L \mathbf{e}_x << \mathbf{k}$ and the dominant contributions to the intersubband coherence can be expected for $\omega \approx \omega_L$, we can simplify Eq. (VI.B.10) further

$$\mathbf{P}(z,\omega) \approx \frac{1}{A}\sum_{\mathbf{k},m}\Big\{p_{\mathbf{k}}^{(m)}(\omega)+c.c.\Big\}\mathbf{d}_{12}(z)$$

and find that the macroscopic polarization is here composed of intersubband coherences which are diagonal in $\mathbf{k}$.

Using $-\mathrm{i}\,\omega \mathrm{e}^{-\mathrm{i}\,\omega t} = d/dt\,\mathrm{e}^{-\mathrm{i}\,\omega t}$ we obtain therewith the generated field in the form

$$E_z(z,t) = -\sum_{m=1}^{N}\int_{(m)} dz' \Big\{\frac{\mu_0\omega_L}{2Q_\perp^L}\sin^2\theta_L\big[\Theta(z-z')+\Theta(z'-z)\big]\,\frac{\mathrm{d}}{\mathrm{d}t}\mathbf{P}^{(m)}(z',t-\frac{Q_\perp^L}{\omega_L}|z-z'|) + \frac{1}{\epsilon_\infty}\delta(z-z')\mathbf{P}^{(m)}(z',t)\Big\} \tag{VI.B.11}$$

Next, we insert the complete transverse field, i.e. the *transverse part of Eq. (VI.B.11)* together with the external applied field $E_0(z,t)$ in the carrier-field part of the microscopic equations of motion for the intersubband coherence and the occupation numbers. In this way, the influence of radiative coupling can be investigated by solving the microscopic equations for every quantum well with a self-consistently determined radiation field.

Note, that in contrast to the linear regime, where we could determine the linear response of a multiple quantum well system by solving the microscopic equations of motion for the intersubband coherence of *one single quantum well only*, we now have to solve an equation of motion for the intersubband coherence of *each single quantum well.* In addition to this, we have to solve equations of motion for the occupation of the two subbands. This means, that we have to solve the microscopic equations for $3N$ quantities in a N quantum well sample. Thereby, for each quantity we have to solve nk single equations of motions, where nk is the number of wave vectors $\mathbf{k}$, as intersubband coherence and occupation are dependent on the wave number. Consequently, the required cpu-time is increasing enormously. Whereas a calculation including mean-field calculations and carrier-phonon interaction is still settled in an acceptable time frame, the inclusion of carrier-carrier scattering is almost impossible without a draw back on certain approximations. For example, the calculation of the nonlinear response of a 51 quantum well sample would - with inclusion of carrier-carrier scattering in its complete form - have a run-time of at least 3 months. The time frame could in principle be reduced by reducing the number of wave vectors, but this yields the risk of inaccuracies and misleading results. Therefore, we here include "only" mean-field carrier-carrier contributions and carrier-phonon scattering in the microscopic equations of motion.

1. Numerical Results

In the following, we investigate the temporal behavior of the relative population in the upper subband in each well in a multiple quantum well system - with and without regard to different dephasing contributions. The system is composed of 80 electronically uncoupled quantum wells, each a 10 nm AlGaAs/GaAs well with a carrier density of $n = 1.0\times^{12}$ cm^{-2} at a lattice temperature of $T = 50$ Kelvin, separated by $Al_{0.35}Ga_{0.65}As$ barriers with a thickness of $D - L = 20$ nm. The system is assumed to be in quasi-equilibrium before excited resonantly by an external applied field. We consider two different scenarios: a) complete neglection of possible nonparabolicity effects, i.e. the subbands are supposed to be parallel and thus the transition energy is independent from the in-plane wave vector and b) consideration of nonparabolicity effects in effective mass approximation.

We start with scenario a and concentrate first only on one of the quantum wells described above. Without carrier-phonon interaction the well reacts exactly as a simple two level system. Excited resonantly by a Gaussian pulse with pulse area $\Theta = 1\pi$, all electrons in the lower subband of

the well are exited to the upper subband [cf. thick grey line in the front of Fig. VI.B.1(a1)]. Including carrier-phonon interaction as dephasing contribution, the excitation is suppressed partly and complete inversion can not be achieved [cf. thick grey line in Fig. VI.A.2(a2)]. Including the non-parabolicity of the conduction band, i.e. different in-plane energy dispersion for the two subbands, the excitation of all electrons is not possible [cf. thick grey line in the front of Fig. VI.B.2(b1)]; the remaining excitation even further suppressed by carrier-phonon interaction [cf. thick grey line in the front of Fig. VI.B.2(b1)].

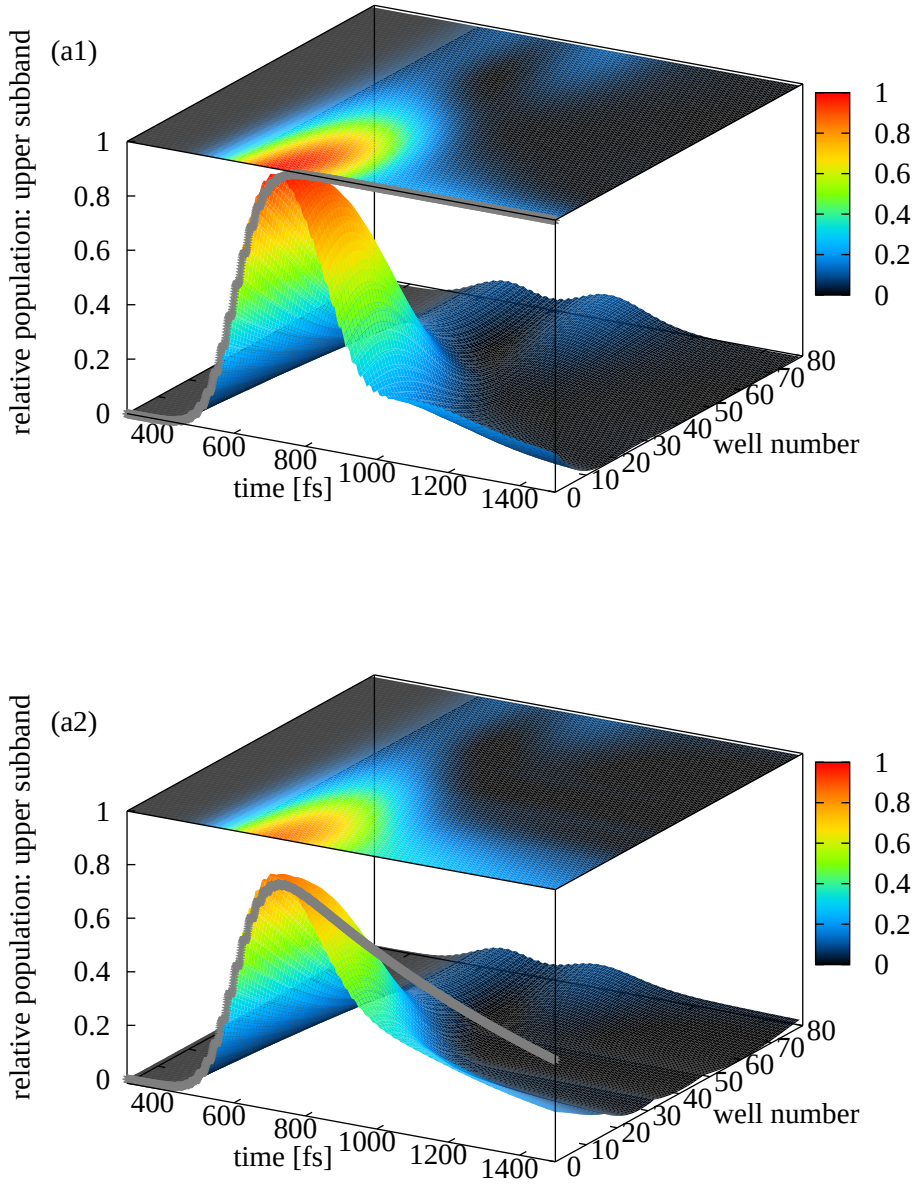

Figure VI.B.1 — Density oscillations in 80 QW System (Equal Subband Dispersion): Relative population in the upper subband in each quantum well of a 80 quantum well sample for equal in-plane energy dispersion (a1) without carrier-phonon interaction and (a2) with inclusion of carrier-phonon interaction. In all cases, the population excited in a sample containing only a single-quantum well, is plotted additionally in the front (grey line)

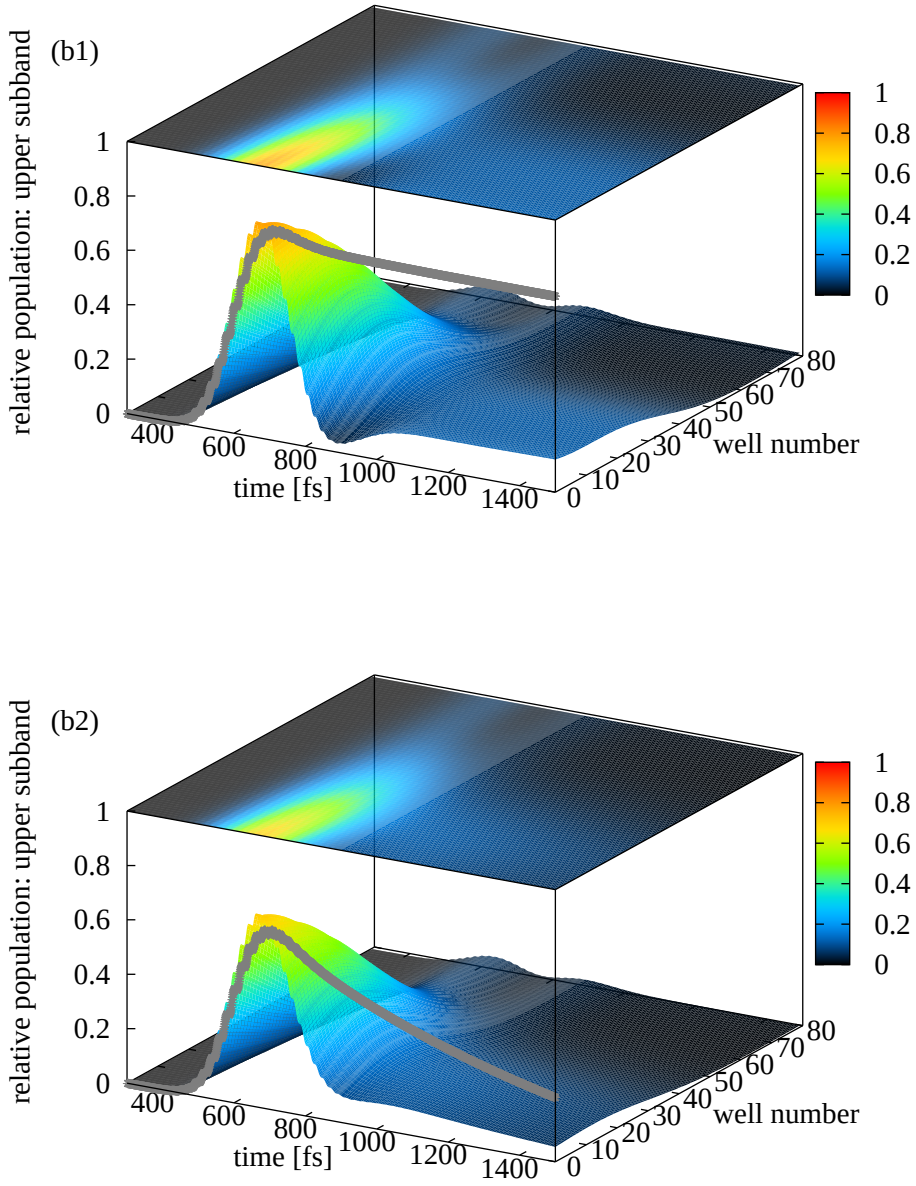

Figure VI.B.2 — Density oscillations in 80 QW System (Different Subband Dispersion): Relative population in the upper subband in each quantum well of a 80 quantum well sample for different in-plane energy dispersion (b1) without carrier-phonon interaction and (b2) with inclusion of carrier-phonon interaction. In all cases, the population excited in a sample containing only a single-quantum well, is plotted additionally in the front (grey line)

Next, we consider the full system with all 80 quantum wells (still in scenario a). In Fig. VI.A.2a, we present the population in the upper subband of each quantum well with and without carrier-phonon interaction, angle of incidence $\theta = 63°$. Due to radiative coupling between the wells, the local field in each quantum well is varying strongly in the sample. Whereas the first quantum wells exhibit a local field strong enough to excite all electrons in the upper subband, only a weak

field is present at the rear wells exciting only a small number of electrons in the upper subband. Dephasing due to carrier-phonon interaction suppresses the overall excitation of electrons, similar to the case of the single quantum well considered before. But radiative damping is clearly the dominant contribution in the example considered here. The same conclusion is valid for scenario b. Whereas the first wells in the 80 quantum well sample experience a local field strong enough to excitate electrons to the upper sample, almost none electrons are excited in the rear wells. Again, the impact of carrier-phonon interaction is strongest for the 1 quantum well sample and has almost negligible impact on the 80-wells sample.

Generally, the impact of radiative coupling is mostly dependent on the relation of oscillator strength to pulse area/amplitude of external applied field. If the applied field is considerably larger than contributions of the generated fields, local field effects become less important. Two different examples are shown in Fig. VI.B.3 (in both cases nonparabolicity and carrier-phonon interaction is neglected). For small angle of incidence, where the oscillation strength is comparatively weak, the impact of radiative coupling is almost neglectable - as can be seen in Fig. VI.B.3(a) for the example of a 1π pulse. The electrons in all wells are excited to roughly the same extent (with a small time delay) and there is almost no difference between the excitation of a single well and the whole sample. In contrast to the situation arising for a larger angle, cf. again Fig. VI.A.2. The same is valid for MQW samples with low carrier density (not shown). For a larger angle of incidence, here $\theta = 63^\circ$, exciting with a stronger pulse yields a similar effect. With increasing pulse area, the sample reacts longer like one quantum well exhibiting complete Rabi flops. However, different states of excitation can still be observed at the end of the excitation [cf. Fig. VI.B.3(b)].

Thus, radiative coupling between the quantum wells of a multiple quantum well system can dominate the Rabi oscillations of the subband populations. Especially for samples with high oscillator strength due to large carrier density, radiative coupling between wells can yield completely different excitation states in the wells of a MQW sample. However, the effect can be evaded or at least reduced by either exciting under a small angle which results in a reduced oscillator strength or on the other hand using external fields with amplitudes considerably stronger than those of the generated fields.

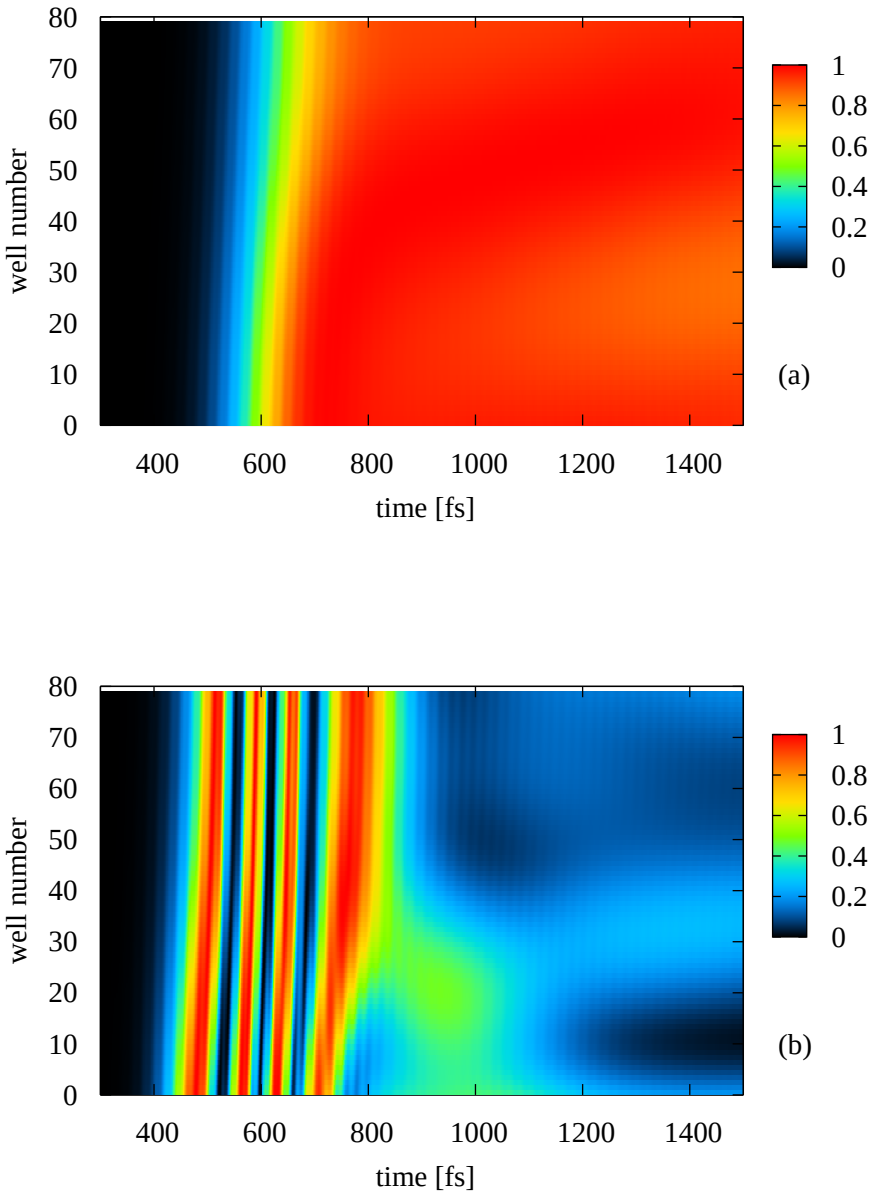

Figure VI.B.3 — Density oscillations in 80 QW System: Relative population in the upper subband in each quantum well of the 80 quantum well sample: (a) Weak oscillator strength due to small angle of incidence $\theta = 23^{\circ}$; (b) Exciting with a pulse considerably larger than the contributions due to generated fi elds (here with area $\Theta = 8\pi$) the MQW sample exhibits complete Rabi oscillations. At the end of the excitation the influence of local fi eld effects become visible.

CHAPTER VII
Comparison with Experimental Results[1]

In a last part, we will now compare the derived theory with experimental results - in both the linear and the nonlinear regime. All experiments compared with, have been performed at the Max-Planck Institute in Berlin in the group of T. Elsaesser, M. Woerner and K. Reimann.

A. Experimental Setup

The sample geometry is the same in all measurements. The actual probe differs in carrier density. In detail we distinguish sample A and B.

- Sample A is a multiple quantum well sample consisting of 51 GaAs quantum wells, each with width $L = 10$ nm, and separated by $Al_{0.35}Ga_{0.65}As$ barriers, each with a thickness of $D-L = 20$ nm (Fig. VII.A.1). The center of every barrier is n-type δ-doped with Si, resulting in an electron concentration of $n_e = 5 \times 10^{10}$ cm^{-2} in each quantum well.
- Sample B has the same sample geometry, but a different carrier density $n_e = 1.2 \times 10^{12}$ cm^{-2} in each quantum well.

In both cases, the sample was processed into a prism and mounted in the total-reflection geometry (single-pass prism geometry) shown in Fig. VII.A.1. This achieves a strong coupling between the p-polarized light and the intersubband transition dipoles. Mid-infrared absorption spectra were measured using a Biorad FTS 45-A Fourier transform spectrometer. The samples were mounted inside a closed-cycle cryostat equipped with broadband KRS-5 windows to allow measurements at different sample temperatures. A small aperture with razor blade edges ensures that light is only transmitted through the sample facets. Furthermore, a broadband wire-mesh polarizer allows to obtain polarization-dependent spectra both for p polarization (the electric field has a component perpendicular to the quantum well layers) and for s polarization (electric field parallel to the quantum well layers). This serves to clearly identify intersubband transitions, since they are dipole-allowed only for p polarization [WFL$^+$04].

The corresponding theoretical setup is presented in Fig. VII.A.2.

[1] The here presented results are partially published in [WFL$^+$04] and [SRW$^+$04]

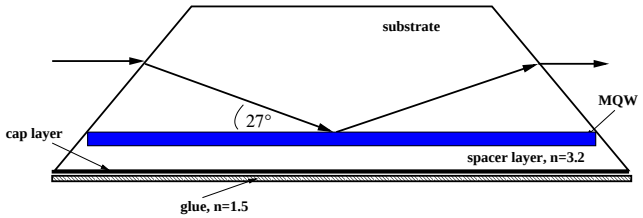

Figure VII.A.1 — Experimental Setup: Single-pass prism geometry as used in the experiments. Details are given in the text and in [WFL$^+$04]

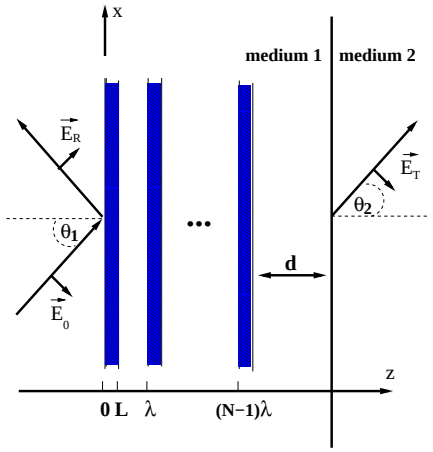

Figure VII.A.2 — Theoretical Model System for single-pass prism geometry: :MQW system with respect to total reflection at a medium-1/medium-2 interface in order to enhance the absorption (standing wave): $\mathbf{E}_{in} = \mathbf{E}_{in}\hat{\mathbf{p}}_+ e^{i\,\mathbf{q}_+\cdot\mathbf{r}}$ ($\mathbf{E}_{out} = E_{out}\hat{\mathbf{p}}_- e^{i\,\mathbf{q}_-\cdot\mathbf{r}}$) denotes the ingoing (outgoing) p-polarized field. In the experiment the spacing between the last well and the prism base (medium-1/medium-2 interface) is $d = 1.26$ μm to center the wells at the anti-node of the standing wave, and the angle of incidence is $\theta = 63^\circ$.

B. Results

1. Linear Regime

In Fig. VII.B.1, measurements of the linear absorption on sample A are given for three different temperatures. One can clearly see the symmetric IS absorption line around 100 meV. With increasing temperature we observe a shift towards lower energy, a decrease of the amplitude, and an increase of the linewidth.

As can be seen in Fig. VII.B.2 the theory yields satisfactory agreement with the experiment (line shape, linewidth, peak position, and height). For this sample, at low temperatures the linewidth is determined to approximately equal amounts by the lifetime in subband 2, by intrasubband scattering processes, and by radiative coupling. The absorption lines are almost Lorentzian-like. With increasing temperature, the absorption peak shifts ($\approx$ 3 meV between 100 and 300 K) to lower energies. As stated before, the non-diagonal correlation contributions have the effect of compensating the diagonal ones to a large extent. Neglecting the non-diagonal correlation contributions in this case, the linewidth varies between 20 meV at 100 K to 50 meV at 300 K (not shown). Comparing the broadening due to the different dephasing contributions [Fig. VII.B.2(II)], we see that carrier-carrier and

carrier-phonon interactions yield here again not additive dephasing mechanisms, due to interference effects of the diagonal and non-diagonal correlation contributions. Remember that the strength of these interference effects depends on both carrier density and the difference in the effective masses [cf. Chapter IV]. Comparing the linewidth including cc- and cp-correlations of a single quantum well only (c) and all 51 wells (d), we find that even for the moderate density considered here, radiative damping leads to an additional broadening of $\Delta E_{\text{rad}} \approx 1$ meV, which is about 12% (at 300 K) to 25% (at 100 K) of the final linewidth.

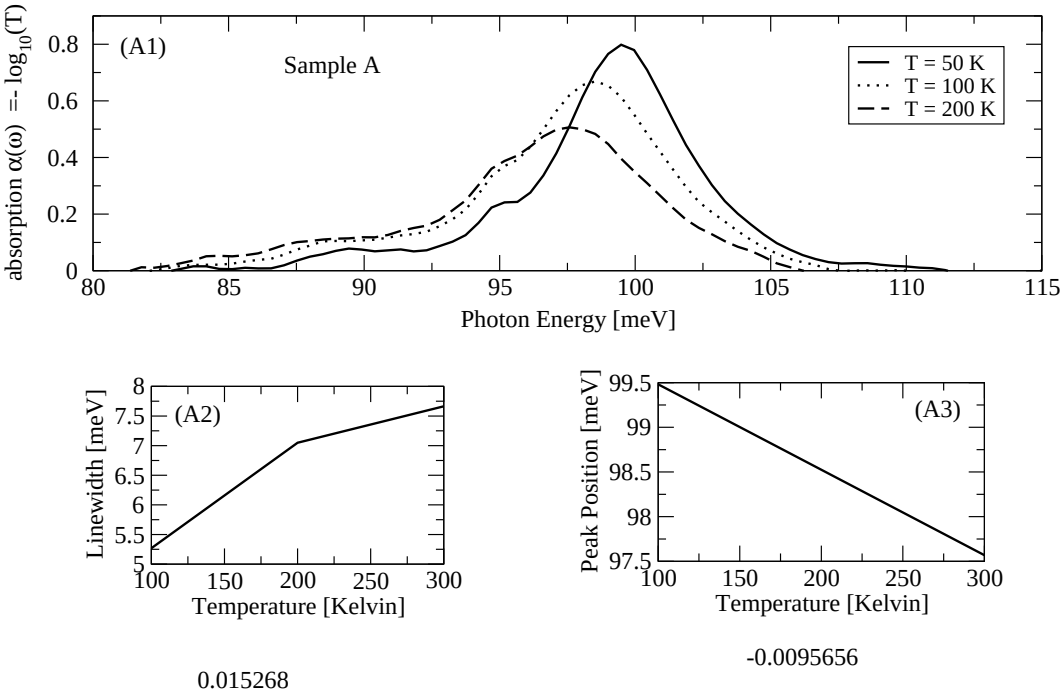

Figure VII.B.1 — Linear Absorption: Experimental Results: Linear Absorption at sample A consisting of 51 GaAs quantum wells, each with width $L = 10$ nm, and separated by $Al_{0.35}Ga_{0.65}As$ barriers, each with a thickness of $D - L = 20$ nm (Fig. VII.A.1). The center of each barrier is n-type δ-doped with Si, resulting in an electron concentration of $n_e = 5 \times 10^{10}$ cm^{-2} in each quantum well. With courtesy of R.A. Kaindl et al. [cf. [WFL$^+$04]]

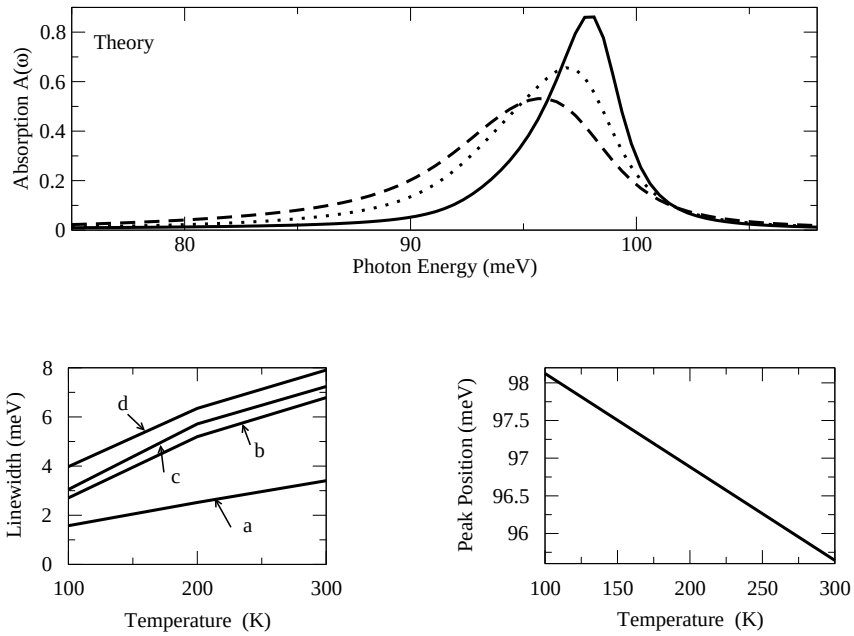

Figure VII.B.2 — Linear Absorption: Theoretical Results: (I) Simultaneous inclusion of cc-/cp-correlation contributions and different effective masses of the MQW sample. (II) Comparison of the linewidth with regard to different dephasing contributions: linewidth of a single quantum well with (a) only cc-correlations, (b) only cp-correlations, (c) cc- and cp-correlations; (d) linewidth of full theory, i.e., with radiative interaction.

2. Nonlinear Results

To conclude we compare very recently obtained theoretical and experimental results in the nonlinear regime. The experimental situation is the following: A coherent IS excitation is created by a femtosecond MIR pulse with a center frequency resonant to the $1 \leftrightarrow 2$ IS transition. The incident applied excitation pulse $E_{\rm in}(t)$ and the light transmitted through the sample $E_{\rm out}(t)$ are fully characterized by measuring their amplitude and phase using ultrafast electro-optic sampling. Experiments were performed for different field strengths of the excitation pulses. The mid-infrared pulses with a duration of 200 fs and electric field amplitudes of up to 1 MV/cm are generated via difference frequency mixing of intense 25-fs pulses at 800 nm in thin GaSe crystals [LRW$^+$04].

In Fig. VII.B.3 we compare the measured and calculated transmitted field of Sample B with increasing excitation (a) 5 KV/cm, (b) 45 kV/cm, (c) 100 kV/cm. Whereas for low excitation the field amplitude is slightly reduced, for an intermediate amplitude a surprisingly low amplitude is observed, for high amplitude the transmitted field gradually approaches the shape and amplitude of the incident field. Remember, that in the total-reflection geometry considered here, the transmitted field is composed of both the reflected field and the field which really is transmitted through the structure. The observed effect can be completely explained with radiative coupling. For low external excitation, the incident field is largely reflected at the high oscillator strength of the first quantum wells (similar to the discussion in Chapter B). With increasing excitation, the amplitudes of the re-emitted fields reach the saturation values. For further increasing excitation fields, e.g. 100 kV/cm, the incident field is stronger than the saturated re-emitted fields decreasing the importance of radiative coupling. Further details are given in [SRW$^+$04].

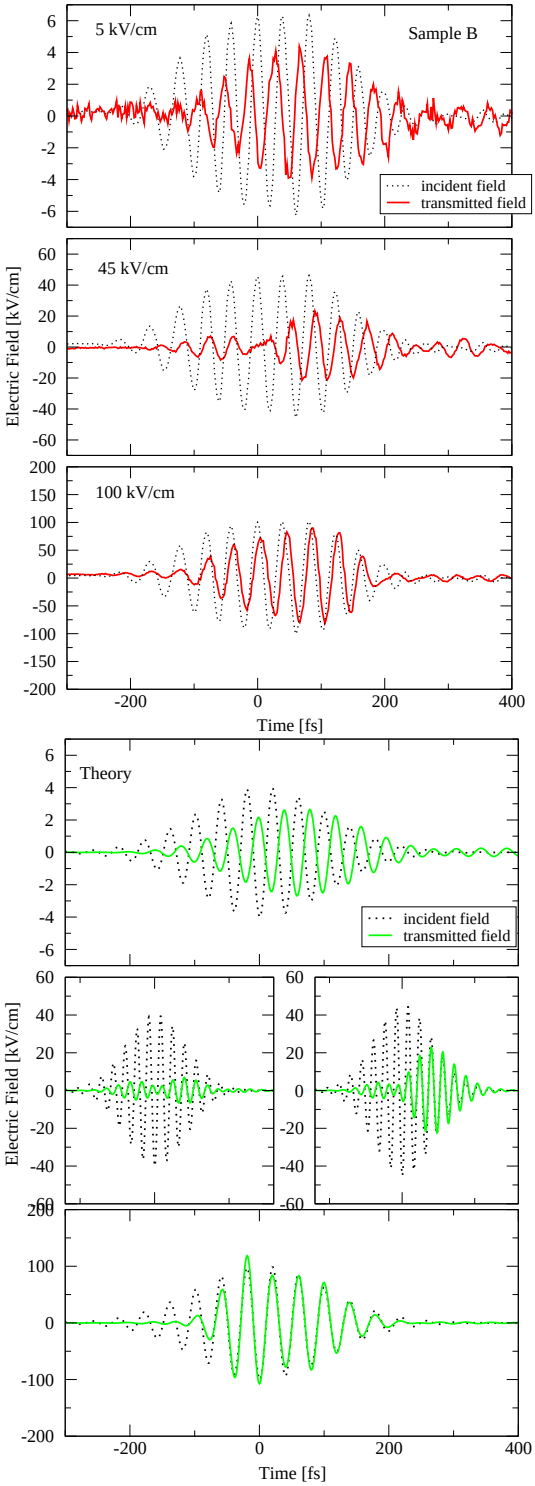

Figure VII.B.3 — Transmitted Field of High-Density Sample (Experiment, Theory): Comparison of the measured and calculated field of Sample B with increasing excitation (a) 5 KV/cm, (b) 45 kV/cm, (c) 100 kV/cm. Whereas for low excitation the field amplitude is slightly reduced, for an intermediate amplitude a surprisingly low amplitude is observed, for high amplitude the transmitted field gradually approaches the shape and amplitude of the incident field. The theoretical results are in good agreement with the experiments.

CHAPTER VIII
Conclusion

In conclusion, we have presented a microscopic theory for the linear and nonlinear description of intersubband excitations. Thereby many particle interactions such as carrier-carrier and carrier-phonon interaction and radiative coupling have been taken into account. Considering first only a single quantum well, we have investigated the impact of the microscopic contributions for a wide range of parameters in the linear regime. Furthermore, we have seen that in the nonlinear regime, where the many-particle effects destroy the ability of the system to oscillate in a manner comparable to Rabi oscillations, we could counteract the impact of these contributions by exciting the quantum well with a controlled detuning. Best results were achieved for ultrashort pulses which still have a wide spectral width. After including radiative coupling into the theory, we investigated the linear and nonlinear response of multiple quantum well systems. Especially interesting is the impact of radiative coupling in the nonlinear regime. The impact of radiative coupling in highly doped quantum wells on the density oscillations is effectively stronger than the impact of many-particle interactions. Comparison with experimental results showed excellent agreement in both the linear and nonlinear regime.

APPENDICES

APPENDIX A

Matrixelements

In the following the carrier-field and carrier-carrier matrix elements are derived.

1. Carrier-Field: Semiclassical

Inserting Eq. (II.A.71) in Eq. (II.A.42) the semiclassical carrier-field Hamiltonian reads

$$H_{\rm cf} = e\int_V d^3r\,\hat{\psi}^\dagger(\mathbf{r})\mathbf{E}(\mathbf{r},t)\cdot\mathbf{r}\hat{\psi}(\mathbf{r}) \tag{APP A.1}$$

$$\begin{aligned} &= \frac{e}{A}\sum_{i,j} a_i^\dagger a_j \int d^3r\, \mathrm{e}^{-\mathrm{i}\,(\mathbf{k}_i-\mathbf{k}_j)\cdot\mathbf{r}_{||}}\zeta^*_{w_i,n_i}(\mathbf{r}_\perp)\zeta_{w_j,n_j}(\mathbf{r}_\perp)u^*_{\sigma_i,\mathbf{k}_i\approx 0}(\mathbf{r})u_{\sigma_j,\mathbf{k}_j\approx 0}(\mathbf{r}) \\ &\quad\times\big[\mathbf{E}(\mathbf{r},t)\cdot\mathbf{r}\big] \\ &= \frac{e}{A}\sum_{i,j} a_i^\dagger a_j \sum_{\mathbf{R}}\int_{\Omega_{\rm EC}} d^3\hat{r}\,\mathrm{e}^{-\mathrm{i}\,(\mathbf{k}_i-\mathbf{k}_j)\cdot(\mathbf{R}_{||}+\hat{\mathbf{r}}_{||})}\zeta^*_{w_i,n_i}(\mathbf{R}_\perp+\hat{\mathbf{r}}_\perp)\zeta_{w_j,n_j}(\mathbf{R}_\perp+\hat{\mathbf{r}}_\perp) \\ &\quad\times u^*_{\sigma_i,\mathbf{k}_i\approx 0}(\mathbf{R}+\hat{\mathbf{r}})u_{\sigma_j,\mathbf{k}_j\approx 0}(\mathbf{R}+\hat{\mathbf{r}})\big[\mathbf{E}(\mathbf{R}+\hat{\mathbf{r}},t)\cdot(\mathbf{R}+\hat{\mathbf{r}})\big]\,, \end{aligned} \tag{APP A.2}$$

where in the last step we have split the position vector $\mathbf{r}$ in lattice vector $\mathbf{R}$ of the underlying Bravais lattice and intra-cell vector $\hat{\mathbf{r}}$ according to $\mathbf{r}=\mathbf{R}+\hat{\mathbf{r}}$. Using a Taylor expansion around the lattice vector, we can express any function $f(\mathbf{R}+\hat{\mathbf{r}})$ as

$$f(\mathbf{R}+\hat{\mathbf{r}}) = \sum_{n_0}^{\infty}\frac{1}{n!}(\hat{\mathbf{r}}\cdot\nabla)^n f(\mathbf{R})\,. \tag{APP A.3}$$

Therewith we obtain

$$\begin{aligned} &\mathrm{e}^{-\mathrm{i}\,(\mathbf{k}_i-\mathbf{k}_j)\cdot(\mathbf{R}_{||}+\hat{\mathbf{r}}_{||})}\big[\mathbf{E}(\mathbf{R}+\hat{\mathbf{r}},t)\cdot(\mathbf{R}+\hat{\mathbf{r}})\big]\zeta^*_{w_i,n_i}(\mathbf{R}_\perp+\hat{\mathbf{r}}_\perp)\zeta_{w_j,n_j}(\mathbf{R}_\perp+\hat{\mathbf{r}}) \\ &= (1+\hat{\mathbf{r}}\cdot\nabla)\Big\{\mathrm{e}^{-\mathrm{i}\,(\mathbf{k}_i-\mathbf{k}_j)\cdot\mathbf{R}_{||}}\big[\mathbf{E}(\mathbf{R},t)\cdot\mathbf{R}\big]\zeta^*_{w_i,n_i}(\mathbf{R}_\perp)\zeta_{w_j,n_j}(\mathbf{R}_\perp)\Big\}+... \end{aligned} \tag{APP A.4}$$

Keeping only the first two contributions (monopole and dipole contribution) yields the carrier-field Hamilton in dipole approximation

$$\begin{aligned} H_{\rm cf} &= \frac{e}{A}\sum_{i,j} a_i^\dagger a_j \sum_{\mathbf{R}}\int_{\Omega_{\rm EC}} d^3\hat{r}\,\big[1+\hat{\mathbf{r}}\cdot\nabla_{\mathbf{R}}\big]u^*_{\sigma_i,\mathbf{k}_i\approx 0}(\hat{\mathbf{r}})u_{\sigma_j,\mathbf{k}_j\approx 0}(\hat{\mathbf{r}}) \\ &\quad\times\mathrm{e}^{-\mathrm{i}\,(\mathbf{k}_i-\mathbf{k}_j)\cdot\mathbf{R}_{||}}\zeta^*_{w_i,n_i}(\mathbf{R}_\perp)\zeta_{w_j,n_j}(\mathbf{R}_\perp)\big[\mathbf{E}(\mathbf{R},t)\cdot\mathbf{R}\big] \\ &= \frac{e}{A}\Omega_{\rm EC}\sum_{i',j'}\sum_{\mathbf{q},\mathbf{Q}} a^\dagger_{i',\mathbf{q}+\mathbf{Q}/2}a_{j',\mathbf{q}-\mathbf{Q}/2}\sum_{\mathbf{R}}\mathrm{e}^{-\mathrm{i}\,\mathbf{Q}\cdot\mathbf{R}_{||}} \\ &\quad\times\zeta^*_{w_{i'},n_{i'}}(\mathbf{R}_\perp)\zeta_{w_{j'},n_{j'}}(\mathbf{R}_\perp)\big[\mathbf{E}(\mathbf{R},t)\cdot\mathbf{R}\big]\delta_{\sigma_{i'},\sigma_{j'}} \end{aligned} \tag{APP A.5}$$

Here we have used that the Bloch factors of the conduction band are (a) orthogonal and (b) symmetric functions [YC99]

$$(a)\ \frac{1}{\Omega_{\rm EC}}\int_{\Omega_{\rm EC}} d^3\hat{r}\,u^*_{\sigma_i,\mathbf{k}_i\approx 0}(\hat{\mathbf{r}})u_{\sigma_j,\mathbf{k}_j\approx 0}(\hat{\mathbf{r}}) = \delta_{\sigma_i,\sigma_j} \tag{APP A.6}$$

$$(b)\ \int_{\Omega_{\rm EC}} d^3\hat{r}\,u^*_{\sigma_i,\mathbf{k}_i\approx 0}(\hat{\mathbf{r}})\,\hat{\mathbf{r}}\,u_{\sigma_j,\mathbf{k}_j\approx 0}(\hat{\mathbf{r}}) = 0 \tag{APP A.7}$$

and switched to centre of mass coordinates and relative coordinates:

$$\mathbf{q} = \frac{\mathbf{k}_i + \mathbf{k}_j}{2}\,, \qquad \mathbf{Q} = \mathbf{k}_i - \mathbf{k}_j \tag{APP A.8}$$

Therefore the compound indices i, j are replaced by new indices i', j' containing only well number, subband number and spin.

Note that Eq. (APP A.5) consists only of the monopole contribution, the dipole contribution of the multipole expansion has vanished. This is due to the restriction of transitions in the conduction band. Allowing transitions between conduction and valence band, the dipole contribution would not vanish, because of the interband dipole moment (cf. for example [War96, Kuh98]).

For convenience we proceed for the two contribution ($H_{\mathrm{cf}}|_{\mathbf{R}_{||}}, H_{\mathrm{cf}}|_{\mathbf{R}_\perp}$) separately.

$$\begin{aligned}
H_{\mathrm{cf}}|_{\mathbf{R}_{||}} = \;& e \sum_{i',j'} \sum_{\mathbf{q},\mathbf{Q}} a^\dagger_{i',\mathbf{q}+\mathbf{Q}/2} a_{j',\mathbf{q}-\mathbf{Q}/2}\, l_\perp \sum_{\mathbf{R}_\perp} \zeta^*_{w_{i'},n_{i'}}(\mathbf{R}_\perp)\zeta_{w_{j'},n_{j'}}(\mathbf{R}_\perp) && \text{(APP A.9)}\\
& \times \frac{1}{N_{||}} \sum_{\mathbf{R}_{||}} \mathrm{e}^{-\mathrm{i}\,\mathbf{Q}\cdot\mathbf{R}_{||}}\, \mathbf{R}_{||} \cdot \mathbf{E}(\mathbf{R}_{||}, \mathbf{R}_\perp, t)\delta_{\sigma_{i'},\sigma_{j'}} && \text{(APP A.10)}\\
= \;& e \sum_{i',j'} \sum_{\mathbf{q},\mathbf{Q}} a^\dagger_{i',\mathbf{q}+\mathbf{Q}/2} a_{j',\mathbf{q}-\mathbf{Q}/2}\, l_\perp \sum_{\mathbf{R}_\perp} \zeta^*_{w_{i'},n_{i'}}(\mathbf{R}_\perp)\zeta_{w_{j'},n_{j'}}(\mathbf{R}_\perp) && \text{(APP A.11)}\\
& \times \mathrm{i}\,\nabla_{\mathbf{Q}} \cdot \underbrace{\frac{1}{N_{||}} \sum_{\mathbf{R}_{||}} \mathrm{e}^{-\mathrm{i}\,\mathbf{Q}\cdot\mathbf{R}_{||}} \mathbf{E}_{||}(\mathbf{R}_{||}, \mathbf{R}_\perp, t)}_{:=\mathbf{E}_{||}(\mathbf{Q},\mathbf{R}_\perp,t)}\, \delta_{\sigma_{i'},\sigma_{j'}} && \text{(APP A.12)}\\
= \;& e \sum_{i',j'} \sum_{\mathbf{q},\mathbf{Q}} a^\dagger_{i',\mathbf{q}+\mathbf{Q}/2} a_{j',\mathbf{q}-\mathbf{Q}/2} \delta_{\sigma_{i'},\sigma_{j'}} && \text{(APP A.13)}\\
& \times \underbrace{\mathrm{i} \int_{L_\perp} dR_\perp \zeta^*_{w_{i'},n_{i'}}(R_\perp)\zeta_{w_{j'},n_{j'}}(R_\perp)\nabla_{\mathbf{Q}} \cdot \mathbf{E}_{||}(\mathbf{Q}, R_\perp, t)}_{F^{i',j'}_{||}(\mathbf{Q},t)}\,. && \text{(APP A.14)}
\end{aligned}$$

Note that we have replaced the sum over $\mathbf{R}_\perp$ in the continuum limit by an integral expression (using $dx \sum_x \to \int dx$,where dx denotes the distance between the different x-values, i.e. the discretisation of x).

$$\begin{aligned}
H_{\mathrm{cf}}|_{\mathbf{R}_\perp} = \;& e \sum_{i',j'} \sum_{\mathbf{q},\mathbf{Q}} a^\dagger_{i',\mathbf{q}+\mathbf{Q}/2} a_{j',\mathbf{q}-\mathbf{Q}/2}\, l_\perp \sum_{\mathbf{R}_\perp} \zeta^*_{w_{i'},n_{i'}}(\mathbf{R}_\perp)\zeta_{w_{j'},n_{j'}}(\mathbf{R}_\perp) && \text{(APP A.15)}\\
& \times \mathbf{R}_\perp \cdot \underbrace{\frac{1}{N_{||}} \sum_{\mathbf{R}_{||}} \mathrm{e}^{-\mathrm{i}\,\mathbf{Q}\cdot\mathbf{R}_{||}} \mathbf{E}(\mathbf{R}_{||}, \mathbf{R}_\perp, t)}_{:=\mathbf{E}(\mathbf{Q},\mathbf{R}_\perp)}\, \delta_{\sigma_{i'},\sigma_{j'}} && \text{(APP A.16)}\\
= \;& e \sum_{i',j'} \sum_{\mathbf{q},\mathbf{Q}} a^\dagger_{i',\mathbf{q}+\mathbf{Q}/2} a_{j',\mathbf{q}-\mathbf{Q}/2} \delta_{\sigma_i,\sigma_j} && \text{(APP A.17)}\\
& \times \underbrace{\int_{L_\perp} dR_\perp \zeta^*_{w_{i'},n_{i'}}(R_\perp)\zeta_{w_{j'},n_{j'}}(R_\perp)\, R_\perp E_\perp(\mathbf{Q}, R_\perp, t)}_{F^{i',j'}_{\perp}(\mathbf{Q},t)}\,.
\end{aligned}$$

Eventually we arrive at the final result

$$H_{\mathrm{cf}} = \; e \sum_{i',j'} \sum_{\mathbf{q},\mathbf{Q}} a^\dagger_{i',\mathbf{q}+\mathbf{Q}/2} a_{j',\mathbf{q}-\mathbf{Q}/2} \Big[F^{i',j'}_{||}(\mathbf{Q},t) + F^{i',j'}_{\perp}(\mathbf{Q},t) \Big] \delta_{\sigma_{i'},\sigma_{j'}}\,. \tag{APP A.18}$$

2. Carrier-Carrier

$$H_{\rm cc} = \frac{1}{2}\sum_{a,b,c,d} V_{abcd} a_a^\dagger a_b^\dagger a_d a_c \tag{APP A.19}$$

with

$$\begin{aligned} V_{abcd} = \quad & \frac{1}{A^2}\frac{e^2}{4\pi\epsilon_0}\int d^3r \int d^3r' \mathrm{e}^{-\mathrm{i}\,(\mathbf{k}_a-\mathbf{k}_c)\cdot\mathbf{r}_{||}}\,\mathrm{e}^{-\mathrm{i}\,(\mathbf{k}_b-\mathbf{k}_d)\cdot\mathbf{r}'_{||}}\frac{1}{|\mathbf{r}-\mathbf{r}'|} \\ & \times \zeta^*_{w_a,n_a}(\mathbf{r}_\perp)\zeta^*_{w_b,n_b}(\mathbf{r}'_\perp)\zeta_{w_c,n_c}(\mathbf{r}_\perp)\zeta_{w_d,n_d}(\mathbf{r}'_\perp) \\ & \times u^*_{\sigma_a,\mathbf{k}_a\approx 0}(\mathbf{r})u^*_{\sigma_b,\mathbf{k}_b\approx 0}(\mathbf{r}')u_{\sigma_c,\mathbf{k}_c\approx 0}(\mathbf{r})u_{\sigma_d,\mathbf{k}_d\approx 0}(\mathbf{r}') \end{aligned} \tag{APP A.20}$$

Similar to Sec.APP A.1 we split the position vectors in lattice vectors and intracell-vectors and use multipole expansions over the elementary lattice cells. Again only the monopole and dipole contributions of the expansions are taken into account. Due to the restriction to transitions in the conduction band [cf. Eq. (APP A.7)], monopole-dipole and dipole-dipole contributions vanish, leaving only monopole-monopole contributions:

$$\begin{aligned} V_{abcd} = \quad & \frac{1}{A^2}\frac{e^2}{4\pi\epsilon_0}\sum_{\mathbf{R},\mathbf{R}'}\int d^3\hat{r}\int d^3\hat{r}' \mathrm{e}^{-\mathrm{i}\,(\mathbf{k}_a-\mathbf{k}_c)\cdot(\mathbf{R}_{||}+\hat{\mathbf{r}}_{||})}\,\mathrm{e}^{-\mathrm{i}\,(\mathbf{k}_b-\mathbf{k}_d)\cdot(\mathbf{R}'_{||}+\hat{\mathbf{r}}'_{||})}\frac{1}{|\mathbf{R}+\hat{\mathbf{r}}-\mathbf{R}'-\hat{\mathbf{r}}'|} \\ & \times \zeta^*_{w_a,n_a}(\mathbf{R}_\perp+\hat{\mathbf{r}}_\perp)\zeta^*_{w_b,n_b}(\mathbf{R}'_\perp+\hat{\mathbf{r}}'_\perp)\zeta_{w_c,n_c}(\mathbf{R}_\perp+\hat{\mathbf{r}}_\perp)\zeta_{w_d,n_d}(\mathbf{R}'_\perp+\hat{\mathbf{r}}'_\perp) \\ & \times u^*_{\sigma_a,\mathbf{k}_a\approx 0}(\mathbf{R}+\hat{\mathbf{r}})u^*_{\sigma_b,\mathbf{k}_b\approx 0}(\mathbf{R}'+\hat{\mathbf{r}}')u_{\sigma_c,\mathbf{k}_c\approx 0}(\mathbf{R}+\hat{\mathbf{r}})u_{\sigma_d,\mathbf{k}_d\approx 0}(\mathbf{R}'+\hat{\mathbf{r}}'), \\ = \quad & \frac{1}{A^2}\frac{e^2}{4\pi\epsilon_0}\Omega_0^2\sum_{\mathbf{R},\mathbf{R}'}\mathrm{e}^{-\mathrm{i}\,(\mathbf{k}_a-\mathbf{k}_c)\cdot\mathbf{R}_{||}}\,\mathrm{e}^{-\mathrm{i}\,(\mathbf{k}_b-\mathbf{k}_d)\cdot\mathbf{R}'_{||}}\frac{1}{|\mathbf{R}-\mathbf{R}'|} \\ & \times \zeta^*_{w_a,n_a}(\mathbf{R}_\perp)\zeta^*_{w_b,n_b}(\mathbf{R}'_\perp)\zeta_{w_c,n_c}(\mathbf{R}_\perp)\zeta_{w_d,n_d}(\mathbf{R}'_\perp)\delta_{\sigma_a,\sigma_c}\delta_{\sigma_b,\sigma_d}, \\ = \quad & \frac{1}{A^2}\frac{e^2}{4\pi\epsilon_0}\int d^3R\int d^3R' \mathrm{e}^{-\mathrm{i}\,(\mathbf{k}_a-\mathbf{k}_c)\cdot\mathbf{R}_{||}}\,\mathrm{e}^{-\mathrm{i}\,(\mathbf{k}_b-\mathbf{k}_d)\cdot\mathbf{R}'_{||}}\frac{1}{|\mathbf{R}-\mathbf{R}'|} \\ & \times \zeta^*_{w_a,n_a}(\mathbf{R}_\perp)\zeta^*_{w_b,n_b}(\mathbf{R}'_\perp)\zeta_{w_c,n_c}(\mathbf{R}_\perp)\zeta_{w_d,n_d}(\mathbf{R}'_\perp)\delta_{\sigma_a,\sigma_c}\delta_{\sigma_b,\sigma_d}\,. \end{aligned} \tag{APP A.21}$$

For convenience we switch to center and relative coordiante $\tilde{\mathbf{R}}_{||} = 0.5(\mathbf{R}_{||}+\mathbf{R}'_{||})$ and $\tilde{\mathbf{r}}_{||} = \mathbf{R}_{||} - \mathbf{R}'_{||}$ and replace $R_\perp$ by z. Using $\frac{1}{N_{||}}\sum_{\mathbf{R}}\mathrm{e}^{\mathrm{i}\,(\mathbf{q}-\mathbf{q}')\cdot\mathbf{R}} = \delta_{\mathbf{q},\mathbf{q}'} \to \frac{1}{A}\int d^2R\mathrm{e}^{\mathrm{i}\,(\mathbf{q}-\mathbf{q}')\cdot\mathbf{R}} = \delta_{\mathbf{q},\mathbf{q}'}$ [cf. [Czy00, p. 35 (3.37)]] and

$$\int d^2\tilde{r}\frac{\mathrm{e}^{-\mathrm{i}\,\mathbf{k}\cdot\tilde{\mathbf{r}}}}{\sqrt{\tilde{r}^2+z^2}} = \quad \int_0^\infty d\tilde{r}\,\tilde{r}\int_0^{2\pi}d\zeta\,\frac{\mathrm{e}^{-\mathrm{i}\,|\mathbf{k}|\,\tilde{r}\cos\zeta}}{\sqrt{\tilde{r}^2+z^2}} = \int_0^\infty d\tilde{r}\,\tilde{r}\frac{2\pi J_0[|\mathbf{k}|\tilde{r}]}{\sqrt{\tilde{r}^2+z^2}} = 2\pi\frac{\mathrm{e}^{-|\mathbf{k}||z|}}{|\mathbf{k}|} \tag{APP A.22}$$

we obtain finally

$$\begin{aligned} V_{abcd} = \quad & \frac{1}{A^2}\frac{e^2}{4\pi\epsilon_0}\int d^2\tilde{R}_{||}\mathrm{e}^{-\mathrm{i}\,(\mathbf{k}_a-\mathbf{k}_c+\mathbf{k}_b-\mathbf{k}_d)\cdot\tilde{\mathbf{R}}_{||}}\delta_{\sigma_a,\sigma_c}\delta_{\sigma_b,\sigma_d} \\ & \times\int dz\int dz'\int d^2\tilde{r}_{||}\mathrm{e}^{-0.5\mathrm{i}\,(\mathbf{k}_a-\mathbf{k}_c-\mathbf{k}_b+\mathbf{k}_d)\cdot\tilde{\mathbf{r}}_{||}} \\ & \times\frac{1}{\sqrt{\tilde{r}_{||}^2+(z-z')^2}}\zeta^*_{w_a,a}(z)\zeta^*_{w_b,n_b}(z')\zeta_{w_c,n_c}(z)\zeta_{w_d,n_d}(z'), \\ = \quad & \frac{1}{A}\frac{e^2}{2\epsilon_0}\delta_{\mathbf{k}_a+\mathbf{k}_b,\mathbf{k}_c+\mathbf{k}_d}\delta_{\sigma_a,\sigma_c}\delta_{\sigma_b,\sigma_d} \\ & \times\int dz\int dz'\frac{\mathrm{e}^{-|\mathbf{k}_a-\mathbf{k}_c||z-z'|}}{|\mathbf{k}_a-\mathbf{k}_c|}\zeta^*_{w_a,n_a}(z)\zeta^*_{w_b,n_b}(z')\zeta_{w_c,n_c}(z)\zeta_{w_d,n_d}(z')\,. \end{aligned} \tag{APP A.23}$$

Here, the final result is

$$H_{\mathrm{cc}} = \frac{1}{2} \sum_{a,b,c,d} V_{abcd} a_a^\dagger a_b^\dagger a_d a_c, \tag{APP A.24}$$

with

$$V_{abcd} = \frac{1}{A} \frac{e^2}{2\epsilon_0} \int dz \int dz' \frac{\mathrm{e}^{-|\mathbf{k}_a - \mathbf{k}_c||z-z'|}}{|\mathbf{k}_a - \mathbf{k}_c|} \zeta^*_{w_a,n_a} a(z) \zeta^*_{w_b,n_b}(z') \times \tag{APP A.25}$$

$$\times \zeta_{w_c,n_c}(z) \zeta_{w_d,n_d}(z') \delta_{\mathbf{k}_a+\mathbf{k}_b,\mathbf{k}_c+\mathbf{k}_d} \delta_{\sigma_a,\sigma_c} \delta_{\sigma_b,\sigma_d}. \tag{APP A.26}$$

APPENDIX B

Coulomb and Fröhlich Form Factors

In the following the form factors of the various Coulomb and Fröhlich matrix elements are plotted for different well width. At the end the influence of the actual quantum well model is investigated. Thereby *IW* denotes the infinite-barrier well, *FW* the finite-barrier well and *EWL* the effective well width approximation.

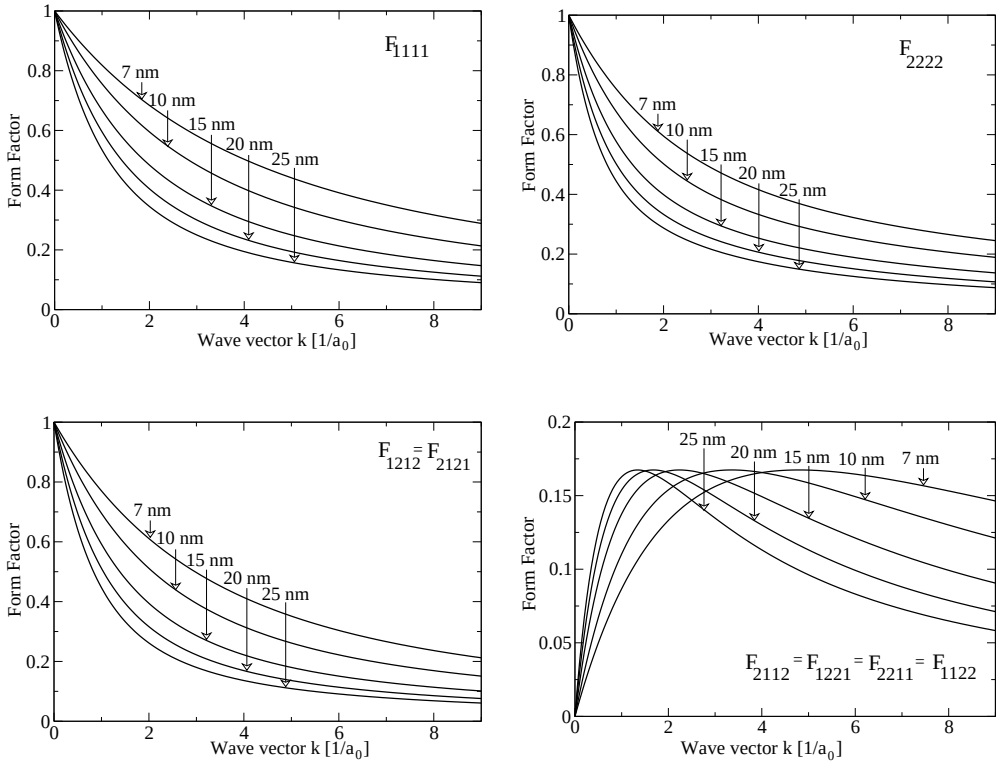

Figure VIII.APP B.1 — Coulomb Form Factors for a quantum well with infi nite barriers

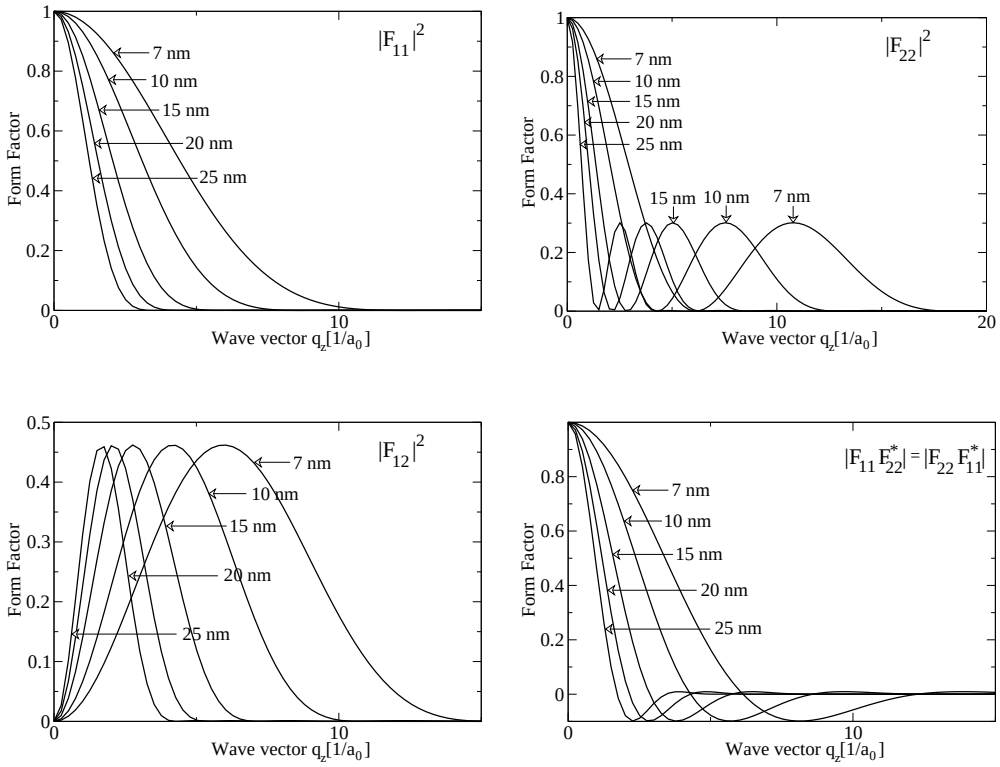

Figure VIII.APP B.2 — Phonon Form Factors for a quantum well with infi nite barriers

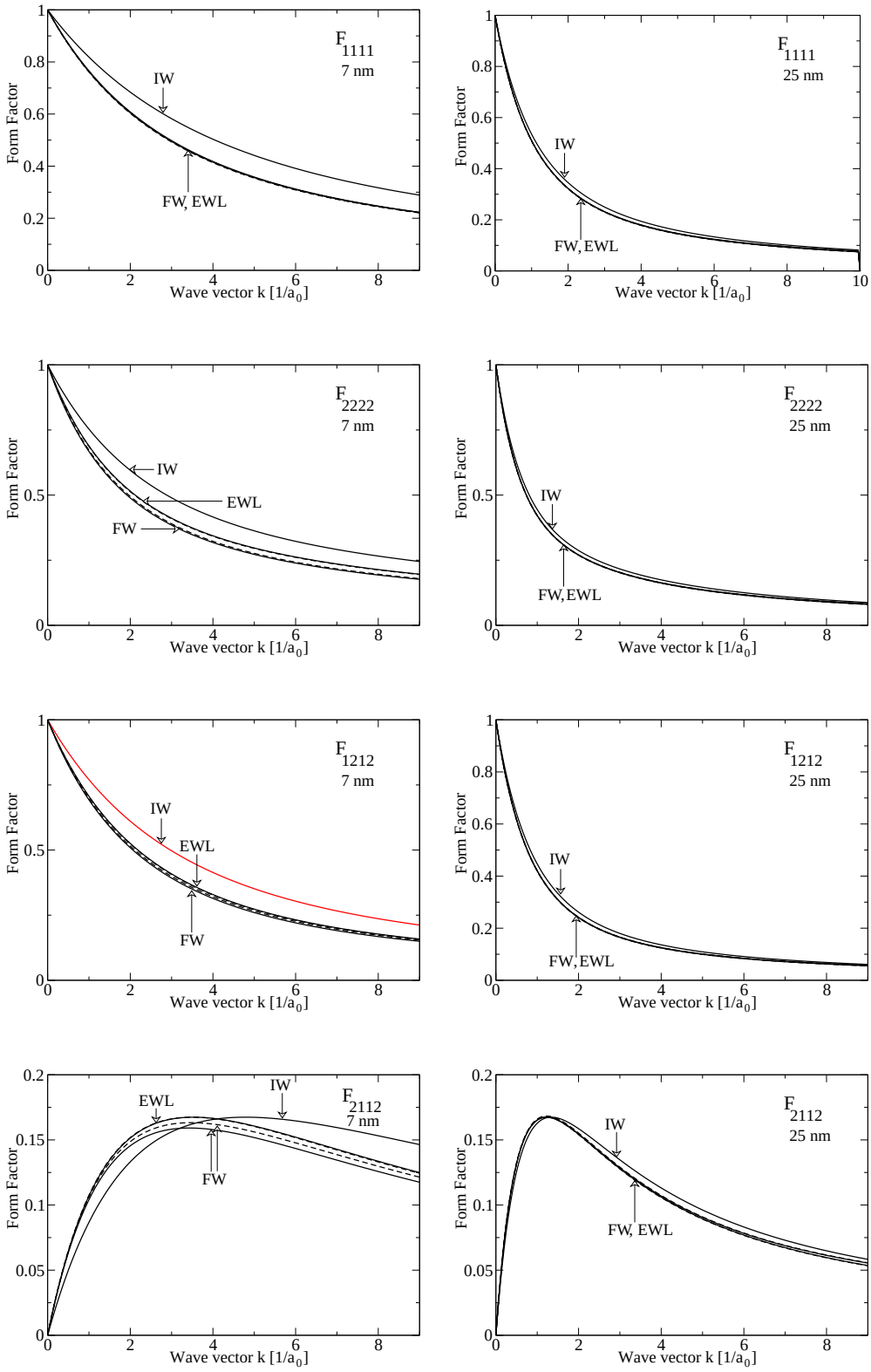

Figure VIII.APP B.3 — Coulomb Form Factors II: Comparison of Coulomb Form Factors of a quantum well with infi nite barriers, fi nite barriers and in effective well-width approximation

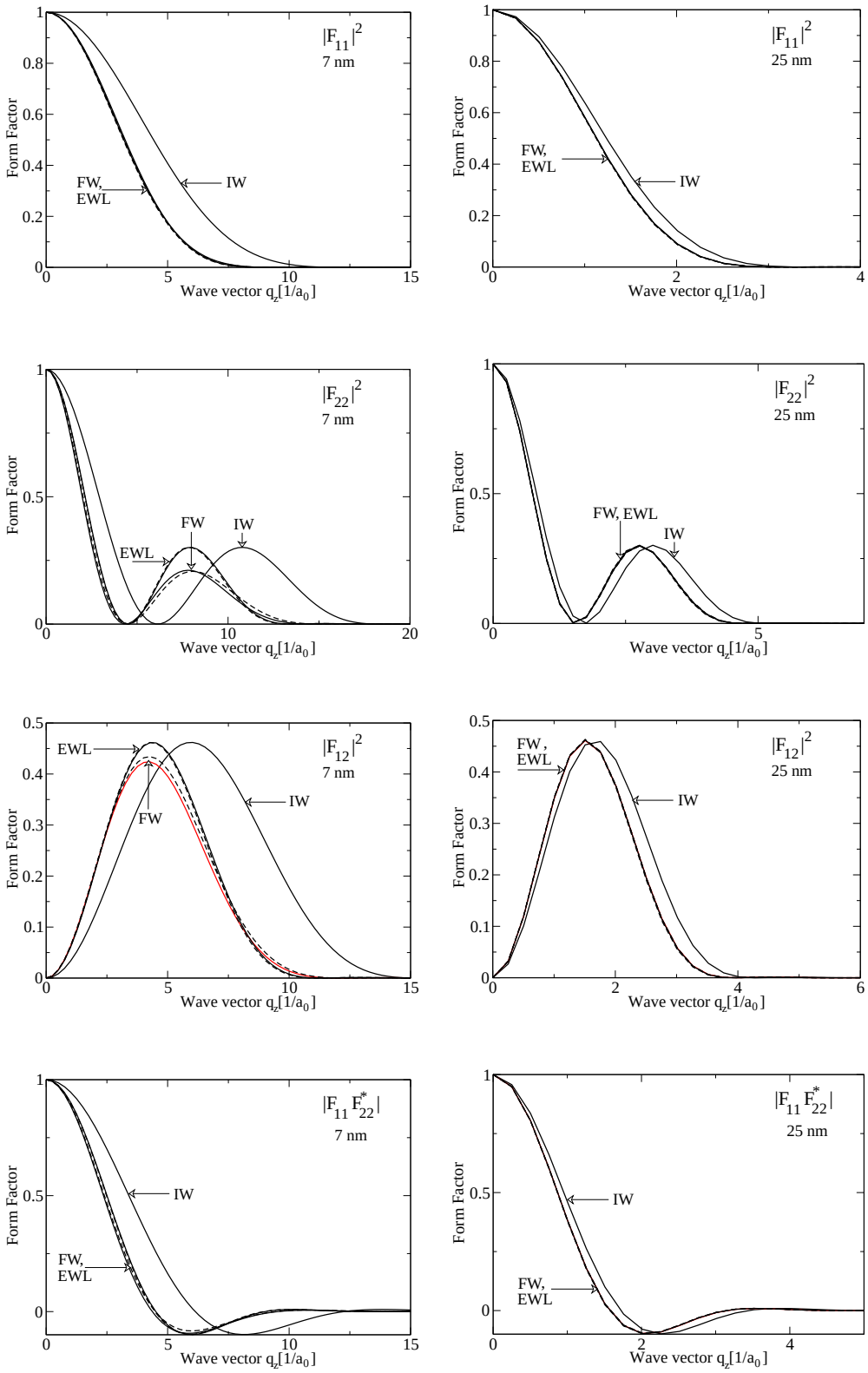

Figure VIII.APP B.4 — Fröhlich Form Factors II: Comparison of Phonon Form Factors of a quantum well with infi nite barriers, fi nite barriers and in effective well-width approximation

APPENDIX C

Time Evolution Operator and Time (Anti-)Ordering Operator

In the following we derive the superoperator for the time evolution of the density matrix operator (time evolution superoperator) [FS90]

$$\sigma(t) = \mathcal{U}(t,t')\sigma(t'), \quad \text{with} \quad \mathcal{U}(t',t') = \mathbb{1}\,. \tag{APP C.1}$$

Combining Eq. (APP C.1) with the von Neumann-equation, Eq. (III.C.8), yields an equation of motion

$$\frac{\mathrm{d}}{\mathrm{d}t}\mathcal{U}(t,t') = -\mathrm{i}\,\mathcal{L}(t)\mathcal{U}(t,t')\,, \tag{APP C.2}$$

which can be formally integrated

$$\int_{t'}^{t} dt_1 \frac{d}{dt_1}\mathcal{U}(t_1,t') = -\mathrm{i}\int_{t'}^{t} dt_1 \mathcal{L}(t_1)\mathcal{U}(t_1,t') \tag{APP C.3}$$

$$\rightarrow \mathcal{U}(t,t') = \mathbb{1} - \mathrm{i}\int_{t'}^{t} dt_1 \mathcal{L}(t_1)\mathcal{U}(t_1,t')\,. \tag{APP C.4}$$

An iteration of this result shows, that $\mathcal{U}(t,t')$ can be expressed in form of the von Neumann series

$$\begin{aligned}
\mathcal{U}(t,t') &= \mathbb{1} + \sum_{n=1}^{\infty}\mathcal{U}^{(n)}(t,t'),\\
\mathcal{U}^{(n)}(t,t') &= (-\mathrm{i})^n \int_{t'}^{t} dt_1 \int_{t'}^{t_1} dt_2 ... \int_{t'}^{t_{n-1}} dt_n \mathcal{L}(t_1)\mathcal{L}(t_2)...\mathcal{L}(t_n)\\
&\qquad \text{with } (t \geq t_1 \geq t_2 \geq ... \geq t_n \geq t')\,.
\end{aligned} \tag{APP C.5}$$

With the time ordering superoperator

$$\mathcal{T}_+\Big(A(t_1)B(t_2)\Big) = \begin{cases} A(t_1)B(t_2) & \text{for } t_1 > t_2,\\ B(t_2)A(t_1) & \text{for } t_2 > t_1. \end{cases}$$

we can express the time evolution superoperator in a very compact form:

$$\begin{aligned}
\mathcal{U}(t,t') &= \mathbb{1} + \sum_{n=1}^{\infty}(-\mathrm{i})^n \frac{1}{n!}\int_{t'}^{t} dt_1 ... \int_{t'}^{t} dt_n \mathcal{T}_+\Big(\mathcal{L}(t_1)...\mathcal{L}(t_n)\Big),\\
\rightarrow \mathcal{U}(t,t') &= \mathcal{T}_+ \mathrm{e}^{-\mathrm{i}\int_{t'}^{t}\mathrm{d}t''\mathcal{L}(t'')}\,.
\end{aligned} \tag{APP C.7}$$

In the same way, we derive a time evolution operator for the irrelevant part of the Liouville operator, $\mathcal{Q}\mathcal{U} = \mathcal{U}_\mathcal{Q}$, with

$$\frac{\mathrm{d}}{\mathrm{d}t}\mathcal{U}_\mathcal{Q}(t,t') = -\mathrm{i}\,\mathcal{L}_\mathcal{Q}(t)\mathcal{U}_\mathcal{Q}(t,t')\,, \quad \mathcal{U}_\mathcal{Q}(t',t') = \mathbb{1} \tag{APP C.8}$$

and obtain

$$\mathcal{U}_\mathcal{Q}(t,t') = \mathcal{T}_+ \mathrm{e}^{-\mathrm{i}\int_{t'}^{t}\mathrm{d}t''\mathcal{L}_\mathcal{Q}(t'')}\,. \tag{APP C.9}$$

The two operators are then connected by the two operator identities [FS90]

$$\mathcal{U}(t,t') = \mathcal{U}_{\mathcal{Q}}(t,t') - \mathrm{i}\int_{t'}^{t} \mathrm{d}t''\, \mathcal{U}(t,t'')\, \mathcal{L}_{\mathcal{P}}(t'')\, \mathcal{U}_{\mathcal{Q}}(t'',t')\,, \tag{APP C.10}$$

$$\mathcal{U}(t,t') = \mathcal{U}_{\mathcal{Q}}(t,t') - \mathrm{i}\int_{t'}^{t} \mathrm{d}t''\, \mathcal{U}_{\mathcal{Q}}(t,t'')\, \mathcal{L}_{\mathcal{P}}(t'')\, \mathcal{U}(t'',t')\,. \tag{APP C.11}$$

Similar to the derivation of Eq. (APP C.7), we can express the density operator at a given time $t' < t$ using the time-antiordering operator:

$$\mathcal{T}_{-}\Big(A(t_1)B(t_2)\Big) = \begin{cases} A(t_1)B(t_2) & \text{for } t_1 < t_2, \\ B(t_2)A(t_1) & \text{for } t_2 < t_1. \end{cases}$$

Therefor we integrate the von-Neumann equation formally in time

$$\begin{aligned} \int_{t'}^{t} dt_1 \frac{d}{dt_1}\sigma(t_1) &= -\mathrm{i}\int_{t'}^{t} dt_1 \mathcal{L}(t_1)\sigma(t_1), \\ &\rightarrow \sigma(t') = \sigma(t) + \mathrm{i}\int_{t'}^{t} dt_1 \mathcal{L}(t_1)\sigma(t_1) \end{aligned} \tag{APP C.13}$$

and iterate the result

$$\begin{aligned} \sigma(t') = \quad & \sigma(t) + \mathrm{i}\int_{t'}^{t} dt_1 \mathcal{L}(t_1)\sigma(t) + \mathrm{i}^{\,2}\int_{t'}^{t} dt_1 \int_{t_1}^{t} dt_2 \mathcal{L}(t_1)\mathcal{L}(t_2)\sigma(t) \qquad \text{(APP C.14)} \\ & + \cdots + \mathrm{i}^{\,n-1}\int_{t'}^{t} dt_1 \int_{t_1}^{t} dt_2 .. \int_{t_{n-2}}^{t} dt_{n-1} \mathcal{L}(t_1)\mathcal{L}(t_2)..\mathcal{L}(t_{n-1})\sigma(t) \\ & + \mathrm{i}^{\,n}\int_{t'}^{t} dt_1 \int_{t_1}^{t} dt_2 .. \int_{t_{n-1}}^{t} dt_n \mathcal{L}(t_1)\mathcal{L}(t_2)..\mathcal{L}(t_n)\sigma(t_n) \\ & \text{with } (t \geq t_n \geq .. \geq t_2 \geq t_1 \geq t')\,. \qquad \text{(APP C.15)} \end{aligned}$$

Since $\lim_{n\to\infty}(t - t_{n-1}) = 0$, the last term is infinitesimal small. Thus we obtain

$$\begin{aligned} \sigma(t') = \quad & \Big[\mathbb{1} + \mathrm{i}\int_{t'}^{t} dt_1 \mathcal{L}(t_1) + \mathrm{i}^{\,2}\int_{t'}^{t} dt_1 \int_{t_1}^{t} dt_2 \mathcal{L}(t_1)\mathcal{L}(t_2) \qquad \text{(APP C.16)} \\ & + \cdots + \mathrm{i}^{\,n-1}\int_{t'}^{t} dt_1 \int_{t_1}^{t} dt_2 .. \int_{t_{n-2}}^{t} dt_{n-1} \mathcal{L}(t_1)\mathcal{L}(t_2)..\mathcal{L}(t_{n-1})\Big]\sigma(t), \\ = \quad & \mathcal{T}_{-}\mathrm{e}^{\mathrm{i}\int_{t'}^{t}\mathrm{d}t''\mathcal{L}(t'')}\sigma(t) \qquad \text{(APP C.17)} \end{aligned}$$

and along the lines for the relevant part of the density operator:

$$\begin{aligned} &\frac{\mathrm{d}}{\mathrm{d}t}\sigma_{\mathrm{rel}}(t) = -\mathrm{i}\ \mathcal{P}[\sigma_{\mathrm{rel}}(t)]\ \mathcal{L}(t)\ \sigma(t) \\ &\rightarrow \sigma_{\mathrm{rel}}(t') = \sigma_{\mathrm{rel}}(t) + \mathrm{i}\int_{t'}^{t} dt_1 \mathcal{P}[\sigma_{\mathrm{rel}}(t_1)]\mathcal{L}(t_1)\sigma(t_1), \\ &\qquad = \mathcal{T}_{-}\mathrm{e}^{\mathrm{i}\int_{t'}^{t}\mathrm{d}t''\mathcal{P}[\sigma_{\mathrm{rel}}(t'')]\mathcal{L}(t'')}\sigma(t)\,. \end{aligned} \tag{APP C.18}$$

APPENDIX D

Factorization of Six-Operator-Terms

In this section we derive an expression for six operator terms which is needed for the derivation of the carrier-carrier correlation contributions. Proceeding analog the lines of III.C.4.b.3 yields first

$$\begin{aligned}
&\mathrm{tr}(a_1^\dagger a_2^\dagger a_3^\dagger a_4 a_5 a_6 \sigma_{\mathrm{rel,e}}) = && \text{(APP D.1)}\\
&= \sum_{\{n_\alpha\}} \sum_{a,b,c,d,e,f} U_{a1} U_{b2} U_{c3} U_{d4}^* U_{e5}^* U_{f6}^* \langle \{n_\alpha\} | d_a^\dagger d_b^\dagger d_c^\dagger d_d d_e d_f \prod_n \frac{\mathrm{e}^{-\lambda_n \hat{n}_n}}{1+\mathrm{e}^{-\lambda_n}} | \{n_\alpha\} \rangle,\\
&= \sum_{\{n_\alpha\}} \sum_{a,b,c} \Big[U_{a1} U_{a4}^* \left(U_{b2} U_{c3} U_{c5}^* U_{b6}^* - U_{b2} U_{c3} U_{b5}^* U_{c6}^* \right)\\
&\quad + U_{a1} U_{a5}^* \left(U_{b2} U_{c3} U_{c6}^* U_{b4}^* - U_{b2} U_{c3} U_{b6}^* U_{c4}^* \right)\\
&\quad + U_{a1} U_{a6}^* \left(U_{b2} U_{c3} U_{c4}^* U_{b5}^* - U_{b2} U_{c3} U_{b4}^* U_{c5}^* \right) \Big] \langle \{n_\alpha\} | n_a n_b n_c \prod_n \frac{\mathrm{e}^{-\lambda_n \hat{n}_n}}{1+\mathrm{e}^{-\lambda_n}} | \{n_\alpha\} \rangle,\\
&= \mathrm{tr}(a_1^\dagger a_4 \sigma_{\mathrm{rel,e}}) \mathrm{tr}(a_2^\dagger a_3^\dagger a_5 a_6 \sigma_{\mathrm{rel,e}}) + \mathrm{tr}(a_1^\dagger a_5 \sigma_{\mathrm{rel,e}}) \mathrm{tr}(a_2^\dagger a_3^\dagger a_6 a_4 \sigma_{\mathrm{rel,e}})\\
&\quad + \mathrm{tr}(a_1^\dagger a_6 \sigma_{\mathrm{rel,e}}) \mathrm{tr}(a_2^\dagger a_3^\dagger a_4 a_5 \sigma_{\mathrm{rel,e}}) && \text{(APP D.2)}
\end{aligned}$$

and thus we obtain

$$\begin{aligned}
\mathrm{tr}(a_1^\dagger a_2^\dagger a_3^\dagger a_4 a_5 a_6 \sigma_{\mathrm{rel}}) = &\ \langle a_1^\dagger a_4 \rangle \mathrm{tr}(a_2^\dagger a_3^\dagger a_5 a_6 \sigma_{\mathrm{rel}}) + \langle a_1^\dagger a_5 \rangle \mathrm{tr}(a_2^\dagger a_3^\dagger a_6 a_4 \sigma_{\mathrm{rel}})\\
&+ \langle a_1^\dagger a_6 \rangle \mathrm{tr}(a_2^\dagger a_3^\dagger a_4 a_5 \sigma_{\mathrm{rel}}),\\
= &\ \langle a_1^\dagger a_4 \rangle \left\{ \langle a_2^\dagger a_6 \rangle \langle a_3^\dagger a_5 \rangle - \langle a_2^\dagger a_5 \rangle \langle a_3^\dagger a_6 \rangle \right\}\\
&+ \langle a_1^\dagger a_5 \rangle \left\{ \langle a_2^\dagger a_4 \rangle \langle a_3^\dagger a_6 \rangle - \langle a_2^\dagger a_6 \rangle \langle a_3^\dagger a_4 \rangle \right\}\\
&+ \langle a_1^\dagger a_6 \rangle \left\{ \langle a_2^\dagger a_5 \rangle \langle a_3^\dagger a_4 \rangle - \langle a_2^\dagger a_4 \rangle \langle a_3^\dagger a_5 \rangle \right\}
\end{aligned} \qquad \text{(APP D.3)}$$

APPENDIX E

Commutators

During the scope of this work, the following commutators appear:

$$[a_i^\dagger\, a_j, a_k^\dagger\, a_l\,] = \, a_i^\dagger\, a_l\, \delta_{j,k} - a_k^\dagger\, a_j\, \delta_{i,l} \tag{App E.1}$$

$$\begin{aligned}[a_1^\dagger a_2^\dagger a_3 a_4, a_5^\dagger a_6] &= -[a_5^\dagger a_6, a_1^\dagger a_2^\dagger a_3 a_4],\\ &= \quad a_1^\dagger a_2^\dagger a_3 a_6 \delta_{5,4} - a_k^\dagger a_2^\dagger a_3 a_4 \delta_{6,1}\\ &\quad - a_1^\dagger a_5^\dagger a_3 a_4 \delta_{6,2} - a_1^\dagger a_2^\dagger a_4 a_6 \delta_{5,3}\end{aligned} \tag{App E.2}$$

$$\begin{aligned}[a_a^\dagger a_b^\dagger a_d a_c, a_1^\dagger a_2^\dagger a_3 a_4] = \quad & a_a^\dagger a_b^\dagger a_d a_2^\dagger a_3 a_4 \delta_{1,c} - a_a^\dagger a_b^\dagger a_c a_2^\dagger a_3 a_4 \delta_{d,1} + a_1^\dagger a_a^\dagger a_b^\dagger a_d a_3 a_4 \delta_{c,2}\\ & - a_1^\dagger a_a^\dagger a_b^\dagger a_3 a_4 a_c \delta_{d,2} + a_1^\dagger a_2^\dagger a_a^\dagger a_4 a_d a_c \delta_{b,3} - a_1^\dagger a_2^\dagger a_b^\dagger a_4 a_d a_c \delta_{3,a}\\ & + a_1^\dagger a_2^\dagger a_3 a_a^\dagger a_d a_c \delta_{b,4} - a_1^\dagger a_2^\dagger a_3 a_b^\dagger a_d a_c \delta_{4,a}\end{aligned} \tag{App E.3}$$

$$[a_1^\dagger b_{\mathbf{Q}'} a_2, a_3^\dagger b_{\mathbf{Q}} a_4] = a_1^\dagger a_4 b_{\mathbf{Q}'} b_{\mathbf{Q}} \delta_{2,3} - a_3^\dagger a_2 b_{\mathbf{Q}'} b_{\mathbf{Q}} \delta_{1,4}\,, \tag{App E.4}$$

$$[a_1^\dagger b_{\mathbf{Q}'}^\dagger a_2, a_3^\dagger b_{\mathbf{Q}} a_4] = a_1^\dagger a_4 b_{\mathbf{Q}'}^\dagger b_{\mathbf{Q}} \delta_{2,3} - a_3^\dagger a_2 b_{\mathbf{Q}'}^\dagger b_{\mathbf{Q}} \delta_{1,4} - a_3^\dagger a_4 a_1^\dagger a_2 \delta_{\mathbf{Q}',\mathbf{Q}} \tag{App E.5}$$

1. Free-Carrier: Bandstructure

$$H_{0,e} = \sum_i \, \epsilon_i \, a_i^\dagger \, a_i \tag{App E.6}$$

$$\begin{aligned}[H_0, a_k^\dagger\, a_l\,] &= \sum_i \, \epsilon_i \, [a_i^\dagger \, a_i\,, a_k^\dagger \, a_l\,],\\ &= \sum_i \epsilon_i \, (\, a_i^\dagger \, a_l \, \delta_{i,k} - a_k^\dagger \, a_i \, \delta_{i,l}),\\ &= (\epsilon_k - \epsilon_l)\, a_k^\dagger \, a_l\end{aligned} \tag{App E.7}$$

2. Carrier-Field: Semiclassical

$$H_{\rm cf} = e \sum_{i,j} \sum_{\mathbf{q},\mathbf{Q}} a^\dagger_{i,\mathbf{q}+\mathbf{Q}/2} a_{j,\mathbf{q}-\mathbf{Q}/2} \Big[F^{i,j}_{||}(\mathbf{Q},t) + F^{i,j}_{\perp}(\mathbf{Q},t) \Big] \delta_{\sigma_i,\sigma_j} \tag{App E.8}$$

index i,j contain well number, subband number and spin.

$$\begin{aligned}[H_{\rm cf}, a^\dagger_{k,\mathbf{k}_k} a_{l,\mathbf{k}_l}] &= e \sum_{i,j} \sum_{\mathbf{q},\mathbf{Q}} F^{i,j}(\mathbf{Q},t) [a^\dagger_{i,\mathbf{q}+\mathbf{Q}/2} a_{j,\mathbf{q}-\mathbf{Q}/2}, a^\dagger_{k,\mathbf{k}_k} a_{l,\mathbf{k}_l}] \delta_{\sigma_i,\sigma_j},\\ &= e \sum_{i,j} \sum_{\mathbf{q},\mathbf{Q}} F^{i,j}(\mathbf{Q},t) \Big\{ a^\dagger_{i,\mathbf{q}+\mathbf{Q}/2} a_{l,\mathbf{k}_l} \delta_{k,j} \delta_{\mathbf{k}_k,\mathbf{q}-\mathbf{Q}/2} - a^\dagger_{k,\mathbf{k}_k} a_{j,\mathbf{q}-\mathbf{Q}/2} \delta_{l,i} \delta_{\mathbf{k}_l,\mathbf{q}+\mathbf{Q}/2} \Big\} \delta_{\sigma_i,\sigma_j},\\ &= e \sum_i \sum_{\mathbf{Q}} \Big\{ F^{i,k}(\mathbf{Q},t) a^\dagger_{i,\mathbf{k}_k+\mathbf{Q}} a_{l,\mathbf{k}_l} \delta_{\sigma_i,\sigma_k} - F^{l,i}(\mathbf{Q},t) a^\dagger_{k,\mathbf{k}_k} a_{i,\mathbf{k}_l-\mathbf{Q}} \delta_{\sigma_l,\sigma_i} \Big\}\,.\end{aligned} \tag{App E.9}$$

Inserting the definition of $F^{i,j}(\mathbf{Q},t)$ yields

$$\begin{aligned}[H_{\rm cf}, a_k^\dagger a_l] = \quad & e\sum_i \sum_{\mathbf{Q}} \Big\{ \int dz \phi^*_{w_i,n_i}(z)\phi_{w_k,n_k}(z)\Big[zE_z(\mathbf{Q},z,t)), \\ & + \mathrm{i}\ \nabla_{\mathbf{Q}}\cdot\mathbf{E}_{||}(\mathbf{Q},z,t)\Big] a^\dagger_{i,\mathbf{k}_k+\mathbf{Q}} a_{l,\mathbf{k}_l}\delta_{\sigma_i,\sigma_k} \\ & - \int dz \phi^*_{w_l,n_l}(z)\phi_{w_i,n_i}(z)\Big[zE_z(\mathbf{Q},z,t)) \\ & + \mathrm{i}\ \nabla_{\mathbf{Q}}\cdot\mathbf{E}_{||}(\mathbf{Q},z,t)\Big] a^\dagger_{k,\mathbf{k}_k} a_{i,\mathbf{k}_l-\mathbf{Q}}\delta_{\sigma_l,\sigma_i}\Big\}\end{aligned} \tag{APP E.10}$$

which can be rewritten using integration by parts

$$\begin{aligned}[H_{\rm cf}, a_k^\dagger a_l] = \quad & e\sum_i \sum_{\mathbf{Q}} \Big\{ \int dz \phi^*_{w_i,n_i}(z)\phi_{w_k,n_k}(z)\Big[zE_z(\mathbf{Q},z,t)) a^\dagger_{i,\mathbf{k}_k+\mathbf{Q}} a_{l,\mathbf{k}_l}, \\ & - \mathrm{i}\ \mathbf{E}_{||}(\mathbf{Q},z,t)\cdot\nabla_{\mathbf{Q}}\ a^\dagger_{i,\mathbf{k}_k+\mathbf{Q}} a_{l,\mathbf{k}_l}\Big]\delta_{\sigma_i,\sigma_k} \\ & - \int dz \phi^*_{w_l,n_l}(z)\phi_{w_i,n_i}(z)\Big[zE_z(\mathbf{Q},z,t)) a^\dagger_{k,\mathbf{k}_k} a_{i,\mathbf{k}_l-\mathbf{Q}} \\ & - \mathrm{i}\ \mathbf{E}_{||}(\mathbf{Q},z,t)\cdot\nabla_{\mathbf{Q}}\ a^\dagger_{k,\mathbf{k}_k} a_{i,\mathbf{k}_l-\mathbf{Q}}\Big]\delta_{\sigma_l,\sigma_i}\Big\}\end{aligned} \tag{APP E.11}$$

3. Carrier-Carrier

$$H_{\rm cc} = \frac{1}{2}\sum_{a,b,c,d} V_{abcd} a_a^\dagger a_b^\dagger a_d a_c \tag{APP E.12}$$

with

$$V_{abcd} = \quad \frac{1}{A}\frac{e^2}{2\epsilon_0}\int dz \int dz' \frac{\mathrm{e}^{-|\mathbf{k}_a-\mathbf{k}_c||z-z'|}}{|\mathbf{k}_a-\mathbf{k}_c|}\phi^*_{w_a,n_a}a(z)\phi^*_{w_b,n_b}(z')\times \tag{APP E.13}$$

$$\times\ \phi_{w_c,n_c}(z)\phi_{w_d,n_d}(z')\delta_{\mathbf{k}_a+\mathbf{k}_b,\mathbf{k}_c+\mathbf{k}_d}\delta_{\sigma_a,\sigma_c}\delta_{\sigma_b,\sigma_d} \tag{APP E.14}$$

$$\begin{aligned}[H_{\rm cc}, a_k^\dagger a_l] = \quad & \frac{1}{2}\sum_{a,b,c,d} V_{abcd}[a_a^\dagger a_b^\dagger a_d a_c, a_k^\dagger a_l], \\ = \quad & \frac{1}{2}\sum_{a,b,c,d} V_{abcd}\Big\{ - a_k^\dagger a_b^\dagger a_d a_c \delta_{l,a} - a_a^\dagger a_k^\dagger a_d a_c \delta_{l,b} \\ & - a_a^\dagger a_b^\dagger a_c a_l\,\delta_{k,d} + a_a^\dagger a_b^\dagger a_d a_l\,\delta_{k,c}\Big\}, \\ = \quad & \frac{1}{2}\Big\{ - \sum_{b,c,d} V_{lbcd} a_k^\dagger a_b^\dagger a_d a_c - \sum_{a,c,d} V_{alcd} a_a^\dagger a_k^\dagger a_d a_c \\ & - \sum_{a,b,c} V_{abck} a_a^\dagger a_b^\dagger a_c a_l + \sum_{a,b,d} V_{abkd} a_a^\dagger a_b^\dagger a_d a_l\Big\}.\end{aligned} \tag{APP E.15}$$

Using the symmetry of the Coulomb matrix element, $V_{abcd} = V_{badc}$ (cf. Eq. (APP E.13)), and the commutation relations we can simplify further Eq. (APP E.15)

$$[H_{\rm cc}, a_k^\dagger a_l] = \sum_{a,b,c}\Big[V_{abkc}\, a_a^\dagger a_b^\dagger a_c a_l\ - V_{labc}\, a_k^\dagger a_a^\dagger a_c a_b\Big]. \tag{APP E.16}$$

4. Carrier-Phonon

Hamiltonian:

$$H_{\rm cp} = \sum_{a,b,\mathbf{k},\underline{\mathbf{q}}} \left[g^{a,b}_{\underline{\mathbf{q}}} a^\dagger_{a,\mathbf{k}_a} b_{\underline{\mathbf{q}}} a_{b,\mathbf{k}_a - \underline{\mathbf{q}}_{||}} + g^{*a,b}_{\underline{\mathbf{q}}} a^\dagger_{b,\mathbf{k}_a - \underline{\mathbf{q}}_{||}} b^\dagger_{\underline{\mathbf{q}}} a_{a,\mathbf{k}_a} \right] \tag{APP E.17}$$

$\underline{\mathbf{q}}$ denotes a 3d wave vector, indices a, b denotes well number, subband and spin.

Using Eq. (APP E.1) we obtain immediately

$$\begin{aligned}
[H_{\rm cp}, a^\dagger_{k,\mathbf{k}_k} a_{l,\mathbf{k}_l}] = & \sum_{a,b,\mathbf{k}_a,\underline{\mathbf{q}}} \Big\{ g^{a,b}_{\underline{\mathbf{q}}} b_{\underline{\mathbf{q}}} \Big(a^\dagger_{a,\mathbf{k}_a} a_{l,\mathbf{k}_l} \delta_{b,k} \delta_{\mathbf{k}_a - \underline{\mathbf{q}}_{||},\mathbf{k}_k} - a^\dagger_{k,\mathbf{k}_k} a_{b,\mathbf{k}_a - \underline{\mathbf{q}}_{||}} \delta_{a,l} \delta_{\mathbf{k}_a,\mathbf{k}_l} \Big) \\
& + g^{*a,b}_{\underline{\mathbf{q}}} b^\dagger_{\underline{\mathbf{q}}} \Big(a^\dagger_{b,\mathbf{k}_a - \underline{\mathbf{q}}_{||}} a_{l,\mathbf{k}_l} \delta_{a,k} \delta_{\mathbf{k}_a,\mathbf{k}_k} - a^\dagger_{k,\mathbf{k}_k} a_{a,\mathbf{k}_a} \delta_{b,l} \delta_{\mathbf{k}_a - \underline{\mathbf{q}}_{||},\mathbf{k}_l} \Big) \Big\}, \\
= & \sum_{a,\underline{\mathbf{q}}} \Big\{ g^{a,k}_{\underline{\mathbf{q}}} b_{\underline{\mathbf{q}}} a^\dagger_{a,\mathbf{k}_k + \underline{\mathbf{q}}_{||}} a_{l,\mathbf{k}_l} - g^{l,a}_{\underline{\mathbf{q}}} b_{\underline{\mathbf{q}}} a^\dagger_{k,\mathbf{k}_k} a_{a,\mathbf{k}_l - \underline{\mathbf{q}}_{||}} \\
& + g^{*k,a}_{\underline{\mathbf{q}}} b^\dagger_{\underline{\mathbf{q}}} a^\dagger_{a,\mathbf{k}_k - \underline{\mathbf{q}}_{||}} a_{l,\mathbf{k}_l} - g^{*a,l}_{\underline{\mathbf{q}}} b^\dagger_{\underline{\mathbf{q}}} a^\dagger_{k,\mathbf{k}_k} a_{a,\mathbf{k}_l + \underline{\mathbf{q}}_{||}} \Big\}
\end{aligned} \tag{APP E.18}$$

APPENDIX F

Correlation Contributions (Scattering Rates)

Below, the used abbreviations are given for subband $i = 1$, the terms for $i = 2$ are obtained by exchanging the subband indices 1 and 2.

$$\Gamma_{\mathrm{d}}^{1,\mathrm{cp}} = 2\sum_{\underline{\mathbf{q}}}\Big[\delta(-\epsilon^1_{\mathbf{k}}+\epsilon^1_{\mathbf{k}+\underline{\mathbf{q}}_{||}}-\hbar\omega_{LO})|g^{11}_{\underline{\mathbf{q}}}|^2\left\{n_{\underline{\mathbf{q}}}(1-f^1_{\mathbf{k}+\underline{\mathbf{q}}_{||}})+\left(n_{\underline{\mathbf{q}}}+1\right)f^1_{\mathbf{k}+\underline{\mathbf{q}}_{||}}\right\}+\delta(-\epsilon^1_{\mathbf{k}}+\epsilon^1_{\mathbf{k}+\underline{\mathbf{q}}_{||}}+\hbar\omega_{LO})|g^{11}_{\underline{\mathbf{q}}}|^2\left\{\left(n_{\underline{\mathbf{q}}}+1\right)(1-f^1_{\mathbf{k}+\underline{\mathbf{q}}_{||}})+n_{\underline{\mathbf{q}}}f^1_{\mathbf{k}+\underline{\mathbf{q}}_{||}}\right\}$$
$$+\delta(-\epsilon^2_{\mathbf{k}}+\epsilon^1_{\mathbf{k}+\underline{\mathbf{q}}_{||}}-\hbar\omega_{LO})|g^{12}_{\underline{\mathbf{q}}}|^2\left\{n_{\underline{\mathbf{q}}}(1-f^1_{\mathbf{k}+\underline{\mathbf{q}}_{||}})+\left(n_{\underline{\mathbf{q}}}+1\right)f^1_{\mathbf{k}+\underline{\mathbf{q}}_{||}}\right\}+\delta(-\epsilon^2_{\mathbf{k}}+\epsilon^1_{\mathbf{k}+\underline{\mathbf{q}}_{||}}+\hbar\omega_{LO})|g^{12}_{\underline{\mathbf{q}}}|^2\left\{\left(n_{\underline{\mathbf{q}}}+1\right)(1-f^1_{\mathbf{k}+\underline{\mathbf{q}}_{||}})+n_{\underline{\mathbf{q}}}f^1_{\mathbf{k}+\underline{\mathbf{q}}_{||}}\right\}\Big]$$

(App F.1)

$$\begin{aligned}\Gamma_{\mathrm{d}}^{1,\mathrm{cc}} = \quad & 2\sum_{\mathbf{k}',\mathbf{q}}\Big[\delta(\epsilon^1_{\mathbf{k}}+\epsilon^1_{\mathbf{k}'}-\epsilon^1_{\mathbf{k}'-\mathbf{q}}-\epsilon^1_{\mathbf{k}+\mathbf{q}})V^{1111}_{\mathbf{q}}(2V^{1111}_{\mathbf{q}}-V^{1111}_{\mathbf{k}'-\mathbf{k}-\mathbf{q}})\left\{f^1_{\mathbf{k}'}(1-f^1_{\mathbf{k}'-\mathbf{q}})(1-f^1_{\mathbf{k}+\mathbf{q}})+f^1_{\mathbf{k}'-\mathbf{q}}f^1_{\mathbf{k}+\mathbf{q}}(1-f^1_{\mathbf{k}'})\right\}\\
& +\delta(\epsilon^1_{\mathbf{k}}+\epsilon^1_{\mathbf{k}'}-\epsilon^2_{\mathbf{k}'-\mathbf{q}}-\epsilon^2_{\mathbf{k}+\mathbf{q}})V^{1122}_{\mathbf{q}}(2V^{1122}_{\mathbf{q}}-V^{1122}_{\mathbf{k}'-\mathbf{k}-\mathbf{q}})\left\{f^1_{\mathbf{k}'}(1-f^2_{\mathbf{k}'-\mathbf{q}})(1-f^2_{\mathbf{k}+\mathbf{q}})+f^2_{\mathbf{k}'-\mathbf{q}}f^2_{\mathbf{k}+\mathbf{q}}(1-f^1_{\mathbf{k}'})\right\}\\
& +\delta(\epsilon^1_{\mathbf{k}}+\epsilon^2_{\mathbf{k}'}-\epsilon^1_{\mathbf{k}'-\mathbf{q}}-\epsilon^2_{\mathbf{k}+\mathbf{q}})V^{1221}_{\mathbf{q}}(2V^{1221}_{\mathbf{q}}-V^{1212}_{\mathbf{k}'-\mathbf{k}-\mathbf{q}})\left\{f^2_{\mathbf{k}'}(1-f^1_{\mathbf{k}'-\mathbf{q}})(1-f^2_{\mathbf{k}+\mathbf{q}})+f^1_{\mathbf{k}'-\mathbf{q}}f^2_{\mathbf{k}+\mathbf{q}}(1-f^2_{\mathbf{k}'})\right\}\\
& +\delta(\epsilon^1_{\mathbf{k}}+\epsilon^2_{\mathbf{k}'}-\epsilon^2_{\mathbf{k}'-\mathbf{q}}-\epsilon^1_{\mathbf{k}+\mathbf{q}})V^{1212}_{\mathbf{q}}(2V^{1212}_{\mathbf{q}}-V^{1221}_{\mathbf{k}'-\mathbf{k}-\mathbf{q}})\left\{f^2_{\mathbf{k}'}(1-f^2_{\mathbf{k}'-\mathbf{q}})(1-f^1_{\mathbf{k}+\mathbf{q}})+f^2_{\mathbf{k}'-\mathbf{q}}f^1_{\mathbf{k}+\mathbf{q}}(1-f^2_{\mathbf{k}'})\right\}\Big].\end{aligned}$$

(App F.2)

$$
\begin{aligned}
\Gamma^{1,\mathrm{cp}}_{\mathrm{nd}} &= \delta(-\epsilon^1_{\mathbf{k}} + \epsilon^1_{\mathbf{k}+\underline{\mathbf{q}}_{||}} - \hbar\omega_{LO})\, g^{11*}_{\underline{\mathbf{q}}} g^{22}_{\underline{\mathbf{q}}} \left\{ \left(n_{\underline{\mathbf{q}}} + 1 \right) (1 - f^1_{\mathbf{k}}) + n_{\underline{\mathbf{q}}} f^1_{\mathbf{k}} \right\} \\
&\quad + \delta(-\epsilon^1_{\mathbf{k}} + \epsilon^1_{\mathbf{k}+\underline{\mathbf{q}}_{||}} + \hbar\omega_{LO})\, g^{11*}_{\underline{\mathbf{q}}} g^{22}_{\underline{\mathbf{q}}} \left\{ n_{\underline{\mathbf{q}}} (1 - f^1_{\mathbf{k}}) + \left(n_{\underline{\mathbf{q}}} + 1 \right) f^1_{\mathbf{k}} \right\} , \\
\tilde{\Gamma}^{1,\mathrm{cp}}_{\mathrm{nd}} &= \delta(-\epsilon^1_{\mathbf{k}} + \epsilon^2_{\mathbf{k}+\underline{\mathbf{q}}_{||}} - \hbar\omega_{LO})\, |g^{12}_{\underline{\mathbf{q}}}|^2 \left\{ \left(n_{\underline{\mathbf{q}}} + 1 \right) (1 - f^1_{\mathbf{k}}) + n_{\underline{\mathbf{q}}} f^1_{\mathbf{k}} \right\} \\
&\quad + \delta(-\epsilon^1_{\mathbf{k}} + \epsilon^2_{\mathbf{k}+\underline{\mathbf{q}}_{||}} + \hbar\omega_{LO})\, |g^{12}_{\underline{\mathbf{q}}}|^2 \left\{ n_{\underline{\mathbf{q}}} (1 - f^1_{\mathbf{k}}) + \left(n_{\underline{\mathbf{q}}} + 1 \right) f^1_{\mathbf{k}} \right\} , \\
\Gamma^{1,\mathrm{cc}}_{\mathrm{nd1}} &= \delta(\epsilon^1_{\mathbf{k}} + \epsilon^2_{\mathbf{k}'} - \epsilon^1_{\mathbf{k}'-\mathbf{q}} - \epsilon^2_{\mathbf{k}+\mathbf{q}}) V^{2222}_{\mathbf{q}} (2V^{1221}_{\mathbf{q}} - V^{1212}_{\mathbf{k}'-\mathbf{k}-\mathbf{q}}) \{ f^2_{\mathbf{k}+\mathbf{q}} (1 - f^1_{\mathbf{k}})(1 - f^2_{\mathbf{k}'}) + f^1_{\mathbf{k}} f^2_{\mathbf{k}'} (1 - f^2_{\mathbf{k}+\mathbf{q}}) \} \\
&\quad + \delta(\epsilon^1_{\mathbf{k}} + \epsilon^1_{\mathbf{k}'} - \epsilon^1_{\mathbf{k}'-\mathbf{q}} - \epsilon^1_{\mathbf{k}+\mathbf{q}}) V^{1221}_{\mathbf{q}} (2V^{1111}_{\mathbf{q}} - V^{1111}_{\mathbf{k}'-\mathbf{k}-\mathbf{q}}) \{ f^1_{\mathbf{k}+\mathbf{q}} (1 - f^1_{\mathbf{k}})(1 - f^1_{\mathbf{k}'}) + f^1_{\mathbf{k}} f^1_{\mathbf{k}'} (1 - f^1_{\mathbf{k}+\mathbf{q}}) \}, \\
\tilde{\Gamma}^{1,\mathrm{cc}}_{\mathrm{nd1}} &= \delta(\epsilon^1_{\mathbf{k}} + \epsilon^1_{\mathbf{k}'} - \epsilon^2_{\mathbf{k}'-\mathbf{q}} - \epsilon^2_{\mathbf{k}+\mathbf{q}}) V^{2121}_{\mathbf{q}} (2V^{1221}_{\mathbf{q}} - V^{1221}_{\mathbf{k}'-\mathbf{k}-\mathbf{q}}) \{ f^2_{\mathbf{k}+\mathbf{q}} (1 - f^1_{\mathbf{k}})(1 - f^1_{\mathbf{k}'}) + f^1_{\mathbf{k}} f^1_{\mathbf{k}'} (1 - f^2_{\mathbf{k}+\mathbf{q}}) \} \\
&\quad + \delta(\epsilon^1_{\mathbf{k}} + \epsilon^2_{\mathbf{k}'} - \epsilon^2_{\mathbf{k}'-\mathbf{q}} - \epsilon^1_{\mathbf{k}+\mathbf{q}}) V^{1221}_{\mathbf{q}} (2V^{1212}_{\mathbf{q}} - V^{1221}_{\mathbf{k}'-\mathbf{k}-\mathbf{q}}) \{ f^1_{\mathbf{k}+\mathbf{q}} (1 - f^1_{\mathbf{k}})(1 - f^2_{\mathbf{k}'}) + f^1_{\mathbf{k}} f^2_{\mathbf{k}'} (1 - f^1_{\mathbf{k}+\mathbf{q}}) \}, \\
\Gamma^{1,\mathrm{cc}}_{\mathrm{nd2}} &= \sum_{\mathbf{k}'} \Big[\delta(\epsilon^1_{\mathbf{k}} + \epsilon^2_{\mathbf{k}'} - \epsilon^2_{\mathbf{k}'-\mathbf{q}} - \epsilon^1_{\mathbf{k}+\mathbf{q}}) V^{2222}_{\mathbf{q}} (2V^{1212}_{\mathbf{q}} - V^{1221}_{\mathbf{k}'-\mathbf{k}-\mathbf{q}}) \{ f^2_{\mathbf{k}'-\mathbf{q}} (1 - f^1_{\mathbf{k}})(1 - f^2_{\mathbf{k}'}) + f^1_{\mathbf{k}} f^2_{\mathbf{k}'} (1 - f^2_{\mathbf{k}'-\mathbf{q}}) \} \\
&\qquad + \delta(\epsilon^1_{\mathbf{k}} + \epsilon^1_{\mathbf{k}'} - \epsilon^1_{\mathbf{k}'-\mathbf{q}} - \epsilon^1_{\mathbf{k}+\mathbf{q}}) V^{2121}_{\mathbf{q}} (2V^{1111}_{\mathbf{q}} - V^{1111}_{\mathbf{k}'-\mathbf{k}-\mathbf{q}}) \{ f^1_{\mathbf{k}'-\mathbf{q}} (1 - f^1_{\mathbf{k}})(1 - f^1_{\mathbf{k}'}) + f^1_{\mathbf{k}} f^1_{\mathbf{k}'} (1 - f^1_{\mathbf{k}'-\mathbf{q}}) \} \Big], \\
\tilde{\Gamma}^{1,\mathrm{cc}}_{\mathrm{nd2}} &= \sum_{\mathbf{k}'} \Big[\delta(\epsilon^1_{\mathbf{k}} + \epsilon^1_{\mathbf{k}'} - \epsilon^2_{\mathbf{k}'-\mathbf{q}} - \epsilon^2_{\mathbf{k}+\mathbf{q}}) V^{1221}_{\mathbf{q}} (2V^{1221}_{\mathbf{q}} - V^{1221}_{\mathbf{k}'-\mathbf{k}-\mathbf{q}}) \{ f^2_{\mathbf{k}'-\mathbf{q}} (1 - f^1_{\mathbf{k}})(1 - f^1_{\mathbf{k}'}) + f^1_{\mathbf{k}} f^1_{\mathbf{k}'} (1 - f^2_{\mathbf{k}'-\mathbf{q}}) \} \\
&\qquad + \delta(\epsilon^1_{\mathbf{k}} + \epsilon^2_{\mathbf{k}'} - \epsilon^1_{\mathbf{k}'-\mathbf{q}} - \epsilon^2_{\mathbf{k}+\mathbf{q}}) V^{1221}_{\mathbf{q}} (2V^{1221}_{\mathbf{q}} - V^{1212}_{\mathbf{k}'-\mathbf{k}-\mathbf{q}}) \{ f^1_{\mathbf{k}'-\mathbf{q}} (1 - f^1_{\mathbf{k}})(1 - f^2_{\mathbf{k}'}) + f^1_{\mathbf{k}} f^2_{\mathbf{k}'} (1 - f^1_{\mathbf{k}'-\mathbf{q}}) \} \Big], \\
\Gamma^{1,\mathrm{cc}}_{\mathrm{nd3}} &= \sum_{\mathbf{q}} \Big[\delta(\epsilon^1_{\mathbf{k}} + \epsilon^2_{\mathbf{k}'} - \epsilon^2_{\mathbf{k}'-\mathbf{q}} - \epsilon^1_{\mathbf{k}+\mathbf{q}}) V^{1221}_{\mathbf{q}} (2V^{1212}_{\mathbf{q}} - V^{1221}_{\mathbf{k}'-\mathbf{k}-\mathbf{q}}) \{ f^1_{\mathbf{k}} (1 - f^2_{\mathbf{k}'-\mathbf{q}})(1 - f^1_{\mathbf{k}+\mathbf{q}}) + f^2_{\mathbf{k}'-\mathbf{q}} f^1_{\mathbf{k}+\mathbf{q}} (1 - f^1_{\mathbf{k}}) \} \\
&\qquad + \delta(\epsilon^1_{\mathbf{k}} + \epsilon^2_{\mathbf{k}'} - \epsilon^1_{\mathbf{k}'-\mathbf{q}} - \epsilon^2_{\mathbf{k}+\mathbf{q}}) V^{1212}_{\mathbf{q}} (2V^{1221}_{\mathbf{q}} - V^{1212}_{\mathbf{k}'-\mathbf{k}-\mathbf{q}}) \{ f^1_{\mathbf{k}} (1 - f^1_{\mathbf{k}'-\mathbf{q}})(1 - f^2_{\mathbf{k}+\mathbf{q}}) + f^1_{\mathbf{k}'-\mathbf{q}} f^2_{\mathbf{k}+\mathbf{q}} (1 - f^1_{\mathbf{k}}) \} \Big] \\
\tilde{\Gamma}^{1,\mathrm{cc}}_{\mathrm{nd3}} &= \sum_{\mathbf{q}} \Big[\delta(\epsilon^1_{\mathbf{k}} + \epsilon^1_{\mathbf{k}'} - \epsilon^1_{\mathbf{k}'-\mathbf{q}} - \epsilon^1_{\mathbf{k}+\mathbf{q}}) V^{1221}_{\mathbf{q}} (2V^{1111}_{\mathbf{q}} - V^{1111}_{\mathbf{k}'-\mathbf{k}-\mathbf{q}}) \{ f^1_{\mathbf{k}} (1 - f^1_{\mathbf{k}'-\mathbf{q}})(1 - f^1_{\mathbf{k}+\mathbf{q}}) + f^1_{\mathbf{k}'-\mathbf{q}} f^1_{\mathbf{k}+\mathbf{q}} (1 - f^1_{\mathbf{k}}) \} \\
&\qquad + \delta(\epsilon^1_{\mathbf{k}} + \epsilon^1_{\mathbf{k}'} - \epsilon^2_{\mathbf{k}'-\mathbf{q}} - \epsilon^2_{\mathbf{k}+\mathbf{q}}) V^{1111}_{\mathbf{q}} (2V^{1221}_{\mathbf{q}} - V^{1221}_{\mathbf{k}'-\mathbf{k}-\mathbf{q}}) \{ f^1_{\mathbf{k}} (1 - f^2_{\mathbf{k}'-\mathbf{q}})(1 - f^2_{\mathbf{k}+\mathbf{q}}) + f^1_{\mathbf{k}'-\mathbf{q}} f^2_{\mathbf{k}+\mathbf{q}} (1 - f^2_{\mathbf{k}}) \} \Big].
\end{aligned}
$$

The contributions nonlinear in the polarization are given by

$$\Xi_{\text{nl}} = \sum_{\mathbf{k}',\mathbf{q}} \Gamma^{\text{cc}}_{\text{nl}} \tag{App F.3}$$

with

$$\begin{aligned}
\Gamma^{\text{cc}}_{\text{nl}} = \quad & \Big[\delta(\epsilon^1_{\mathbf{k}} + \epsilon^1_{\mathbf{k}'} - \epsilon^1_{\mathbf{k}'-\mathbf{q}} - \epsilon^1_{\mathbf{k}+\mathbf{q}})(2V^{1111}_{\mathbf{q}} - V^{1111}_{\mathbf{k}'-\mathbf{k}-\mathbf{q}})\Big[p^{21}_{\mathbf{k}}\Big(V^{1221}_{\mathbf{q}} p^{21}_{\mathbf{k}'} p^{12}_{\mathbf{k}+\mathbf{q}} - V^{1221}_{\mathbf{q}} p^{12}_{\mathbf{k}'-\mathbf{q}} p^{12}_{\mathbf{k}+\mathbf{q}} + V^{1212}_{\mathbf{q}} p^{21}_{\mathbf{k}'} p^{12}_{\mathbf{k}'-\mathbf{q}}\Big) - V^{2222}_{\mathbf{q}} p^{21}_{\mathbf{k}+\mathbf{q}} p^{21}_{\mathbf{k}'-\mathbf{q}} p^{12}_{\mathbf{k}'}\Big] \\
& + \delta(\epsilon^1_{\mathbf{k}} + \epsilon^1_{\mathbf{k}'} - \epsilon^2_{\mathbf{k}'-\mathbf{q}} - \epsilon^2_{\mathbf{k}+\mathbf{q}})(2V^{1221}_{\mathbf{q}} - V^{1221}_{\mathbf{k}'-\mathbf{k}-\mathbf{q}})\Big[p^{21}_{\mathbf{k}}\Big(V^{1221}_{\mathbf{q}} p^{21}_{\mathbf{k}'} p^{21}_{\mathbf{k}'-\mathbf{q}} - V^{1111}_{\mathbf{q}} p^{21}_{\mathbf{k}+\mathbf{q}} p^{21}_{\mathbf{k}'-\mathbf{q}} + V^{1212}_{\mathbf{q}} p^{21}_{\mathbf{k}+\mathbf{q}} p^{21}_{\mathbf{k}'}\Big) - V^{1221}_{\mathbf{q}} p^{12}_{\mathbf{k}+\mathbf{q}} p^{12}_{\mathbf{k}'-\mathbf{q}} p^{12}_{\mathbf{k}'}\Big] \\
& + \delta(\epsilon^1_{\mathbf{k}} + \epsilon^2_{\mathbf{k}'} - \epsilon^1_{\mathbf{k}'-\mathbf{q}} - \epsilon^2_{\mathbf{k}+\mathbf{q}})(2V^{1221}_{\mathbf{q}} - V^{1212}_{\mathbf{k}'-\mathbf{k}-\mathbf{q}})\Big[p^{21}_{\mathbf{k}}\Big(V^{1111}_{\mathbf{q}} p^{12}_{\mathbf{k}'} p^{21}_{\mathbf{k}+\mathbf{q}} - V^{1212}_{\mathbf{q}} p^{21}_{\mathbf{k}+\mathbf{q}} p^{12}_{\mathbf{k}'-\mathbf{q}} + V^{1221}_{\mathbf{q}} p^{12}_{\mathbf{k}'} p^{12}_{\mathbf{k}'-\mathbf{q}}\Big) - V^{1221}_{\mathbf{q}} p^{12}_{\mathbf{k}+\mathbf{q}} p^{21}_{\mathbf{k}'-\mathbf{q}} p^{21}_{\mathbf{k}'}\Big] \\
& + \delta(\epsilon^1_{\mathbf{k}} + \epsilon^2_{\mathbf{k}'} - \epsilon^2_{\mathbf{k}'-\mathbf{q}} - \epsilon^1_{\mathbf{k}+\mathbf{q}})(2V^{1212}_{\mathbf{q}} - V^{1221}_{\mathbf{k}'-\mathbf{k}-\mathbf{q}})\Big[p^{21}_{\mathbf{k}}\Big(V^{1111}_{\mathbf{q}} p^{21}_{\mathbf{k}'} p^{21}_{\mathbf{k}'-\mathbf{q}} - V^{1221}_{\mathbf{q}} p^{12}_{\mathbf{k}+\mathbf{q}} p^{12}_{\mathbf{k}'-\mathbf{q}} + V^{1221}_{\mathbf{q}} p^{12}_{\mathbf{k}'} p^{12}_{\mathbf{k}+\mathbf{q}}\Big) - V^{1212}_{\mathbf{q}} p^{21}_{\mathbf{k}+\mathbf{q}} p^{12}_{\mathbf{k}'-\mathbf{q}} p^{21}_{\mathbf{k}'}\Big] \\
& + \delta(\epsilon^2_{\mathbf{k}} + \epsilon^2_{\mathbf{k}'} - \epsilon^2_{\mathbf{k}'-\mathbf{q}} - \epsilon^2_{\mathbf{k}+\mathbf{q}})(2V^{2222}_{\mathbf{q}} - V^{2222}_{\mathbf{k}'-\mathbf{k}-\mathbf{q}})\Big[p^{21}_{\mathbf{k}}\Big(V^{1221}_{\mathbf{q}} p^{21}_{\mathbf{k}'} p^{12}_{\mathbf{k}+\mathbf{q}} - V^{1221}_{\mathbf{q}} p^{12}_{\mathbf{k}'-\mathbf{q}} p^{12}_{\mathbf{k}+\mathbf{q}} + V^{1212}_{\mathbf{q}} p^{21}_{\mathbf{k}'} p^{12}_{\mathbf{k}'-\mathbf{q}}\Big) - V^{1111}_{\mathbf{q}} p^{21}_{\mathbf{k}+\mathbf{q}} p^{21}_{\mathbf{k}'-\mathbf{q}} p^{12}_{\mathbf{k}'}\Big] \\
& + \delta(\epsilon^2_{\mathbf{k}} + \epsilon^2_{\mathbf{k}'} - \epsilon^1_{\mathbf{k}'-\mathbf{q}} - \epsilon^1_{\mathbf{k}+\mathbf{q}})(2V^{1221}_{\mathbf{q}} - V^{1221}_{\mathbf{k}'-\mathbf{k}-\mathbf{q}})\Big[p^{21}_{\mathbf{k}}\Big(V^{1221}_{\mathbf{q}} p^{21}_{\mathbf{k}'} p^{21}_{\mathbf{k}'-\mathbf{q}} - V^{2222}_{\mathbf{q}} p^{21}_{\mathbf{k}+\mathbf{q}} p^{21}_{\mathbf{k}'-\mathbf{q}} + V^{1212}_{\mathbf{q}} p^{21}_{\mathbf{k}+\mathbf{q}} p^{21}_{\mathbf{k}'}\Big) - V^{1221}_{\mathbf{q}} p^{12}_{\mathbf{k}+\mathbf{q}} p^{12}_{\mathbf{k}'-\mathbf{q}} p^{12}_{\mathbf{k}'}\Big] \\
& + \delta(\epsilon^2_{\mathbf{k}} + \epsilon^1_{\mathbf{k}'} - \epsilon^2_{\mathbf{k}'-\mathbf{q}} - \epsilon^1_{\mathbf{k}+\mathbf{q}})(2V^{1221}_{\mathbf{q}} - V^{1212}_{\mathbf{k}'-\mathbf{k}-\mathbf{q}})\Big[p^{21}_{\mathbf{k}}\Big(V^{2222}_{\mathbf{q}} p^{12}_{\mathbf{k}'} p^{21}_{\mathbf{k}+\mathbf{q}} - V^{1212}_{\mathbf{q}} p^{21}_{\mathbf{k}+\mathbf{q}} p^{12}_{\mathbf{k}'-\mathbf{q}} + V^{1221}_{\mathbf{q}} p^{12}_{\mathbf{k}'} p^{12}_{\mathbf{k}'-\mathbf{q}}\Big) - V^{1221}_{\mathbf{q}} p^{12}_{\mathbf{k}+\mathbf{q}} p^{21}_{\mathbf{k}'-\mathbf{q}} p^{21}_{\mathbf{k}'}\Big] \\
& + \delta(\epsilon^2_{\mathbf{k}} + \epsilon^1_{\mathbf{k}'} - \epsilon^1_{\mathbf{k}'-\mathbf{q}} - \epsilon^2_{\mathbf{k}+\mathbf{q}})(2V^{1212}_{\mathbf{q}} - V^{1221}_{\mathbf{k}'-\mathbf{k}-\mathbf{q}})\Big[p^{21}_{\mathbf{k}}\Big(V^{2222}_{\mathbf{q}} p^{21}_{\mathbf{k}'} p^{21}_{\mathbf{k}'-\mathbf{q}} - V^{1221}_{\mathbf{q}} p^{12}_{\mathbf{k}+\mathbf{q}} p^{12}_{\mathbf{k}'-\mathbf{q}} + V^{1221}_{\mathbf{q}} p^{12}_{\mathbf{k}'} p^{12}_{\mathbf{k}+\mathbf{q}}\Big) - V^{1212}_{\mathbf{q}} p^{21}_{\mathbf{k}+\mathbf{q}} p^{12}_{\mathbf{k}'-\mathbf{q}} p^{21}_{\mathbf{k}'}\Big]\Big].
\end{aligned} \tag{App F.4}$$

and

$$\Xi_{\text{nl},f_i} = \sum_{\underline{\mathbf{q}}} \Gamma^{\text{cp}}_{\text{nl},f_i} + \sum_{\mathbf{k}',\mathbf{q}} \Gamma^{\text{cc}}_{\text{nl},f_i} \tag{App F.5}$$

with

$$
\begin{aligned}
\Gamma^{\text{cp}}_{\text{nl},f_i} = \; & \Big[-\delta(-\epsilon^j_{\mathbf{k}} + \epsilon^j_{\mathbf{k}+\underline{\mathbf{q}}_{||}} - \hbar\omega_{LO})\, g^{ii}_{\underline{\mathbf{q}}} g^{jj*}_{\underline{\mathbf{q}}} p^{ji}_{\mathbf{k}} p^{ij}_{\mathbf{k}+\underline{\mathbf{q}}_{||}} + \delta(-\epsilon^j_{\mathbf{k}} + \epsilon^j_{\mathbf{k}+\underline{\mathbf{q}}_{||}} + \hbar\omega_{LO})\, g^{jj*}_{\underline{\mathbf{q}}} g^{ii}_{\underline{\mathbf{q}}} p^{ij}_{\mathbf{k}} p^{ji}_{\mathbf{k}+\underline{\mathbf{q}}_{||}} \\
& - \delta(-\epsilon^j_{\mathbf{k}} + \epsilon^i_{\mathbf{k}+\underline{\mathbf{q}}_{||}} - \hbar\omega_{LO})\, g^{ji}_{\underline{\mathbf{q}}} g^{ij*}_{\underline{\mathbf{q}}} p^{ji}_{\mathbf{k}} p^{ji}_{\mathbf{k}+\underline{\mathbf{q}}_{||}} + \delta(-\epsilon^j_{\mathbf{k}} + \epsilon^i_{\mathbf{k}+\underline{\mathbf{q}}_{||}} + \hbar\omega_{LO})\, g^{ji*}_{\underline{\mathbf{q}}} g^{ij}_{\underline{\mathbf{q}}} p^{ij}_{\mathbf{k}} p^{ij}_{\mathbf{k}+\underline{\mathbf{q}}_{||}} \Big] + c.c.\,, \\
\Gamma^{\text{cc}}_{\text{nl},f_i} = \; & \Big[\delta(\epsilon^i_{\mathbf{k}} + \epsilon^i_{\mathbf{k}'} - \epsilon^i_{\mathbf{k}'-\mathbf{q}} - \epsilon^i_{\mathbf{k}+\mathbf{q}})(2V^{iiii}_{\mathbf{q}} - V^{iiii}_{\mathbf{k}'-\mathbf{k}-\mathbf{q}}) \Big[V^{ijji}_{\mathbf{q}} \Big(1 - f^i_{\mathbf{k}} - f^i_{\mathbf{k}'}\Big) p^{ji}_{\mathbf{k}+\mathbf{q}} p^{ji}_{\mathbf{k}'-\mathbf{q}} + V^{ijji}_{\mathbf{q}} \Big(f^i_{\mathbf{k}} - f^i_{\mathbf{k}'-\mathbf{q}}\Big) p^{ij}_{\mathbf{k}+\mathbf{q}} p^{ji}_{\mathbf{k}'} + V^{ijij}_{\mathbf{q}} \Big(f^i_{\mathbf{k}} - f^i_{\mathbf{k}+\mathbf{q}}\Big) p^{ij}_{\mathbf{k}'} p^{ji}_{\mathbf{k}'-\mathbf{q}} \Big] \\
& + \delta(\epsilon^i_{\mathbf{k}} + \epsilon^i_{\mathbf{k}'} - \epsilon^j_{\mathbf{k}'-\mathbf{q}} - \epsilon^j_{\mathbf{k}+\mathbf{q}})(2V^{ijji}_{\mathbf{q}} - V^{ijji}_{\mathbf{k}'-\mathbf{k}-\mathbf{q}}) \Big[V^{iiii}_{\mathbf{q}} \Big(1 - f^i_{\mathbf{k}} - f^i_{\mathbf{k}'}\Big) p^{ji}_{\mathbf{k}+\mathbf{q}} p^{ji}_{\mathbf{k}'-\mathbf{q}} + V^{ijji}_{\mathbf{q}} \Big(f^i_{\mathbf{k}} - f^j_{\mathbf{k}+\mathbf{q}}\Big) p^{ji}_{\mathbf{k}'-\mathbf{q}} p^{ji}_{\mathbf{k}'} + V^{ijij}_{\mathbf{q}} \Big(f^i_{\mathbf{k}} - f^i_{\mathbf{k}'-\mathbf{q}}\Big) p^{ji}_{\mathbf{k}'} p^{ji}_{\mathbf{k}+\mathbf{q}} \Big] \\
& + \delta(\epsilon^i_{\mathbf{k}} + \epsilon^j_{\mathbf{k}'} - \epsilon^i_{\mathbf{k}'-\mathbf{q}} - \epsilon^j_{\mathbf{k}+\mathbf{q}})(2V^{ijji}_{\mathbf{q}} - V^{ijij}_{\mathbf{k}'-\mathbf{k}-\mathbf{q}}) \Big[V^{iiii}_{\mathbf{q}} \Big(f^i_{\mathbf{k}} - f^i_{\mathbf{k}'-\mathbf{q}}\Big) p^{ij}_{\mathbf{k}+\mathbf{q}} p^{ji}_{\mathbf{k}'} + V^{ijji}_{\mathbf{q}} \Big(f^i_{\mathbf{k}} - f^j_{\mathbf{k}+\mathbf{q}}\Big) p^{ji}_{\mathbf{k}'-\mathbf{q}} p^{ji}_{\mathbf{k}'} + V^{ijij}_{\mathbf{q}} \Big(1 - f^i_{\mathbf{k}} - f^j_{\mathbf{k}'}\Big) p^{ji}_{\mathbf{k}'-\mathbf{q}} p^{ij}_{\mathbf{k}+\mathbf{q}} \Big] \\
& + \delta(\epsilon^i_{\mathbf{k}} + \epsilon^j_{\mathbf{k}'} - \epsilon^j_{\mathbf{k}'-\mathbf{q}} - \epsilon^i_{\mathbf{k}+\mathbf{q}})(2V^{ijij}_{\mathbf{q}} - V^{ijji}_{\mathbf{k}'-\mathbf{k}-\mathbf{q}}) \Big[V^{iiii}_{\mathbf{q}} \Big(f^i_{\mathbf{k}} - f^i_{\mathbf{k}+\mathbf{q}}\Big) p^{ij}_{\mathbf{k}'} p^{ji}_{\mathbf{k}'-\mathbf{q}} + V^{ijji}_{\mathbf{q}} \Big(f^i_{\mathbf{k}} - f^j_{\mathbf{k}'-\mathbf{q}}\Big) p^{ji}_{\mathbf{k}+\mathbf{q}} p^{ji}_{\mathbf{k}'} + V^{ijji}_{\mathbf{q}} \Big(1 - f^i_{\mathbf{k}} - f^j_{\mathbf{k}'}\Big) p^{ji}_{\mathbf{k}'-\mathbf{q}} p^{ij}_{\mathbf{k}+\mathbf{q}} \Big] \\
& + \delta(\epsilon^j_{\mathbf{k}} + \epsilon^j_{\mathbf{k}'} - \epsilon^j_{\mathbf{k}'-\mathbf{q}} - \epsilon^j_{\mathbf{k}+\mathbf{q}})(2V^{jjjj}_{\mathbf{q}} - V^{jjjj}_{\mathbf{k}'-\mathbf{k}-\mathbf{q}}) \Big[V^{ijij}_{\mathbf{q}} \Big(f^j_{\mathbf{k}'} - f^j_{\mathbf{k}'-\mathbf{q}}\Big) p^{ij}_{\mathbf{k}} p^{ji}_{\mathbf{k}+\mathbf{q}} + V^{ijji}_{\mathbf{q}} \Big(f^j_{\mathbf{k}'} - f^j_{\mathbf{k}+\mathbf{q}}\Big) p^{ji}_{\mathbf{k}'-\mathbf{q}} p^{ij}_{\mathbf{k}} - V^{ijji}_{\mathbf{q}} \Big(1 - f^j_{\mathbf{k}+\mathbf{q}} - f^j_{\mathbf{k}'-\mathbf{q}}\Big) p^{ji}_{\mathbf{k}'} p^{ji}_{\mathbf{k}} \Big] \\
& + \delta(\epsilon^j_{\mathbf{k}} + \epsilon^j_{\mathbf{k}'} - \epsilon^i_{\mathbf{k}'-\mathbf{q}} - \epsilon^i_{\mathbf{k}+\mathbf{q}})(2V^{ijji}_{\mathbf{q}} - V^{ijji}_{\mathbf{k}'-\mathbf{k}-\mathbf{q}}) \Big[V^{ijij}_{\mathbf{q}} \Big(f^j_{\mathbf{k}'} - f^i_{\mathbf{k}+\mathbf{q}}\Big) p^{ij}_{\mathbf{k}} p^{ij}_{\mathbf{k}'-\mathbf{q}} + V^{ijji}_{\mathbf{q}} \Big(f^j_{\mathbf{k}'} - f^i_{\mathbf{k}'-\mathbf{q}}\Big) p^{ji}_{\mathbf{k}} p^{ji}_{\mathbf{k}+\mathbf{q}} - V^{iiii}_{\mathbf{q}} \Big(1 - f^i_{\mathbf{k}+\mathbf{q}} - f^i_{\mathbf{k}'-\mathbf{q}}\Big) p^{ji}_{\mathbf{k}} p^{ji}_{\mathbf{k}'} \Big] \\
& + \delta(\epsilon^j_{\mathbf{k}} + \epsilon^i_{\mathbf{k}'} - \epsilon^j_{\mathbf{k}'-\mathbf{q}} - \epsilon^i_{\mathbf{k}+\mathbf{q}})(2V^{ijji}_{\mathbf{q}} - V^{ijij}_{\mathbf{k}'-\mathbf{k}-\mathbf{q}}) \Big[V^{ijji}_{\mathbf{q}} \Big(f^i_{\mathbf{k}'} - f^j_{\mathbf{k}'-\mathbf{q}}\Big) p^{ji}_{\mathbf{k}} p^{ji}_{\mathbf{k}+\mathbf{q}} + V^{iiii}_{\mathbf{q}} \Big(f^i_{\mathbf{k}'} - f^i_{\mathbf{k}+\mathbf{q}}\Big) p^{ij}_{\mathbf{k}} p^{ji}_{\mathbf{k}'-\mathbf{q}} - V^{ijij}_{\mathbf{q}} \Big(1 - f^j_{\mathbf{k}'-\mathbf{q}} - f^i_{\mathbf{k}+\mathbf{q}}\Big) p^{ij}_{\mathbf{k}} p^{ji}_{\mathbf{k}'} \Big] \\
& + \delta(\epsilon^j_{\mathbf{k}} + \epsilon^i_{\mathbf{k}'} - \epsilon^i_{\mathbf{k}'-\mathbf{q}} - \epsilon^j_{\mathbf{k}+\mathbf{q}})(2V^{ijij}_{\mathbf{q}} - V^{ijji}_{\mathbf{k}'-\mathbf{k}-\mathbf{q}}) \Big[V^{ijji}_{\mathbf{q}} \Big(f^i_{\mathbf{k}'} - f^j_{\mathbf{k}+\mathbf{q}}\Big) p^{ij}_{\mathbf{k}} p^{ij}_{\mathbf{k}'-\mathbf{q}} + V^{iiii}_{\mathbf{q}} \Big(f^i_{\mathbf{k}'} - f^i_{\mathbf{k}'-\mathbf{q}}\Big) p^{ij}_{\mathbf{k}} p^{ji}_{\mathbf{k}+\mathbf{q}} - V^{ijji}_{\mathbf{q}} \Big(1 - f^i_{\mathbf{k}'-\mathbf{q}} - f^j_{\mathbf{k}+\mathbf{q}}\Big) p^{ij}_{\mathbf{k}} p^{ji}_{\mathbf{k}'} \Big] \Big] + c.c. \\
& [j = 1, 2, j \neq i] \qquad \text{(App F.6)}
\end{aligned}
$$

APPENDIX F

Bibliography

[AE87] L. Allen and J.H. Eberly. *Optical Resonance and Two–Level Atoms*. Dover Publications, Inc., New York, 1987. Unabriged and corrected edition of the work originally published in 1975 by John Wiley & Sons, Inc., New York.

[Ahn94] D. Ahn. First-order correction to phonon scattering due to dynamical screening in quantum wells. *Physical Review B*, 50(3):1713–1716, July 1994.

[AK04] V.M. Axt and T. Kuhn. Femtosecond spectroscopy in semiconductors: a key to coherences, correlations and quantum kinetics. *Reprots on Progress in Physics*, 67(4):433 – 512, 2004.

[AW97] A.M. Alcalde and G. Weber. Nonparabolicity effects on electron-optical-phonon scattering rates in quantum wells. *Physical Review B*, 56(15):9619–9624, October 1997.

[Bas88] G. Bastard. *Wave Mechanics applied to Semiconductor Heterostructures*. Les Editions de Physique, France, 1rd edition, 1988.

[BC04] A.A. Batista and D.S. Citrin. Rabi flopping in a two-level system with a time-dependent energy renormalization: Intersubband transitions in quantum wells. *Phys. Rev. Lett.*, 92(12):1274041 –1274044, 2004.

[BFWK04] S Butscher, J Forstner, I Waldmuller, and A Knorr. Polaron signatures in the line shape of semiconductor intersubband transitions: quantum kinetics of the electron-phonon interaction. *Physica Status Solidi (b)*, 241(11):R49 – R51, 2004.

[BHKP96] J.J. Baumberg, A.P. Heberle, K. Kohler, and K. Ploog. Ultrafast coherent carrier control in quantum wells. *Journal of the Optical Socitey of America B*, 13(6):1246 – 1250, 1996.

[BKL+90] R. Binder, S.W. Koch, M. Lindberg, N. Peyghambarian, and W. Schäfer. Ultrafast adiabatic following in semiconductors. *Physical Review Letters*, 65(7):899–902, August 1990.

[BKP01] H.-P. Breuer, B. Kappler, and F. Petruccione. The time-convolutionless projection operator technique in the quantum theory of dissipation and decoherence. *Annals of Physics*, 291(1):36–70, July 2001.

[BLS+02] P. Borri, W. Langbein, S. Schneider, U. Woggon, R.L. Sellin, D. Ouyang, and D. Bimberg. Coherent light-matter interaction in ingaas quantum dots: Dephasing time and optical rabi oscillations. *Phys. Status Solidi B-Basic Res.*, 233(3):391 – 400, 2002.

[BR85] M Braun and U Rossler. Magneto-optic transitions and non-parabolicity parameters in the conduction-band of semiconductors. *Journal of Physics C*, 18(17):3365 – 3377, 1985.

[BSP+92] R. Binder, D. Scott, A.E. Paul, M. Lindberg, K. Henneberger, and S.W. Koch. Carrier-carrier scattering and optical dephasing in highly excited semiconductors. *Physical Review B*, 45(3):1107–1115, January 1992.

[But04] S. Butscher. *Theory of the Non-markovian Intersubband Dynamics of Semiconductor Quantum Wells*. diploma thesis, Technische Universität Berlin, 2004.

[CK99] W.W. Chow and S.W. Koch. *Semiconductor–Laser Fundamentals — Physics of the Gain Material*. Springer Verlag, Berlin, 1999.

[CKF+94] S.T. Cundiff, A. Knorr, J. Feldmann, S.W. Koch, E.O. Göbel, and H. Nickel. Rabi flopping in semiconductors. *Physical Review Letters*, 73(8):1178–1181, August 1994.

[CT84] D.P. Craig and T. Thirunamachandran. *Molecular quantum electrodynamics: An Introduction to Radiation-Molecule Interactions*. Academic Press, Inc., London, 1984.

[CTDRG89] C. Cohen-Tannoudji, J. Dupont-Roc, and G. Grynberg. *Photons and Atoms*. John Wiley & Sons, Inc., Chichester, 1rd edition, 1989.

[Czy00] G. Czycholl. *Theoretische Festkörperphysik*. vieweg, Braunschweig/Wiesbaden, 1rd edition, 2000.

[Eke87] U. Ekenberg. Enhancement of nonparabolicity effects in a quantum well. *Physical Review B*, 36(11):6152–6155, October 1987.

[Eke89] U. Ekenberg. Nonparabolicity effects in a quantum well: Sublevel shift, parallel mass, and landau levels. *Physical Review B*, 40(11):7714–7726, October 1989.

[FÖ4] J. Förstner. *Light Propagation and Many-Particle Effects in Semiconductor Nanostrucutres*. Dissertation, Technische Universität Berlin, 2004.

[FS90] E. Fick and G. Sauermann. *The Quantum Statistics of Dynamical Processes*. Springer Verlag, Berlin, 1990.

[FWDK03] J. Förstner, C. Weber, J. Danckwerts, and A. Knorr. Phonon-assisted damping of rabi oscillations in semiconductor quantum dots. *Phys. Rev. Lett.*, 91(12):274011–274014, 2003.

[GSKB00] S Graf, H Sigg, K Kohler, and W Bachtold. Direct observation of depolarization shift of the intersubband resonance. *Physical Review Letters*, 84(12):2686 – 2689, 2000.

[Har00] P. Harrison. *Quantum Wells, Wires and Dots — Theoretical and Computational Physics*. John Wiley & Sons, Inc., Chichester, 2000.

[Hei84] W. Heitler. *The Quantum Theory of Radiation*. Dover Publications, Inc., New York, 3rd edition, 1984. Reprint.

[HK94] H. Haug and S.W. Koch. *Quantum Theory of the Optical and Electronic Properties of Semiconductors*. World Scientific Publishing Co. Pte. Ltd., Singapore, 3rd edition, 1994.

[HKK+96] S Hughes, A Knorr, SW Koch, R Binder, R Indik, and JV Moloney. The influence of electron-hole-scattering on the gain spectra of highly excited semiconductors. *Solid State Communications*, 100(8):555 – 559, 1996.

[IR01] R. Iotti and F. Rossi1. Nature of charge transport in quantum-cascade lasers. *Physical Review Letters*, 87(14):1466031–1466034, October 2001.

[Jac98] J.D. Jackson. *Classical Electrodynamics*. John Wiley & Sons, Inc., Chichester, 3rd edition, 1998.

[JKK+96] F. Jahnke, M. Kira, S.W. Koch, G. Khitrova, E.K. Lindmark, Jr. T.R. Nelsona, D.V. Wick, J.D. Berger, O. Lyngnes, H.M. Gibbs, and K. Tai. Excitonic nonlinearities of semiconductor microcavities in the nonperturbative regime. *Physical Review Letters*, 77(26):5257–5260, December 1996.

[JKK97] F. Jahnke, M. Kira, and S.W. Koch. Linear and nonlinear optical properties of excitions in semiconductor quantum wells and microcavities. *Z. Phys. B*, 104:559–572, 1997.

[KB89] L.P. Kadanoff and G. Baym. *Quantum Statistical Mechanics*. Addison-Wesley, California, reprint edition, 1989.

[KJHK99] M. Kira, F. Jahnke, W. Hoyer, and S.W. Koch. Quantum theory of spontaneous emission and coherent effects in semiconductor microstructures. *Progress in Quantum Electronics*, 23(6):189 – 279, 1999.

[Kli95] C.F. Klingshirn. *Semiconductor Optics*. Springer Verlag, Berlin, 1995.

[Kni76] Z. Knittl. *Optics of Thin Films - An Optical Multilayer Theory*. John Wiley & Sons, Inc., London, 1976.

[Kno97] A. Knorr. *Spatial effects in the Ultrafast Optics and Kinetics of Semiconductors*. Habilitationsschrift, Philipps–Universität Marburg, July 1997.

[Koh61] W Kohn. Cyclotron resonance and de haas-van alphen oscillations of an interacting electron gas. *Physical Review*, 123(4):1242, 1961.

[Kuh94] T. Kuhn. *Ladungsträgerdynamik in Halbleitersystemen fern vom Gleichgewicht: Elektronisches Rauschen und kohärente Prozesse*. Habilitationsschrift, Universität Stuttgart, 1994.

[Kuh98] T. Kuhn. Density matrix theory of coherent ultrafast dynamics. In E. Schöll, editor, *Theory of Transport Properties of Semiconductor Nanostructures*, volume 4 of *Electronic Materials*, chapter 6, pages 173–214. Chapman & Hall, 1998.

[LG99] S.-C. Lee and I. Galbraith. Intersubband and intrasubband electronic scattering rates in semiconductor quantum wells. *Physical Review B*, 59(24):15796–15805, June 1999.

[LG00] S.-C. Lee and I. Galbraith. Influence of exchange scattering and dynamic screening on electron–electron scattering in semiconductor quantum wells. *Physical Review B*, 62(23):15327–15330, December 2000.

[Liu94] A. Liu. Local-field effect on the linear optical intersubband absorption in multiple quantum wells. *Physical Review B*, 50(12):8569–8576, September 1994.

[LK88] M Lindberg and SW Koch. Effective bloch equations for semiconductors. *Physical Review B*, 38(5):3342 – 3350, 1988.

[LN03] JZ Li and CZ Ning. Interplay of collective excitations in quantum-well intersubband resonances. *Physical Review Letters*, 91(9), 2003.

[LN04] J Li and CZ Ning. Effects of electron-electron and electron-phonon scatterings on the linewidths of intersubband transitions in a quantum well. *Physical Review B*, 70(12), 2004.

[Lou00] R. Loudon. *The Quantum Theory of Light*. Oxford University Press, New York, 3rd edition, 2000.

[LRW+04] C.W. Luo, K. Reimann, M. Woerner, T. Elsaesser, R. Hey, and K.H. Ploog. Phase-resolved nonlinear response of a two-dimensional electron gas under femtosecond intersubband excitation. *Physical Review Letters*, 92(4):0474021–0474024, January 2004.

[Muk95] S. Mukamel. *Principles of nonlinear optical spectroscopy*. Oxford University Press, New York, 1995.

[MVO03] D. McPeake, F.T. Vasko, and E.P. O'Reilly. Rabi oscillations of two-dimensional electrons under ultrafast intersubband excitation. *Physical Review B*, 68(19):1933061–1933064, November 2003.

[N+97] D. Nikonov et al. Collective intersubband excitations in quantum wells: Couloumb interaction versus subband dispersion. *Physical Review Letters*, 79(23):4633–4636, December 1997.

[NIS99] D.E. Nikonov, A. Imamoğlu, and M.O. Scully. Fano interference of collective excitations in semiconductor quantum wells and lasing without inversion. *Physical Review B*, 59(19):12212–12215, June 1999.

[Nol97] W. Nolting. *Grundkurs Theoretische Physik 3: Elektrodynamik*. vieweg, Braunschweig/Wiesbaden, 5rd edition, 1997.

[PAL00] S.H. Park, D. Ahn, and Y.T. Lee. Screening effects on electron-longitudinal optical-phonon intersubband scattering in wide quantum well and comparison with experiment. *Japanese Journal of applied physics Part 1*, 39:6601 – 6605, 2000.

[Pre98] F. Prengel. *Hot Electrons in Quantum Wires: Intersubband Impact Ionization*. Dissertation, Technische Universität Berlin, July 1998. Published by Mensch & Buch Verlag, Berlin, 1998.

[PS99] F. Prengel and E. Schöll. Delayed intersubband relaxation in quantum wires due to quantum kinetic coulomb scattering. *Physical Review B*, 59(8):5806 – 5816, 1999.

[SBD+99] A Schulzgen, R Binder, ME Donovan, T Lindberg, K Wundke, HM Gibbs, G Khitrova, and N Peyghambarian. Direct observation of excitonic rabi oscillations in semiconductors. *Physical Review Letters*, 82(11):2346 – 2349, 1999.

[Sip87] J.E. Sipe. New green-function formalism for surface optics. *Journal of the Optical Society of America B*, 4(4):481–4893???, April 1987.

[SMM+04] G.Y. Slepyan, A. Magyarov, S.A. Maksimenko, A. Hoffmann, and D. Bimberg. Rabi oscillations in a semiconductor quantum dot: Influence of local fields. *Phys. Rev. B*, 70(4):045320 –045325, 2004.

[SRW+04] T. Shih, K. Reimann, M. Woerner, T. Elsaesser, I. Waldmüller, A. Knorr, R. Hey, and K.H. Ploog. Nonlinear response of radiatively coupled intersubband transitions of quasi-two-dimensional electrons. *submitted to Physical Review Letters*, 2004.

[TRN+00] S Tsujino, M Rufenacht, H Nakajima, T Noda, C Metzner, and H Sakaki. Peak position of the intersubband absorption spectrum of quantum wells with controlled electron concentrations. *Physical Review B*, 62(3):1560 – 1563, 2000.

[Vas04] F.T. Vasko. Spin-dependent rabi oscillations in single quantum dots. *Phys. Rev. B*, 70(7):073305 –073308, 2004.

[WAK03] T. Wolterink, V.M. Axt, and T. Kuhn. Role of exchange interaction in coulomb quantum kinetics. *Physical Review B*, 67(11), 2003.

[Wal02] I. Waldmüller. *Many Particle Theory of the Optical Gain of Intersubband Transitions*. diploma thesis, Technische Universität Berlin, 2002.

[War96] T. Warncke. *Coherent dynamics of readiatively coupled quantum wells*. Dissertation, Philipps–Universität Marburg, December 1996. Published by Verlag Görich & Weiershäuser GmbH, Marburg, 1996.

[WFK04] I. Waldmüller, J. Förstner, and A. Knorr. Self-consistent projection operator theory of intersubbnad absorbance in semiconductor quantum wells. In K. Morawetz, editor, *Nonequilibrium Physics at Short Time Scales*, chapter 1, pages 251–272. Springer Verlag, 2004.

[WFL+04] I Waldmuller, J Forstner, SC Lee, A Knorr, M Woerner, K Reimann, RA Kaindl, T Elsaesser, R Hey, and KH Ploog. Optical dephasing of coherent intersubband transitions in a quasi-two-dimensional electron gas. *Physical Review B*, 69(20), 2004.

[WGW+96] RJ Warburton, C Gauer, A Wixforth, JP Kotthaus, B Brar, and H Kroemer. Intersubband resonances in inas/alsb quantum wells: Selection rules, matrix elements, and the depolarization field. *Physical Review B*, 53(12):7903 – 7910, 1996.

[YC99] P.Y. Yu and M. Cardona. *Fundamentals of Semiconductors — Physics and Material Properties*. Springer Verlag, Berlin, 2nd edition, 1999.

[Zal84] M Zaluzny. On the influence of the depolarization field on the intersubband absorption in thin semiconductor-films. *Physica Status Solidi (b)*, 123(1):K57 – K62, 1984.

[Zal91] M. Zaluzny. Intersubband absorption line broadening in semiconductor quantum wells: Nonparabolicity contribution. *Physical Review B*, 43(5):4511–4514, February 1991.

Index

Acknowledgments

I want to seize this chance to thank many people who have contributed to this work in one way or another.
First of all, I would like to thank Prof. Dr. Andreas Knorr, who gave me the chance to continue my research on intersubband transitions. He left me considerable freedom in arranging my work whilst at the same time offering constant guidance and encouragement. I am grateful for his invaluable comments during the whole work with this dissertation. The knowledge of his support was always a reassuring thought.
Special thanks go also to Dr. Michael Wörner, Prof. Dr. Klaus Reimann and Prof. Dr. T. Elsässer from the Max-Born Institute for Nonlinear Optics and Short Pulse Spectroscopy in Berlin not only for their collaboration but also for many fruitful discussions.
It is a great pleasure to thank Jan Schlesner, for his friendship and continuous support (also in the name of Poldi, my poor old battered computer), S.C. Lee for sharing her knowledge and countless valuable discussions, Peter Orlowski, who more than once saved my day by solving hardware problems or accelerating the process of installing new computers, Andrea Schulze who is always ready to help if bureaucracy is threatening to bear the palm, Frau Krupsack-Dabel for her very friendly and encouraging supervision in the framework of the Berliner Chancengleichheitsprogramm and all members of the AG Knorr for cooperations and discussions, tea, cake and fun...
Furthermore, I would like to thank Prof. Dr. E. Schöll and Prof. Dr. E. Sedlmayr for kindly agreeing to act as a co-referee and as a chairman of the examiners commission, respectively. I gratefully acknowledge their and Prof. Knorr's flexibility concerning the time-frame.

And finally,
Bounty, Jörg, Mum
(in alphabetical order)
the three of you mean everything to me.
I would have never done this without your never-ending support and understanding.
You always believed in me!

Financial support by the "Berliner Programm zur Förderung der Chancengleichheit für Frauen in Forschung und Lehre" is gratefully acknowledged.